Biological role of calystegines – isolation from potato sprouts, analysis and dietary perspectives

Dissertation

zur Erlangung des

Doktorgrades der Naturwissenschaften (Dr. rer. nat.)

der

Naturwissenschaftlichen Fakultät I – Biowissenschaften –

der Martin-Luther-Universität

Halle-Wittenberg,

vorgelegt

von Herrn Dipl. Pharm. Nebojša Jocković

geb. am 06.11.1979 in Novi Sad, Serbien

Gutachter:

1. Prof. Dr. Birgit Dräger, Martin-Luther-Universität, Halle-Wittenberg

2. PD Matthias Brandsch, Martin-Luther-Universität, Halle-Wittenberg

3. Prof. Ing. František Kvasnička, CSc., University of Chemistry and Technology, Prague

Halle (Saale), den 16.10.2014   Datum der Verteidigung: 05.03.2015

A. Table of contents

B. List of figures

C. List of schemes

D. List of equations

E. List of tables

F. Abbreviations

Abbreviation	Full name
Aq. bidest.	double-distilled water
BES	*N,N*-bis(2-hydroxyethyl)-2-aminoethanesulfonic acid
BGE	background electrolyte
cal.	calystegine
cpm	counts per minute
DAD	diode array detectio
DNJ	deoxy-nojirimycin
dpm	disintegration per minute
d.w.	dry weight
extr.	extract
FAB6	flux assay buffer pH = 6
FAB7.5	flux assay buffer pH = 7.5
FBS	foetal bovine serum
fract.	fraction
f.w.	fresh weight
GC	gas chromatography
HEC	hydroxyethylcellulose
HEPES	2-[4-(2-hydroxyethyl) piperazine-1-yl]-ethanesulfonic acid
HMDS	hexamethyldisilazane
HPLC	high pressure liquid chromatography
ion exch.	ion exchanger
I.D.	inside diameter
K_m	Michaelis-Menten constant, dissociation coefficient of enzyme-substrate complex dissociation
K_i	dissociation constant of enzyme-inhibitor complex
λ	wavelength
L	litre
L.	length
LDL	low-density lipoprotein
LE	leading electrolyte
m	mass
M1	ion exchanger Merck I
M3	ion exchanger Merck III
M4	ion exchanger Merck IV
MEM	minimal essential medium
MeOH	methanol
MES	2-(*N*-morpholino)ethanesulfonic acid

min	minute
m.v.	mean value
n.d.	not determined
NEAA	non-essential amino acids
n.l.	noise level
p.s.	potato sprouts
PBS	phosphate buffered saline
p-NPG	*para*-nitrophenyl-*β*-D-glucopyranoside
PPAR	peroxisome proliferator-activated receptor
PS-DVB	polystyrene-divinylbenzene
R^2	correlation coefficient
r.e.	raw extract
rpm	revolutions per minute
RT	room temperature
RSD	relative standard deviation
s	second
sol.	solution
s.d.	standard deviation
std. error	standard error
susp.	suspension
TBA	tetrabutylammonium bromide
TE	terminating electrolyte
TEER	transepithelial electrical resistance
TLC	thin layer chromatography
TMCS	trimethylchlorosilane
TMS	tetramethylsilane
Tris	2-amino-2-hydroxymethyl-propane-1,3-diol
USB	ultrasonic bath
UV	ultraviolet
VLDL	very low-density lipoprotein
V_{max}	maximal speed of enzyme specific activity
w.	weight

G. Publications and poster presentations

Publications:

Kvasnička, František; Jocković, Nebojša; Dräger, Birgit; Ševčík, Rudolf; Čepl, Jaroslav; Voldřich Michal (2008) Electrophoretic determination of calystegines A_3 and B_2 in potato. *J. Chromatogr. A*, **1181**, 137–144

Jocković, Nebojša; Fischer, Wiebke; Brandsch, Matthias; Brandt, Wolfgang; Dräger, Birgit (2013) Inhibition of Human Intestinal α-Glucosidases by Calystegines, *J. Agric. Food Chem.*, **61 (23)**, 5550–5557

Poster presentations:

2009, Botaniker Tagung der Deutschen Botanischen Gesellschaft, Leipzig:
Kvasnička, František; <u>Jocković, Nebojša</u>; Dräger, Birgit; Ševčík, Rudolf; Čepl, Jaroslav; Voldřich Michal, Electrophoretic determination of calystegines A_3 and B_2 in potato

1. Introduction

1.1.   Calystegines

1.1.1.   Structure. Physical and chemical properties

Calystegines are secondary plant metabolites discovered by Tepfer and colleagues in 1988 in *Calystegia sepium* (Convolvulaceae) (Tepfer et al., 1988). Their structure was elucidated two years later (Ducrot and Lallemand, 1990; Goldmann et al., 1990): they were described as nitrogen containing, low-weight molecules and bicyclic compounds. The skeleton of calystegines is 8-azabicyclo[3.2.1]octane, to which 3–5 hydroxyl groups are attached. Distinctive for calystegines is an aminoketal functionality, built by a tertiary hydroxyl group at the bicyclic bridgehead C1 with the nitrogen bridge atom (Figure 1). Other hydroxyl groups are secondary ones, in axial or equatorial position to the skeleton. According to the number of the hydroxy groups attached on the nortropane ring, calystegines are divided in three main classes: A (three hydroxyl groups), B (four hydroxyl groups) and C (five hydroxyl groups). If an amino group is located on the C1 bridgehead, calystegines are classified as *N*-calystegines. The nitrogen atom is methylated in *N*-methyl calystegines. To date, 14 different calystegines and 2 glycosidated calystegines have been discovered (Asano et al., 1997c; Biastoff and Dräger, 2007). No calystegine esters have been found.

Since the nitrogen in the bicyclic structure is not methylated, calystegines are structurally classified, regarding the skeleton, as polyhydroxynortropanes. This implies that they are hydrophilic and water soluble. Their octanol–water partition coefficient is below zero. If calystegines are regarded as norpseudotropine derivatives, they are more polar than norpseudotropine itself because of the greater extent of hydroxylation of their skeleton. On the other hand, existence of the hydroxyl group on the C1 bridgehead influences the basicity: calystegines are less basic than norpseudotropine. Among calystegines there is a gradient considering basicity. The more hydroxyl groups are present, the less basic is calystegine (Dräger, 2002). That is, calystegines of group A are more basic than the C calystegines. This fact is due to the positive inductive effect of the hydroxyl groups, which attract the free electron pair of the nitrogen bridge atom, making it less susceptible for protonation. Number and positions of hydroxyl groups in calystegines affect not only basicity and polarity, but also their cyclic structure balance. Although naturally occurring calystegines were found in bicyclic form only, ring-opening and isomerisation are possible and may be a reason for the variety of calystegine structures (Boyer et al., 1992; Dräger, 2004). The equatorial position of

hydroxyls is energetically more stable than the axial one and is more frequent in naturally occurring calystegines (Dräger, 2004; Skaanderup and Madsen, 2003).
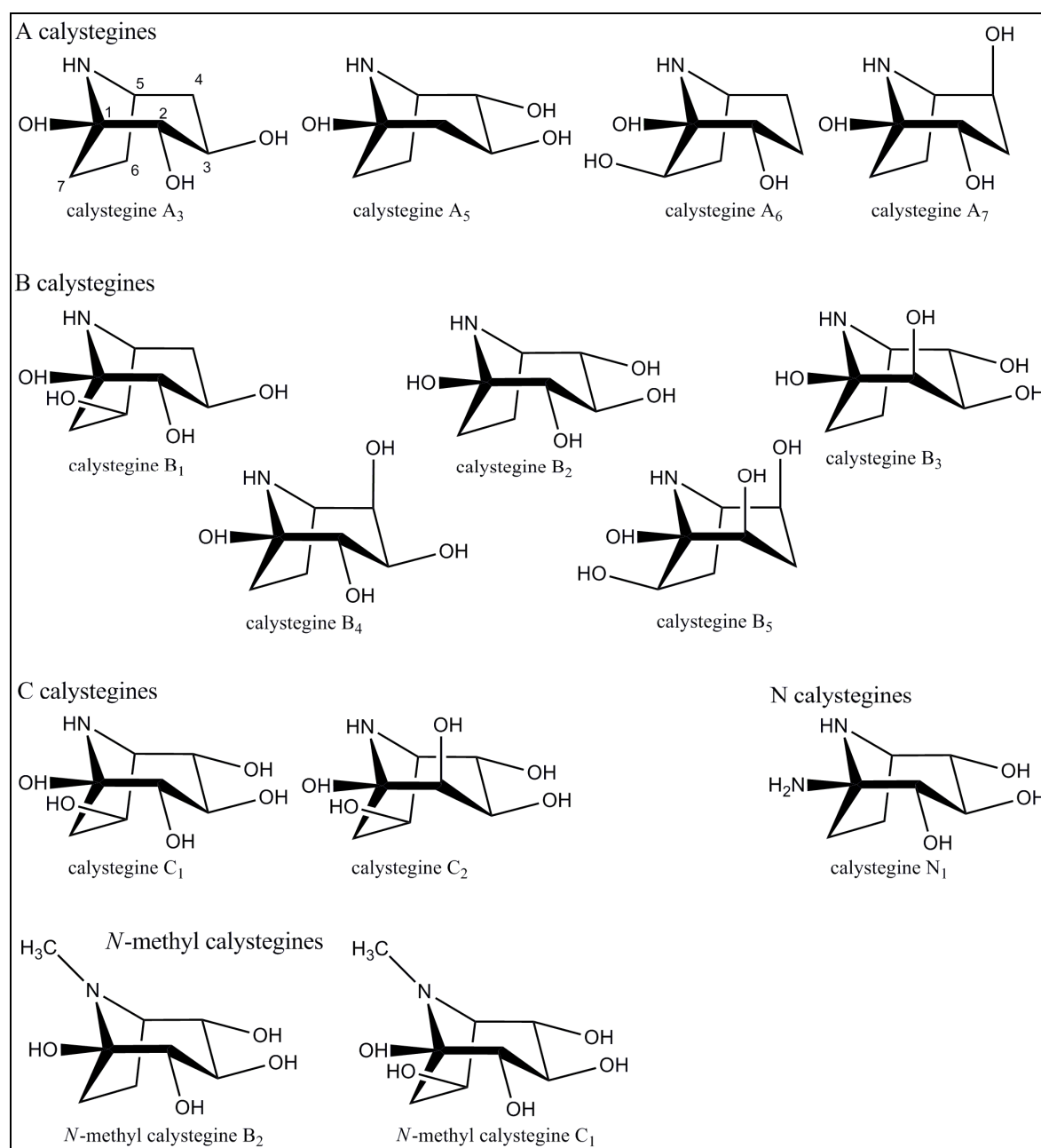
Figure 1: Classification of calystegines

1.1.2. Occurrence and distribution of calystegines

Calystegines have been found exclusively in the plant species Brassicaceae, Convolvulaceae, Erythroxylaceae, Moraceae and Solanaceae up to now (Asano et al., 2001a; Brock et al., 2005; Brock et al., 2006; Dräger, 2004; Schimming et al., 1998). Some representatives of

these plant families are used in the human everyday diet, like sweet peppers, aubergines and potatoes (Asano et al., 1997b; Friedman et al., 2003; Keiner and Dräger, 2000).

Calystegines normally appear in combinations of several (iso)forms, amount and composition of the mixtures depend on the plant species. The most widespread calystegines are calystegines B_2, A_3 and B_1 (Dräger, 2004). Calystegine B_2 appears as the most common among them, since it occurs in nearly all plants known to produce calystegines. Only some Convolvulaceae species lack calystegine B_2 (Biastoff and Dräger, 2007). Young meristematic tissues, including flowers and fruits, possess the highest concentrations of calystegines. Certain organs in some plants are especially rich in calystegines. Localisation of calystegines in cells has not been possible and extracellular calystegines were not found (Biastoff and Dräger, 2007).

Enzymes for biosynthesis of tropane alkaloids are localised in the root pericycle and in the endodermis (Nakajima and Hashimoto, 1999; Suzuki et al., 1999). Production of calystegines can be affected by alteration of biosynthesis pathways or by increase of sugar supply. When 5% sucrose was applied to root cultures of *Atropa belladonna*, ratios of calystegine to hyoscyamine, the latter (nearly) unaffected by sucrose application, were up to four-fold higher than in untreated controls (Rothe et al., 2001). *A. belladonna* and *Hyoscyamus* species are known for their content of the tropane alkaloids hyoscyamine (Asano et al., 1996c) and scopolamine. Leaves of *A. belladonna* typically contain 3 mg/g dry mass hyoscyamine (Yun et al., 1992), more than calystegines A_3, B_1, and B_2 together (ca. 1.5 mg/g dry mass). Also in the roots of the plant, hyoscyamine concentration (2–3 mg/g dry mass) was higher than that of the total calystegine alkaloids (ca. 300 µg/g dry mass). Still, a considerable fraction of the total tropane alkaloid content that is produced in these plants is for calystegine formation, in particular in young tissues.

Calystegines in potato (*Solanum tuberosum*, L.)

Potato (*Solanum tuberosum* L.) is a member of Solanaceae. It is native in South America, but meanwhile has been spread around the globe, mainly due to its significant role as food plant. Currently, after wheat and rice, it is the third most common food crop worldwide (Ji et al., 2012). Most commercial potato cultivars are tetraploid, designated as *S. tuberosum* spp. *tuberosum*, whereas indigenous South American cultivars are predominantly diploid (e.g. *S. tuberosum* spp. Phureja) (Griffiths et al., 2008). The tuber is the edible plant organ and its major nutritional components are carbohydrates, mostly starch. Up to 70% of sucrose

transported into the tuber is metabolised into starch, providing up to 20% starch related to total potato fresh mass (ap Rees and Morrell, 1990).

Calystegine have been detected in potatoes for the first time in 1993 (Nash et al., 1993) and were found to be ubiquitous. The aerial tissues with the highest calystegine concentrations are flowers and young leaves (Keiner and Dräger, 2000). Underground organs are especially rich in calystegines (Keiner and Dräger, 2000; Nash et al., 1993; Richter et al., 2007). Their content in plant organs may vary considerably, depending on cultivar. Although the concentration of calystegine in tuber peel is usually up to twice as high as in tuber flesh, both the distribution and the total amount of calystegines in tubers show within-species variability (Friedman et al., 1997). The growth stage of the potato plant also has an influence on calystegine accumulation in tubers. Dormant tubers directly after harvest contain less calystegines in all parts than sprouting tubers. Calystegine content also shows variations concerning organ position or localisation. Higher calystegine concentrations are present in upper leaves and sprout tips than in lower leaves or lower parts of sprouts. This again indicates pronounced accumulation of calystegines in young meristematic tissues.

Calystegines B_2, A_3 and B_4 are the main representatives in potato. Beside them, calystegines B_1, B_3 and A_5 are also present, but in lower concentrations. The highest calystegine concentrations in potato were generally measured in sprouts. Maximal concentrations were reported for young potato tuber sprouts, with more than 3 mg/g fresh mass (Keiner and Dräger, 2000). Calystegine content in sprouts is indirectly proportional to spout length. Long sprouts contain more water than short sprouts, but calystegine accumulation decreases during sprouts elongation, resulting in a lower calystegine concentration in long sprouts relative to dry mass (Keiner and Dräger, 2000). The concentration of calystegine B_2 is greater than that of calystegine A_3 and the ratio of calystegine B_2/A_3, is approximately 2 times greater in sprouts than in tuber flesh or peel. Up to now, no correlation is known between concentrations of calystegines in sprouts and either flesh or peel (Griffiths et al., 2008).

1.1.3. Biosynthesis

Calystegine biosynthesis starts with enzymatic decarboxylation of arginine or ornithine to putrescine (Figure 2). Further enzymatic processing through intermediates *N*-methyl putrescine and 4-methylaminobutanal leads to the *N*-methylpyrrolinium cation, a common precursor for calystegines and other structurally similar alkaloids (e.g. atropine, cocaine or nicotine), with which calystegines occur together (Brock et al., 2005; Stenzel et al., 2006).
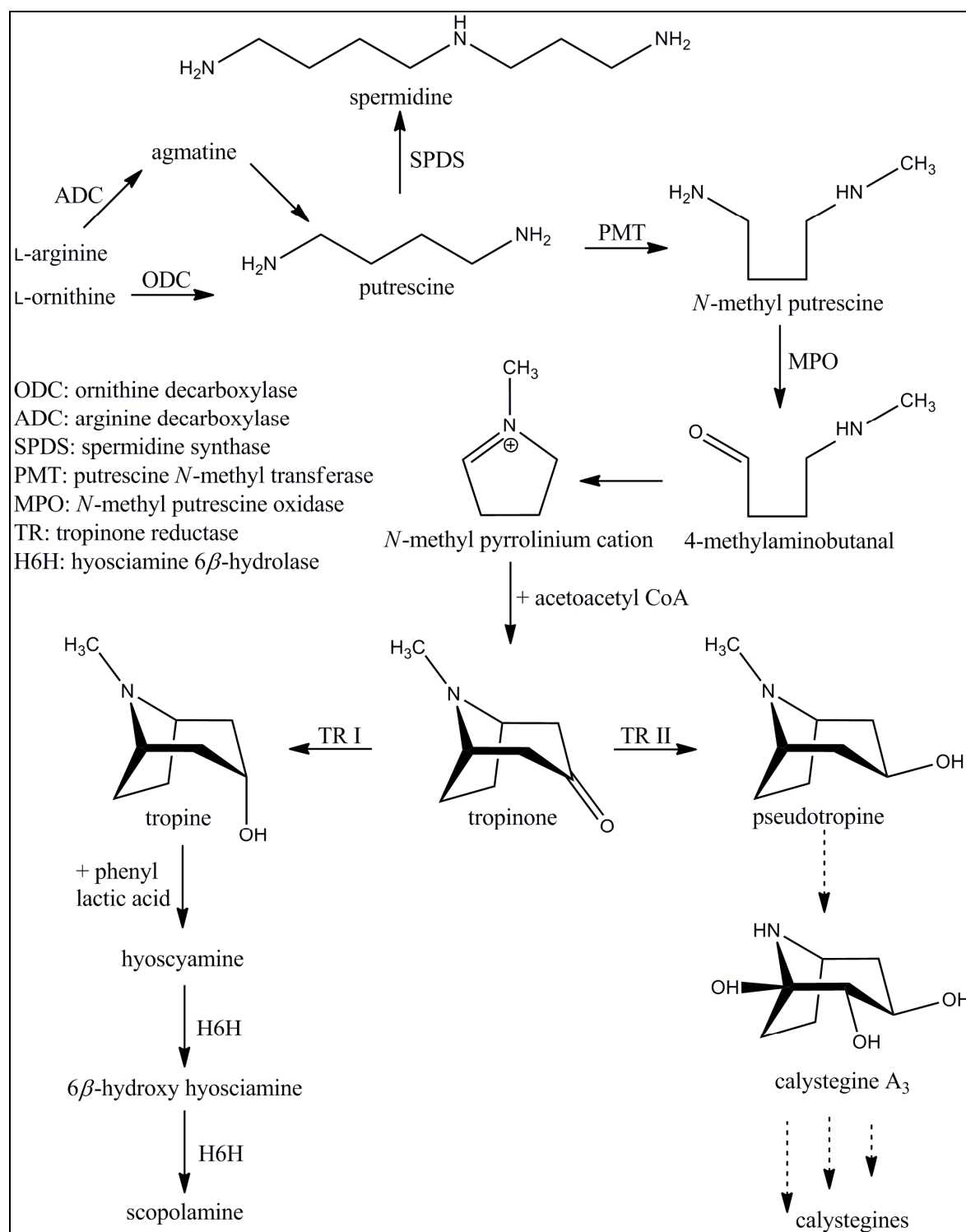
Figure 2: Pathway of calystegine biosynthesis

Reaction of the *N*-methylpyrrolinium cation with acetoacetyl CoA then leads to the formation of tropinone, the first intermediate with a tropane ring and substrate for either of two tropinone reductases, TRI and TRII. Both reductases dehydrogenate the ketone at C3 of tropine, but with different stereospecificities. TRI generates an axial hydroxyl group, producing tropine that is further processed to hyoscyamine and scopolamine. By generation of

an equatorial hydroxyl group at C3, TRII produces pseudotropine that is the first specific precursor of the calystegines, as was already assumed soon after the elucidation of calystegine structure (Dräger et al., 1994). After the elucidation of the structure of calystegine, it was assumed, that pseudotropine is the first specific precursor for the calystegines (Dräger et al., 1994). Confirmation came from isolation of both TRI and TRII from *Datura stramonium* (Portsteffen et al., 1992; Portsteffen et al., 1994) and from *Hyoscyamus niger* (Hashimoto et al., 1992), plants that contain calystegines besides tropine esters hyoscyamine and scopolamine. TRII was also cloned and characterised in potato, another confirmation of the specific role of TRII in synthesis of calystegines (Keiner et al., 2002).

The nortropane skeleton and an equatorial hydroxyl group on C3 indicate that calystegines are related with pseudotropine. However, not all of the calystegines have a hydroxylated C3, which is the result of keto-enol tautomerism, a nonenzymatical process of ring opening at the acid labile aminoketal group (Asano et al., 1996a).

1.1.4.   Chemical synthesis

Ever since their discovery, calystegines have been objects of interest for chemical synthesis. Their sugar-like structure suggests suitability of methods developed for synthesis of sugars. The presence of chiral carbon atoms and defined hydroxyl group orientations require enantioselective preparation, which can be complex and difficult (Dräger, 2004). Several approaches for synthesis of calystegine A_3 have been described. When starting with 3-aminocyclohexanone and applying 4 synthesis steps, a racemic mixture of calystegine A_3 is obtained (Boyer et al., 1992). Both enantiomers of calystegine A_3 are also obtained with a synthetic procedure in which cycloheptatriene is the starting compound, over 6-azido derivatives of *meso*-2-cycloheptene-1,4-diol (Johnson and Bis, 1995). Recently, a new variation of a method for calystegine A_3 synthesis has been published that starts from 2-deoxy-D-glucose and applies a diastereoselective allylation protocol (Rasmussen and Jensen, 2011). Enantioselective synthesis of calystegine B_2 (Boyer and Lallemand, 1992; Boyer and Lallemand, 1994; Duclos et al., 1992; Faitg et al., 1999) and calystegine B_4 (Moosophon et al., 2010) may also be performed in several ways. However, those methods yield low product amounts and consist of lengthy synthetic procedures.

A practical way starts with benzyl-protected methyl 6-iodo-glycoside. A zinc-mediated tandem reaction, followed by ring-closing metathesis, converts iodo-sugars into carbocycles (cycloheptenes) in just two steps. These are converted to cycloheptanones by regioselective

oxidation and after reductive deprotection of hydroxyl groups, the nortropane skeleton forms spontaneously (Boyer and Hanna, 2001; Boyer et al., 2001; Marco-Contelles and de Opazo, 2002). An advantage of this synthesis is that other calystegines can also be formed by this modified way. Calystegines B_3 and B_4 were synthesised following this procedure, starting with D-galactose and D-mannose (Skaanderup and Madsen, 2001; Skaanderup and Madsen, 2003). Csuk and colleagues described a procedure for synthesis of a chiral pool of calystegine A_7 from methyl α-D-glucopyranoside. This method is also based on a Zn-mediated tandem ring opening reaction followed by a Grubbs' catalyst-mediated ring closure metathesis (Csuk et al., 2008).

1.1.5.   Purification and analysis of calystegines

<u>Purification</u>

Calystegine hydrophilicity implies processing raw plant material with either hot water or aqueous methanol or ethanol. High temperature during extraction ensures deactivation of enzymes present in fresh tissue and precipitation of coagulated proteins. In water–alcohol extraction liquids, a high water percentage of >50% enables transition of water soluble components from the raw material into the liquid phase, whereas alcohol, e.g. methanol, influences the denaturation of proteins (Sinanoglu and Fernández, 1985).

The hydrophilicity of the calystegines also distinguishes them from the majority of the alkaloids and the fact that customary alkaloid extraction techniques may not be applied in their case is a reason why they were discovered later than other alkaloids. The basic nature and water solubility of calystegines implies the use of ion-exchange chromatography for purification. The most applied and reliable purification technique comprises a series of runs on different types of ion-exchange material. The primary step, purification on a strong cation exchange column, is universal. Being alkaline compounds, the calystegines are retained through the positive charge of their secondary amino group (Dräger et al., 1995) whereas acidic and neutral components of the raw extract are washed away with water. The calystegines are thereafter eluted with diluted ammonia, along with some contaminating amino acids and amino sugars. The following step is purification on a strong anion exchange column (OH^- form): the calystegines pass through almost without retention, but ions with negative charge and zwitterions, e.g. amino acids, are bound to the column. Finally, a weak cation exchange column (NH_4^+ form) is used for fractionation and separation of the calystegines that are eluted with water. The order of appearance of the calystegines in eluate fractions depends on the polarity of the nitrogen atom: less basic calystegines will appear

early while more basic ones elute late. The order of elution is generally as follows: calystegine C–B–A. The order of the columns may be varied, but typically purification then takes more time and yields may be reduced.

Other techniques for separation and concentration of calystegines, following the initial purification step on the strong cation exchanger, were also developed (Biastoff and Dräger, 2007; Dräger, 2004). Concentration was achieved, for example, using *Agrobacterium tumefacies*, while separation of calystegine A_3 was performed on Sephadex LH20 columns or by multilayer coil countercurrent chromatography (MLCCC). However, these alternatives proved to be either unreliable or excessively complex.

Analysis

Although the calystegines belong to a large group of alkaloids, their detection and analysis were not always as favourable and easy. When discovered, calystegines were detected by paper electrophoresis. The method for sugars was modified, since calystegines can be considered aminosugars.

A two step staining treatment with $AgNO_3$ and NaOH was applied for detection (Molyneux et al., 1996; Tepfer et al., 1988). Applying similar conditions, TLC was also successful (Dräger, 1995; Molyneux et al., 1996). An upgraded, automated TLC method was developed (AMD−TLC = automated multiple development thin layer chromatography), which is more favourable for single type calystegine separation (Scholl et al., 2001).

Since the calystegines, due to their structure, do not have chromophores, HPLC is not a method of choice for detection and quantification, although refractometric detection after passage over an amino column is possible. This method is basically an adaptation of an analytical procedure for sugars. However, refractometry is not sufficiently sensitive for direct detection from plant matrices or low concentration samples (Dräger, 2002; Goldmann et al., 1990).

Capillary electrophoresis (CE) can also be applied for analysis of calystegines, especially since there are hydrophilic compounds, positively charged in aqueous solutions due to the free electron pair on the nitrogen atom. However, the lack of chromophores complicates also this procedure. Again, a sugar analysis procedure was modified, whereby calystegines were firstly derivatised with borate and calystegine-borate complexes were separated and detected at 191 nm, the detection wavelength for borates (Daali et al., 2000;Dräger, 2002). Direct detection of calystegines in CE can be performed by electrochemical oxidation (Rüttinger and Dräger, 2001). Unlike indirect detection using borate, this is a sensitive method, but a disadvantage is

that it is not very robust and the instrumentation is not easily obtainable. Overall, CE is a promising technique for future investigation.

The method of choice for calystegine quantitation still remains gas chromatography (GC). Calystegines are neither volatile nor lipophilic and require transformation in a volatile form. Before GC analysis, calystegines are derivatised with mild silylation agents, trimethylchlorosilane (TMCS) and hexamethyldisilazane (HMDS), with addition of pyridine (Sweeley et al., 1963). Pyridine is an organic nitrogen base, which reacts with the released HCl and the trimethylsilyl chloride. Using this silylating combination increases the silylating potential of the single reagent. Calystegine molecule structure remains undamaged and derivatisation is complete, which is essential for quantification. Hydroxyl groups are silylated, forming trimethylsilyl ether derivatives, whereas the nitrogen atom remains intact (Dräger, 1995). The precipitated ammonium or pyridine chloride salts do not affect the GC analysis.

$$3\ R\text{-}(OH)_3 + (CH_3)_3SiCl + (CH_3)_3Si\text{-}NH\text{-}Si(CH_3)_3 \longrightarrow 3\ R\text{-}(O\text{-}Si(CH_3)_3)_3 + NH_4Cl$$
$$R\text{-}(OH)_3 = \text{calystegine } A_3$$
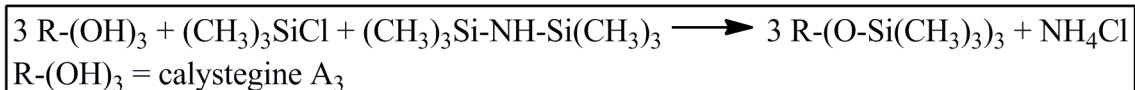
Equation 1: Simplified silylation scheme of calystegines

During GC, the silylated calystegine derivatives are separated according to their affinity to the hydrophobic stationary phase. Interaction increases with the number of hydroxyl groups, which is directly proportional to retention time, resulting in the order of appearance A-B-C of calystegine groups on a GC chromatogram. Individual calystegines are identified by comparison to(defined) retention times of pure references. GC can be coupled to mass spectrometry (MS), which allows more reliable confirmation of calystegine identity according the known mass spectra. However, absolute configuration can be determined only with nuclear magnetic resonance (NMR). GC analysis of calystegines is reliable for quantification, but the complex sample preparation is disadvantageous, providing many possibilities for errors or losses (Biastoff and Dräger, 2007; Dräger, 2002).

1.1.6. Biological properties of calystegines

Structure–effect relations between calystegines and glycosidases – Calystegines inhibit plant and mammal glycosidases (Asano et al., 1994b). The structure of calystegine resembles the pyranose form of monosaccharides, which infers their glycosidase inhibitory activity. Glycosidases are significant catalysts in numerous enzymatic reactions like digestion of

polysaccharides, synthesis and modification of the glycoside chains on glycoproteins and lysosomal decomposition of glycoconjugates (Asano et al., 2000; Watson et al., 2001). The sugar-like composition of calystegines indicated their potential involvement in carbohydrate metabolism, which was later confirmed in extensive assays showing the inhibitory properties of calystegines for various bacterial, plant and mammal glycosidases (Asano et al., 1995a; Asano et al., 2001a; Kato et al., 1997; Molyneux et al., 1993).

Calystegine B_2 inhibited almond β-glycosidase and coffee bean α-galactosidase stronger than calystegine A_3. Calystegine B_1 did not inhibit coffee bean α-galactosidase, but inhibited bovine liver β-galactosidase and β-glycosidases of almond and *Caldocellum saccharolyticum* (Asano et al., 1995a). Calystegine B_2 was a surprisingly weak inhibitor of human lysosomal liver enzymes (Asano et al., 1997b). Calystegine C_1 showed an identical inhibitory spectrum and, compared with calystegine B_2, inhibited almond β-glycosidase stronger and coffee α-galactosidase weaker (Asano et al., 1994b). Calystegines did not inhibit mannosidase, with the exception of calystegine C_2 from *D. leichhardtii* (Kato et al., 1997).

Taking all these accounts into consideration, the number of hydroxyl groups in the calystegines does not correlate well with their inhibitory effect on glycosidases: there are variations depending of the type of enzyme. Still, some factors generally have the same effect. The main condition for effective glycosidase inhibition is a hydroxyl group on the bridgehead carbon (C2) (Asano et al., 1997c; García-Moreno et al., 2001), as glucosylation of this hydroxyl group (calystegine esters) leads to reduction of the inhibitory potency (Asano et al., 1997a). the orientations of the hydroxyl groups to the nortropane skeleton also plays an important role for inhibitory strength, equatorial positions being more favourable. Calystegines with equatorial hydroxyl groups, e.g. B_1 and C_1, are strong inhibitors of β-galactosidases, whereas calystegines with axial hydroxyl groups (B_3 and B_4) lack the inhibitory effect (Asano et al., 1997c). Methylation of calystegines (*N*-methylcalystegines) enhanced inhibition of coffee bean α-galactosidase, except in the case of calystegine C_1, whereas it nearly abolished the inhibitory effect of calystegines A_3 and B_4 on almond β-glycosidase and trehalase (Asano et al., 1997c).

Mechanism of inhibition of calystegines – Calystegines normally act as competitive glycosidase inhibitors, which is common for most polyhydroxy alkaloids (Asano et al., 1997b; Asano et al., 1997c; Asano et al., 1995a; Dräger, 2004). Some, however, act as noncompetitive inhibitors, such as calystegine N_1 for pig kidney trehalase, or glycosilated calystegine B_1 for rice α-glycosidase (Asano et al., 1997c; Asano et al., 1996c). Calystegines exclusively inhibit activity of exoglycosidases that cleave at the non-reducing end of a

saccharide chain, while endoglycosidases, which cleave within a saccharide chain releasing oligo- or disaccharides, mostly remain unaffected (Watson et al., 2001).

O-glycosidases form a large group of various enzymes that differ in hydrolytic mechanism and substrate specificity (Bourne and Henrissat, 2001). The orientation of the oxygen at the anomeric chiral carbon, located in the semi-acetal (aldoses) or semi-ketal (ketoses) functionality, in the cyclic monosaccharides released by their activity may be retained or inversed (Davies et al., 2003; Vasella et al., 2002). Calystegines exhibit inhibition of glycosidases due to their sugar mimicking structure, since the nitrogen in the nortropane skeleton resembles the glycosidic oxygen of a saccharide molecule. During enzymatic *O*-catalysis, the sugar oxygen atom is protonated by the donor group of the enzyme, whereby a planar oxocarbenium ion is formed. In retaining hydrolases, this ion is stabilised (additionally) by a nucleophilic carboxylate residue (Davies et al., 2003; Nerinckx et al., 2003). A similar course of interaction is expected also for the calystegines. They may occupy the active site of an enzyme in relaxed chair conformation, with the protonated nitrogen in the position that corresponds to that of the anomeric carbon atom of a saccharide substrate. The nitrogen is in contact with both donor and nucleophile residues of the enzyme, which altogether corresponds to the transition state. These observations resulted from crystallisation of calystegine B_2 with *β*-glycosidase from *Thermotoga maritima* (TmGH1) (PDB 2CBV) (Gloster et al., 2006). Taking all these variations into consideration, it is still hard to define an exact model of the mechanism of inhibition by calystegine (Biastoff and Dräger, 2007).

<u>*Toxicity*</u> − A potential toxic effect of calystegines was suspected, based on their glycosidase inhibitory effects. Fodder plants containing alkaloidal glycosidase inhibitors were identified to cause strong and lethal intoxications in farm animals (Haraguchi et al., 2003). Typical lesions were observed in neural and glandular tissues after the hydoxylated alkaloids had been absorbed from the feed into the blood of the animals (Cholich et al., 2009). The toxic plants, e. g. *Ipomoea* species, contain calystegines, but also additional glycosidase inhibitors of strong toxicity like swainsonine (Figure 6). Calystegines alone proved non-toxic in experiments performed on mice (Stegelmeier et al., 2008).

<u>*Role and function in* <u>p</u>lants</u> − The function of calystegines within plants themselves has not been completely explained. It was noticed that calystegines occur with structurally similar alkaloids (atropine, cocaine and nicotine) (Brock et al., 2005). The biosynthetic precursors, such as *N*-methylputrescine and the methylpyrrolinium cation, are common to all of them (Stenzel et al., 2006).

Investigations on interaction of calystegines with the rhizosphere gave rise to speculations, that they are the carbon and nitrogen sources of choice for calystegine catabolising soil bacteria. Involvement of calystegines in nodulation was excluded. It was also assumed that calystegines may possess allelopathic properties, since it had been shown that naturally occurring enantiomer of calystegine B_2 inhibits alfalfa seed germination (Schimming et al., 1998).

Medicinal application – Calystegines and some other glycosidase inhibitors are designated as "pharmacological chaperones" or "pharmacoperones" (Amaral, 2006). Chaperones are proteins that assist other proteins in obtaining and maintaining correct folding. Pharmacoperones are folding helpers for some mutated human glycosidases, since they can bind to the active site or another protein target structure and support the correct folding (Arakawa et al., 2006; Bernier et al., 2004). This therapeutic approach is also called enzyme enhancement therapy (Desnick, 2004). Most of the pharmacological chaperones applied for treatment of lysosomal storage disorders are competitive inhibitors, stabilising the conformation of the mutant enzymes (Asano, 2009). However, a noncompetitive inhibitor has recently been reported as a chaperone (Kuriyama et al., 2008). Application of calystegines has recently been considered for treatment of lysosomal storage diseases, e.g. Morbus Gaucher and Morbus Fabry (Asano, 2003). These diseases are the results of mutations in the genes encoding the lysosomal glycosidases glucosylceramidase or glucocerebrosidase, EC 3.2.1.45 (Morbus Gaucher), and α-galactosidase A, EC 3.2.1.22 (Morbus Fabry). Accumulation of toxic glucosylceramide in lysosomes of macrophages is observed in M. Gaucher patients (Cox et al., 2003; Cox et al., 2000; Pastores et al., 2004), which leads to hepatomegaly, splenomegaly, blood tissue functional disorders, hypermetabolism, skeletal pathology, growth retardation and/or pulmonary diseases.

M. Fabry is a glucosphingolipid metabolism disorder resulting in lysosomal accumulation of globotriaosyl ceramide. This causes chronic pain and vascular degeneration, renal failure, cardiac abnormalities like premature myocardial infarctions and strokes. The severity of the disease correlates with the residual amount of enzymatic activity (Fan et al., 1999). Early application of pharmacological chaperones for restoration of intracellular mutant enzymes was implemented for Fabry disease (Fan et al., 1999). Iminosugars also act as chaperones. According to Asano et al. (Asano et al., 2001b), 1-deoxynojirimycin (1-DNJ), a strong inhibitor of lysosomal α-galactosidase, can increase the activity of mutated α-galactosidase in Morbus Fabry lymphoblasts, acting as a chemical chaperone.

N-butyl-1-deoxynojirimycin (Miglustat, Zavesca™), a derivative of 1-DNJ and an inhibitor of ceramide glucosyltransferase (EC 2.4.1.80), the enzyme that produces glucosylceramide, was introduced as a means for therapy of Morbus Gaucher Type 1 (Cox et al., 2003; Cox et al., 2000; Platt et al., 1994). Incubation of fibroblast carrying the asparagine-to-serine mutation in position 370 (N370S) of glucocerebrosidase that is a cause of Morbus Gaucher with calystegines A_3, B_1, B_2, C_1 (and other inhibitors) led to increased enzyme activity (Chang et al., 2006). These results support the theory that calystegines can act as low molecular weight chaperones of enzyme actives centers (Ikeda et al., 2003).

Further applications of calystegine-containing plants are described in Chapter 1.3.2 Therapy of D. mellitus type 2.

1.2.   Digestion and resorption of carbohydrates in human GIT

1.2.1.   Enzymes of carbohydrate degradation: *α*- and *β*-glycosidases

The digestion of carbohydrates starts right after the ingestion. Food starch is degraded by amylases from saliva and later from the pancreas. The main part of this process, and the following resorption, take place in the small intestine by glycosidases. The specificity of cleavage of glycosidic bonds depends on the number and type of monosaccharide subunits and on the configuration of the hydroxyl groups in the substrate, as well as on the position of the cleavage site (Kimura et al., 2007; Park et al., 2008). The breakdown products, maltose, isomaltose and dextrins with chain lengths of 2 to 8 glucose units, are further cleaved into monomers by glucoamylase, maltase, and isomaltase. Sucrose, a major sweetener of human food, is an *α*-glycoside of fructose and cleaved by intestinal sucrase.

These four enzyme activities are structurally organised and localised in a heterodimeric complex of two multidomain proteins: maltase-glucoamylase (MGAM) and sucrase-isomaltase (SI) (Figure 3 (Sim et al., 2008)). They are tethered in the cell membrane of intestinal brush border cells with the enzymatically active domains in the intestinal lumen. MGAM and SI each contain two catalytic domains: an N-terminal domain proximal to the luminal wall and a C-terminal, distal domain. The domains are characterised by high amino acid sequence identities of 40% between the N- and C-terminal domains within MGAM as well as between those within SI, while the N-terminal domains of MGAM and SI share 60 % amino acid identity, as do the C-terminal domains (Nichols et al., 2003; Nichols et al., 1998).
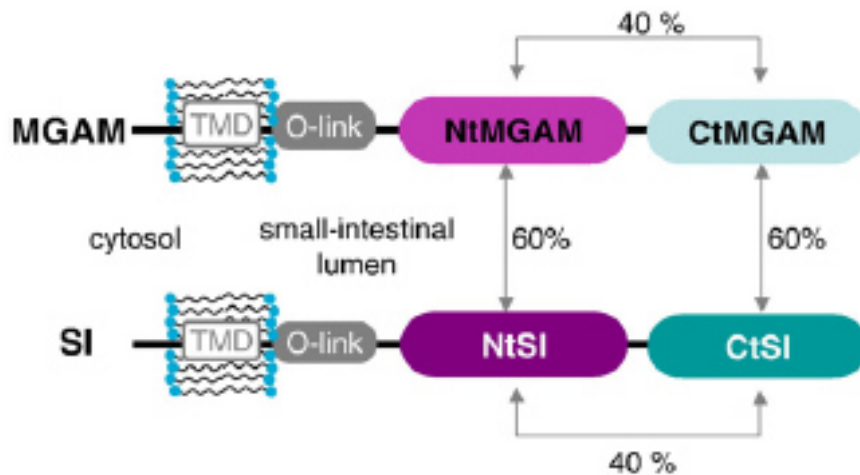
Figure 3: Linear schematic representation of the protein organisation of MGAM and SI

(Sim et al., 2008) Domains of the enzyme: cytosolic domain (small, ~26 residues), TMD (transmembrane domain, ~20 residues), *O*-link (*O*-glycosylated linker, ~55 residues), NtMGAM and CtMGAM, NtSI and CtSI (pair of two homologous catalytic domains each, ~900 residues per domain). Sequence identity between the catalytic subunits is indicated in percents.
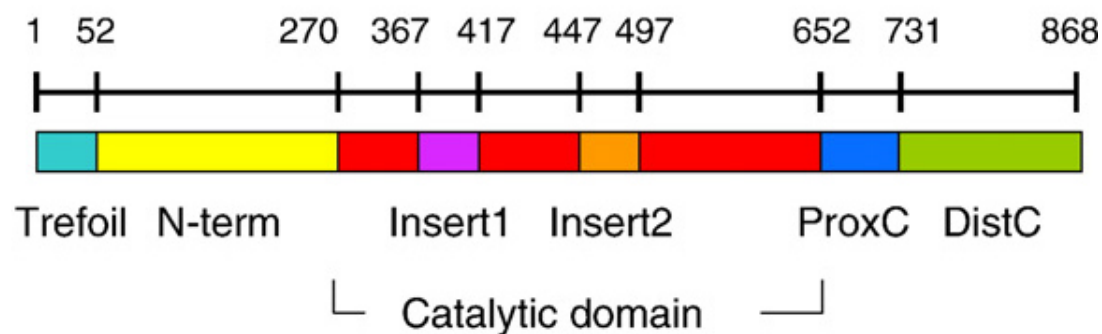
Figure 4: Linear schematic representation of the NtMGAM domain with amino acid boundaries

(Sim et al., 2008) Individual domains are coloured as follows: trefoil Type-P domain (cyan), N-terminal domain (yellow), catalytic (β/α)$_8$ domain (red), catalytic domain Insert 1 (purple), catalytic domain Insert 2 (orange), proximal C-terminal domain (ProxC) (blue), distal C-terminal domain (DistC) (green).

The two catalytic domains of MGAM, as well as those of SI, contain the conserved active site amino acid sequence WiDMNE ("i" stands for a variable residue), which is also characteristic of subgroup four of glycoside hydrolase family 31 (GH31) (Ernst et al., 2006). All four domains exhibit overlapping and complementary substrate specificity and show α-glycosidase activity. However, substrate preferences are somewhat variable between the domains. SI contributes almost all sucrase activity, all isomaltase activity, and 80% of the maltase activity. MGAM exercises all glucoamylase activity, 20% of the maltase activity and 1% of the

sucrase activity. Therefore total maltase activity can be ascribed to additive $\alpha(1-4)$ cleavage action of all four domains, whereas sucrase activity ($\alpha(1-2)$ glycosidic bond cleavage) is derived from the CtSI domain (Heymann and Günther, 1994; Semenza and Auricchio, 1989). Despite the overall similarity in amino acid sequence and atomic structure, different biochemical and structural properties of the enzymatic domains were also reported by Jones et al. (Jones et al., 2011).

Maltase (EC 3.2.1.20) and sucrase (EC 3.2.1.48) are major carbohydrate digesting α-glycosidases in the mammalian small intestine. They are grouped into GH31 based on their amino acid sequences (Henrissat and Davies, 1997). These enzymes are mucosal exoglycosidases acting at the nonreducing end of oligosaccharides. Maltase was considered the intestinal α-glycosidic enzyme with the highest glucogenic capacity (Heymann and Günther, 1994), which was later confirmed in an investigation carried out with human recombinant enzymes. Although theoretically representing a very potent enzyme according to the kinetic parameters (high V_{max},), maltase is held in a narrow operating range by the "substrate brake" (Quezada-Calvillo et al., 2008), which, combined with the quantitative molecular excess of sucrase, allows sucrase to be considered as the default α-glycosidase during carbohydrate-rich meals (Quezada-Calvillo et al., 2007). Recently, the N-terminal moieties of both proteins were crystallised after heterologous expression in insect cells (Sim et al., 2008; Sim et al., 2010), providing insights into substrate- and inhibitor-binding to these enzyme domains.

Reaction mechanism of α- and β-glycosidases

The mechanism of enzymatic hydrolysis of disaccharides comprises the formation of an oxycarbocation, cleavage of the glycosidic linkage, and charge neutralization by water. A carboxylic function at the enzyme active site stabilises the electron-deficient transition state (Cogoli and Semenza, 1975; Jensen et al., 1986). During catalysis, one carboxylic acid side chain attacks the anomeric centre as a catalytic nucleophile and the other acts as an acid catalyst weakening the C–O bond by protonation. The positioning of those two carboxylic acid side chains during catalysis differs between α- and β-glycosidase, Figure 5 (Heightman and Vasella, 1999).

Maltase and sucrase are retaining glycosidases (Henrissat and Davies, 1997) and their catalytic acid-base and nucleophile residues attack the glycosidic bond in a two-step mechanism. Each step inverts the configuration of the anomeric glycoside oxygen, which leads to an overall retention of the oxygen configuration (Vuong and Wilson, 2010).
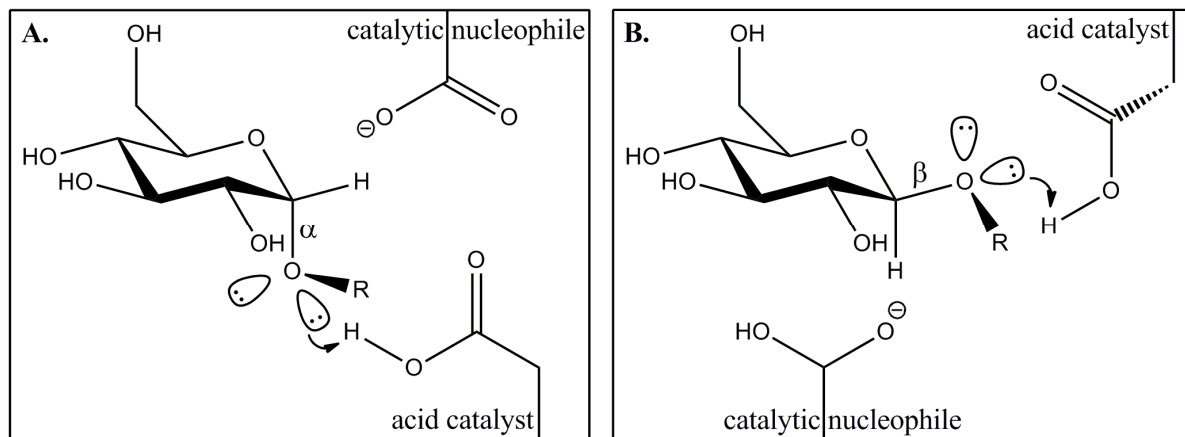
Figure 5: Positioning of the carboxylic acid side chains during catalysis of *α*- and *β*-glycosidase (Heightman and Vasella, 1999) A. interaction of the catalytic acid of *α*-glycosidases with an *α*-glycoside; B. *syn* protonation of a *β*-glycosidase

1.2.2. Caco-2 cells as model system for GIT resorption studies

Since maltase and sucrase reside at the human intestinal mucosa, Caco-2 cells were chosen for this investigation because of their similarity to human enterocytes regarding their morphology, their protein-related composition and functions (Chantret et al., 1988; Grasset et al., 1984; Meunier et al., 1995; Pinto et al., 1983; Zweibaum et al., 1984), and their protein activity (Hauri et al., 1985; Hidalgo et al., 1989; Rousset et al., 1989). Monolayers of Caco-2 cells are established as a culture model system of human intestinal cells for experiments on inhibition of *α*-glycosidase (Hansawasdi et al., 2001; Nishioka et al., 1998; Toda et al., 2000) and drug transport (Boulenc et al., 1993; Cogburn et al., 1991; Hilgers et al., 1990).

1.3. Carbohydrate metabolism disorders

1.3.1. Diabetes mellitus type 2

Diabetes mellitus type 2 is related to abnormal postprandial increase of the blood glucose level (hyperglycaemia), which in the long term provokes micro- and macrovascular damage, with detrimental coronary, optical, neuronal and renal alternations (Adler et al., 2003; Di Carli et al., 2003; Fowler, 2008; Stevens et al., 2001). Postprandial hyperglycaemia stimulates secretion of insulin by the *β* cells of the Langerhans' islets in the pancreas, depleting insulin reserves in the cells (Odaka et al., 1992). Insulin acts as the primary regulator of blood

glucose, but it also inhibits lipolysis in adipocytes, hepatocytes and muscle cells (Ludwig, 2002; Saltiel and Kahn, 2001). Hyperglycaemia in diabetes type 2 is additionally strengthened by elevated hepatic glucose output (Ferrannini et al., 1988; Firth et al., 1986; Mitrakou et al., 1990).

Diabetes mellitus type 2 appears in adults and shows a gradual onset, unlike autoimmunity-related diabetes mellitus type 1, which starts abruptly and affects predominantly children. Diabetes type 2 is rising worldwide, due to it correlation with adverse life styles, everyday habits and diet. Previous to full expression of the disease, a complex of signs points out a pre-diabetes status, which is designated as metabolic syndrome. The syndrome comprises high blood pressure, obesity and increased blood glucose levels after meals due to reduced insulin sensitivity of target tissues. Regular consumption of energetically rich meals with high glycemic effect leads to increasing insulin resistance and dysfunction of pancreatic β-cells, accompanying the metabolic syndrome (Eckel et al., 2005; Ludwig, 2002; Venn and Green, 2007). Patients with these signs should avoid consumption of food that leads to a sudden rise of glucose in the blood. Blood glucose can be controlled by a suitable alimentary selection and schedule, like carbohydrates that are slowly digested or have a low glycemic index. The glycemic index (GI) is a term developed by Jenkins and al. (Jenkins et al., 1981) and a relative measure of the postprandial glycaemia caused by carbohydrates in the diet. The GI is also a physiological indicator for carbohydrate-rich foods, describing their blood glucose raising capacity. Foods with GI >70 are classified as high GI, and when GI < 50, it is low (Ek et al., 2012; Jenkins et al., 1981). In order to reduce the risk of diabetes, low GI foodstuffs should preferably be consumed (Brand-Miller et al., 2009; Willett et al., 2002). Inhibition of carbohydrate degradation and absorption in the small intestine is another option for reducing the postprandial hyperglycaemia: α-glycosidase inhibitors are applied as anti-diabetic agents clinically (Goto et al., 1995; Miura et al., 1998; Odaka et al., 1992).

1.3.2. Therapy of D. mellitus type 2

Insulin treatment

Human insulin is produced by recombinant DNA technology. It is usually applied subcutaneously. According to the duration of action, insulin formulations are classified as fast and short acting, intermediate acting and long acting. The pharmacological effect and kinetics depend on solubility (solution or suspension, precipitated with protamine or zinc),

formulation complexity (single insulin or different activity insulin mixture) or alignment of certain amino acids.

Oral hypoglycaemic agents

Oral antidiabetic medicines comprise have different mechanisms of actions and are classified according to their chemical structures.

Biguanides act as insulin sensitizers. They increase glucose uptake and consumption in peripheral organs and also reduce hepatic gluconeogenesis and intestinal glucose absorption. Metformin is the main representative of this group. It does not stimulate appetite, which may lead to gain of body weight.

Thiazolidinediones ("glitazones") are peroxisome proliferator-activated receptor agonists. Glitazones lower blood glucose by increasing insulin sensitivity in organs and tissues, i.e. they act as insulin sensitizers.

Sulfonylureas act as insulin secretagogues, stimulating insulin secretion. An unfavourable side effect directly concerning the therapy is the tendency to provoke hypoglycaemia as a result of stimulation of appetite.

Meglitinides ("glinides") are another class of insulin secretagogues. Like sulfonylureas, they also exhibit their effect only if the β-cells of the pancreas are functional. The risk of hypoglycaemia is lower in their case.

- Therapy of D. mellitus type 2 by α-glycosidase inhibitors (synthetic and natural)

Herbal medicines have been used in folk medicine for diabetes prevention or treatment around the world, including traditional Chinese medicine (Asano et al., 2001a), ayurvedic medicine (Bhandari et al., 2008; Grover et al., 2002) and among the native population in South America (Ranilla et al., 2010). In traditional Chinese medicine, the extract from mulberry leaves is used orally for prevention and treatment of diabetes. Mulberry extract contains glycosidase inhibitors and lowers postprandial blood glucose (Miyahara et al., 2004). Oriental medicine prescribes root bark of mulberry trees for antiinflammatory, antipyretic and antitussive action and against diuretic complications whereas mulberry fruits are used as a sedative and tonic (Asano et al., 2001a). Mulberry leaves have been used traditionally in Chinese medicine to prevent and cure diabetes ("Xiao-ke") (Chen et al., 1995). Significant antihyperglycaemic effects of extracts of mulberry leaves as well of mulberry root bark were observed in both normal and hyperglycemic induced mice (Hikino et al., 1985; Kimura, 1995).

1-deoxynojirimycin (1-DNJ, Figure 6), originally named moranoline after the mulberry tree, is a piperidine alkaloid isolated from mulberry root bark (Yagi et al., 1976). It was designated as a strong antidiabetic agent for its considerable suppression of postprandial hyperglycaemia in rats and potent inhibition of α-glycosidase (Yoshikuni, 1988). Suppression of postprandial blood glucose elevation and insulin secretion by DNJ was observed in humans as well. Advantageously, long-term application of DNJ did not provoke hypoglycaemia (Kimura et al., 2007). Besides 1-DNJ, other azasugars were found in mulberry material (Asano et al., 1994b; Asano et al., 1994c), some of which were proven to be strong inhibitors of mammalian α-glycosidase (Asano et al., 1995b; Asano et al., 1994a).

Ayurvedic traditional Indian medicine uses water extracts of stems and roots of *Salacia reticulata* WIGHT for treatment of diabetes mellitus type 2. Salacinol and kotalanol (Figure 6) were identified as the active components of this plant (Yoshikawa et al., 1998; Yoshikawa et al., 1997). Clinical trials applying water extracts of *S. reticulata* on human patients with type 2 diabetes mellitus confirmed antidiabetic functionality of this plant through effective glycemic control and good tolerance (Jayawardena et al., 2005).

Further treatments from traditional folk medicine for prevention of the onset of diabetes or obesity by application of herbal medicines or dietary supplements derived from herbal sources remain to be discovered (Asano et al., 2001a).

Natural glycosidase inhibitors were reviewed and compared to compounds of the same effect already in therapeutic use against diabetes type 2 (Asano, 2009; Kawanishi and Farnsworth, 2000). Calystegines were also regarded as natural glycosidase inhibitors and were among those reviewed (Kawanishi and Farnsworth, 2000).

Various inhibitors against glycosidases have been isolated and structurally elucidated, which raised interest in their further investigation as subjects of application on different issues in biochemical areas and enzymology (Asano et al., 1994c). Alkaloidal glycosidase inhibitors isolated from natural sources have been classified into five major structural types: polyhydroxylated piperidines, pyrrolidines, pyrrolines, indolizidines, and pyrrolizidines. Figure 6 demonstrates some of the representatives of these compound groups.

Administration of glycosidase inhibitors leads to lowered postprandial blood glucose levels (Ratner, 2001). Inhibition of α-glycosidases has become an important option for the treatment of diabetes, since the activity of these enzymes is rate-limiting for carbohydrate digestion (Quezada-Calvillo et al., 2007). The activity of maltase and sucrase has been a focus of researchers working on treatment of diabetes type 2.

IMINOSUGARS (arch. AZASUGARS)

Pyrrolidines

DMDP*

Pyrrolizidines

australine

casuarine

Piperidines

compound	R_1	R_2	R_N
fagomine	-H	-H	-H
1-DNJ**	-H	-OH	-H
nojirimycin	-OH	-OH	-H
miglitol	-H	-OH	$-C_2H_5OH$

Indolizidines

castanospermine*

swainsonine

THIOSUGARS

compound	R
salacinol	-H
kotalanol	$-CH(OH)CH(OH)CH_2OH$

Tetrahydrothiophene sulfonium ion

CARBAGLYCOSYLAMINES (PSEUDOAMINOSUGARS)

valienamine unit

acarviosione unit

maltose

$(\alpha\ 1{\rightarrow}4)$

acarbose

Figure 6: Naturally occurring glycosidase inhibitors

Pyrrolizidine derivative = fusion of two pyrrolidine rings;
DMDP* = 2,5-dihydroxymethyl-3,4-dihydroxypyrrolidine; 1-DNJ** = 1-deoxynojirimycin

It was presumed that the inhibition of these enzymes would attenuate the postprandial blood glucose rise, which is one of the main problems that the patients suffering from this disease have to deal with (Puls et al., 1977). One of the active agents discovered was the pseudotetrasaccharide acarbose (Figure 6) (Bischoff, 1994). While its structure resembles oligosaccharide molecules that are generated during the digestion of starch in small intestine, it is the acarviosine unit that is responsible for the α-glycosidase inhibitory effect. The unsaturated double bond of valienamine is similar to the glucose transition state during cleavage of the glycoside bond, and the positively charged imine nitrogen atom occupies the position of the carboxyl group of the catalytic nucleophile (Krasikov et al., 2001). It is also reported that not all the enzyme active sites posses the same susceptibility for acarbose, due to different enzyme production and inhibition assay methods (Breitmeier et al., 1997; Quezada-Calvillo et al., 2008; Sim et al., 2008; Sim et al., 2010). Miglitol (Figure 6) is another inhibitor of maltase-glucoamylase and sucrase-isomaltase that also diminishes absorption of carbohydrates and ameliorates blood glucose peaks.

1.4.   Aims and questions

Calystegines are present in human nutrition. The central question therefore was whether calystegines in the diet have dietary effects on humans.

- The first goal was to provide sufficient amounts of calystegines with satisfying purity for the later investigations. Potato sprouts were chosen as extraction material since they are known to be a rich source of calystegines and are easily available. Another objective was to perform the purification in a concise and practical way. Because of the structural resemblance, separation of calystegines on the ion exchange columns demands long purification time and repetition of purification steps. There are no precise protocols up to now considering the material amount, and exact type, order and length of purification steps for calystegine isolation. A new approach was attempted within the already established ion exchange chromatography of calystegines in order to achieve a feasible and abridged scheme for calystegine separation.

- Besides the established GC method for analysis and determination of calystegines, a new method was tested for reliable calystegines quantitation. Calystegines are easily

protonated in solutions with a pH lower than the corresponding calystegine pK_a. Attempts to separate and quantify calystegines as cations using capillary zonal electrophoresis (CZE) found limited application up to now, mostly due to complicated derivatisation procedures (Daali et al., 2000) or the necessity for frequent recalibration (Rüttinger and Dräger, 2001). A new approach, using CZE and capillary isotachophoresis (cITP), appeared attractive as an alternative to the robust but tedious GC analysis of calystegines.

Calystegines are inhibitors of plant and animal glycosidases. The inhibiting effect of calystegines would enable delayed uptake of monosaccharides and a smaller rise of blood glucose after a meal.

- The structure of calystegines resembles other polyhydroxy alkaloids that act as inhibitors of plant and animal glycosidases. Some of these alkaloids were proved to be toxic. Assessment of the potential toxic effect of calystegines was necessary. As possible resorption in the intestine was also to be investigated, transepithelial transport tests with Caco-2 cells as transport model were to be performed.

- Harmfulness of the calystegine solutions, applied in the concentrations for the transepithelial test, to Caco-2 cell monolayer had to be examined, and monolayer integrity tests had to be performed.

- The main objective of this study was to assess the potential effects of calystegines present in food on the digestion of carbohydrates.

  Docking studies were to be performed for a preliminary evaluation of the interaction between calystegines and the enzymatic active centres of α-glycosidases, for which crystal structure models are available.

  The effect of calystegines isolated from potato on human α-glycosidases was to be tested, since enzyme sensitivity towards inhibitors tested *in vitro* varies substantially, depending on the source of the enzyme and on the way of preparation. Caco-2 cells were used as the source of the proteins, as it is known that maltase and sucrase are the most active disaccharidases in the small intestine.

  The extent of the glycosidase inhibition was to be described in terms of kinetic parameters of the enzymes and inhibitor-enzyme dissociation constants.

2. Material and methods

2.1.   Material

2.1.1.   Plant material − potatoes

Purification of calystegines

Potato tubers (total 30 kg) of cultivar Rosara (late harvest − late August, early September) were supplied by "Gemüsekiste" (Halle-Diemitz, Germany) and kept in a cold room (in the dark at 5 °C (±1)) for 4 months for dormancy. The tubers were subsequently laid out at room temperature in the dark and occasionally sprinkled with water to maintain moisture. Sprouting started after 4 weeks and sprouts of ca. 1.0−1.5 cm were collected every 7 days over a period of 2 months. After every harvest, the sprouts were stored at −20 °C. The total yield of sprouts was 548.6 g of fresh weight.

Before extraction, sprouts were pooled, homogenised, split into 5 approximately equal aliquots and lyophilised.

Table 1: Potato sprouts (cultivar Rosara) harvested for extraction and separation of calystegines

harvest No.	1	2	3	4	5	6	7	8	9	10	11
days old [*]	28	31	38	45	52	59	66	73	80	87	94
f.w. yield [g]	66.3	24.3	94.6	114.1	90.5	72.6	41.8	25.8	11.4	5.7	1.6
f.w./(total f.w.) [%]	12.1	4.4	17.2	20.8	16.5	13.2	7.6	4.7	2.1	1.0	0.3

[*] days after the transfer to room temperature

Analysis of calystegines by CZE, cITP and GC

Samples of potatoes (Table 2 , Table 3 and Table 4) were obtained from the Potato Research Institute at Havlíčkův Brod (Czech Republic), unless stated otherwise.

Table 2: Potato material[*] used for comparison of cITP with CZE

source	Stachy[**]	Valečov[**]	Přerov[**]	Suchdol[**]
cultivar	Ditta	Ditta	Ditta	Ditta
	Impala	−	Impala	Impala
	Karin	Karin	Karin	Karin
	Saturna	Saturna	Saturna	Saturna

[*]samples taken from whole fresh potato tubers; [**] location of origin of tubers

Table 3: Potato material used for comparison of CZE with GC

cultivar designation	material designation
Ditta	whole potato (flesh and skin) flesh skin (potato material lyophilised)
Granola	
Karin	
Magda	
Samanta	

Table 4: Potato material* used for comparison of cITP with GC

cultivar designation	material designation
Agria	whole potato (flesh and skin)
British Columbia Blue	flesh whole potato (flesh and skin) sprouts
potato cultivar (source Čepl)	sprouts, batch 1 and batch 2
commercially purchased potatoes	sprouts, batch 1a and batch 1b sprouts, batch 2a and batch 2b
Desirée	sprouts, a sprouts, b

* potato material lyophilised;
  "a" and "b" designation of batches: extraction procedure repetitions

2.1.2. Cell culture (Caco-2 cells)

The Caco-2 cell line was obtained from the German Collection of Microorganisms and Cell Cultures (Braunschweig, Germany).

2.1.3. Media, buffers and standard solutions for cytological methods

Table 5: Composition of the cell growth medium for Caco-2 cells (cell cultivation)

Cell growth medium:
- Minimum Essential Medium Eagle (MEM) with Earle's salts and L-glutamine, with addition of:
- foetal bovine serum (10%)
- MEM-non essential amino acids (1%)
- gentamicin (50 µg/mL)

Table 6: Composition of Dulbecco's PBS for Caco-2 cells (cell subcultivation)

Dulbecco's PBS (pH=7.0−7.5)

(phosphate buffered saline without Ca^{2+} and Mg^{2+}):

- 137 mM NaCl
- 2.7 mM KCl
- 1.5 mM Na_2HPO_4
- 8.1 mM KH_2PO_4

Table 7: Composition of trypsinisation solution for Caco-2 cells (cell subcultivation)

Trypsin EDTA solution:

- 0.05% trypsin
- 0.022% EDTA (Titriplex III)
- in PBS (without Ca^{2+} and Mg^{2+})

Table 8: Composition of flux assay buffer for transepithelial flux measurements

Flux assay buffer (FAB) Transwell® compartment components	pH 6.0 donor [mM]	pH 7.5 acceptor [mM]
NaCl	140	140
KCl	5.4	5.4
$CaCl_2$	1.8	1.8
$MgSO_4$	0.8	0.8
glucose	5	5
MES	25	−
HEPES	−	25
Tris	to set pH value	

[^{14}C] D-mannitol solution (Moravek Biochemicals, Brea, USA): specific activity = 53 mCi/mmol, radioactive concentration = 250 µCi/2.5 mL, concentration = 1.89 mM in original solution.

Scintillation cocktail: ROTISZINT® ECO PLUS, LSC-universal cocktail (Carl Roth GmbH + Co. KG, Karlsruhe, Germany).

2.1.4.   Buffers, standards and stock solutions for enzymatic calystegine determination (*β*-glycosidase assay)

Phosphate buffer solution pH 5 (PB5) − modified phosphate buffer according to Sörensen: Aqueous 1M stock solutions of KH_2PO_4 and Na_2HPO_4 were prepared, divided into aliquots and kept frozen at −20 °C. For assays, aliquots of both stock solutions were thawed and diluted with Aq. bidest. to 150 mM. Buffer PB5 was produced by adding 150 mM Na_2HPO_4 to 150 mM KH_2PO_4 until the pH reached 5.0.

150 mM PB5 was used as a solvent for the enzymatic reaction, since it has been proven to be capable of buffering the flux test buffers (FAB6 of donor and FAB7.5 of acceptor compartment, Table 8) that were eventually to be added for the calystegine quantitation. The buffering capacity of 150 mM PB5 is shown in Table 9.

Table 9: Buffering capacity of 150 mM PB5 with Transwell® compartment buffers FAB6 and 7.5 for the flux test

150 mM PB5 [mL]	FAB6 [mL]	FAB7.5 [mL]	reaction mix. [mL]	pH value
2.25	–	–	2.25	5.00
1.50	0.75	–	2.25	5.35
1.50	–	0.75	2.25	5.54
–	+	–	FAB6	6.00
–	–	+	FAB7.5	7.50

Volumes are 30 times larger than in the enzyme assay; ratios of components are the same: 2/3 PB5 (substrate and enzyme) and 1/3 flux sample (FAB6 or 7.5)

Reaction product standard series: 25 mL of a 10 mM *p*-nitrophenol (*p*-NP) stock solution (in PB5) was produced. A standard concentration series ranging from 0.01−0.3 mM was produced by diluting the *p*-NP stock solution with PB5 (Table 10).

Substrate solution: 50 mL of a 50 mM *p*-nitrophenyl-*β*-D-glucopyranoside (*p*-NPG) stock solution was prepared in 150 mM PB5. A concentration series of the substrate solution was produced by diluting the stock solution with PB5 in the range of 0.45−45 mM (Table 11). Substrate solutions were produced fresh dayly and kept in an ice bath while under ultra sound treatment. Particular attention was paid to the colour of the solution: yellowish colour indicates substrate decomposition, setting *p*-NP free in the solution.

Table 10: *p*-nitrophenol dilution series (standard substance)

stock sol. volume [µL]	dilutions (10 mL[*])	
	dilution No.	concentration [mM]
10	1	0.01
20	2	0.02
30	3	0.03
50	4	0.05
100	5	0.10
150	6	0.15
200	7	0.20
250	8	0.25
300	9	0.30

[*] Dilutions were filled up with 150 mM PB5 to 10 mL in volumetric flasks

Table 11: *p*-nitrophenyl *β*-D-glucopyranoside dilution series (substrate)

stock sol. volume [mL]	dilutions (10 mL[*])	
	dilution No.	concentration [mM]
0.09	1	0.45
0.3	2	1.5
0.6	3	3
1.2	4	6
1.8	5	9
2.4	6	12
3.0	7	15
4.2	8	21
5.4	9	27
9.0	10	45

[*] Dilutions were filled up with 150 mM PB5 to 10 mL in volumetric flasks

Enzyme solution: The stock solution of sweet almond *β*-D-glycosidase (EC 3.2.1.21) was 0.2 mg/mL in PB5. It was kept on ice during the assay and was diluted 20-fold with PB5 to 0.01 mg/mL for each measurement.

Stop solution: A 1M solution of sodium carbonate in Aq. bidest.

Calystegine solutions: Stock solutions of 5 mM each of calystegines A_3 and B_2 were made of purified calystegine pools obtained from sprouts of potato cultivar Rosara (see Chapter 2.2.1 for separation details and Chapter 3.1.1 for calystegine pool content and purity). The stock solutions were diluted to produce concentration series of 0.5, 2.5, 5, 25 and 50 µM (Table 12). Calystegines were dissolved in PB5 for measuring the kinetic parameters and K_i values. They were also dissolved in flux test buffers pH 6.0 and 7.5 each, in order to generate the calibration curves for calystegine determination in the transepithelial transport tests and in the calystegine flux calculations. Each concentration series was produced by diluting the stock solutions with the appropriate buffers.

Table 12: Dilutions for calystegine A$_3$ and B$_2$ concentration series

stock solution	dilutions (10 mL[*])	
V	dilution No.	concentration
[µL]		[mM]
1	1	0.0005
5	2	0.0025
10	3	0.005
50	4	0.025
100	5	0.05

[*] Dilutions were filled up to 10 mL in volumetric flasks. Diluent was either FAB6, FAB7.5 or PB5 (see Chapters 2.1.3 and 2.1.4 for buffer composition)

2.1.5. Buffer and stock solutions for determination of calystegine inhibitory activity by the human intestinal disaccharidase activity assay

Substrates: 10 mL stock solutions of 1575 mM of assay substrates (disaccharides: maltose and sucrose) were produced in Aq. bidest, of which dilution series with final concentrations of 10.5, 105, 525, 1050 and 1575 mM were made.

Calystegine solutions: Aqueous solutions of 2.5 and 5 mM each of calystegines A$_3$ and B$_2$ were produced from corresponding calystegine pools, which were obtained following the procedure described in Chapter 2.2.1. An aqueous solution of acarbose of 52.5 µM was produced to serve as inhibition control. Lyophilised calystegine pool samples and acarbose were dissolved separately in double distilled water.

Phosphate buffer solution pH 6 (PB6) − modified phosphate buffer according to Sörensen: Aqueous 1M stock solutions of both KH_2PO_4 and Na_2HPO_4 were prepared, divided in aliquots and kept frozen at −20 °C. For the assay, aliquots were thawed and diluted with Aq. bidest. to 20 mM and PB6 was produced by adjusting the pH value of 20 mM KH_2PO_4 to pH = 6 with 20 mM Na_2HPO_4.

2.1.6. Buffers for capillary zone electrophoresis (CZE) and capillary isotachophoresis (cITP)

For reasons of conciseness, buffer composition is described in Chapter 2.2.5.with explanation of the measurement methods.

2.1.7. Chemicals and standards

Cell culture reagents were purchased from PAA Laboratories GmbH (Cölbe, Germany), except for foetal bovine serum (Biochrom, Berlin, Germany).

[^{14}C] D-mannitol solution (1.89 mM, specific radioactivity 53 mCi/mmol, radioactive concentration 100 µCi/mL) was obtained from Moravek Biochemicals (Brea, USA).

Materials and reagents for calystegine purification and derivatisation were obtained from Merck (Darmstadt, Germany), except for silylation reagents, which were purchesed from AppliChem (Darmstadt, Germany).

Calystegine standards were kindly provided by Dr. Naoki Asano (Hokuriku University, Kanazawa, Japan). Purity of these standards was assessed by GC.

Sweet almond β-D-glycosidase (EC 3.2.1.21, 7.0 units/mg solid, 7.0 units/mg protein (Biuret)) was purchased from Sigma-Aldrich, (St. Louis, MO, USA), and p-nitrophenyl β-D-glycoside from Diagonal (Münster, Germany). Acarbose was acquired from Bayer (Leverkusen, Germany).

Bidistilled water (TKA GenPure water purification unit, Niederelbert, Germany) was used for preparation of all solutions and buffers, except for those for CZE and cITP (see under 2.2.5).

For measurements by CZE and cITP, calystegine B$_2$ (purity $\geq 98\%$) was purchased from GeneTiCa Ltd. (Prague, Czech Republic) as an additional standard. L-Histidine, acetic acid, methanol, and ammonium hydroxide were purchased from Lachema (Brno, Czech Republic). BES, TBA and HEC were obtained from Sigma-Aldrich (Prague, Czech Republic). Other substances were purchased from Merck (Darmstadt, Germany), Roth (Karlsruhe, Germany), Sigma (Taufkirchen, Germany) or VEB Laborchemie (Apolda, Germany). All substances were of analytical grade "p.a.".

2.2. Methods

2.2.1. Extraction, purification, separation and derivatisation of calystegines

Extraction of calystegines

Isolation of calystegines − For extraction, potato sprouts (Table 1) were mixed, divided into 5 aliquots, and subsequently lyophilised (lyophilisator: Christ® GAMMA 1-20, Osterode, Germany). Dry sprouts were weighed and ground to a fine powder in an electrical mill (WARING, Waring Products Division, New Hartford, CT, USA). The ground material, divided in 2 aliquots, was extracted with 50% methanol (methanol:Aq. bidest = 1:1) in a ratio of 1:20 (g:mL) in an ultrasonic bath (Sonorex RK 100, Bandelin Electronic, Berlin, Germany) for 30 min. The supernatant was decanted, and the same extraction procedure was repeated with material leftovers.

After the second extraction step, the supernatants were combined, centrifuged for 20 min at 9000 rpm (temperature 7 °C) (Sorvall® RC-5B Superspeed, Du Pont Instruments, Newtown, CT, USA; rotor type GS-3), and vacuum-filtrated through narrow-pored filter paper (Filtrak, Bärenstein, Germany). A total volume of 4.6 L of 50% MeOH was applied for the complete extraction of all sprout material.

The volume of the raw extract was reduced under vacuum using a rotary evaporator (Büchi R-10, Glasapparatefabrik, Flawil, Switzerland)) at ca. 60 °C until all methanol was eliminated and the extract eventually became viscous. The extract was then liquefied with Aq. bidest. by washing the rotary evaporator balloon and transferred into centrifuge bottles. It was subsequently centrifuged for 20 min, at 15000 rpm (temperature 5 °C) (Sorvall® RC-5B Superspeed, rotor type SS-45). The supernatant was vacuum filtered using narrow-pored filter paper. The aqueous raw extract was filled up with Aq. bidest. in a 1000 mL volumetric flask.

Five aliquots of 10 mL each (corresponding to 1% (1.14 g) of the total sprout dry weight each) were lyophilised to determine the dry weight of the raw aqueous potato sprout extract. These samples were added to the bulk of the raw extract again before the purification.

Preparation of potato material for comparison of GC with CZE/cITP analysis − The potato material described in Tables 2, 3 and 4 was extracted essentially as described for calystegine extraction, except that for fresh material, a ratio of material:50% MeOH of 1:4 was used, taking into consideration a fresh weight:dry weight ratio of approximately five. For each sample group, the state of the potato material (fresh or lyophilised) is indicated in the presentation of the results.

For CZE analysis, fresh potato samples of 50 g were vortexed in 200 mL of 50% methanol for 2 min. The extracts were filtered through 0.2 µm nylon filters, diluted if necessary and

analysed. Lyophilised potato samples (2 g dry sprouts in 50 mL of 50% methanol) were extracted in the ultrasonic bath for 30 min and, after filtration and/or dilution, directly analysed by CZE. For cITP analysis, sample treatment was the same as for CZE, except that the filtrate was diluted five-fold with water prior to analysis (injection volume was 10 µL)

Purification of calystegines (step 1): strongly acidic cation exchanger

Raw aqueous potato sprout extract was applied onto a column packed with a strongly acidic cation exchanger (Ion exchanger I, Merck, Germany) (Table 13). The column was regenerated with 2M HCl to saturate the matrix with H^+ counter ions and washed with Aq. bidest. until the pH was neutral. Neutral and acid constituents of the raw potato sprout extract flowed through the column during application of the extract (fraction "flow through 1") and washing the column with Aq. bidest. (fraction "flow through 2") until the pH was neutral again. These fractions together were designated as the flush. It was discarded, although a general check for calystegines was also performed in order to exclude the possibility of insufficient ion exchange capacity or too high elution speed (GC analysis and comparison between raw extract flow through 1 and Merck I extract, see Chapter 3.1.1, Figure 10).

During the ion exchange process, calystegines and other positively charged constituents of the extract are bound onto the matrix surface, replacing H^+ ions as counter ions to the fixed, negativly charged exchanger surface. The result of the ion exchange is an acidic pH of the flush fraction. As long as the eluate pH remains acidic during sample aplication and column washing, it indicates that ion exchange is taking place and that the ion exchmange capacity of the column has not been exceeded.

Calystegines were eluted with 2M NH_3 until the pH of the eluate became strongly basic. The column was then eluted with five column volumes Aq. bidest.. The ammonia and Aq. bidest. eluates were combined and the volume was reduced under vacuum at 60 °C until the ammonia was eliminated. This reduced eluate was designated as extract "M1". It was transferred into a volumetric flask of 50 mL and filled up quantitatively with Aq. bidest. Four aliquots of 2 mL each (corresponding to 4%, i.e. 4.56 g of the total sprout dry weight each) were taken for determination of the extract dry weight by lyophilisation. Those samples were added to the bulk of the M1 extract again before the following purification step.

Potato material purification for comparison of GC vs. CZE/cITP – Purification of potato extract for comparison of analysis by GC and by CZE/cITP was done as described above. The differences in the purification specifications are as indicated below.

Potato material shown in Table 3: 0.5 g dry weight material prepared crude extract was purified on 1 mL Merck I. The column was cleansed with Aq. bidest. until sample wash out was pH neutral. Calystegines were eluted with 3 mL of 2M NH_3. The pH of the eluate was strongly basic. The column was thereafter eluted with 10 mL Aq. bidest.

Potato sprouts of the cultivars shown in Table 4 were prepared for analysis: extracts from 1 g dry weight sprouts were purified on 2 mL Merck I column. The columns were cleansed with Aq. bidest. until sample wash out was pH neutral. Calystegines were eluted with 6 mL 2M NH_3 until the eluate pH became strongly basic. The column was further eluted with 20 mL Aq. bidest. Ammoniac and Aq. bidest. eluates were joined for further sample analysis.

Purification of calystegines (step 2): strongly basic anion exchanger

Extract M1 was applied onto a column packed with a strongly basic anion exchanger (Ion exchanger III, Merck, Germany) (Table 13). The column was regenerated with 2M NaOH to saturate the matrix with OH^- counter ions and then washed with Aq. bidest. until the pH became neutral. During sample loading, the OH^- ions were substituted with negatively charged and polar molecules from the extract. Calystegines flew through the column and were collected immediately, together with five to seven column volumes of Aq. bidest. eluate. They were combined together and this eluate was named "M3" extract. The volume of the extract was reduced under vacuum at 60 °C and then filled up to exactly 100 mL with Aq. bidest. in a volumetric flask. Complete extract was lyophilised in order to determine M3 extract weight. The lyophilised extract was stored at −20 °C before the following purification step.

Separation of calystegines (step 3): weakly acidic cation exchanger

Finally, a weakly acidic cation exchanger (Ion exchanger IV, Merck, Germany) (Table 13) was used for separation of the calystegines. The column was regenerated with 2M NH_3 to be completely saturated with NH_4^+ counter ions, during which, due to particles swelling, bed volume increased 1.5 to 1.7-fold. Then the column was rinsed with Aq. bidest. until the pH of the flow through was neutral. The volume of Aq. bidest. necessary for washing reached between 100 and 200 times the regenerated bed volume, which resulted in prolonged preparation times for separations.

Lyophilised frozen extract M3 was thawed and dissolved in 25 mL Aq. bidest. for calystegine separation. It was applied onto the column and eluted with Aq. bidest. that was applied to the column using a peristaltic pump (Pump P-1, Pharmacia Biotech, Upsala, Sweden), while the

fractions were collected using an automatic fraction collector (CYGNET™ fraction collector, ISCO, Columbus, OH, USA). Fractionation was performed during daytime over a period of 10 days. For storage overnight, the column was secured and kept in the cold room at 5 °C. Before elution was continued, the column was tempered to room temperature. Finally, elution with 2M NH_3 was performed in order to wash down the eventually remaining calystegines. Calystegine fractionation was continually monitored by GC during the separation process. Fractions were pooled according to the obtained calystegine elution flow profile. Flow lines were constructed by measuring calystegines in collected fractions, expressed as flame ionisation detector (FID) signal values (pA×s). In order to increase pool purity, pool limits were not set at the signal interceptions of different calystegines, but at the points at which elution of the succeeding calystegine was noticed.

The fractions containing the major potato sprout calystegines (cal. A_3, B_2 and B_4) were pooled separately. Pool volumes were reduced under vacuum and then filled up to 50 mL with Aq. bidest. in volumetric flasks. From each single calystegine pool 4 aliquots of 10 mL each were lyophilised to determine the pool dry weights.

Mixed calystegine pools, containing the fraction in which elution profiles of neighbouring individual calystegines overlap, were also reduced under vacuum and filled up to 10 mL in volumetric flasks, but dry weights were not determined.

The calystegine content of every single pool was measured by GC, as well as purity, that was calculated as the percentage of every calystegine FID signal related to the sum of all the visible signals in FID chromatogram, excluding impurity peaks derived from silylation mixture components, internal standard and solvents.

For more detailed information concerning extraction, purification and separation procedures, column proportions and dynamic characteristics, refer to Table 13, Table 14.

Table 13: Ion exchange material used for calystegine purification and separation

Designation	Ion exchanger I	Ion exchanger III	Ion exchanger IV
Ion exchanger type	strongly acidic cation	strongly basic anion	weakly acidic cation
Ion form (counter ion)	H^+	OH^-	$H^{+\ *}$
Fixed ion functional type	$-SO_3^-$	$-N^+(CH_3)_3$	$-COO^-$
Ion exchange capacity	1.7 mmol/mL	0.9 mmol/mL	3.2 mmol/mL
Particle size (average)	0.3–1.2 mm	n.s.	n.s.
Purification step number	1	2	3
Process type	step 1: purification	step 2: purification	step 3: separation
Abbreviation (column, extract)	M1	M3	M4
Regeneration liquid	2M HCl	2M NaOH	2M NH_3
Elution liquid	2M NH_3	Aq. bidest.	Aq. bidest.

n.s. = not stated; producer: Merck (Darmstadt, Germany);
* for calystegine separation/fractionation used: NH_4^+ form (regenerated with 2M NH_3);
ion exchanger matrix composition: cross linked polymer (PS-DVB = polystyrene-divinylbenzene resin)

POTATO SPROUTS

PREPARATION & EXTRACTION of material:
→ fresh sprouts lyophilised, ground to fine powder;
→ extraction with 50% MeOH, (MeOH: Aq. bidest.=1:1);
→ sprouts dry weight:V(50% MeOH), [g:mL]=1:20;
→ methanol eliminated by volume reduction under vacuum

RAW EXTRACT (AQUEOUS)

PURIFICATION STEP #1:
purified over Merck I column, H^+ form (regenerated with 2N HCl)
→ neutral and negative charged compounds in flush fraction;
→ calystegines and dipole charged compounds bound onto the column;
→ calystegines eluted with $2N$ NH_3

M1 EXTRACT

PURIFICATION STEP #2:
purified over Merck III column, OH^- form (regenerated with 2N NaOH)
→ negative and dipole charged compounds bound onto the column,
→ calystegines eluted with water

M3 EXTRACT

PURIFICATION STEP #3 ⇔ SEPARATION OF CALYSTEGINES:
fractionated over Merck IV column, NH_4^+ form (regenerated with $2N$ NH_3)
→ calystegines eluted with water, fractions eventually pooled according to the calystegine content

M4: cal. B_2 pool   **M4: cal. B_4 pool**   **M4: cal. A_3 pool**

Scheme 1: Summary of steps for extraction and purification of calystegines

Calystegines arranged according the order of elution (left to right); on the left are represented the different extraction/purification/separation steps; on the right short description of the processes.

Table 14: Purification and separation of calystegines: dynamic parameters and characteristics of the columns

Column		PURIFICATION		SEPARATION	
		step 1 Merck I	step 2 Merck III	step 3 Merck IV, H$^+$	Merck IV, NH$_4^+$
	V(ion exch.) [mL]	120	60	50	68
	column dimens. (h × w), [cm]	19 × 2.8	21 × 1.9	22 × 1.7	30 × 1.7
	column dimens. ratio (h : w)	6.8	11.1	13	17.6
	ratio (sprouts d.w. : V(ion exch.), [g : mL]	0.9	1.9	2.3	1.7
	v(elu.) [mL/min]	2	2	2	2
	v(elu.) [V(col.)/h]	1	2	1.7	2.3
	dead vol. [mL]	~ 47	~ 30	–	42 (first 3 fract. 14 mL each)
regeneration		2M HCl, until pH = 1	2M NaOH, until pH = 12	2M NH$_3$, until pH = 12	–
		Aq. bidest. until pH ≈ 7	Aq. bidest. until pH ≈ 7	Aq. bidest. until pH ≈ 7	–
sample application		1060 mL raw aq. extract	50 mL extr. (Merck I purif., vol. reduced under vacuum)		25 mL extr. (Merck III purif., vol. reduced under vacuum)
sample wash	sample wash (column flushing) (Aq.bidest), [mL]	1000	–		cal. elution (fractionation): 11371
	ratio V(Aq. bidest. : ion exch.) [mL : mL]	8.3	–		167
calystegine elution	basic elution, 2M NH$_3$ [mL]	250	–		120
	ratio V(NH$_3$: ion exch.) [mL : mL]	2.1	–		1.8
	column wash out (Aq. bidest.), [mL]	600	380		600
calystegine elution	ratio V(Aq. bidest. : ion exch.), [mL : mL]	5	6.4		8.8
purif. extr.		50 mL extr. Merck I purif.	100 mL extr. Merck III purif.		see the pooled fractions

Overview of the characteristics of the columns used for calystegine purification and separation, including solutions and volumes applied and the ratios related to bed volumes.

Derivatisation of calystegines – silylation

HMDS and TMCS are silylation agents (weak and strong) that are both selective for hydroxyl groups (secondary amino groups remain underivatised). Pyridine is both solvent and catalyst. Hexane is used as neutral matrix solvent for the reaction. Azobenzine (1 mg/mL in hexane) was chosen as internal standard. Samples for GC analysis were silylated in total volumes of 125 or 250 µL, depending on sample type. Calystegine eluate samples were normally silylated in 125 µL. Wash fractions and other samples containing substantial amounts of impurities were silylated in 250 µL. For each GC run, 1–3 µL of supernatant, cleared by centrifugation, was injected. The number of GC samples for each measurement was 3–5, and each of the samples corresponded to raw extract from 10–20 mg sprout dry weight. Calystegine contents represent mean values of sample group members, whereas the highest standard deviation tolerated was 10% of the mean value.

Table 15: Silylation conditions for analysis of calystegines and sugars

Silylation reaction in125 µL Components and steps:	V [µL]
pyridine	15
HMDS	20
TMCS	5
vortex; keep at 60 °C for 30 min; cool down to RT	
n-hexane	60
azobenzine sol. (1 mg/mL hexane)	25
vortex, centrifuge[*]	

[*] silylated samples with internal standard were centrifuged in Eppendorf 5415 D centrifuge at 12000 rpm for 5 min (RT).

2.2.2. Gas chromatography

GC was performed under the following conditions for qualitative and quantitative analysis of calystegines:

Table 16: Components of the GC system

DEVICE:	HP Agilent 6890 GC gas chromatograph, HP G1512A controller and communications module and HP G1513A injector
COLUMN:	FS-Supreme-5, Macherey-Nagel, Germany
Dimensions:	L. = 30 m, ID = 0.25 mm, film thickness 25 µm
Stationary phase:	95% methylsiloxane, 5% phenylsiloxane
Carrier gas:	helium
DETECTORS:	flame ionisation (FID) and nitrogen phosphorus (NPD)
Combustion gas:	hydrogen/synthetic air mixture

Table 17: GC program for separation of calystegines and sugars

INLETS:			
Mode:	split	Split ratio:	20 to 1
Heater:	250 °C	Split flow:	19.9 mL/min
Pressure:	120 kPa	Gas saver:	15 mL/min at 3 min
Total flow:	23.6 mL/min		
GAS FLOW:			
Pressure:	120 kPa		
Initial flow:	1 mL/min	Post flow:	1.5 mL/min
Run time:	24 min	Run time:	24–26 min
Average velocity:	30 cm/s		
DETECTORS:	Front:	Back:	
Type:	NPD	FID	
Heater:	310 °C	310 °C	
H_2 flow:	3 mL/min	40 mL/min	
Air flow:	60 mL/min	450 mL/min	

Table 18: Oven temperature profile for the GC separation program[*]

Oven ramp	°C/min	Temp. [°C]	Hold [min]	Total run time [min]
Initial	–	160	2	2
Ramp 1	5	240	0	18
Ramp 2	10	300	0	24
Post run	–	300	2	26

[*] initial oven temperature is 160 °C; overall run time is 26 min, cooldown time to oven initial temperature is 4 min

Qualitative analysis of calystegines and sugars

Individual calystegines were identified by their FID signal retention times. Since calystegines contain one nitrogen atom, their presence was additionally confirmed by the corresponding NPD signals, using the FID/NPD signal ratio for peak purity (Dräger, 1995). Sugar substrates and products in the α-glycosidase assay were identified by their retention times.

Table 19: List of retention times in GC of calystegines, sugars and some relevant compounds

Compound	Rt [min]	Compound	Rt [min]
calystegine A_5	7.93−8.00	fructose	8.80, 8.89, 9.08, 9.14, 9.46
calystegine A_3	8.39−8.40	glucose	10.33, 11.88
calystegine B_4	9.91−9.98	maltose	21.35, 21.77, 22.26
calystegine B_3	10.48−10.55	sucrose	21.00
calystegine B_1	10.68−10.75	trehalose	22.00
calystegine B_2	12.34−12.37	azobenzine	7.64−7.69
calystegine C_1	14.17	castanospermine	13.45

Azobenzine was used as internal standard, castanospermine for calibration of calystegines.

All the sugar signals appeared as multiple peaks, except for sucrose and trehalose (single peaks). Calibration curves for sugars with multiple peaks were constructed by applying the sum of signals on the ordinate, except for fructose, for which the two last signals were most prominent and were regarded as robust (the early fructose signals, marked in the table with grey script, had poor resolution and were therefor designated as unreliable for calibration curve construction).

Quantitative analysis of calystegines and sugars

Calibration curves for the analysis of calystegines – A calibration curve for calystegines was produced using castanospermine, as it is similar to calystegines in structural and molecular properties and is commercially available in high purity. An aqueous stock solution of 5 mg/mL castanospermine was prepared. This was diluted 1:10 with water and nine different sample volumes were taken in order to prepare silylated solutions for GC. The samples were lyophilised and silylated in 500 µL (according to Table 15, using double volumes of derivatisation agents, filled up to 500 µL with n-hexane), thus providing a series of nine silylated castanospermine solutions with concentrations ranging from 0.01 to 0.6 mg/mL (0.01, 0.025, 0.05, 0.1, 0.15, 0.2, 0.3, 0.45, 0.6 mg/mL). Injection volume was 1 µL, which resulted in injecting 0.01 to 0.6 µg of castanospermine absolute, in order of increasing concentrations. Each concentration was injected three times. The highest standard deviation was 2.6% of the corrected mean value. Corrected mean values of recorded FID signals were plotted against silylated castanospermine standard concentrations. The limit of quantification was determined at 0.01 mg/mL sylilated castanospermine, corresponding to 10 ng per injection. Linearity was confirmed up to 0.6 mg/mL, i.e. 600 ng per injection. The resulting calibration curve is described by the following equation and correlation coefficient:

$y = 272.18x$ ($R^2 = 0.9992$); y = corrected FID signal peak area, (pA×s),

x = calystegine concentration in silylated mixture (mg/mL)

Equation 2: Calibration curve of castanospermine (for quantifications of calystegines)

Quantification of calystegines and sugars was done using the FID signals corrected area (pA×s), which was obtained by dividing the detected FID peak area by the injection volume (in µL) and then multiplying with a correction coefficient that was calculated by dividing the FID peak of the internal standard (azobenzine) in the sample by the mean value of azobenzine FID peaks of all samples in a series of measurements.

Calibration curves for sugar analysis – Aqueous stock solutions of both sugar substrates (maltose, sucrose and trehalose) and products (glucose and fructose) for the α-glycosidase assay were prepared with concentrations of 50 mg/mL. From these, concentration series ranging from 0.01–50 mg/mL in ten steps (0.01, 0.05, 0.1, 0.5, 1, 2.5, 5, 10, 25, 50 mg/mL Aq. bidest.) were made and 10 µL of each were silylated in 125 µL, corresponding to 0.8 µg to 4 mg sugar per mL of silylation mixture. Injection volume was 3 µL. Linearity of calibration curves was observed from 0.8 µg/mL silylation mixture, corresponding to 2.4 ng

sugar injected (limit of quantification) up to 4 mg sugar per mL of silylation mixture, i.e. 12 µg sugar injected. The GC sample volumes of the assay samples were chosen to lie within this range.

Table 20: Equations of calibration curves of sugars (α-glycosidase inhibition assay)

Compound ~	Trend line equation	Trend line correl. coef. (R^2)
fructose	y = 222.76x	0.9987
glucose	y = 362.92x	0.9995
maltose	y = 229.17x	0.9988
sucrose	y = 266.45x	0.9992
trehalose	y = 219.23x	0.9992

y = corrected FID signal peak area (pA×s);
x = sugar concentration in silylated mixture (mg/mL)

2.2.3. Gas chromatography and mass spectrometry (GC-MS)

The GC device was a Trace GC 2000 Series from ThermoQuest CE Instruments (Austin, TX, USA). The GC column and separation program were equivalent to the GC method described previously (2.2.2), except for the following alterations: injection was splitless, inlet temperature was 200 °C, split flow was 19 mL/min.

The MS device was an Automass multi from ThermoQuest Finnigan (France). The emission current was 300−400 µA, ionization energy was 70 eV, detector gain [PM] was set at 580 V. Mass detection range was set to 50−550 m/z.

Table 21: Oven temperature profile for the GC-MS separation program for calystegines[*]

Oven ramp	°C/min	Temp. [°C]	Hold [min]	Total run time [min]
Initial	−	50	2	2
Ramp 1	20	160	0	7.5
Ramp 2	−	160	1	8.5
Ramp 3	5	240	0	24.5
Ramp 4	−	240	2	26.5
Ramp 5	10	300	0	32.5
Post run	−	300	2	34.5

[*] initial oven temperature was 50 °C; overall run time was 34.5 min, cooldown time to oven initial temperature was 4 min.

Table 22: GC retention times and mass spectra of calystegines (GC-MS)

Compound	Rt [min]	Mass spectra [m/z]
azobenzine	12.32	77-105-152-**182**
calystegine A_5	13.13	73-**156**-204-242-259-285-360-375
calystegine A_3	13.43	73-**156**-244-258-285-360-375
calystegine B_4	15.10	73-147-**217**-244-259-284-374
calystegine B_3	15.72	73-147-**217**-244-259-284-373
calystegine B_1	16.01	73-129-147-217-**244**-258-284-332-374
calystegine B_2	17.56	73-147-**217**-244-259-284-373
castanospermine	18.76	73-116-129-147-172-217-230-258-272-298-**361**-387-462-477
calystegine C_1	19.68	73-147-**217**-244-258-291-317-332-347-373-462

Bold script indicates the most prominent mass spectrum signals

Sample preparation and application were as described previously for GC. GC-MS was performed exclusively for structure confirmation by MS-spectra for control and evaluation of the purification procedure. Sugars were not confirmed by MS, as these were purchased commercially and were of high purity according to the supplier.

Table 23: Retention times for sugars (GC-MS)

Compound	Peak 1 Rt [min]	Peak 2 Rt [min]	Peak 3 Rt [min]	Peak 4 Rt [min]	Peak 5 Rt [min]
fructose	15.92	16.12	16.95	17.20	18.51
glucose	18.69	20.37	–	–	–
maltose	31.62	32.13	32.61	–	–
sucrose	29.90	30.70	31.34	–	–
trehalose	31.30	32.39	–	–	–
Grey script: signals with pour resolution, that were not taken in consideration for confirmation of identity					

2.2.4. Nuclear magnetic resonance (NMR) spectroscopy

NMR spectra of purified calystegine pools were measured on a Varian Spectrometer 400 in deuterised water (D_2O). Chemical shifts (δ) are expressed in ppm and the coupling constants (J) are in Hz. The temperature for measurements was 25 °C. ^{13}C NMR spectra were recorded at 100 MHz and ^1H spectra at 400 MHz. The amount of sample prepared for NMR analysis was 12–13 mg of lyophilised calystegine pool, dissolved in 0.7 mL D_2O.

NMR spectra were visually processed using the program MestReCLite (version 4.7.0.0, copyright 2005) from Mestrelab Research (Santiago de Compostela, Galícia/Spain).

Chemical shifts found in ^{13}C NMR spectra were analysed for structure confirmation of obtained pure calystegines. Resonances are referenced in relation to the tetramethylsilane.

2.2.5. Capillary zone electrophoresis (CZE) and capillary isotachophoresis (cITP)
Capillary zone electrophoresis (CZE)

Calystegines A_3 and B_2 served as external standard for quantitative CZE analysis. Stock solutions of 1 mg/mL were produced by dissolving the calystegines in 50% methanol and stored cool at 4–8 °C. The calibration standards (five concentrations of 5, 10, 20, 30 and 50 µg/mL in 20% methanol) were prepared from the stock solutions. Coefficients of calibration equation describing relationship between peak area corrected on migration time (peak are in mAUs divided by migration time in minutes gives unit mAUs/min) and concentration of calystegine solution (µg/mL) was calculated (Table 34). For routine quantitative analysis, a solution of tetrabutylammonium bromide (TBA, 100 µg/mL in 20% methanol) was used as auxiliary standard instead of calystegines.

Table 24: Conditions for capillary zone electrophoresis (CZE) of calystegines

Device	electrophoretic analyser Hewlett Packard 3DCE (HPST Ltd., Prague, Czech Republic)
Capillary	fused silica separation capillary, total length: 500 mm, effective length: 415 mm, 50 µm I.D.
Capillary washing	prior the use: demineralised water (5 min), 0.1 M NaOH (10 min), demineralised water (5 min), and finally BGE (10 min); between analyses: 0.1 M NaOH (2 min), demineralised water (2 min), eventually equilibrated with BGE (3 min)
Background electrolyte (BGE)	20 mM L-histidine, 20 mM BES, and 20% methanol in demineralised water, filtrated (0.2 µm nylon membrane)
Sample injection	pressure (25 mbar for 25 s)
Separation conditions	constant voltage: +30 kV (ca. 3 µA); analysis time: 4 min
Detection	DAD, λ = 210 nm (indirect detection)
Electropherogram evaluation	Chemstation software package
External standards	calystegines A_3 and B_2; TBA auxiliary standard (100 µg/mL in 20% methanol) for routine quantitative analysis

BES = *N,N*-bis(2-hydroxyethyl)-2-aminoethanesulfonic acid; washing the capillary between the runs in order to preserve high reproducibility of migration times

Capillary isotachophoresis (cITP)

Stock solutions (1 mg/mL) of calystegines A_3 and B_2 were used for preparation of calibration solutions, five different volumes of which each were injected: 0.5, 1, 2, 5 and 10 µL corresponding to 25, 50, 100, 250 and 500 ng. Coefficients of calibration equation describing relationship between step length in seconds and injected amount of calystegine in ng was calculated (Table 35). Calystegines A_3 and B_2 were also added to samples at levels of 50% and 100% of the calystegines concentration measured in the samples in order to test accuracy. As for CZE, TBA (100 µg/mL in 20% methanol) was used as auxiliary standard instead of calystegines for routine analysis.

Table 25: Conditions for capillary isotachophoresis (cITP) of calystegines

Device	column-coupling electrophoretic analyser EA 101 (Villa-Labeco, Slovak Republic)
Capillary	FEP pre-separation capillary (110 mm × 0.8 mm I.D.) FEP analytical capillary (90 mm × 0.3 mm I.D.)
Leading electrolyte (LE)	5 mM NH$_4$OH, 10 mM BES, 0.05% HEC and 20% methanol in demineralised water
Terminating electrolyte (TE)	5 mM L-histidine, 5 mM acetic acid and 30% methanol in demineralised water
Sample injection	Hamilton syringe of 10 µL
Separation	constant driving current: 150 µA pre-separation capillary, 20 µA analytical capillary, 5 µA during detection; cationic mode
Analysis duration	20 min
Detection	contact conductivity detector
Isotachopherograms evaluation	PC software package supplied with analyser (KasComp Ltd., Slovakia)
External standard technique	TBA auxiliary standard (100 µg/mL in 20% methanol)

FEP = copolymer of tetrafluoroethylene with hexafluoropropylene;
TBA = tetrabutylammonium bromide; HEC = hydroxyethylcellulose

2.2.6. Liquid scintillation counting

In the samples of the transepithelial Caco-2 cell layer impermeability test (Chapter 2.4.2, Impermeability test of the intact Caco-2 cell layer), the applied radiolabelled marker [^{14}C] D-mannitol was measured. This radionuclide undergoes β-decay, emitting electrons that, in suitable media, create luminescence photons, which are detected by a photomultiplier and transformed into voltage impulses. Those detected impulses are recorded as cpm (counts per minute), or after quench correction, as dpm (disintegration per minute) (Römpp et al., 1992).

Samples of 100 µL were collected as described in Chapter 2.4.2., mixed with 2.8 mL of scintillation cocktail (Rotiszint® eco plus, Carl Roth, Karlsruhe, Germany) and measured in a liquid scintillation spectrometer (Tri-Carb-2100 TR, Packard, USA), 5 min per sample. Three standard samples of 25 µL each (10 µM [^{14}C] D-mannitol in FAB6) were prepared in the same way as the assay samples and measured along with them. Refering to the measured dpm values of the standards, the concentration of radioactivity (dpm) per marker amount (volume of mannitol standard times its concentration) was determined [dpm/pmol]. That ratio (radioactivity concentration) was used to calculate the amounts of marker in flux assay samples, according to their dpm registered by scintillation counting. Based on these relations, marker amounts and concentrations in the compartments were calculated for every sampling time point in the assay. Transepithelial flow of [^{14}C] D-mannitol through the Caco-2 cells monolayer was expressed as flux (J) (%/(h×cm^2)) (see Equation 6 and Equation 7 in Chapter 2.6.1: Calculation of transepithelial flux).

2.2.7. Quantification of cell lysate proteins

Cell lysate proteins (Chapter 2.4.3: Protein extraction from the cell culture) for the α-glycosidase assay (Chapter 2.5.2) were quantified according to Bradford (Bradford, 1976). Proteins form intensively blue coloured complexes with Coomassie Brilliant Blue G-250 dye, since the dye builds complexes with cationic and acidic side chains of proteins. Protein solutions were diluted 1:10 to 1:20 with phosphate buffer pH = 6. Volumes of 50 µL of diluted solutions were mixed with 1 mL of Bradford reagent, diluted 1:4, in quartz glass cuvettes and left for 5 min. Samples were measured in a Shimadzu UV-160A double beam spectrophotometer (λ = 595 nm). Blank samples were prepared and measured identically, only with adding PB6 instead of protein samples. Bovine serum albumin (BSA) was used for creation of the calibration curve, which was linear within a concentration range of 25−200 µg protein/mL, corresponding to an absorption range of 0.12−0.65.

y = Kx + B (K=334.02, B= −15.353);

y = absorption, x = concentration of protein (µg/mL)

Equation 3: Calibration curve for protein quantification

2.3. *In silico* methods – docking

All ligands for docking were constructed with the SYBYL modelling suite (SYBYL version 8.0, Tripos International, St. Louis, MO, USA). Energy was minimised with the TRIPOS force field (Clark et al., 1989) using Gasteiger charges (Gasteiger and Marsili, 1978; Gasteiger and Marsili, 1980). The X-ray crystal structures of the N-terminal domain of sucrase-isomaltase (3LPP) (Sim et al., 2010) and of human intestinal maltase-glucoamylase (3L4X and 2QMJ) (Sim et al., 2008) are available from the protein database (PDB at the Research Collaboratory for Structural Bioinformatics (RCSB) www.pdb.org). All hydrogen atoms were added using the 3d-protonate module of MOE (Molecular Operating Environment, version 2007.09, Chemical Computing Group Inc., Montreal, QC, Canada). Partial charges were assigned by Gasteiger charges. All ligands were docked to the active sites of the proteins under standard settings of GOLD (Genetic Optimised Ligand Docking, Cambridge Crystallographic Data Centre) (Jones et al., 1995; Nissink et al., 2002; Verdonk et al., 2003), whereby a maximum output of 30 docking arrangements was allowed. The active sites were defined by a radius of 15 Å around the $O_{\delta 2}$ atoms of Asp443 (3L4X) and Asp472 (3LPP). Ligands with the best docking score (Table 45) were optimised with the Tripos force field. For this purpose only those amino acid residues in direct interaction with the ligands were considered to be flexible whereas all other atoms of the protein were fixed. The resulting interaction energies were calculated by subtraction of the energies of the empty enzymes and the isolated ligands from the energy of the complex. Solvent effects were not included.

2.4. Cytological methods

2.4.1. Cultivation and subcultivation

Caco-2 cells were cultivated in 75 cm^2 culture flasks (Greiner, Frickenhausen, Germany) with cultivation medium, composition shown in Chapter: 2.1.3), in a 5% CO_2–95% air atmosphere at 37 °C (cell culture chamber, Heraeus, Hanau, Germany). Medium was replaced on the day after seeding and thereafter every 2 days. Cell density for the cultivation was 8×10^5 per flask. After 4 days 80–90% confluence was reached (observed under a microscope: Axiovert 25, Zeiss, Jena, Germany) (Fischer et al., 2010). The confluent cell layers were dispersed by trypsinisation, resuspended in medium and subcultured in 175 cm^2 culture flasks for α-glycosidase enzyme assays (Chapter 2.5.2). Total cell number seeded in assay flasks was

7×10^6 (cell density $4 \times 10^4 / cm^2$). Flasks were used for α-glycosidase enzyme measurements 7 days after subcultivation, since sucrase and maltase activity increase during cultivation (Blais et al., 1987; Ferruzza et al., 2012). Enzyme activity may increase in older cell cultures, but cell culture time is not that important factor for harvesting of cells and cell isolation as long as the activity of the necessary enzyme is measurable. It has been shown that the differentiation rate of cells cultured on impermeable plastic support solely depends on the cell number. For example, Caco-2 cells seeded at a density of 8×10^5 cells in 35 mm plastic dishes reach confluence in 24 h and are fully differentiated after 7 days. After that, monolayers are tight, polarised, approximately 30 µm thick and of skin-like appearance. Domes appear after already 3–4 days, indicating that the monolayers are very tight. In previous studies beginning 1992 (AG Brandsch, Biozentrum, MLU Halle-Wittenberg), microvilli and polarization were observed electron-microscopically. If cultivation lasts too long, after 10–14 days the monolayer sheets start to detach from plastic support in a skin-like manner (source: personal communication, Dr. Mathias Brantsch).

Basic steps for the cell cultivation and subcultivation are shown in Scheme 2.
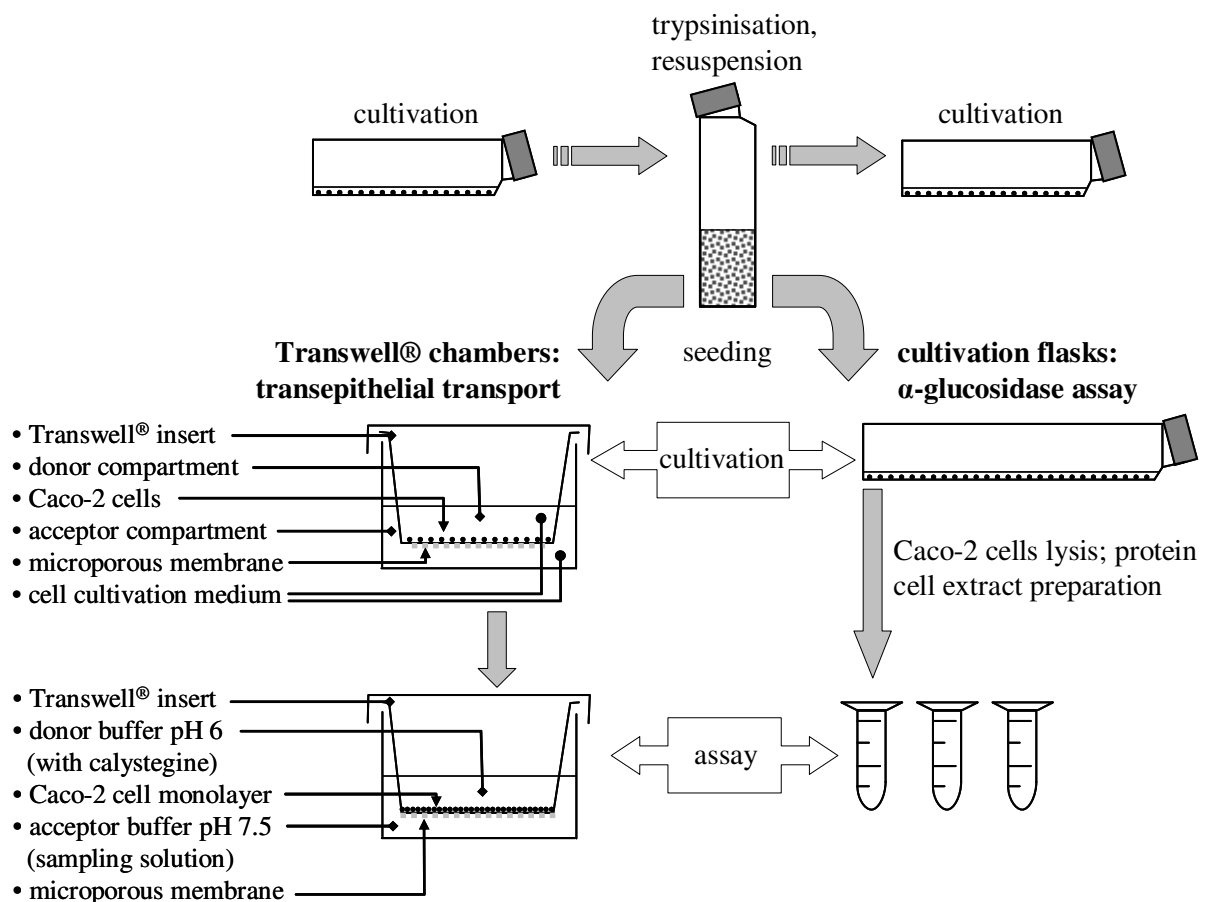
Scheme 2: Schematic presentation of Caco-2 cell cultivation and subcultivation

2.4.2. Transepithelial transport test for calystegines: Flux test

- Transepithelial transport of calystegines

Caco-2 cells were used as a model for intestinal transport. Transport assays were performed in plates with 6 Transwell® permeable inserts of microporous polycarbonate membrane of 4.67 cm^2, pore size 3 µm (Corning Life Sciences, Schiphol-Rijk, The Netherlands). Cell suspensions were pipetted on the insert membranes at a density of 4.3×10^4–4.4×10^4 cells/cm^2 and cultivated for 21 days. Medium was changed on the day after subculture, then every two days and on the day before the experiment. Transepithelial electrical resistance (TEER) of cell monolayers was checked on the day of the experiment using an ohmmeter (Millicell ERS, Millipore Co., Bedford). The cell culture medium was removed and the membranes were rinsed two times with donor buffer (37 °C). Donor and acceptor buffer composition was previously shown (Table 8, Chapter 2.1.3). The experiment started by filling the donor (luminal) compartments with 2.5 and 5 mM calystegine A$_3$ and B$_2$ solutions in donor buffer, each in triplicate. Samples were collected from donor and acceptor compartments. Donor samples (100 µL) were taken after 0 and 120 min. Acceptor compartment samples (200 µL) were taken after 10, 30, 60 and 120 min. Immediately after sampling, compartments were supplemented with volumes of buffer corresponding to the sample volumes. During the experiment, multiwell Transwell® chambers were kept in the table incubator (Thermostar, BMG Lab Technologies) at 37 °C and 150 rpm. Three assays were prepared for each calystegine concentration. After 120 min, TEER was again measured to confirm the integrity of the monolayer (Artursson, 1990). Calystegine B$_2$ in the acceptor buffer was measured enzymatically by the inhibition of sweet almond β-glycosidase cleavage of p-NPG, based on competitive inhibition (method description in the Chapter 2.5.1). The samples were corrected for dilution. Transepithelial transport of calystegines was calculated and expressed as flux [%/(h×cm^2)] (see Equation 6 and Equation 7 in the Chapter 2.6.1: Calculation of transepithelial flux).

- Impermeability test of the intact Caco-2 cell layer

Besides measuring the transepithelial electrical resistance, Caco-2 cell monolayer integrity in presence of calystegines during the permeability assay was also monitored by measuring the transepithelial flux of [^{14}C] D-mannitol, used as a paracellular marker for integrity verification (Dawson, 1977). The [^{14}C] D-mannitol (Moravek Biochemicals, Brea, CA, USA) solution possessed a specific activity of 53 mCi/mmol and a radioactive concentration of 100 µCi/mL

(250 µCi/2.5 mL, as indicated on the package label), thus providing a concentration of 1.89 mM mannitol in the original solution. This commercial solution was included in donor calystegine solutions (FAB6) to obtain 10 µM mannitol. Calystegine concentration was 5 mM, which corresponds to the higher calystegine concentration applied in the transepithelial transport assay. The intention was to show the harmlessness of the calystegine solution to the integrity of the Caco-2 cell monolayer. Parallel to mannitol-containing calystegine, calystegine-free mannitol blanks were prepared in donor buffer. The assay was performed in three wells for each test combination (blanks, calystegines).

The corrected mannitol amounts were related to the initial amount of mannitol applied in the donor compartment in the beginning of the experiment (0 min), expressed as percentages and eventually divided by the surface of the Transwell$^{®}$ inserts, i.e. the surface of the cell monolayer. The transepithelial flux of mannitol is obtained by using the 60 min time point, since flux is usually shown as percental transport of the measured substance per cm^2 and per 1h.

The course of the assay was as previously described for the transepithelial transport test, with samples taken at the same time points, only that here sample volume was 100 µL. The measured mannitol amounts in the acceptor wells at each of the four measuring time points (10, 30, 60 and 120 min) were corrected for the acceptor compartment sample dilution by replacing the taken sample volumes with acceptor buffer. The sample dilution wes corrected during calculation. The samples were measured in a liquid scintillation spectrometer (Tri-Carb-2100 TR, Packard, USA), see Chapter 2.2.6 for explanation of analytical method.

2.4.3.   Protein extraction from the cell culture

Caco-2 cells cultured for 7 days were washed twice with ice-cold 20 mM phosphate buffer pH 6.0 (Conklin et al., 1975), scraped with rubber cell scrapers (Sarstedt, Germany), resuspended and homogenised in 8−10 mL buffer per flask. The cells were lysed by freezing at −80 °C and thawing at 37 °C twice, then pulled through 24 G cannulas (Braun-Sterican®, Melsungen, Germany) twice. The homogenised cell lysate was centrifuged for 30 min at 12000 g and 4 °C (Ultracentrifuge SORVALL® ULTRA Pro 80). Protein content was determined with the method by Bradford (Bradford, 1976).

2.5.   Enzymatic methods

2.5.1.   Enzymatic determination of calystegines (*β*-D-glycosidase enzymatic assay)

<u>Generation of a calibration curve for *p*-NP</u>

The absorbance of *p*-NP was measured using a Multiskan-Ascent spectrophotometer with the following specification (Table 26). The volumes of *p*-NP dilution series solutions (Table 10) pipetted in the microtitre plate wells were equal to the reaction volume (75 µL) in the *β*-D glycosidase assay. One row of wells, filled with the same amount of PB5, served as blanks, whose absorption was subtracted from the *p*-NP solution samples. The microtitre plate was shaken for 1 min at 960 rpm and incubated in the spectrophotometer for 10 min at 37 °C to simulate the enzyme assay conditions. Addition of a basic agent (50 µL of 1M Na_2CO_3 stop solution) to the enzyme assay mixture stops the enzymatic reaction and develops the yellow colour of *p*-NP liberated from the artificial substrate (*p*-NPG) during the assay.

Table 26: Device parameters of microtitre plate reader

Spectrophotometer:	Multiskan-Ascent (Thermo Labsystems, Helsinki, Finland)
Photometric measuring principle:	single beam photometer
Optical system:	light source: quartz halogen lamp (Osram 64222, 6V/10W) filter: interference filter, wave length 340, 405, 414, 450, 492, 540, 620, 690 nm
Wavelength range:	340−850 nm
Wavelength error:	± 2 nm
Detector:	silicone photodetector
Incubator:	5 °C−40 °C
Temperature distribution:	± 0.8 °C
Agitation function:	slow (8 Hz), middle fast (12 Hz), fast (16 Hz)
Microtitre plate types:	96 and 384 well plates

Accordingly, 50 µL of stop solution was also added to each standard curve sample and the microtitre plate was shaken again for 1 min at 960 rpm. Absorption values ($\lambda = 405$ nm) were measured and plotted against the corresponding *p*-NP concentrations. The regression line provides the equation for calculation of *p*-NP concentration from the absorbance of the enzyme assay reaction mixture.

$y = 7.5287x + 0.0039 \ (R^2 = 0.9998)$

y = absorption, x = c(*p*-NP) in mM (reaction mixture volume)

Equation 4: Regression line equation of *p*-NP absorbance after adding 1M Na$_2$CO$_3$

The equation for *p*-NP concentration in the stopped enzyme assay mixture:

$x = (A - 0.0039)/7.5287$

x = c (*p*-NP) in mM; A = absorption measured at the end of assay

Equation 5: Equation for quantification of *p*-NP and indirectly calystegine B$_2$

The concentration of *p*-NP in the stopped reaction mixture was converted to the amount of *p*-NP in the well, which equals the amount of *p*-NP liberated from *p*-NPG during the enzyme reaction. The amount of the substrate cleaved by the enzyme was divided by the assay duration (seconds) and the total amount of protein present in the reaction (mg). Enzyme specific activity is expressed as amount of substrate cleaved per second per mg of total protein and expressed as nkat/mg [nmol/(s×mg)].

The pipetting scheme for generation of the *p*-nitrophenol calibration curve is shown in the Appendix section (Scheme 3: Pipetting scheme for generation of *p-nitrophenol* calibration curve).

For calculation of the kinetic parameters and their evaluation, SigmaPlot (Version 10.0, Systat Software, Inc.) and its additional module Enzyme Kinetics (Version 1.3) were used.

<u>Determination of kinetic parameters of *β*-glycosidase (K$_m$ and *V*$_{max}$)</u>

Enzyme activity of *β*-glycosidase was verified using the synthetic substrate *p*-PNG. The microtitre plate was filled with 25 µL each of substrate solutions 1−10 (Table 11) in duplicate, in two columns and four rows.

25 µL buffer was added to each well: PB5 for regular determination of enzyme parameters, FAB6 and FAB7.5 for determination of enzyme kinetics with flux test assay samples (donor and acceptor samples). Odd plate columns were filled with 25 µL PB5 per well (serving as blank samples for the neighbouring column with enzyme, added later). The plate was agitated for 1 min at 960 rpm and incubated for 5 min at 37 °C. 25 µL of enzyme solution (0.01 mg/mL) was added fast successively in the wells of the even plate columns. The plate was agitated for 1 min at 960 rpm and incubated for 10 min (nominal assay duration time) at 37 °C. Then enzyme reactions were halted by adding 50 µl of stop solution in all wells, the plate

was agitated again for 1 min at 960 rpm and absorbance was immediately measured at 405 nm.

The effective enzyme assay duration is 11 min: the assay is started by adding the enzyme solution into the prewarmed reaction mixture, which is then homogenised by agitation (1 min) and incubated for 10 min. The enzyme is deactivated by adding highly basic 1M Na_2CO_3 that stops the assay and enables the yellow colour of *p*-NP to develop. The colour was photometrically measured at 405 nm immediately after shaking the mixture. The pipetting scheme is shown in the Appendix (Scheme 4: Determination of Km value of substrate (*p*-NPG) for *β-d-glycosidase*).

The odd columns, with buffer pipetted instead of the enzyme solution, were blanks, whose absorption was subtracted from the wells with enzyme applied. The first two rows of the plate were filled with substrate solutions 3–10 for the enzyme activity control, also used in other kinetics tests of *β*-glycosidase.

Inhibition of *β*-glycosidase with calystegines A$_3$ and B$_2$: determination of kinetic parameters; creation of calibration curves for calystegine determination in the transepithelial transport test

Determination of kinetic parameters of β-glycosidase inhibited with calystegines A$_3$ and B$_2$ – The same procedure was applied as for the determination of kinetic parameters of *β*-glycosidase. Instead of filling wells with buffer solutions (PB5, FAB6 or 7.5), wells were filled with one of the 6 different calystegine solutions (Chapter 2.1.4, Table 12) in appropriate buffer. Kinetic parameters were determined for each one of the calystegine solutions. The pipetting scheme is shown in the Appendix (Scheme 5: Inhibition of *β-d-glycosidase* with calystegine. Determination of Ki value).

Calystegines act as competitive *β*-glycosidase inhibitors. The amount of the liberated enzyme reaction product (*p*-NP) is thus reduced, and the final colour of the reaction mixture is less intense than of the uninhibited enzyme mixtures. The colour reduction, which is proportional to the increase of calystegine concentration, is also noticeable visually.

Creation of calibration curves for calystegine determination in the transepithelial transport test – The enzyme activity was measured using only one substrate concentration, close to the substrate K_m value. All of the 6 different calystegine solutions were pipetted in duplicate in two columns and four rows (FAB6 or 7.5, buffer type corresponding to the flux test donor and acceptor samples). The subsequent procedures and pipetting steps were analogous to the previous enzyme kinetic measuring schemes. The pipetting scheme is shown in the Appendix

(Scheme 6: Inhibition of *β-d-glycosidase* with calystegine. Generation of the equation for calystegine quantification in flux assay samples).

Calibration curves for calystegines in both FABs were constructed separately by applying specific enzyme activity (nkat/mg) on the ordinate and calystegine concentration in the enzyme reaction mixture on the abscissa. Regression lines were of the exponential type, according to the highest correlation factors. The equations of those exponential curves of *β*-glycosidase specific activity with calystegines in FAB6 and FAB7.5 were transformed into logarithmic ones, in order to obtain the appropriate form (calystegine concentration) for quantitation of calystegine in samples of donor and acceptor compartments during the transepithelial transport assay. The equations for calystegine B_2 are shown in Table 27.

Table 27: Equations of the regression lines for calystegine B_2 in FAB6 and FAB7.5 for inhibition of *β*-glycosidase in 3 mM *p*-NPG.

Transwell® compartment	flux assay buffer (pH)	regression line equation with correlation coefficient	equation for calystegine B_2 quantitation in FAB
donor	FAB6	$y = 61.121e^{-0.081x}$ $(R^2 = 0.9814)$	$x = Ln(y/61.121)/(-0.0810)$
acceptor	FAB7.5	$y = 56.749e^{-0.0823x}$ $(R^2 = 0.9920)$	$x = Ln(y/56.749)/(-0.0823)$
y = absorption, x = concentration in of calystegine B_2 in the assay mixture volume (µM)			

- <u>Determination of calystegine content in the transepithelial transport test</u>

Samples were taken from the Transwell chamber as described in Chapter 2.4.2., representing both calystegine concentrations applied for the transport assay (2.5 or 5 mM), both compartments (donor or acceptor) and all specified time points (10, 30, 60 and 120 min). Samples from the donor compartment were diluted with appropriate buffer: 1:100 for the 2.5 mM and 1:200 for the 5 mM calystegine solution. The detection limit of the *β*-glycosidase assay was 30 ng/mL calystegine B_2, which is approximately 5 times lower than the GC detection limit.

2.5.2. Enzyme assay for determination of human intestinal disaccharidase (*α*-glycosidase) activity

<u>*α*-glycosidase assay</u>

The enzymes used for the determination of kinetics were contained in the Caco-2 cell lysate (Chapter 2.4.3). The assay was based on the method of Dahlqvist (Dahlqvist, 1968) and was

performed in 1.5 mL Eppendorf test tubes (Eppendorf, Hamburg, Germany). Table 28 shows the individual steps of the assay.

The volume of Caco-2 cell protein extract applied in the assay was 450 µL. Following the pipetting scheme of the assay (25 µL of substrate solution applied), the concentration of maltose or sucrose in the assay mixture ranged from 0.5–75 mM (0.5, 5, 25, 50 and 75 mM). For determination of kinetic parameters of uninhibited enzymes, 50 µL of bidest. water was added, and effective buffer concentration was 17 mM. The assay was started by adding the protein extract into the assay mixture. Blank samples were prepared with inactivated protein extract (heated for 10 min at 95 °C while shaking at 24 rpm) in the assay mixture. Control experiments contained 20 mM phosphate buffer pH = 6 instead of protein extract. Samples were incubated in a thermomixer for 60 min at 37 °C and 600 rpm (Eppendorf Thermomixer 5436). Reactions were stopped by heating the samples for 10 min at 95 °C and 24 rpm (VORTEMP-UniEquip, Martinsried bei München, Germany). Flocculated proteins were removed by centrifugation for 10 min at 12000 g and 4 °C (Biofuge fresco, Heraeus, Hanau, Germany). Besides maltase and sucrase activity, trehalase activity was also checked, since trehalase is also known as brush border glycosidase, inhibited by calystegines (Asano et al., 1996b; Asano et al., 1994b).

Table 28: Overview of the assay steps for human intestinal glycosidase activity

	Substrate	Aq. bidest./ inhibitor	Protein solution (Caco-2 cell lysate)
Component volume [µL]	25	50	450
Incubation conditions	60 min, 37 °C, 600 rpm shaking		
Assay stopping (protein deactivation)	10 min, 95 °C, 24 rpm shaking		
Centrifugation	10 min, 12000 g, 4 °C $\rightarrow$ supernatant		

<u>Enzyme product analysis; Determination of enzyme kinetic parameters for maltase and sucrase (K$_m$ and V_{max} values)</u>

After centrifugation of the inactivated assay mixtures, supernatant samples were taken for the GC sugar and calystegine analyses. GC sample volumes were chosen such that the amount of sugar in the assay (substrate) and possible amount of released sugar (products) would fit in the ranges of the calibration curves: 150 µL (0.5–5 mM substrate concentration), 30 µL (25 and 50 mM substrate in assay) and 20 µL (75 mM substrate). The samples for GC analysis were silylated (silylation volume 125 µL) and measured according to the procedure described in Chapters 2.2.1 ("Derivatisation of calystegines – silylation") and 2.2.2 ("GC").

Quantitation of glucose released in the assay samples (used as reference product for the substrate cleaving activity of the enzymes) was performed according to the calibration curve equation show in Chapter 2.2.2 (Gas chromatography → Quantitative analysis of calystegines and sugars).

Maltase and sucrase specific activities were calculated via glucose released from maltose or sucrose and were indicated as pkat/mg protein. One molecule of maltose cleaved yields two molecules of glucose, whereas one cleaved molecule of sucrose yields one molecule of glucose and one molecule of fructose. Enzyme activity expressed as one katal (kat) corresponds to one mol substrate cleaved per second. If related to the enzyme amount applied in the assay (mg), specific enzyme activity is obtained. The specific enzyme activity values for each substrate concentration were used for calculation of enzyme kinetic parameters. Enzyme kinetic parameters of maltase and sucrase (K_m and V_{max}) were calculated by using the program SigmaPlot 10.0 (Systat Software Inc., San Jose, CA, USA) and its Enzyme Kinetics 1.3 module, and given as means ± standard errors of 3–6 assay samples.

Inhibition tests with calystegines; Determination of K_i-values for calystegines

The assay procedure for enzyme inhibition was identical to the previously described steps for enzyme kinetics determination. 50 µL of Aq. bidest. was replaced by 50 µL of 1.25 or 5 mM calystegine A_3 or B_2 aqueous solution (Chapter 2.2.1). Effective calystegine concentration in the assay was 119 or 476 µM. Selection of calystegine sample concentration in the assay is described in Chapter 2.6.2, Equation 8. As a positive control for inhibition, an equal volume of acarbose (52.5 µM) was added (Chapter 2.1.5). The concentration of acarbose in the assay was therefore 5 µM, close to the published acarbose K_i value (Breitmeier et al., 1997).

Inhibition constants of calystegines (K_i) were calculated using SigmaPlot 10.0 and the Enzyme Kinetics 1.3 module. Since acarbose was used as inhibition control in only one concentration (5 µM), the K_i value for acarbose was calculated with the equation for single inhibitor concentration (Motulsky and Christopoulos, 2003) using the kinetic parameters obtained by SigmaPlot. Therefore a standard error for the K_i of acarbose is not available. The inhibition type for calystegines was chosen as full competitive.

2.6.   Mathematical methods and statistics

The processing of the experimental results was performed using Microsoft® Excel (Windows XP, v.2002) and SigmaPlot® 10.0 for Windows.

2.6.1. Calculation of transepithelial flux

Transepithelial flux represents the percentage of the examined compound that crosses the cell layer from one chamber (donor) into the other (acceptor) in a given time. Percentages of examined compound that entered the acceptor compartment (ordinate) were plotted against sampling time points (abscissa). Flux values were presented for the time points of 60 min.

$$J = ((n_{tn(corrected)} / n_D) \times 100) / S$$

J = transepithelial flux [%];
$n_{tn(corrected)}$ = corrected amount of substance in the acceptor compartment at the certain time point;
n_D = amount of substance in the donor compartment at $t = 0$ min;
S = surface of the insert membrane, i.e. cell monolayer [cm^2]

Equation 6: Calculation of transepithelial flux

Correction of the acceptor compartment substance amount during the sampling

In order to rectify the dilution effect in Transwell® acceptor chamber due to the taking of the samples and replacing the sample volume with the buffer in defined time points, the following equation was used for corrected substance amount calculation:

$$n_{tn(corrected)} = n_{tn} + (n_{tn-1} \times V_{sample} / V_A))$$

$n_{tn(corrected)}$ = corrected amount of substance in the acceptor compartment at the certain time point t_n;
n_{tn} = amount of substance in the acceptor compartment at the certain time point t_n;
n_{tn-1} = amount of substance in the acceptor compartment at the time point t_{n-1};
V_{sample} = sample volume taken at the certain time point [mL];
V_A = volume of the acceptor compartment t_n [mL]

Equation 7: Correction of the acceptor compartment substance amount during the sampling

2.6.2. Calculation of kinetic parameters

The choice of concentrations for calystegines in the α-glycosidase assay was based on Asano et al. (Asano et al., 1996b) and Quezada-Calvillo et al. (Quezada-Calvillo et al., 2007). Calystegine IC_{50} and maltose K_m values were used to calculate inhibitory concentrations using the Cheng-Prusoff equation (Cheng and Prusoff, 1973), which provided the lower inhibition concentration for calystegines that was applied.

$K_i = IC_{50} / (1 + ([S] / K_m))$,

K_i = dissociation constant of enzyme-inhibitor complex; IC_{50} = concentration of inhibitor at which enzyme activity is 50% of the normal, uninhibited activity;

K_m = Michaelis-Menten constant, concentration of substrate at which enzyme activity reaches half of the maximal value; [S] = substrate concentration

Equation 8: Equation for K_i calculation according to Cheng and Prusoff

– Equation for selecting the level of effective inhibiting calystegine concentration for α-glycosidase assay

Enzyme kinetic parameters of maltase and sucrase (K_m and V_{max}), were calculated in SigmaPlot 10.0 (Systat Software Inc., San Jose, CA, USA). The inhibition type for calystegines was chosen to be competitive, according to literature sources (Asano et al., 1995a; Asano et al., 1994c; Molyneux et al., 1993), as was that for acarbose (Hanozet et al., 1981). K_i values for acarbose as a positive control and for calystegines A_3 and B_2 were calculated using the kinetic parameters obtained from SigmaPlot in the equation for the inhibitor single concentration: Equation for K_i calculation with inhibitor single concentration (according to Motulsky and Christopoulos, 2003 (Motulsky and Christopoulos, 2003)).

$K_m \times (1 + ([I] / K_i)) = K_{m(apparent)}$, $\rightarrow$ $K_i = K_m \times [I]/(K_m \times K_{m(apparent)} - K_m)$

K_m and $K_{m(apparent)}$ = Michaelis-Menten constants for maltose and sucrose for the corresponding enzymes without inhibitor and with inhibitor (apparent), [I] = inhibitor concentration (acarbose of 5 µM, calystegines A_3 and B_2 of 476 µM both)

Equation 9: Equation for K_i calculation with inhibitor single concentration (according to Motulsky and Christopoulos, 2003)

The high concentration of calystegine was chosen because of the weak inhibition noticed when lower concentrations were applied.

2.6.3. Statistical analysis

The amounts of calystegines determined by GC are represented as mean values of GC samples (n = 3–5) with standard deviations. Values were calculated using Microsoft Excel. Values for dry weights of lyophilised potato sprout extracts and calystegine pools are mean values (n = 3–5) with standard deviations, i.e. quantification of variation (scatter) of the measured values and their mean.

Specific activity for α- or β-glycosidases was calculated in Excel using raw data obtained by measuring sugars with GC or released p-NP spectrophotometrically. Enzyme kinetic parameters were obtained and evaluated by SigmaPlot and its Enzyme Kinetic module. Calculated values are mean values of the enzyme assay samples (n = 3−6 for α-glycosidases, and n = 4 for β-glycosidase) with standard errors. Standard error represents quantification of the precision of the mean, and tells how far is the sample mean from the true population mean. It provides precise value of the mean even if the data are very scattered. Values deviating from means by more than 10% were not taken into consideration for calculation.

Relative standard deviation described precision and assay repeatability for CZE and cITP, considering migration time and signal response.

3. Results and Discussion

3.1. Isolation of calystegines: extraction, purification and separation of calystegines

3.1.1. Calystegine content in potato sprouts measured by GC

The ratio of fresh weight (545.2 g) to dry weight (115.3 g) (f.w./d.w.) of potato sprouts of cultivar Rosara was 4.74 ± 0.12 (mean value of 5 lyophilised aliquots, ± standard deviation). The percentage of dry mass in the sprouts was 21.1%. The highest yield of sprouts was noticed between harvests 3 and 6, when 2/3 of the material (fresh weight) was collected. The weight of the lyophilised sprouts after grinding was 113.88 g, which was used as the reference dry weight to whichcalystegine content was related. The yields of the three major calystegines, A_3, B_2 and B_4, from the three chromatographic purification and separation steps are shown in Figure 7.
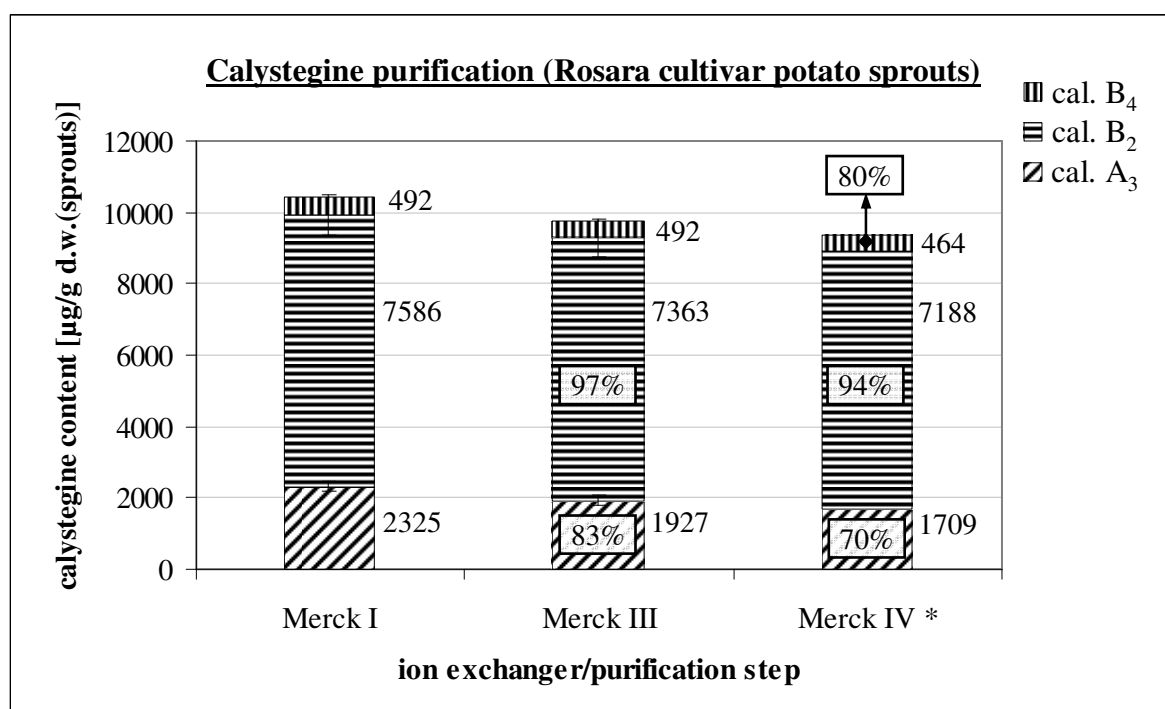
Figure 7: Content of calystegines in the potato sprouts extract corresponding to each purification step. (purification over Merck I & III and separation over Merck IV column)

[*] Merck IV calystegine content consist of the sum of single calystegine pools (see Table 29 for detailed fractionation results); the values in black rectangles represent percental amount of a certain calystegine related to the corresponding calystegine content of purified Merck I extract

3.1.2.   Order of elution of calystegines

Following the established scheme for separation of calystegines (2.2 Methods, Table 14), the order of elution of calystegines over the third column reflects their basicity (Figure 8). Characteristics of fractions and pools from the separation of calystegines over the Merck IV column are presented in Figure 9. For the more complete insight of the elution course, the level of fractionation achieved was additionally characterised with the relationship between the pooled calystegine fractions, representing the distribution and dynamics of calystegine pools during the elution.

Raw extract from potato sprouts underwent two purification steps (step 1 on a Merck I and step 2 on a Merck III ion exchanger column) before the Merck III-purified extract was fractionated over a Merck IV ion exchanger column. GC chromatograms of the extracts after purification steps, that demonstrate the level of extract purity, are show in Figure 9, Figure 10 and Figure 11.
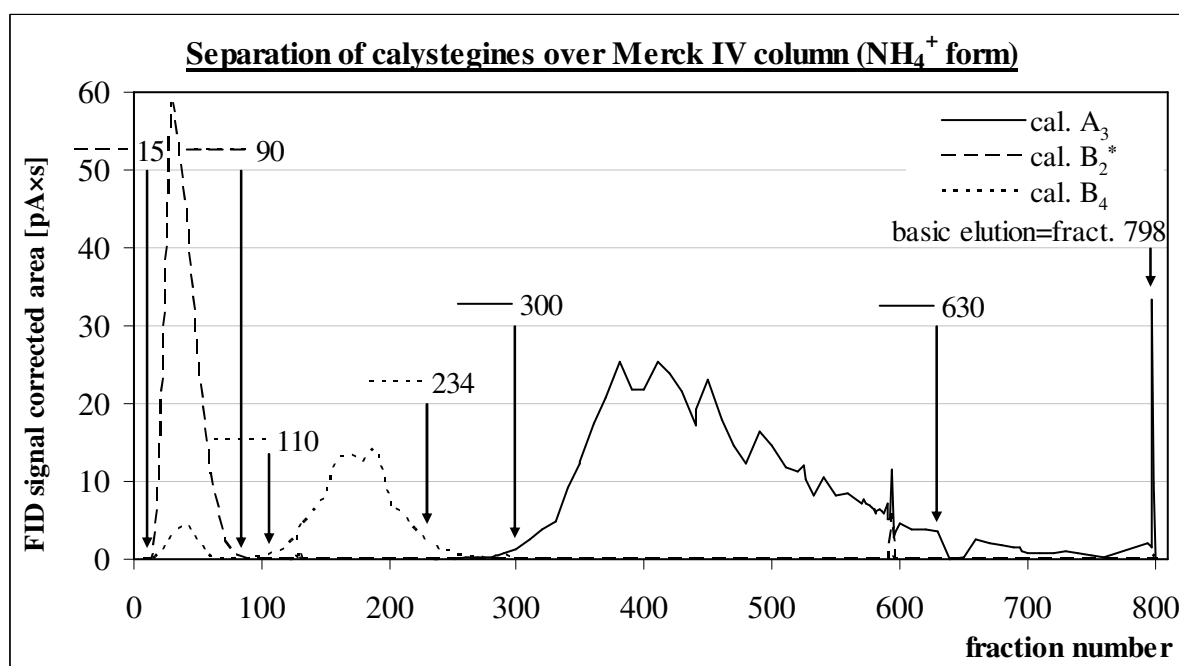
Figure 8: Order of elution of calystegine fractions during the separation on a Merck IV column

Arrows point to the numbers of the bordering fractions of pure calystegine pools. On the far right is shown the first ammonia fraction, that eluted the remaining calystegines from the column (corresponds to the sudden jump of the signal line and abrupt end of the elution); [*] actual corrected areas of FID signal (calystegine B_2) divided by 10, so that all the signal values could fit to the same diagram frame.

In Figure 9, the horizontal bar represents calystegine pool volumes as fractions of the column volume. The percent values were divided by factor 100 for better readability and display of the numbers. Those data represent how many column volume equivalents of water were

necessary in order to elute a certain calystegine pool; the 68 mL Merck IV bed was eluted with a total of 11.4 liters of water or ca. 16700% of bed volume.
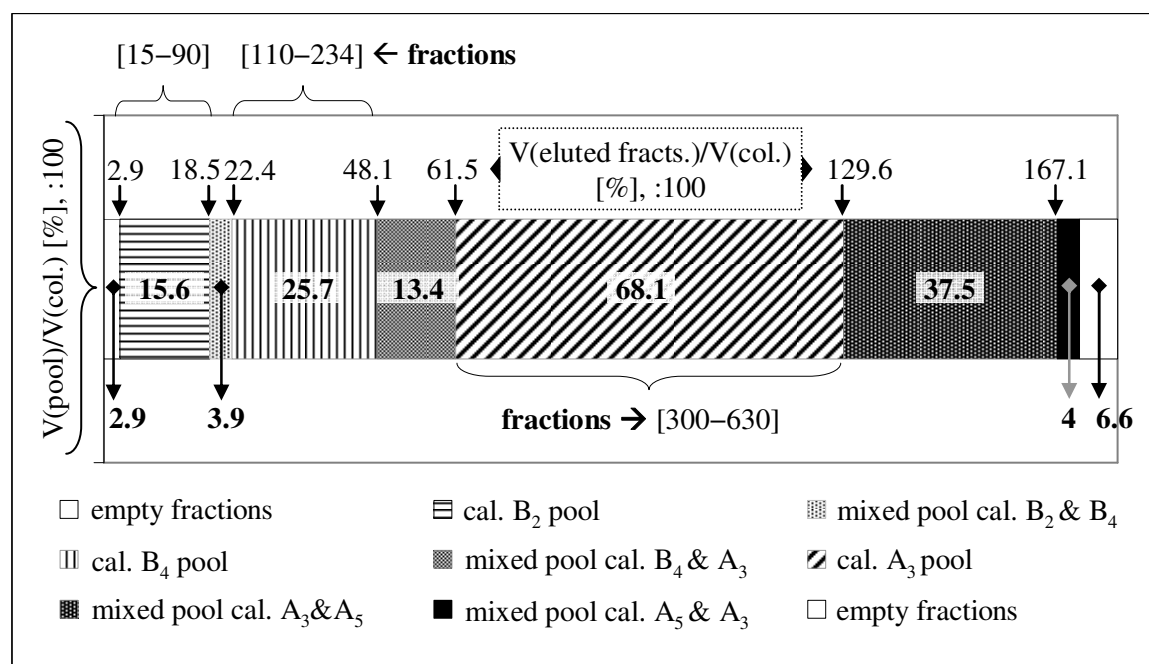
Figure 9: Distribution of the calystegine pools during the elution
– calystegine pools presented as ratios of pool volume to column volume

Curly brackets above and below the bar are demarcations for the pure calystegine pools and indicate pool boundaries with fraction numbers. The last eight fractions (fractions 795–802) were flushes that had bigger volumes than the majority of the fractions (fractions 1–794), about once to twice the column volume.

The pure pool of calystegine B_2 contained only 76 fractions (9.5% of the total fraction number, 8.8% of the total volume eluted, i.e. 15.6 column volumes). The pool of calystegine B_4 comprised fractions 110–234. That amounts to 124 fractions, i.e. 15.6% of all fractions, 14.5% of the total volume eluted (~25.7 column volumes). The pool of calystegine A_3 comprised fractions 300–630; a total of 331 fractionsthat represented 41.3% of all fractions and 38.3% of the total eluted volume (37.5 column volumes).

"Bleeding" of calystegine B_2 from the Merck IV column during fractionation was noticed. Although it should have stopped flowing out soon after the main calystegine B_2 portion was eluted, forming the main calystegine B_2 pool core, calystegine B_2 traces were noticeable in the B_4 pool (which was expected, since they are neighbouring pools), but also later, e.g. in the main calystegine A_3 pool. Here, it still amounted to about 0.14% of the total calystegine B_2 content measured in the eluate from the Merck I column or 0.612% of calystegine $A_3 + B_2$

sum in the pool. In the last pool, mainly a mixture of calystegines A_3 and A_5, B_2 content is still 0.599%. The compositions of the calystegine pools are shown in Table 29 (absolute values, calystegine content) and Table 30 (relative values, percental calystegine content).

Table 29: Calystegine contents of Merck IV pooled fractions

cal. pool fracts.	B_2 15–90	B_2 & B_4 91–109	B_4 110–234	B_4 & A_3 235–299	A_3 300–630	A_3 & A_5 631–797	A_5 & A_3 798–799
cal. A_3	–	–	–	1.01 ± 0.13[*2]	**186.6** **± 14**	5.42 ± 0.09	1.57 ± 0.14
cal. B_2	**816** **± 70**	0.57 ± 0.033	0.61 ± 0.017	0.16 ± 0.018[*3]	1.15 ± 0.12	–	–
cal. B_4	5.77 ± 1.09[*1]	0.43 ± 0.014	**45.12** **± 1.39**	1.48 ± 0.16	–	–	–
cal. A_5	–	–	–	–	4.25 ± 0.25	1.16 ± 0.02	2.44 ± 0.22

Calystegine contents expressed in mg; mean values of 3 samples ± standard deviations. Values in bold script represent contents of the corresponding pure calystegine pools; numerated asterisk signs in exponent show standard deviations above acceptable value of 10% → % s.d. (calystegine content): [*1]=19%; [*2]=12%; [*3]=13%

Table 30: Purity of calystegine pools

pool No.: cal.: fractions:	1 B_2 15–90	2 $B_2 > B_4$ 91–109	3 B_4 110–234	4 $B_4 > A_3$ 235–299	5 A_3 300–630	6 $A_3 > A_5$ 631–797	7 $A_5 > A_3$ 798–799
cal. A_5	–	–	–	–	2.11 (± 0.04)	16.42 (± 0.05)	**43.21** **(± 1.55)**
cal. A_3	~ 0.04	–	0.44 (± 0.14) [‡]	**26.96** **(± 0.14)**	**92.64** **(± 0.14)**	**76.70** **(± 0.04)**	27.76 (± 0.60)
cal. B_4	0.66 (± 0.17) [‡]	**24.94** **(± 0.94)**	**91.37** **(± 0.75)**	**39.55** **(± 0.58)**	–	0.43 (± 0.06) [‡]	0.29 (± 0.07) [‡]
cal. B_3	0.08 (± 0.01)	31.66 (± 0.36)	4.69 (± 0.02)	1.78 (± 0.16)	0.10 (± 0.02) [‡]	0.11 (± 0.003)	0.21 (± 0.04) [‡]
cal. B_1	0.04 (± 0.01) [‡]	3.53 (± 0.11)	–	4.61 (± 1.08) [‡]	0.52 (± 0.14) [‡]	2.35 (± 0.05)	1.04 (± 0.01)
cal. B_2	**92.42** **(± 0.44)**	**32.44** **(± 0.90)**	1.23 (± 0.01)	4.14 (± 0.06)	0.57 (± 0.04)	0.33 (± 0.04) [‡]	0.13 (± 0.02) [‡]

Purity as ratios [%] of calystegine FID signals to total sum of signals in every pool; signals of solution and derivatisation impurities were not taken into consideration; [‡]: % s.d.(m.v.) > 10%; bold script: the prevailing calystegine type in the corresponding pool.
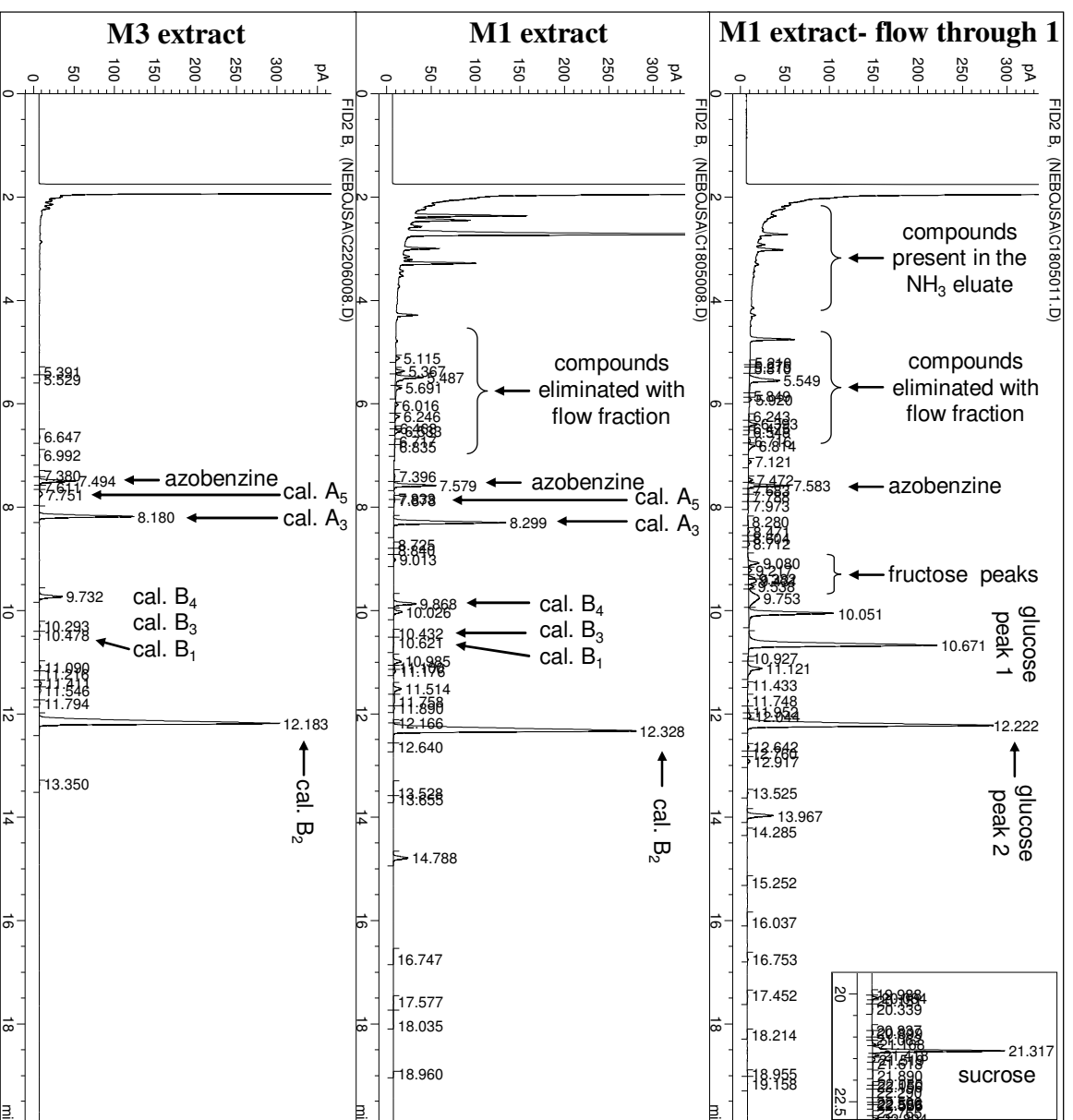
Figure 10: GC chromatograms of eluates from purification steps 1 and 2 (Merck I and III)- difference between flush and eluate fractions

Flow-through 1 was the flow through generated during loading of the raw extract (1060 mL) onto the Merck I column (120 mL bed volume) and was collected as a separate fraction. Then, the column was washed with 8.3 column volumes of Aq. bidest. (see 2.2 Methods, Table 14). This fraction was collected as flow-through 2. M1 extract refers to the ammonia eluate (2.1 column volumes) of the Merck I column, including additional washes with Aq. bidest. (5 column volumes). This extract represents the calystegine-containing fraction of purification step 1. M3 extract represents the calystegine-containing fraction of purification step 2: M1 extract was applied onto the Merck III column and the column was washed with 6.4 column

volumes of Aq. bidest. The wash liquid, containing the calystegines, was immediately caught and saved.
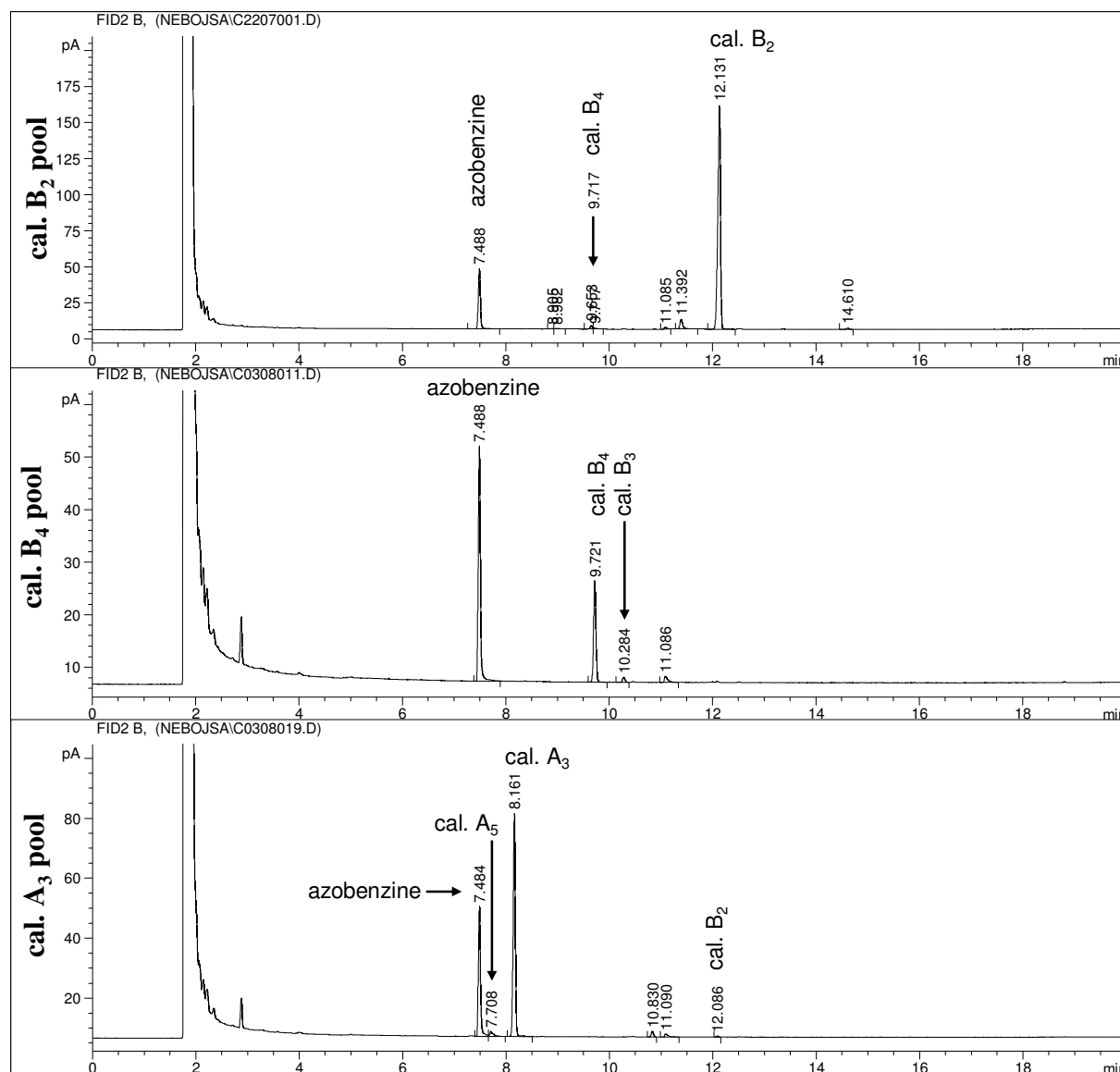
Figure 11: GC chromatograms of separated calystegine B_2, B_4 and A_3 pools (fractionation over Merck IV column, NH_4^+ form)

Overview of dry weights of calystegine-containing fractions after each step of purification – Extract dry weight was determined after each purification step (Figure 12). Percental dry weight of different purification steps was related to 113.88 g of extracted sprouts dry weight. Calystegine dry weight sum of A_3, B_2 and B_4 pool amounted to 1.024% of total sprouts dry weight: that was percental amount of relevant calystegines related to sprouts dry weight. No sum of complete Merck IV pooled fractions dry weight was known, since not all Merck IV pools were lyophilised, but only the ones with high calystegine content.
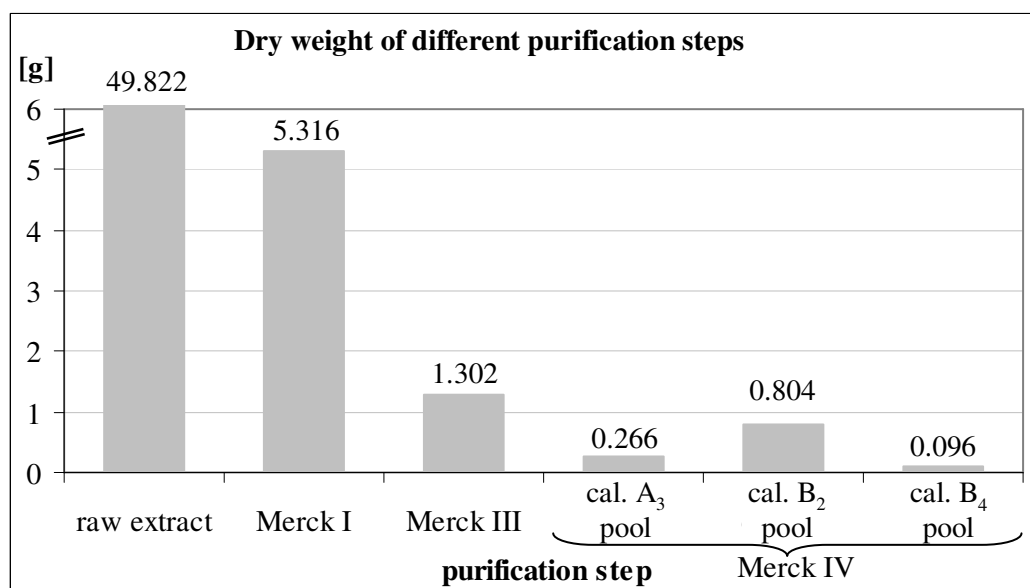
Figure 12: Dry weights after successive purification steps

Table 31 shows the relative amounts, as determined by GC, of the three main calystegines (A_3, B_2 and B_4) in the total material dry weights after the individual steps of purification.

Table 31: Relative calystegine content (GC) in corresponding calystegine pools related to total dry weight of different purification steps

	dry sprouts cal. pool/ (d.w.(sprouts))	**raw extract** [*] cal. pool/ (d.w.(r.e.))	**Merck I** cal. pool/ (d.w.(M1))	**Merck III** cal. pool/ (d.w.(M3))	**Merck IV** [**] cal. pool/ (d.w.(pool))
calystegine pool:	[g/g = %]				
cal. A_3	0.16 ± 0.01	0.37 ± 0.03	3.51 ± 0.27	14.33 ± 1.08	70.23 ± 5.31
cal. B_2	0.72 ± 0.06	1.64 ± 0.14	15.35 ± 1.32	62.68 ± 5.37	101.47 ± 8.70
cal. B_4	0.04 ± 0.001	0.09 ± 0.003	0.85 ± 0.03	3.47 ± 0.11	46.82 ± 1.45
cal. $A_3+B_2+B_4$	0.92 ± 0.05	2.10 ± 0.11	19.71 ± 1.05	80.48 ± 4.28	90.48 ± 4.68

[*] = 50% MeOH extract; [**] = each calystegine type refers to its representing pool (highest content and purity) obtained by separation over Merck IV. Sum of calystegine $A_3+B_2+B_4$ values (90.5) shows how pure calystegine pools are by comparing their calystegine content by GC and pool d.w.; for exact calystegine content and percental calystegine amoint in correcponding pools see Table 29 and Table 30

3.1.3. Confirmation of identity of calystegines − structure analysis
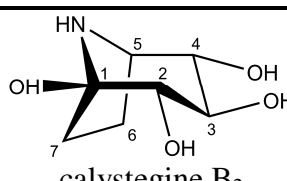
● GC-MS analysis of calystegines

Calystegine signals in GC-MS chromatograms of the pooled calystegine fractions (Figure 53 – Figure 58) corresponded with those of calystegine standards. Spectra of fragments of calystegine samples also corresponded widely with literature data (Dräger, 1995; Molyneux et al., 1993).

● NMR analysis of calystegine pools

Spectral data obtained by ^{13}C NMR in TMS for calystegine A_3, B_2 and B_4 pools are shown in Table 32.

Table 32: ^{13}C NMR spectral data (D_2O, 100 MHz) of calystegines

	literature data			obtained cal. pools			carbon atom (C) functional type
	chemical shift (δ), [ppm]			chemical shift (δ), [ppm]			
calystegine carbon No.	$A_3{}^*$	$B_2{}^*$	$B_4{}^{**}$	A_3	B_2	B_4	calystegine B_2
C-1	93.6	93.2	92.5	n.l.	90.4	n.l.	quaternary C
C-2	82.5	80.4	79.6	79.4	77.7	76.5	methine C
C-3	72.8	77.7	73.8	69.8	74.93	70.9	methine C
C-4	42.6	77.6	74.8	39.4	74.87	72.1	methine C (B_2 & B_4); methylene C (A_3)
C-5	54.3	58.6	59.1	51.7	55.8	56.4	methine C
C-6	29.4	24.5	25.1	26.5	21.8	22.3	methylene C
C-7	31.8	31.5	29.8	28.9	28.8	26.9	methylene C

* : (Asano et al., 1995a)
** : (Asano et al., 1996b)
n.l. = noise level, weak signal

The measured chemical shifts for the calystegines are in accordance with the literature data (Asano et al., 1996b; Asano et al., 1995a; Goldmann et al., 1990). The distinct resonance arising from C-1 is missing in the NMR spectra of calystegines A_3 and B_4, although for B_4 a very weak signal at 90 ppm was noticed. The NMR spectra of calystegines A_3 and B_4

contained some unidentified chemical shifts, which might result from certain impurities. For calystegine A_3, two unidentified minor resonances were detected: 62.6 and 72.1 ppm. For calystegine B_4, the same two unidentified signals, equivalent to those in the spectrum of calystegine A_3, were detected: 62.6, which was more distinct here than for calystegine A_3, and 73.0 (a minor one like for calystegine A_3). Other unidentified signals were minor. Their signal strengths resembled the signal of 73.0, except one: 71.8. This signal was also strongly pronounced, almost as high as the chemical shift belonging to C-4. It might be an alternative C-4 signal, i.e. it was hard to detect with certainty which one of those two tight neighbouring signals is of C-4.

3.1.4. Discussion: Purification, separation (isolation), content and purity of calystegines

<u>**Purification of calystegines**</u>

The overall fresh weight-to-dry weight ratio of the potato sprouts used for calystegine extraction was approximately 5:1, comparable to the results of Keiner and Dräger (Keiner and Dräger, 2000), where also ca. 1 cm long sprouts, which developed from tubers after 5 months of dormancy, made up dry mass 15−20% of fresh mass. The raw methanol extract of the sprouts was coloured ruby-brown, due to polyphenolics, anthocyanins and other pigments (Camire et al., 2009). The presence of starch and sugars gave the extract a thick consistency, especially when its volume was reduced under vacuum and foaming was noticed (enhanced by surface active glycoalkaloids such as the saponins solanine and chaconine) (Friedman et al., 2003).

After the first purification step, over the Merck I column, the colour of the calystegine extract (M1) remained brownish-dark red, but it was significantly more transparent and liquid than the raw extract. The consistency of flow-through 1, obtained during application of the raw extract onto the column, was still thick, mainly because it retained the carbohydrates from the sprouts. No calystegines were found in either flush fraction (flow-through 1 or flow-through 2) after purification step 1. Calystegine content in the Merck I-purified potato sprout extract is comparable to data in the literature (Keiner and Dräger, 2000). The proportion of characteristic calystegines in the potato sprouts also followed the trend already described in literature. Some variations in calystegine content are expected between different cultivars as well as between different plant tissues (Friedman et al., 2003; Keiner and Dräger, 2000). The highest concentrations of calystegines were recorded in short sprouts of potato tubers, 3 mg/g fresh weight, which is approximately 1.5% of dry weight (Keiner and Dräger, 2000). The

calystegine content in the M1 extract shown in Figure 7 (10403 µg/g d.w.), when divided by the f.w./d.w. ratio (4.74), provides a value of 2195 µg/g fresh weight that fits well with the result of Keiner and Dräger (Keiner and Dräger, 2000).

According to the same source, the sum of calystegines A_3, B_2 and B_4 made up about 1.3% of the sprouts dry mass (in this case, the percentage of dry mass of 1 cm long sprouts developing after 5 months of dormancy was approximately 18% of the fresh sprout mass). The sum of calystegines A_3, B_2 and B_4 in the M1 extract of sprouts of cultivar Rosara amounted to 1.04% of sprouts dry weight, while after the final separation of the calystegines on Merck IV, it amounted to 0.94% of sprouts dry weight. When M1 extract was applied onto the Merck III column, darkening of resin particles was noticed, indicating the actual process of anion exchange. The colour of the lower part of the column remained unchanged, which indicated that column exchange capacity was not exceeded. The result of purification step 2 was M3 extract that was lighter in colour than the M1 extract: light yellowish-orange (aqueous solution) or light amber when lyophilised.

Separation of calystegines – Elution order of calystegines

In the separation protocol for weakly acidic ion exchange applied here, the main calystegines are eluted in the following order: B_2, B_4, and A_3. This is related to the structure of calystegine molecules, which affects their basic nature and charge in aqueous environment. Calystegine A_3 has one less hydroxyl group than B_2 and B_4. The lack of that group diminishes the $-I$ effect of $-OH$ groups on the nitrogen free electron pair. Thus, the free electron pair of the nitrogen atom of calystegine A_3 is more disposable for protonation in aqueous environment than that in B-calystegines, making calystegine A_3 more basic than calystegines of the B group. The ion exchange material in the separation column is a weak cation exchanger in NH_4^+ form, i.e. with ammonium ions as counter ions. Being more basic than B-calystegines, calystegine A_3 inclines to more frequent permutation with the NH_4^+ counter ions on the surface of the ion exchanger particles, and because of that was eluted slower and later than calystegines of the B-group.

Calystegine B_2 was the first calystegine to be eluted from the column. Its steep and extremely high and narrow peak (that reached ~600 pA×s, Figure 8) clearly showed that it has by far the lowest affinity for binding on the ion exchanger particles. This difference is emphasised by the calystegine-free (empty) fractions eluting between calystegines B_2 and B_4, while the elution profiles of all other consecutively eluting calystegines overlap to some extent. The minor structural difference between calystegines B_2 and B_4 provides no clear explanation for

this difference in affinity. A transitional period of fractions existed between calystegines B_4 and A_3, which contained both. The overlapping fractions between the two also contained negligible amounts of calystegines B_1 and B_3. The abrupt joint elution of calystegines A_5 and A_3 in the last fractions was due to basic elution of the Merck IV bed with ammonia.

Purity of calystegine pools

The M3 extract (aq.) is transparent and clear yellowish-orange, noticeable especially well when the extract was lyophilised. Subsequent fractionation of the M3 extract took place on a Merck IV (NH_4^+ form) column, resulting in separation of the main extract components – calystegines as well as other substances. After lyophilisation, pools of calystegine fractions showed different colours and consistencies. Calystegines B_4 and A_3 were thick, dark and light brownish-yellow liquids, respectively, while calystegine B_2 formed white-yellowish flake-like crystals. Calystegine B_4 was additionally peculiar and distinguishable because of its amorphous structure, which might be due to some sugar-like components in the pool, invisible in GC. The physical properties of the pure calystegines are summarised in Table 33.

Table 33: List of properties of the main pooled, lyophilised calystegine fractions

Pool (order of elution)	colour	consistency
calystegine B_2	yellowish-white	porous flake-like crystals
calystegine B_4	dark yellowish-brown	amorphous, viscous,
calystegine A_3	light yellowish-brown	amorphous, viscous,

Purity of calystegines according to GC and NMR spectra

The pool of calystegine B_2 contained the corresponding calystegine in the highest purity achieved for any calystegine, regarding content by GC related to lyophilised pool dry weight. The reason for this high purity clearly is the previously dicussed, major difference in affinity for the anion exchange matrix between calystegines B_2 and B_4, which led to clean separation with full yield of calystegine B_2, combined with the 18-fold higher absolute amount of B_2 than of B_4 in their respective pools. Using the same approach of comparison (GC content vs. pool dry weight), calystegine A_3 contains ca. 1/3 (30%) impurities (w/w) and calystegine B_4 ca. 1/2 (53%). Visually these data correlate with the colours of the corresponding lyophilised calystegine pools.

Pool purities considering calystegine amounts only, measured by GC and calculated as percent specific-to-total FID area, indicated high purities of calystegines B_2 (~93%) and A_3

(~91%) and a slightly lower purity of calystegine B_4 (~88%). Chemical shifts detected in ^{13}C NMR spectra of the purified calystegines generally corresponded to literature (Asano et al., 1996b; Asano et al., 1995a), principally confirming succesfull purfication. They are approximately 2.7–3.1 ppm downfield from those signals published.

Only calystegine B_2 was obtained in pure form, however, as confirmed by the NMR spectra. In the NMR spectra of calystegines A_3 and B_4, on the other hand, the presence of additional, unidentified signals were noticed for both calystegines A_3 and B_4. The calystegine B_4 spectrum contains twelve unidentified chemical shifts belonging to impurities. Extent or identity of the impurities could not be determined based on the resonance intensities in the ^{13}C NMR spectral data. Furthermore, in the calystegine B_4 and A_3 NMR spectra, the presumed quaternary C-1 shift resembled a noise peak. The lack of clear quaternary C-1 chemical shifts might be due to their typically smaller intensities than for the other carbon atoms. MS spectra as well as retention times in GC chromatography of the calystegine references, however, confirm the identity of both calystegines A_3 and B_4.

If the relationship between the colours of the lyophilised pools and calystegine pool purity is taken into consideration, it can be concluded that the pools of calystegines A_3 and B_4 contain optically visible impurities that stain the pool and that are invisible in analysis by GC. These impurities could relate to the unknown NMR signals that appear in those two calystegine pools. The fact that the calystegine B_4 pool is coloured more intensively brownish than the light brownish-yellow calystegine A_3 pool correlates with a higher number of unidentified chemical shifts. A reason for not seeing these impurities in GC chromatography may lie in the structure of those compounds. If these molecules were bigger than calystegines, their silylated derivatives would most probably not be vaporised under the GC conditions applied, and could thus neither be detected in GC itself nor, obviously, in secondary MS.

3.2.   Calystegine content by CZE and cITP

3.2.1.   Calystegine content determination by CZE

A series of different background electrolytes ranging from pH 4.5 to 7.5 were tried out. Several cationic compounds containing UV chromophores, such as creatinine, pyridine, quinine, and histidine were applied as carrier cation (data not shown). Background electrolyte (BGE) with creatinine, buffered with caproic acid to pH 4.8, did not allow full separation of calystegines from the matrix. High concentrations of creatinine creatinine ($\geq$ 10 mM) in BGE, for prevention of electrodispersion, led to very high UV absorption, and consequently poor sensitivity. Lower concentrations of creatinine ($\leq$ 2 mM) did not prevent electrodispersion, which caused poor peak shape. Pyridine (pH $\sim$ 5.1) as carrier ion gave similar results. Using quinine as carrier ion (pH > 6), calystegines were separated from the matrix at low concentration of quinine (maximum 5 mM) and background absorption was sufficiently low, but electrodispersion remained. Electrolytes containing histidine and buffered to pH 6.6 with BES appeared to be most suitable for set-ups with detection at 210 nm. The sensitivity of this method was improved with 1 mM quinine as co-ion in the electrolyte. Unfortunately, the separation of calystegine A_3 was disturbed by an eigenpeak and the mobility of calystegine B_2 was low and interfered with EOF at higher pH (pH > 7). The optimised BGE (buffer composition: Chapter 2.2.5, Table 24) had very low conductivity, so high voltage could be applied to accelerate analysis (a current of only 3 μA at 30 kV over the capillary). A detection wavelength of 300 nm was selected for conversion of negative peaks to positive ones and the reference wavelength was set at 210 nm.

The basic characteristics of the CZE method are summarised in Table 34. Typical electropherograms of standard mixture of calystegine A_3 and B_2 and of a sample of potato extract are shown in Figure 13 and Figure 14. Migration times of calystegines in real samples were longer than those of the standard mixture due to matrix effects (huge amounts of alkali and alkaline earth metals and basic amino acids in complex samples), that lead to transient ITP and fluctuations in the strength of the electrical field in the sample zone, which is a known and common phenomenon in capillary zone electrophoresis (Boden and Bächmann, 1996; Johansson et al., 2003).

Table 34: Characteristics of the method of CZE for calystegines determination

Characteristic	calystegine A$_3$	calystegine B$_2$
Migration time (min) [1]	2.08	2.55
Repeatability of migration time (RSD in %) [1]	0.45	0.56
Intra-assay repeatability (RSD in %, n = 6) [2]	4.5	3.8
Accuracy (%, recovery) [3]	95 ± 4	97 ± 6
Linearity (µg/mL) [4]	10–100	10–100
intercept (µg/mL)	−0.63	−0.04
slope (min µg/mL/mAU/s)	3.64	3.89
correlation coefficient	0.9994	0.9999
Limit of detection (µg/mL) [5]	2.9	3.2
Limit of quantification (µg/mL) [6]	9	10

[1] average migration time of five consecutive analyses of a reference mixture of calystegines A$_3$ and B$_2$ (20 µg/mL each); [2] analyses of fresh extracts of whole potatoes, cultivar Karin (Suchdol), (50 g/200 mL 50% methanol) repeatedly extracted and analysed within one day; [3] as [2], with addition of standards A$_3$ and B$_2$ (50 and 100 %); [4] relationship between corrected area and concentration of calystegines; [5] based on signal/noise ratio = 3; [6] based on signal/noise ratio = 10
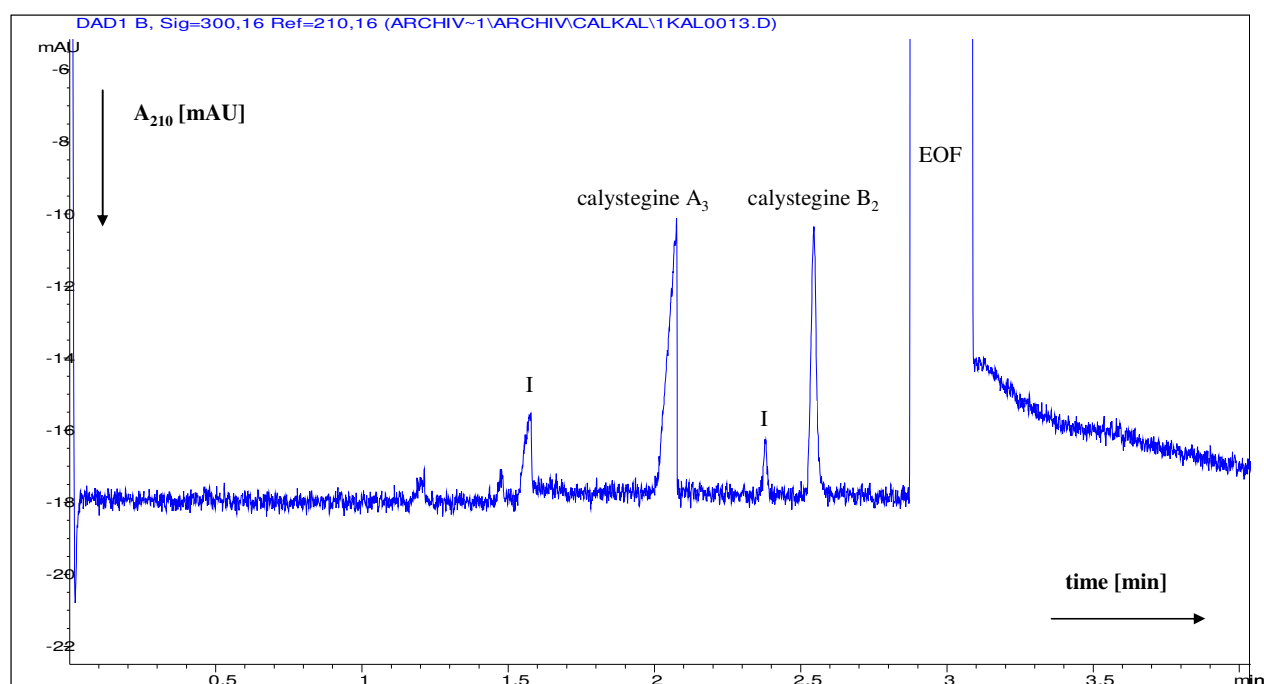
Figure 13: Electropherogram (trace from UV detector) of a mixture of calystegine A$_3$ and B$_2$ references (10 µg/mL each); I = impurity from standards
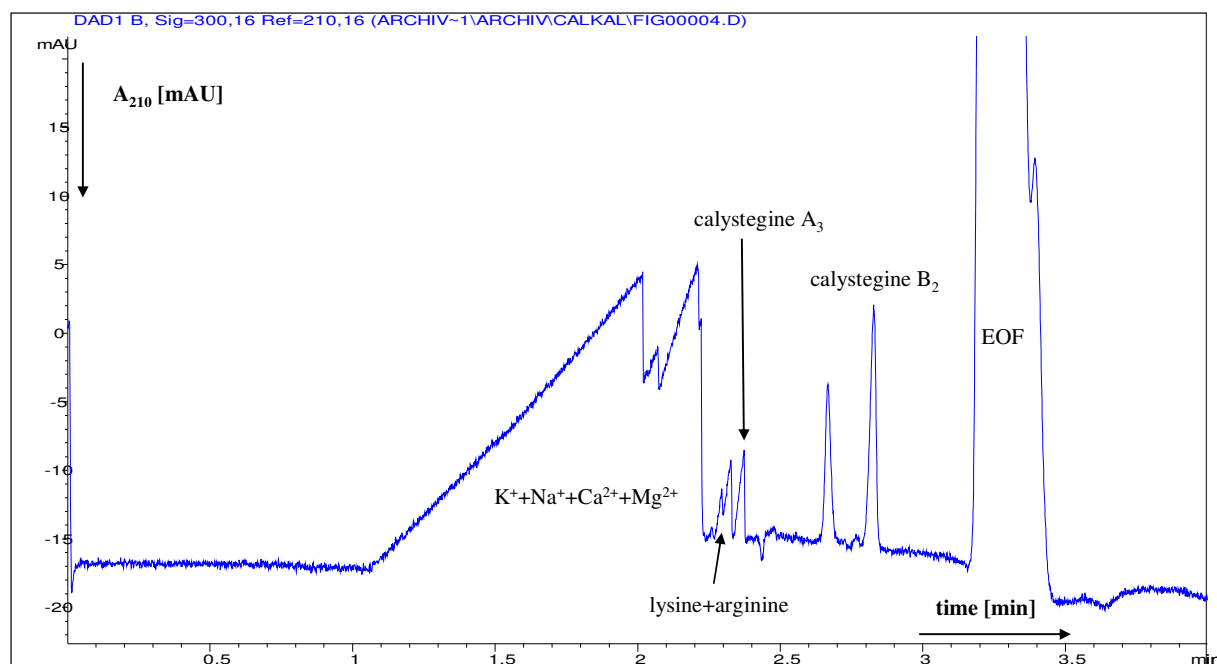
Figure 14: Electropherogram (trace from UV detector) of an extract of potato, cultivar Karin (lyophilised skin, 2 g/50 mL 50% methanol); (K^++Na^++Ca^{2+}+Mg^{2+} = mixture of alkali metal and alkaline-earth metal cations)

3.2.2. Calystegine content determination by cITP

Being medium-strong bases, calystegines are protonated up to pH = 10. Calystegine A_3 is a stronger base (pK_a = 8.3) than B_2 (pK_a = 7.3) (Biastoff and Dräger, 2007), and its molecular weight is 10% lower. In a buffer of approximately pH = 6, calystegine A_3 should have higher mobility than B_2 and their separation should be complete. Preliminary experiments of cITP analysis at pH = 6 of leading electrolyte (LE) confirmed the complete separation of calystegines. Nevertheless, some components from the potato sample (basic amino acids such as lysine and arginine) interfered with the signal of calystegine A_3 (data not shown). Full separation of calystegines from the sample matrix and, additionally, better separation through decreased mobility was observed when leading electrolyte pH was increased to 7 (see RSH value in Table 35). Moreover, methanol was added to both leading (LE) and terminating (TE) electrolytes (Chapter 2.2.5., Table 25) in order to ensure solubility of calystegines and compatibility with the sample extract. The basic characteristics of the cITP method are summarised in Table 35.

Table 35: Characteristics of the cITP method for determination of calystegines

Characteristic	calystegine A_3	calystegine B_2
RSH (-) [1]	0.339 ± 0.02	0.907 ± 0.02
Intra-assay repeatability (RSD in %, n = 6) [2]	3.8	3.3
Accuracy (%, recovery) [3]	97 ± 3	99 ± 5
Linearity (ng)	25–500	25–500
intercept (ng)	1.85	4.42
slope (ng/s)	3.34	3.60
correlation coefficient	0.9998	0.9990
Limit of detection (ng) [4]	3.65	4.01
Limit of quantification (ng) [5]	11	12

[1] RSH = relative step height; mean value from six consecutive analyses of a mixture of calystegines A_3 and B_2 (50 µg/mL each, 5 µL injected); [2] analysis of extract of whole potato tuber, cultivar Karin (Suchdol) (100 g/L in 50% MeOH), repeatedly extracted and analysed within one day; [3] as [2], with addition of A_3 and B_2 standards (50 and 100 %); [4] calculated as minimum detectable step length (1 s). LOD is the *de facto* response factor (= slope); response factors based on molar concentration are practically the same for A_3, B_2 and TBA. Using the sample valve with a fixed internal loop of 30 µL, the LOD corresponds to a concentration as low as 0.1 µg/mL. For injection by syringe (10 µL), LOD corresponds to 0.4 µg/mL; [5] calculated as triple of LOD.

The isotachopherogram of a standard mixture of calystegines A_3 and B_2 is depicted in Figure 15. Figure 16 shows the isotachopherogram of a sample extract from whole potato. Using the optimised leading and terminating electrolytes (Chapter 2.2.5), cITP was sufficiently sensitive and reproducible (RSD $\approx$ 4%) to determine calystegine content in mg per kg potato tubers.
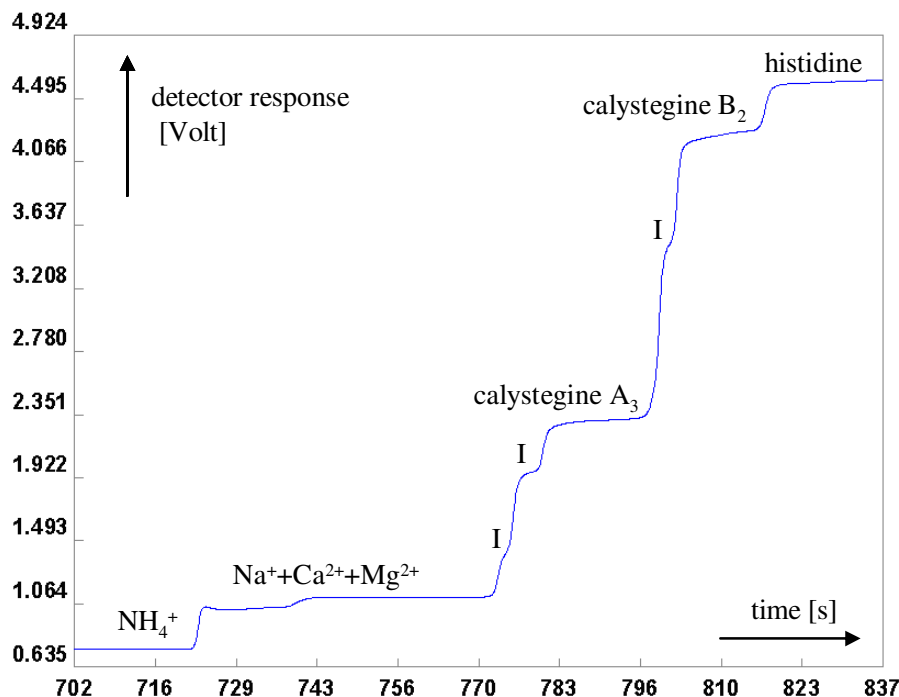
Figure 15: Isotachopherogram (trace from conductometer of analytical capillary) of standard calystegines A$_3$ and B$_2$

(100 ng each, 2 mL of 50 ng/mL), I = impurity from standards.
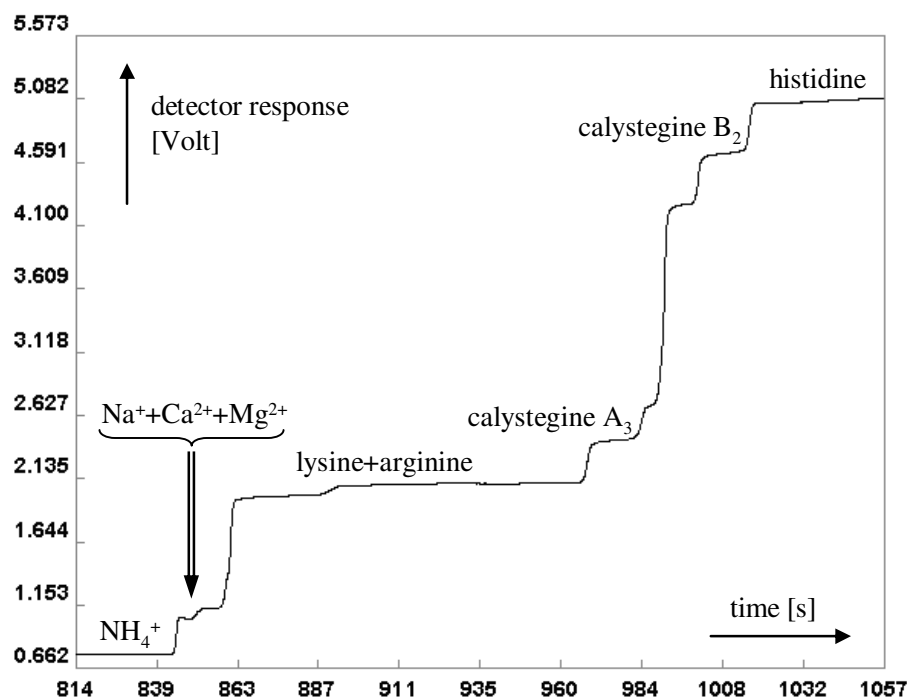
Figure 16: Isotachopherogram (trace from conductometer of analytical capillary) of a sample extract of whole potato, cultivar Karin

(fresh whole potato, 50 g/200 mL of 50% methanol, diluted 5-fold, 10 µL injected). Conditions of analysis were the same as for the previous figure.

3.2.3. Comparison of CZE, cITP and GC analysis for determination of calystegine content

CZE and cITP were compared with conventional gas chromatography for determination of calystegine contents in order to estimate absolute deviations. Since performing all experiments required four months time, the use of the same samples in all experiments was not possible due to lack of long-term stability (fresh potato). In the case of lyophilised samples, only limited amounts were available, for which reason three different sample series were used.

Table 36 summarises measurements by CZE and cITP in a series of potato samples (whole potato). Correlation and regression analysis revealed that both methods identified practically identical amounts of calystegines in potato samples.

Table 36: Comparison of cITP with CZE determination

Potato cultivar and place of origin [*]	cITP (mg/kg)		CZE (mg/kg)	
	cal. A_3	cal. B_2	cal. A_3	cal. B_2
Ditta, Stachy	46	60	48	69
Karin, Stachy	54	67	52	70
Saturna, Stachy	58	75	57	79
Impala, Stachy	74	98	74	108
Ditta, Valečov	62	62	59	64
Karin, Valečov	68	125	69	132
Saturna, Valečov	34	38	34	38
Ditta, Přerov	30	34	30	38
Karin, Přerov	61	58	59	59
Saturna, Přerov	40	45	39	47
Impala, Přerov	20	25	18	24
Ditta, Suchdol	31	40	40	61
Karin, Suchdol	84	119	85	118
Saturna, Suchdol	110	121	117	119
Impala, Suchdol	9	18	11	19

[*] samples taken from whole fresh potato tubers; the same cultivar may have different calystegine content, depending on the place of cultivation

Regression analysis:

calystegine A_3: CZE = 1.02 (± 0.03) × cITP - 0.26 (± 2.0), correlation coefficient 0.9925

calystegine B_2: CZE = 0.99 (± 0.05) × cITP – 4.6 (± 3.4), correlation coefficient 0.9861

The CZE method was compared with GC for a series of potato samples (whole potato, flesh, and peel). Results are shown in Table 37. Regression analysis showed that the slope of the relationship GC vs. CZE is nearly one for both calystegines A_3 and B_2 and the intercepts approach zero (considering standard deviations of coefficients). The somewhat closer relationship for calystegine B_2 could be explained by a generally better separation of this calystegine from the sample matrix than achieved for calystegine A_3.

Table 37: Comparison of CZE with GC determination

potato cultivar	sample [*]	GC (mg/kg)		CZE (mg/kg)	
		cal. A_3	cal. B_2	cal. A_3	cal. B_2
Ditta	whole potato	184	314	146	283
	flesh	196	173	106	131
	peel	258	927	187	772
Granola	whole potato	172	277	131	220
	flesh	196	182	138	139
	peel	132	706	120	756
Karin	whole potato	175	362	184	495
	flesh	120	150	104	115
	peel	325	909	311	868
Samanta	whole potato	150	332	140	333
	flesh	114	189	125	173
	peel	239	717	334	930
Magda	whole potato	233	330	318	397
	flesh	201	253	201	226
	peel	467	870	409	815

[*]: lyophilised material;

Regression analysis:
calystegine A_3: GC = 0.92 ($\pm$ 0.16) $\times$ CZE – 2.6 ($\pm$ 36), correlation coefficient 0.852
calystegine B_2: GC = 0.99 ($\pm$ 0.08) $\times$ CZE + 0.7 ($\pm$ 44), correlation coefficient 0.956

Another series of samples from whole potatoes or parts (flesh or sprouts) was analysed by GC and cITP. In this case, the concentration range of calystegines varied over two orders of magnitude (from tens up to thousands of mg/kg). Both methods gave comparative results (Table 38). Like in the comparison of GC vs. CZE, a tighter relationship was found for calystegine B_2.

Table 38: Comparison of cITP with GC determination

sample (potato cultivar or source and material type [*])	GC (mg/kg)		cITP (mg/kg)	
	cal. A_3	cal. B_2	cal. A_3	cal. B_2
Agria, whole potato	22	34	60	53
British Columbia Blue, flesh	177	233	155	229
British Columbia Blue, whole potato	195	179	191	177
British Columbia Blue, sprouts	1169	3556	1048	3612
sprouts (Čepl, batch 1)	572	1850	669	1829
sprouts (Čepl, batch 2)	614	2010	746	2308
commercially purchased potatoes (sprouts) batch 1a	1522	2450	1381	2407
commercially purchased potatoes (sprouts) batch 1b	1436	2408	1370	2480
commercially purchased potatoes (sprouts) batch 2a	1543	1499	1510	1585
commercially purchased potatoes (sprouts) batch 2b	1554	1531	1342	1513
Desirée, sprouts	712	480	585	414
Desirée, sprouts	846	563	604	433

[*]: all potato samples were lyophilised prior to analysis

Regression analysis:

calystegine A_3: GC = 1. 08 (± 0.07) × cITP – 7 (± 62),   correlation coefficient 0.982

calystegine B_2: GC = 0.96 (± 0.03) × cITP + 38 (± 47), correlation coefficient 0.996

3.2.4. Discussion: Calystegine content determination by CZE and cITP

CZE separation was performed in a fused silica capillary (a hydrodynamically open separation system). Determination of calystegines as borate complexes by CZE with direct UV detection at 191 nm, as published (Bekkouche et al., 2001), had low sensitivity (LOD = 25–50 μg/mL). As derivatisation with a chromophore for enhanced detectability appeared feasible but tedious, indirect UV detection was chosen. However, detector responses for calystegines A_3 and B_2 are very close, showing a difference of only about 3–4% when expressed as RSD (Table 34 and Table 35). Calculation of calystegine content by using an average detector response makes the determination in potato samples more practical.

Calystegine standards are usually difficult to obtain and of variable purity. For routine analysis, an alternative "auxiliary standard" (TBA) was chosen from a number of cationic compounds tested (also lysine, arginine, ornithine, glucosamine). Its advantages are absence in potato samples, economic price, high purity and mobility very close to calystegine A_3. Similar mobility as calystegines and absence of a chromophore in the molecule gave detector responses to TBA, based on molar concentration (CZE) and molar amount (cITP), which were very close to detector response of calystegine A_3. The difference between detector responses to TBA and calystegine A_3, expressed as RSD, is about 2%, which enables calibration of the electrophoretic systems with TBA and quantitative determination of calystegines A_3 and B_2 based on the molar detector response to TBA.

CZE analysis time is half of that of cITP. The total analysis time is about 10 min, including buffer and sample loading. The sensitivity of the indirect UV detection (CZE LOD of 3.2 µg/mL for calystegine B_2, Table 34) is about 15 times better than that published for CZE of borate complexes of calystegines (LOD for calystegine B_2: 50 µg/mL) (Daali et al., 2000). Thus, CZE is still less sensitive than cITP (cITP LOD = 0.1 µg/mL−0.4 µg/mL, Table 35), but nevertheless sufficient for the determination of calystegines in potato samples. The disadvantage of cITP is the duration of analysis (20 min). Shorter columns or higher voltage (driving current) are expected to shorten the run time, but may negatively affect signal separation. Compared to both CZE and cITP, GC is more time consuming and tedious. Since a split injection mode of 1:20 was chosen, sensitivity (GC LOD ≈ 1 µg/mL) was intermediate to those of CZE and cITP. Non-split injection could enhance sensitivity, but larger amounts of silylated samples require frequent cleaning of the injector and installation of the pre-columns.

In conclusion, both the improved CZE and, to a lesser extent, the cITP method of analysis for calystegines appear very suitable for purposes of fast, preliminary screening. However, for sensitive and precise discrimination between and quantification of different, closely related calystegine isoforms (individual members of the A, B or C families, for example), analysis by GC will likely be the reference for some time to come.

3.3.   Transport of calystegines

3.3.1.   Impermeability of the intact Caco-2 cell layer

Prior to performing the calystegine flux assay through monolayer of Caco-2 cells, impermeability of the cell monolayer was tested. High concentrations (5 mM) of calystegines A_3 and B_2 were applied in the donor compartment, together with $[^{14}C]$ D-mannitol, in order to verify the harmlessness of calystegines at that concentration. The electrical resistance of the cell monolayer was 634 ± 40 $\Omega \times cm^2$ before the experiment and after the experiment had increased to 791 ± 225 $\Omega \times cm^2$.

The rate of transport of $[^{14}C]$ D-mannitol, when applied together with 5 mM calystegine A_3 (0.3 %/(h×cm^2)) or B_2 (0.4 %/(h×cm^2)) was below that of $[^{14}C]$ D-mannitol alone (0.5 %/(h×cm^2)), which showed that calystegines did not lead to disruption of the cell monolayer, even in high concentrations (Figure 17).
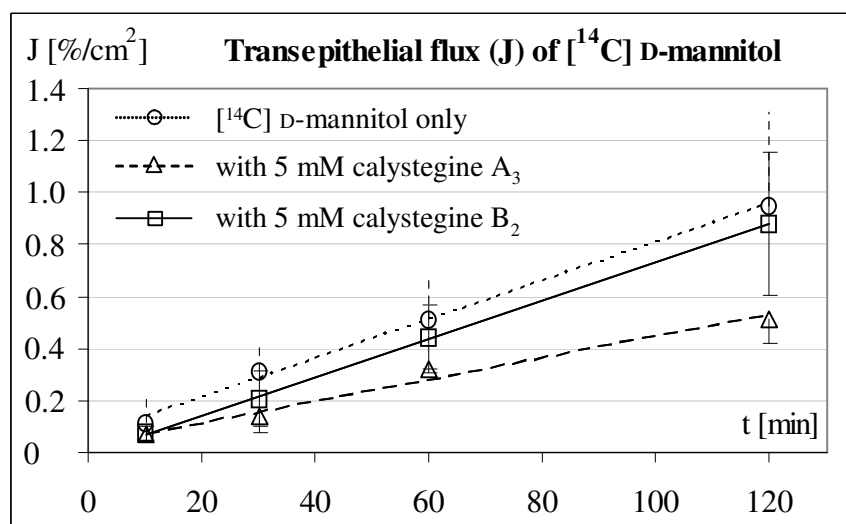
Figure 17: Diagram of transepithelial flux of $[^{14}C]$ D-mannitol alone or with calystegine A_3 or B_2 as a proof for Caco-2 cell monolayer impermeability

Linear regression lines were constructed for $[^{14}C]$ D-mannitol flux values of all the combinations: flux control (mannitol only) and mannitol with calystegine A_3 and B_2 of 5 mM (Table 39).

Table 39: Linear regression line equations for proof of Caco-2 cell monolayer impermeability

sample	linear regression line equation	R^2	transepithelial flux [$\%/(h \times cm^2)$]
[^{14}C] D-mannitol only	y = 0.0074x + 0.0628	0.9970	0.51
--//-- with calystegine A$_3$	y = 0.0041x + 0.0310	0.9826	0.28
--//-- with calystegine B$_2$	y = 0.0074x − 0.0064	0.9996	0.44

y = J (flux) [$\%/cm^2$], x = time [min]

3.3.2. Transport through Caco-2 cells

<u>Kinetics of *β*-glycosidase: basis for the determination of calystegines by enzymatic assay</u>

Transport of calystegine B$_2$ through the Caco-2 cell monolayer was monitored by inhibition of sweet almond *β*-glycosidase. The enzyme assay was used for calystegine B$_2$ quantitation mainly because of its higher sensitivity (LOQ 0.2 µg/mL, LOD 0.03 µg/mL) compared with GC analysis (LOQ 10 µg/mL, LOD 1 µg/mL). Specific activity of sweet almond *β*-glycosidase was 134 ± 2 nkat/mg and K$_m$ for *p*-NPG as substrate was 2.8 ± 0.1 mM (R^2 = 0.99, n = 8, single assays: Appendix, 6.6, Table 47). To assess stability of the assay components and reliability of the assay, eight repetitions were performed with intervals of one hour, using the same solution of all assay components in all repetitions.

Since the *β*-glycosidase assay was designed for quantitation of calystegines in the flux test, the kinetic parameters were determined using the buffers for the Transwell® donor and acceptor compartments. A volume of buffer, corresponding to the sample volume from the flux assay to be used for calystegine determination, was added to the enzyme assay following the pipetting instructions in Scheme 4 (Appendix, 6.6), simulating measurement of flux test compartment samples. The *β*-glycosidase assays for the kinetic parameters at three different pH values were performed in parallel for the direct comparison of the obtained results. K$_m$ values of *p*-NPG in assay with FAB6 and FAB7.5 samples were higher than in PB5 only (3.8 and 3.2 mM compared to 2.5 mM, Table 40). K$_m$ values of substrate in assays with flux samples (FAB6 and 7.5) do not differ significantly from each other (3.8 and 3.2 mM) due to the pH values of the mixtures (Table 9), that are kept very similar by the buffering capacity of PB5.

The Lineweaver-Burk diagram (Appendix, 6.6, Figure 64) demonstrates decreasing V_{max} with increasing pH with FAB6 and 7.5 samples. A slight pH increase (Table 9) leads to a slight decrease of the enzyme activity.

Table 40: Comparison of the kinetic parameters of β-glycosidase in three different pH-environments (enzyme assay PB5 alone and combined with Transwell® compartment buffers for the flux test)

sample name		$V_{max} \pm$ Std. Error [nkat/mg]	$K_m \pm$ Std. Error [mM]	R^2
PB5	(pH = 5.00)	69 ± 1	2.5 ± 0.1	0.9962
PB5 + FAB6	(pH = 5.35)	85 ± 2	3.8 ± 0.3	0.9810
PB5 + FAB7.5	(pH = 5.54)	63 ± 2	3.2 ± 0.2	0.9786

As individual calibration curves for calystegine quantification were necessary for donor (FAB6) and acceptor (FAB7.5) compartments (Appendix, 6.6, Figure 65), to account for the difference in pH, inhibition of β-glycosidase by calystegine B_2 in FAB6 and FAB7.5 was determined. The results were processed using the Enzyme Kinetics Module 1.3 from SigmaPlot, which provided K_i values along with their standard errors. Five different calystegine concentrations in both FAB6 and FAB7.5 were tested for enzyme inhibition; four replicates of each condition were measured (n = 4). Assay set up is described in Chapter 2.5.1, and the pipetting scheme is presented in Scheme 5 (Appendix, 6.6). K_i values of calystegine B_2 for sweet almond β-D-glycosidase were found to be 2.4 ± 0.1 µM (R^2 = 0.9749) in FAB6 and 3.5 ± 0.2 µM (R^2 = 0.9593) in FAB7.5. Inhibition type was selected as competitive (full) (Asano et al., 1996b; Asano et al., 1996c; Asano et al., 1994b; Ikeda et al., 2003; Molyneux et al., 1993). Basically, the same trend was observed in both groups of calculated data: K_m value of the substrate (p-NPG) increased and V_{max} value remained the same with increasing inhibitor concentrations (Appendix, 6.6, Table 48 and Table 49), which additionally implied the full competitive inhibition type.

Table 41: Kinetic parameters for β-glycosidase and inhibition constant of calystegine B_2

inhibitor (solvent)	$V_{max} \pm$ Std. Error (β-glycosidase) [nkat/mg]	$K_m \pm$ Std. Error (p-NPG) [mM]	R^2	$K_i \pm$ Std. Error (cal. B_2) [µM]	R^2
no cal. B_2 (PB5)[‡]	118 ± 2	3.1 ± 0.2	0.9890	-	-
cal. B_2 (FAB6)	108 ± 2	3.2 ± 0.2	0.9871	2.4 ± 0.1	0.9749
cal. B_2 (FAB7.5)	96 ± 3	3.3 ± 0.3	0.9746	3.5 ± 0.2	0.9593

values presented are means ± standard errors (number of samples n = 4, for each one of 5 different substrate concentrations); inhibition type is competitive (full).

Transepithelial flux of calystegine B_2 through Caco-2 cell monolayers

Figure 18 and Table 42 represent transepithelial flux for calystegine B_2. Electrical resistance of the cell monolayer was 911 ± 15 $\Omega \times cm^2$ before the experiment and 1984 ± 905 $\Omega \times cm^2$

thereafter. The amounts of calystegine B_2 in the acceptor compartment were barely quantifiable and ranged from 10–20 µM. The concentration of calystegine B_2 in the acceptor compartment, measured after 2 h, were between 0.1–1% of the initial donor concentration, while the donor compartment concentrations (of calystegine B_2) remained 100 ± 10% of the initially applied test solutions during the whole assay duration of 120 min.
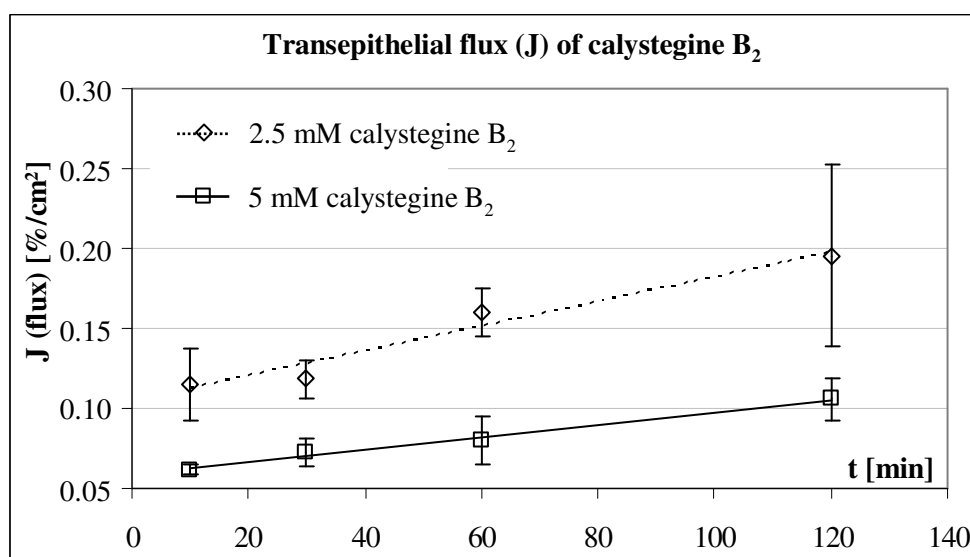
Figure 18: Transepithelial flux of calystegine B_2

Table 42: Linear regression line equations for transepithelial flux of calystegine B_2

sample	linear regression line equation	R^2	transepithelial flux [%/(h×cm²)]
2.5 mM calystegine B_2	y = 0.0008x + 0.1045	0.9584	0.15
5 mM calystegine B_2	y = 0.0004x + 0.0586	0.9928	0.08

y = J (flux) [%/cm²], x = time [min]

Transepithelial flux of calystegine A_3 could not be determined, as weak inhibition of β-glycosidase by calystegine A_3 made quantification far less sensitive than for calystegine B_2 under the same assay conditions. From a concentration series of calystegine A_3, measured to create a calibration curve for inhibition of β-glycosidase, the lowest concentration (0.17 µM) did not inhibit enzyme activity at all, whereas with the highest concentration (16.67 µM) inhibited only about 40% of enzyme activity, i.e. the enzyme retained about 60% its original activity. Compared to that, 16.67 mM of calystegine B_2 inhibited about 80% of enzyme activity.

3.3.3. Discussion: Transport of calystegines

<u>**Impermeability of the intact Caco-2 cell layer**</u>

Mannitol transport did not increase in presence of calystegines, indicating that Caco-2 cell monolayers remained intact and were not damaged even by high concentratins of calystegines within 2 h at 37 °C, which are the conditions for the calystegine flux assay.

<u>**Transport through Caco-2 cells**</u>

Calculations of enzyme activity for the slightly different conditions in the β-glycosidase inhibition assay (PB5 with FAB6 or FAB7.5) (Table 41) showed unaltered K_m, irrespective of pH, while V_{max} decreased slightly with increasing pH. The unaltered K_m value indicated unaffected activity of the enzyme, while the slight alterations of pH, due to the flux test samples, did not impede the β-glycosidase activity. The K_i values for calystegine B_2, both in FAB6 and in FAB7.5, were quite similar and compared well with literature sources (1.2 µM of calystegine B_2 with almond β-glycosidase (Asano et al., 1995a). The confirmation of the inhibition of β-glycosidase by calystegine B_2 also implied that the calibration curve for calystegine B_2 in both Transwell flux test buffers could be considered reliable.

The transepithelial flux of calystegine B_2 was below 0.2 %/(h×cm^2) and the original calystegine concentration in the donor compartments was retained throughout the duration of the assay, which implied, that the transport of calystegine B_2 across confluent Caco-2 cell monolayers was insignificant. The structure of calystegine molecules provides them with hydrophilic features, that impede simple diffusion across cell membranes.

The low level of inhibition of β-glycosidase by calystegine A_3 is in agreement with literature. Judged by their K_i values, calystegine A_3 was described to be an approximately 17-fold weaker inhibitor than calystegine B_2 (Asano et al., 1995a). Since K_i of calystegine A_3 was several times higher than of calystegine B_2, the assay in this set up was not sensitive enough and as that not applicable for measurement of flux of calystegine A_3. Higher concentrations of calystegine A_3 would be needed for inhibition, but additional dilution by taking samples during the flux assay would result in higher volumes of the assay acceptable microtitre plates. Other sample vessels were not attempted and a concentration of calystegine A_3 in the chyme of > 5 mM, as would be necessary in the assay, is not expected.

3.4.   *α*-Glycosidase inhibition

3.4.1. Protein content in the Caco-2 cell lysate

Protein content in Caco-2 cell lysates (Chapter 2.4.1) was determined using the Bradford test (Bradford, 1976). The average yield of soluble protein after clearance by centrifugation was 4.62 ± 0.05 mg of total protein per culture flask (n = 3, Table 43). The cleared protein solutions obtained after harvesting were set to a stock concentration of 0.444 mg/mL of protein dissolved in PB6. Per reaction of the *α*-glycosidase inhibition assay, 450 µL of this protein stock solution was used, containing 200 µg of protein.

Although glucose content in the protein solutions was determined to be up to 5 µg/mL, the glucose signals were hardly detectable even in the large samples for GC, thus allowing this Caco-2 cell-derived glucose to be neglected in the assay.

Table 43: Protein content of three Caco-2 cell passages[*]

No.(passage)	No.(flasks)[**]	V(PB6)/flask [mL]	V(cell susp.) total [mL]	protein/flask [mg]
56	10.43	10	106.8	4.63
75	7	7	49	4.66
83	12	8	96	4.56

[*]   cell passages used for protein extract for three subsequent *α*-glycosidase assay
[**] culture flask surface of 175 cm^2

3.4.2. Kinetic parameters of human maltase and sucrase

Linearity of enzyme activities, measured according to Dahlqvist (Dahlqvist, 1968), was confirmed for protein concentrations between 120 and 490 µg/mL and within a time span of 120 min. Maltase and sucrase kinetic parameters are shown in Table 46. Data are presented as means (n = 3−6) with standard errors, as calculated by SigmaPlot. The activities of both enzymes showed substrate saturation and were suitable for Michaelis-Menten kinetic calculations (Figure 23). The activities of maltase and sucrase, which were measured in the protein extracts, were nicely reproducible. The specific activities were comparable and fit well within the broad range of values found in the literature for extracts from human intestinal mucosa or Caco-2 cells (for maltase: (Quezada-Calvillo et al., 2007; Quezada-Calvillo et al., 2008; Rossi et al., 2006), and for sucrase: (Martin-Latil et al., 2004; Quezada-Calvillo et al., 2007; Trugnan et al., 1986)). Correlating values from the literature are exclusively of the human sources from either intestinal mucosa or Caco-2 cells homogenates, or recombinant

proteins. The K_m value of maltose measured here in Caco-2 cell lysates was 7.3 mM; for human intestinal mucosa, a K_m of 10.7 mM for maltose was reported (Quezada-Calvillo et al., 2007), while the N-terminal maltase moiety of human MGAM, heterologously expressed in *Drosophila* S2 cells, showed a K_m of 4.6 mM (Rossi et al., 2006). A K_m value of sucrose for human sucrase has not been published, so no direct comparison with literature sources of the K_m of 11.1 mM for sucrose, measured in the lysates, was possible.

Another brush border enzyme with α-glycosidase activity is trehalase, which is known to be inhibited by calystegine B_4 (Asano et al., 1996b). For this reason, the Caco-2 cell lysates were also tested for trehalase activity. Although some trehalase activity could be measured, it was barely detectable under the reaction conditions of the α-glycosidase assay. This already low trehalase activity was not favourable for further inhibition assays with calystegine B_4, as enzyme inhibition would result in even lower activities, well below the limit of quantification.

3.4.3. Modeling of the docking of calystegines A_3 and B_2 to recombinant models of human maltase and sucrase

Modeling of possible geometries of docking of calystegines to protein models of maltase and sucrase was examined *in silico* as the first step for preliminary assessment of possible inhibition of intestinal α-glycosidases. In order to assess the reliability of the docking simulations, the highest-scoring arrangement calculated for docking of acarbose to maltase was compared with the experimentally determined arrangement in the X-ray structure of maltase (2QMJ) (Figure 19). The first two moieties of acarbose coincided favourably with each other. They were docked deep in the binding site both in the X-ray stucture and in the calculated model. The other two, solvent exposed, sugar moieties showed slightly different conformations and docking arrangements in model and crystal. These deviations close to the surface of the protein were obviously caused by water molecules, which may stabilise and influence the conformation of acarbose in the X-ray structure, while they were missing in the gas phase docking modeling procedure that was applied here.
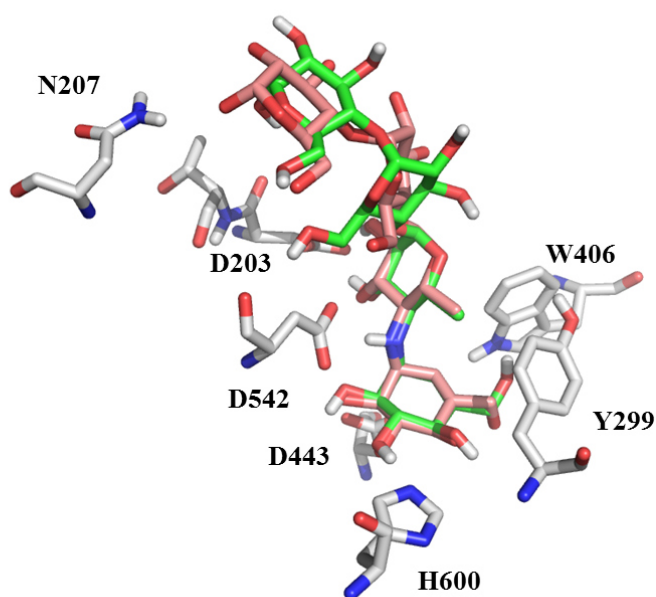
Figure 19: Docking arrangement of acarbose derived from X-ray crystallography (orange carbon atoms) compared to the best calculated docking model (green carbon atoms) on maltase

Figure 20 shows the highest-scoring models caluated for the docking positions of calystegines A_3 (A, B) and B_2 (C, D) in the active sites of maltase (A, C) and sucrase (B, D). Relevant bonds are presented in Table 44.
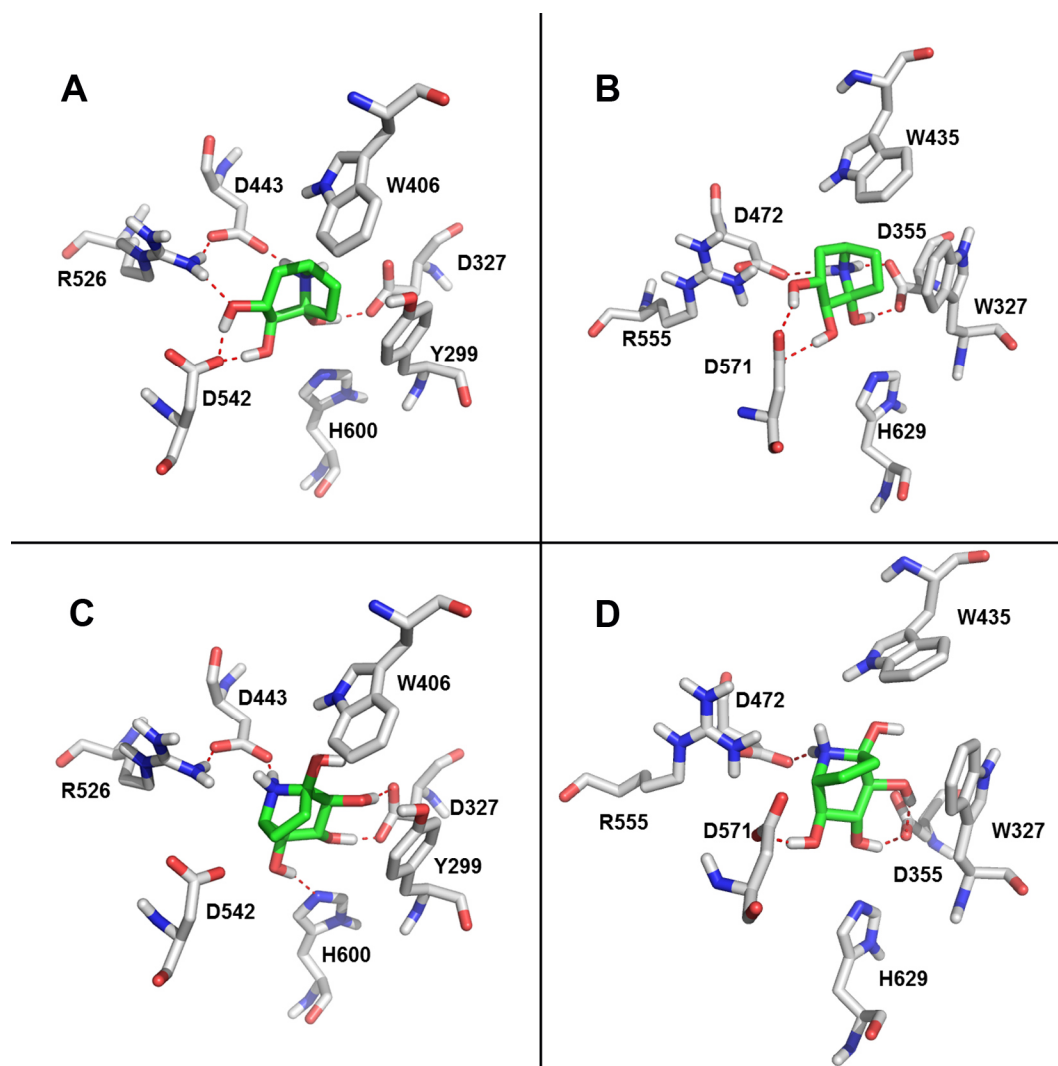
Figure 20: Docking arrangements of calystegines in the active centres of maltase and sucrase

Dotted red lines = H-bonds connecting calystegine hydroxyl and amino groups with amino acid residues; A: calystegine A_3 and maltase, B: calystegine A_3 and sucrase, C: calystegine B_2 and maltase, D: calystegine B_2 and sucrase

Formation of a salt bridge between the positively charged protonated amino groups of calystegines and the aspartate side chains of catalytic nucleophiles (D443 in maltase, D472 in sucrase) was common for all calculated docking arrangements. Further inspection showed that all three hydroxyl groups of calystegine A_3 were modeled to form strong hydrogen bonds to aspartate side chains of acid-base-catalytic residues (D542 and D327 in maltase, D571 and D355 in sucrase). Hydroxyl groups of calystegine B_2 bound to the same aspartate residues, to histidine 600 in maltase and, possibly, to the NH-group of tryptophan 406 in maltase and tryptophan 435 in sucrase.

Table 44: Relevant bonds for docking arrangements of calystegines in the active centres of maltase and sucrase

A calystegine A_3 and maltase		**B** calystegine A_3 and sucrase	
C_1OH	D327	C_1OH	D355
C_2OH	D542 (acid/base catalyst)	C_2OH	D571 (acid/base catalyst)
C_3OH	D542 (acid/base catalyst)	C_3OH	D571 (acid/base catalyst)
C_3OH	R526 [*] (nitrogen)	NH_2^+	D355
NH_2^+	D443 (catalytic nucleophile)	NH_2^+	D472 (catalytic nucleophile)
[*]: NH_2^+ of R526 with (-Ö-) of C_3-OH group		protonated nitrogen atom forms two H-bonds	
C calystegine B_2 and maltase		**D** calystegine B_2 and sucrase	
C_2OH	D327	C_2OH	D355
C_3OH	D327	C_3OH	D355
C_4OH	H600 [**]	C_4OH	D571 (acid/base catalyst)
NH_2^+	D443 (catalytic nucleophile)	NH_2^+	D472 (catalytic nucleophile)
C_1OH	NH-W406 (distance 2.4 Å, not indicated)	C_1OH	NH-W435 (distance 2.5 Å, not indicated)
[**]: with nitrogen of the imidazole ring			

The scores for docking of acarbose to maltase and sucrase, compared to those for calystegines A_3 and B_2, as well as the calculated interaction energies for the calystegines, are listed in Table 45.

Table 45: GOLD docking scores and interaction energies

enzyme⟍ compound	maltase		sucrase	
	GOLD-score	interaction energy [kcal/mol]	GOLD-score	interaction energy [kcal/mol]
acarbose	64.5	n.d.	56.3	n.d.
calystegine A_3	51.3	-49.1	52.7	-55.0
calystegine B_2	48.9	-48.7	49.4	-53.3
GOLD-scores have no unit and reflect fitness of the ligands. Higher values indicate higher affinities of the ligands to the protein. More negative interaction energy indicates higher affinity				

The active sites of maltase and sucrase are almost identical, and the only difference is a single amino acid replacement: tyrosine 299 in maltase with tryptophan 327 in sucrase. Figure 21 shows the superposition of the active sites of both enzymes with calystegine A_3 as ligand.
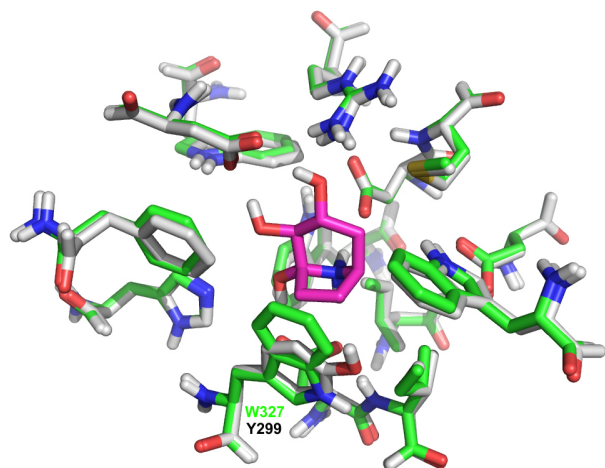
Figure 21: Superposition of the active sites of maltase (pdb: 3L4X) and sucrase (pdb: 3LPP) with calystegine A₃ as ligand

Maltase: grey carbon atoms. Sucrase: green carbon atoms. Calystegine A₃: magenta. The only difference is indicated: tyrosine 299 in maltase replaced by tryptophan 327 in sucrase.

Sucrase with docked calystegine B_2 is shown as ribbon model in Figure 22 as a representative example of a whole enzyme with docked calystegine.
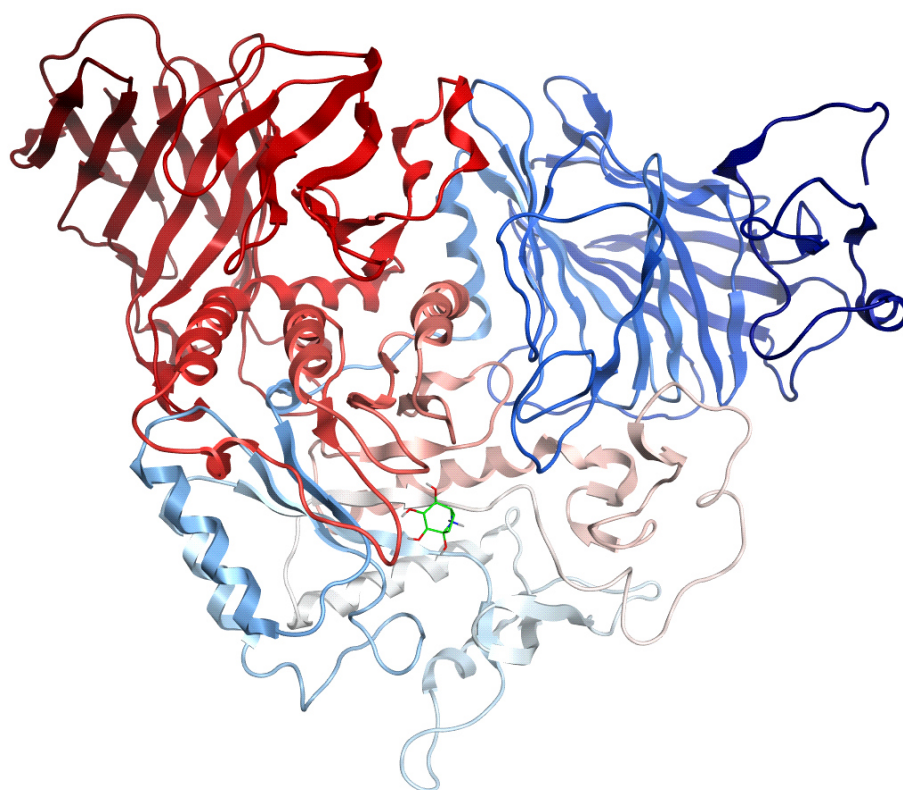
Figure 22: Sucrase (3LPP) backbone with calystegine B₂ docked in the active centre

The nortropane structure of calystegine B₂ (carbon atoms) is marked with green lines. Calystegine oxygen atoms are red, nitrogen is blue. Backbone of the enzyme: the N-terminal part is coloured blue, the C-terminal part red.

3.4.4. Inhibition of human maltase and sucrase by calystegines A_3 and B_2

The K_i values of calystegines A_3 and B_2 for human maltase and sucrase were calculated using the Enzyme Kinetics module 1.3 of SigmaPlot (see Material and Methods, Chapter 2.5.2). Numerical data are shown in Table 46 as means (n = 3−6) with standard errors, as provided by SigmaPlot. Michaelis-Menten plots of the inhibition assay data are presented in Figure 23. The K_i for acarbose was calculated using the equation for a single inhibitor concentration (Motulsky and Christopoulos, 2003), since it was applied as 5 µM only as a positive inhibition control. The same equation was used for single concentration calystegine inhibition tests, for comparison with the data obtained with SigmaPlot. Since only certain mean values were entered into the equation, there are no standard errors for the K_i values obtained with this calculation option. The inhibitory effect of acarbose on maltase and sucrase was confirmed. The positive control for inhibition of maltase and sucrase with 5 µM acarbose showed that both enzymes responded positively to the inhibition: maltase (acarbose K_i = 4.4 µM) is inhibited by acarbose almost twice as strong as sucrase (acarbose K_i = 7.8 µM) (Table 46). This difference in inhibition demonstrated *in vitro* is congruent with the difference in inhibition predicted *in silico* by GOLD docking scores (Table 45).

Both calystegine A_3 and B_2 inhibited maltase and sucrase activities, but compared to acarbose, inhibition is weaker. Calystegine B_2, with a K_i of 55 µM, is a stronger inhibitor of sucrase than calystegine A_3, which has a K_i of 227 µM. For both calystegines, however, the inhibitory effect for maltase is much lower than for sucrase. Inhibition of maltase by 119 µM of calystegine A_3 was hardly detectable, which disabled the calculation of the K_i of calystegine A_3 for maltase. For calystegine B_2, a K_i of 582 µM for maltase was calculated (Table 46).

Whereas the stronger inhibition of sucrase than of maltase by calystegines correlated with the calculated interaction energies for docking (Table 45), the stronger inhibition by B_2 than by A_3 did not reflect the calculated interaction energies.

Table 46: Maltase and sucrase kinetic parameters: without inhibitor and with inhibition by calystegines A$_3$ and B$_2$

inhibitor	V_{max}	K$_m$	R^2 [a]	K$_i$
	[pkat/mg]	[mM]	-	[µM]
	maltase			
no inhibitor	827 ± 12	7.3 ± 0.5	0.9938	-
acarbose 5µM	725 ± 11 [b]	15.6 ± 0.8 [c]	0.9980	4.4 [d]
calystegine A$_3$ (119 µM)	955 ± 15 [b]	9.1 ± 0.6 [c]	0.9957	483 [d]
calystegine A$_3$ (476 µM)	939 ± 23 [b]	11.1 ± 1.1 [c]	0.9913	914 [d]
calystegine A$_3$	901 ± 15 [b]	8.6 ± 0.7 [c]	**0.9819**	[e, f]
calystegine B$_2$ (119 µM)	742 ± 19 [b]	8.6 ± 1.0 [c]	0.9876	668 [d]
calystegine B$_2$ (476 µM)	1016 ± 22 [b]	25.4 ± 1.5 [c]	0.9980	192 [d]
calystegine B$_2$	837 ± 19 [b]	8.7 ± 0.9 [c]	**0.9769**	**582 ± 144 [e]**
	sucrase			
no inhibitor	412 ± 23	11.1 ± 2.5	0.9570	-
acarbose 5µM	166 ± 11 [b]	18.2 ± 3.9 [c]	0.9678	7.8 [d]
calystegine A$_3$ (119 µM)	409 ± 26 [b]	17.1 ± 3.6 [c]	0.9711	220 [d]
calystegine A$_3$ (476 µM)	298 ± 7 [b]	12.5 ± 1.1 [c]	0.9939	3774 [d]
calystegine A$_3$	396 ± 14 [b]	9.9 ± 1.6 [c]	**0.9610**	**227 ± 47 [e]**
calystegine B$_2$ (119 µM)	250 ± 6 [b]	11.4 ± 1 [c]	0.9945	4403 [d]
calystegine B$_2$ (476 µM)	236 ± 8 [b]	25.4 ± 2.3 [c]	0.9948	369 [d]
calystegine B$_2$	378 ± 18 [b]	8.9 ± 1.9 [c]	**0.9439**	**55 ± 12 [e]**

Kinetic parameters are given as means ± standard error (n = 3–6); [a] correlation coefficient, quality of fit between single values and the kinetic parameters derived from the activity curve; [b] apparent V_{max} values for inhibited enzyme; [c] apparent K$_m$ values for inhibited enzyme; [d] K$_i$ according to the single inhibitor concentration equation; [e] K$_i$ according to SigmaPlot; [f] test for inhibition models by SigmaPlot failed, as V_{max} was higher than maltase V_{max} without inhibitor (also Figure 23); kinetic parameter values of calystegines in bold script were obtained by SigmaPlot Enzyme Kinetics Analysis: Single Substrate - Single Inhibitor study.

The relatively low correlation coefficients for the kinetics of sucrase in the presence of calystegines, calculated by SigmaPlot, were similar to the coefficients for sucrase in the presence of acarbose and even without inhibitor present. This indicated that sucrase showed a slight variability independent of inhibitors that may be derived from the procedure for preparation of the protein extract. All of the single concentration enzyme inhibition assays (except sucrase inhibited with 119 µM calystegine A$_3$) have acceptable correlation coefficients of R^2 ≈ 0.99.
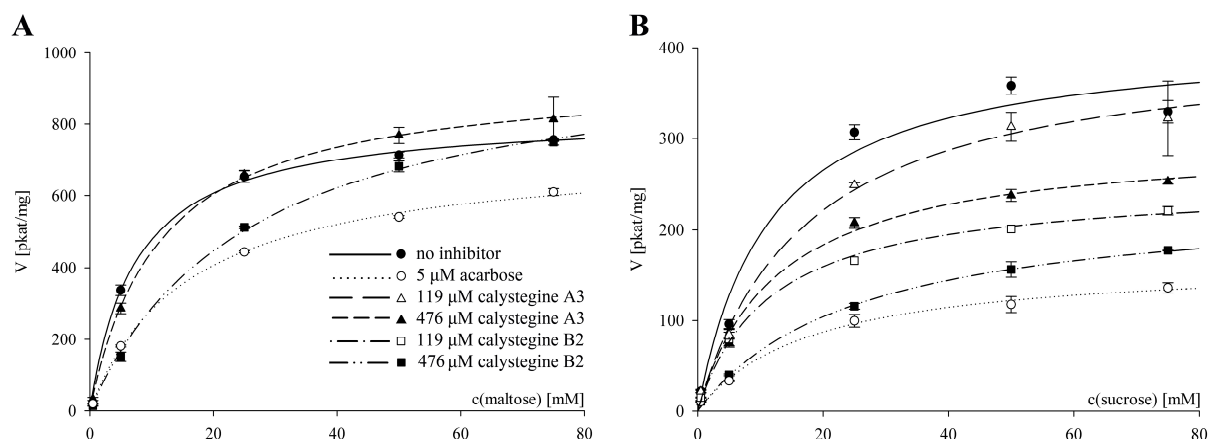
Figure 23: Enzyme activities of maltase (A) and sucrase (B) in Michaelis-Menten plots.

Maltase activity in presence of 119 μM calystegines A_3 and B_2 is not shown, as it was indistinguishable from non-inhibited activity. Error bars on the data points show standard errors (n = 3 – 6).

Apart from the K_i values, the enzyme kinetic parameters (V_{max} and K_m) of calystegines were also estimated with the Enzyme Kinetics module. The fully competitive inhibition type was selected, according to previously published data on the inhibition mechanism of calystegines for glycosidases (Asano et al., 1996b; Asano et al., 1994b; Ikeda et al., 2003), although SigmaPlot showed that the mixed partial inhibition mechanism would fit the data better, according to the correlation coefficients. However, this mechanism scored only 2–3% higher than the full competitive inhibition type by comparison of correlation coefficients. This difference was not taken in consideration, as determining the mechanism of inhibition by calystegines was not an objective of this work. V_{max} and substrate K_m values for the enzymes in general (regarded as not inhibited), obtained within the calculation process for calystegine K_i values, resemble those determined for uninhibited enzymes (Table 46, grey script), supporting the validity of the approach followed in this work.

3.4.5. Discussion: *α*-glycosidase inhibition with calystegines

Cell culture growth

Although it has been noticed that Caco-2 cells in culture increase their protein content and surface enzyme activity especially from days 8 to 15 (Blais et al., 1987; Ferruzza et al., 2012), 7 days old cell culture was used for the *α*-glycosidase assay, since enzyme specific activity was measurable under assay conditions (Chapter 2.5.2).

Enzyme kinetics of maltase and sucrase

Reproduction of the reported enzyme activities of maltase and sucrase was a prerequisite for the enzyme inhibition assays for calystegines A_3 and B_2. Cleared lysates of Caco-2 cells were used as enzyme solutions for the assays, as these provided reproducible results in tests and showed sufficiently high enzyme activities for reliable determination of inhibition. As the enzymes might suffer from the resuspension procedure or the calcium-containing centrifugation medium, results were compared with the data from lysed human small intestine preparations. These comparisons did not indicate major adverse effects of the procedure of preparation of the lysates on enzyme activities. Enzymes obtained from other species or by recombinant techniques may provide different activities (Quezada-Calvillo et al., 2008) and are therefore difficult to be compared to the lysates.

Maltase activity results from four different active sites, i.e. from each one of the catalytic domains of MGAM (maltase-glucoamylase) and of SI (sucrase-isomaltase) (Jones et al., 2011), while sucrase activity is exerted by one active site only, the C-terminal catalytic domain of SI (Quezada-Calvillo et al., 2007). This explains the differences in V_{max} of tha maltase and sucrase activity in Table 46.

Even though the cell lysates contained measurable amounts of glucose (~ 5 µg/mL), it did not interfere with any method for direct measurement of calystegines nor with any enzyme inhibition assay and was thus ignored.

Docking of calystegines A_3 and B_2 to the models of recombinant human maltase and sucrase

The calculated docking positions of the first two moieties of acarbose agreed excelently with those observed in the X-ray structure of acarbose-complexed maltase (2QMJ) (Figure 19), supporting the following docking studies of the calystegines. Due to the larger size of acarbose and the higher number of interactions with the proteins, the docking scores for acarbose in maltase and sucrase were higher than those for the calystegines. The docking scores and interaction energies for maltase and sucrase slightly favoured calystegine A_3 over calystegine B_2 for binding, although calystegine B_2 possesses more hydroxyl groups. Judging from the GOLD docking results, acarbose and calystegines A_3 and B_2 have similar binding geometries in the active centres of maltase and sucrase (see Table 45). The C_4 hydroxyl group of calystegine B_2 forms an H-bond with D542 (acid/base catalyst) of sucrase, but not of maltase. Instead, in interaction with maltase that hydroxyl group forms a H-bond with the nitrogen atom of imidazole in H600. That might partly explain the lower inhibitory effect of

calystegine B_2 on maltase compared with sucrase. The protonated nitrogen atom of calystegine A_3 forms two H-bonds with sucrase at D472 (catalytic nucleophile) and D355. With maltase only one H-bond with the catalytic nucleophile (D443) is formed. As for calystegine B_2, sucrase also appeared more susceptible to inhibition by calystegine A_3, and this difference in number of H-bonds might be part of the explanation. The higher affinity of both calystegines for sucrase than for maltase, that was determined experimentally, was already indicated by their calculated interaction energies (more negative values). The only significant difference in the active sites of the enzymes is replacement of tyrosine 299 in maltase by tryptophan 327 in sucrase, and the better interaction energies for calystegines with sucrase than with maltase may be a result of hydrophobic interaction of the ethylene bridge in the calystegines with the side chain of just this tryptophan in the active centre of sucrase (Figure 21). Considering the small differences in interaction energies between calystegines A_3 and B_2 for sucrase, calystegine A_3 should be stronger inhibitor. However, the *in vitro* data did not confirm this (Chapter 3.4.4, Table 46). Those small differences in calculated interaction energies may consequently be regarded as insignificant. Alternatively, some aspects of the actual interaction of calystegines with glycosidases, which may lead to considerable differences in inhibition *in vivo*, are not adequately covered by *in silico* modeling approaches yet.

Inhibition of human maltase and sucrase by calystegines A_3 and B_2

The nonlinear fit of enzyme parameters indicated that calystegines A_3 and B_2 and acarbose inhibit maltase and sucrase by the competitive mode. The considerably lower K_i values of acarbose for maltase and sucrase, compared to the calystegines (Table 46), agree with the higher calculated docking scores. This can be explained by the larger size of acarbose and by the higher number of interactions with the proteins in comparison with the calystegines.

Inhibition of maltase by the calystegines was generally weak. It is very likely that they displayed different inhibition effect on the maltase activities in each of the two α-glycosidase subunits in the Caco-2 cell wall. This assumption is supported by different inhibitory activity of acarbose on various maltase preparations. Experimentally determined sensitivities of maltase to acarbose vary significantly and depend on the source of the enzyme (species/tissue) and the method of preparation (native, precipitated or heterologously expressed), and on the subunit(s) tested (Quezada-Calvillo et al., 2008), ranging from a K_i of 0.84 µM in human intestinal mucosa lysate (Breitmeier et al., 1997) to a K_i of 62 µM for the heterologously expressed N-terminal subunit of human MGAM (Rossi et al., 2006). The

sensitivity for acarbose of sucrase immuno-precipitated from human intestinal mucosa, with a K_i of 5.3 mM, appeared to be lower (Quezada-Calvillo et al., 2008).

In protein preparations derived from Caco-2 cells, maltase was approximately two times less susceptible (K_i) for inhibition by acarbose than sucrase. With higher concentrations of substrate, acarbose inhibited sucrase more strongly than it did maltase: at 50 mM substrate, sucrase activity decreased to approximately one third of the activity without inhibitor, while the total maltase activity still was at 76% of that of the non-inhibited enzyme (Figure 23). This continuously high maltase activity may be explained by maltase activity being derived from four subunits that are differentially inhibited.

Higher affinity of both calystegines for sucrase was predicted by GOLD in the form of more negative scoring values and interaction energies with sucrase than with maltase (Chapter 3.4.3, Table 45). These observations are in agreement with the experimental results (Chapter 3.4.4, Table 46). Water molecules, which were not included in the docking procedure, may serve as additional stabilisers for the binding of calystegine B_2. That could also explain the lower K_i values of calystegine B_2 in comparison to those of calystegine A_3.

An increase of substrate K_m values was observed for inhibited enzymes compared to uninhibited enzymes: when inhibited by low concentrations of calystegine, the increase of K_m was almost negligible, while under inhibition by high concentrations of calystegines, K_m values almost doubled. Inhibition of sucrase with calystegine A_3 posed an exception, as the K_m of sucrose with 119 µM calystegine A_3 was higher than with 476 µM calystegine A_3. Values of V_{max} basically remained the same. These inhibition kinetics point to competitive type of inhibition.

Calystegine K_i values, calculated with single inhibitor concentration equation, indicated great variability of obtained K_i values for single inhibitor cases, whereby those data corresponded only in wide sense to the values obtained by the SigmaPlot Enzyme Kinetics Module. Reason for this results discrepancy could be relative low level of inhibition with smaller inhibitor concentrations, compared with recognisable extent of inhibition if bigger calystegine concentrations were applied.

Apparent difference between calystegine K_i values obtained in two different calculation ways might indicate as well that K_i values for acarbose calculated using the equation for single inhibitor concentration do not need necessarily to be exact. However, they were found to be in the same scope as the literature data for acarbose K_i as shown in the literature (Breitmeier et al., 1997; Rossi et al., 2006), which was enough to proof and confirm evident inhibition of maltase and sucrase with acarbose as positive control inhibitor.

As mentioned previously, a major reason for the different levels of inhibition of maltase and sucrase, as well as for the variability in measurements of the former, is the fact that maltase activity is provided by both catalytic domains of MGAM as well as by those of SI, while sucrase activity is provided exclusively by the C-terminal catalytic domain of SI. Thus, experiments on enzyme and inhibition characteristics of individually expressed MGAM and SI proteins, as well as the individual active domains, would provide better understanding of intestinal α-glycosidase activities and their inhibition by calystegines and of the effects on carbohydrate degradation.

Perspectives for the application of calystegine-rich diets for lowering the postprandial sugar level in blood

The relevance of these results for carbohydrate digestion was estimated by the calystegine content in vegetables and potato cultivars. Potatoes contain predominantly calystegine B_2, which can amount to up to 57 mg/kg fresh potato flesh without peel (Friedman et al., 2003). When whole tubers were analysed, 239 mg/kg dry mass of calystegine B_2 were found (Griffiths et al., 2008). With dietary portions of 200 grams of those potatoes, the calystegine B_2 concentration in an assumed stomach volume of 1 litre would reach 55-65 µM after the meal (Sherwood, 1997). These concentrations are similar to the K_i of calystegine B_2 for sucrase, indicating a substantial inhibition of sucrose digestion. Even when the stomach content is emptied into the small intestine and further diluted, inhibition is still possible. It has to be tested whether maltose hydrolysis by sucrase is equally inhibited by calystegine B_2. Some other vegetables consumed world-wide are also rich in calystegines. Sweet potatoes (*Ipomoea batatas*), sweet peppers (*Capsicum annuum*) and eggplant (*Solanum melongena*) contain 19, 37 and 73 mg of calystegine B_2 per kg fresh weight (Asano et al., 1997b). 200 gram portions of those vegetables would result in 22–83 µM of calystegine B_2 in the stomach; again concentrations that are estimated to seriously inhibit sucrase. Maltase activity appears rather unaffected by calystegines, but after a starch-rich meal, sucrase becomes the default α-glycosidase due to the the luminal "starch brake" of maltase (Quezada-Calvillo et al., 2008). Targeted application of calystegines could be an approach to control blood glucose level in a more natural way and could increase compliance during therapy.

4. Conclusion

Isolation of calystegines: extraction and separation

- Calystegine concentration in potato sprouts

Potato sprouts were confirmed to be a rich source of calystegines. The calystegine profile was typical for potatoes and calystegine concentration was in usual limits regarding sprout length and considering variations among cultivars. The concentrations of calystegines in potato sprouts, measured after the first purification step on the Merck I column, was as follows: A_3 = 2325 ± 152 µg/g d.w., B_2 = 7586 ± 560 µg/g d.w., B_4 = 492 ± 33 µg/g d.w.

- Calystegine purity

The highest purity was achieved for calystegine B_2: calystegine percental content (relative main-to-total calystegine content) according to GC (A_3 = 92.64% ± 0.14, B_2 = 92.42% ± 0.44 and B_4 = 91.37% ± 0.75) corresponded closely to the GC quantified calystegine content related to total pool dry weight (including non-calystegine impurities; A_3 = 70.23% ± 5.31, B_2 = 101.47% ± 8.70 and B_4 = 46.82% ± 1.45).

Calystegines A_3 and B_4 had high purity according to the percental ratios of calystegine measured by GC, but calystegine content did not match the dry weight of the preparations (approximately 30% difference by calystegine A_3 and 53% by B_4). Impurities, which could be the coloured substances, are not detectable by GC probably due to non-volatility under experimental conditions. Additional purification of calystegine A_3 and B_4 pools using additional ion exchanger columns other chromatographic methods should contribute to the elimination of contaminants.

Quantitation of calystegines with CZE and cITP and comparison with GC

Calystegine contents determined by CZE and cITP correlated well with the results obtained by GC. Electrophoretic methods, compared with GC analysis, possess several advantages:

→ Samples can be prepared directly from the raw material without further purification, but sample filtration and dilution are recommended.

→ Short analysis time.

→ Sensitivity of cITP is higher than GC, so that smaller amounts of compounds can be detected if sample amounts are limited.

Maintenance, service and operation costs of electrophoretic devices are lower than for GC.
The GC method, although more established, is not more sensitive and precise than electrophoretic methods. Analysis takes longer and is more tedious and error-prone due to sample derivatisation prior to analysis.

Transepithelial transport tests

- Calystegines A_3 and B_2 proved to be non-toxic for Caco-2 cell monolayers, suggesting that they can be safely included in therapeutical food products.

- Caco-2 cells did not substantially transport calystegine B_2. Thus, absorption of calystegines into the intestinal mucosa and across the intestinal barrier into the blood would probably be insignificant. Potential systematic toxicity of calystegine to humans is improbable.

Inhibition of human intestinal α-glycosidases

- Docking

Inhibition of maltase and sucrase by calystegines was expected from docking models, but levels of enzyme inhibition were not predictable.
The docking studies support the potential of calystegines as competitive maltase and sucrase inhibitors.

- *In vitro* inhibition of maltase and sucrase by calystegines

The mode of inhibition by calystegines A_3 and B_2 was competitive.
Calystegine B_2 inhibits sucrase ($K_i = 55 \pm 12 \, \mu M$) stronger than maltase ($K_i = 582 \pm 144 \, \mu M$).
Calystegine A_3 inhibits sucrase moderately ($K_i = 227 \pm 47 \, \mu M$), but practically does not inhibit maltase (test for inhibition models by SigmaPlot failed, as V_{max} was higher than maltase V_{max} without inhibitor).

- Diets containing calystegines as support for therapy of Diabetes mellitus type 2

Consumption of conventional meals prepared with foods rich in calystegines may be beneficial for prevention of development of Diabetes mellitus type 2 or as a dietary supporting method for control and treatment of the disease in patients. Better knowledge of qualitative and quantitative aspects of the mechanism of enzyme inhibition will allow appropriate dosage.

4.1. Outlook

Further purification of calystegines A_3 and B_4 by additional ion exchange columns would provide their higher purity. However, application of additional steps prolongs the total time necessary for purification of calystegines.

CZE and cITP proved to be reliable and efficient methods for analysis of calystegines, with promising aspects for further application.

In vitro assays with subunits of intestinal enzyme subunits (available by heterologous expression) would enable to distinguish their catalytic potential. Inhibition of individual human enzyme subunits (M- and S-subunit) would give a differential picture of calystegines inhibitory power.

Further investigations on calystegines for treatment of metabolic disorders related to glycosidases, above all *in vivo* testing, are encouraged by the present results.

5. References

Adler AI, Stevens RJ, Manley SE, Bilous RW, Cull CA and Holman RR (2003) Development and Progression of Nephropathy in Type 2 Diabetes: The United Kingdom Prospective Diabetes Study (UKPDS 64). *Kidney International* **63**:225-232.

Amaral M (2006) Therapy Through Chaperones: Sense or Antisense? Cystic Fibrosis As a Model Disease. *J Inherit Metab Dis* **29**:477-487.

ap Rees T and Morrell S (1990) Carbohydrate Metabolism in Developing Potatoes. *American Journal of Potato Research* **67**:835-847.

Arakawa T, Ejima D, Kita Y and Tsumoto K (2006) Small Molecule Pharmacological Chaperones: From Thermodynamic Stabilization to Pharmaceutical Drugs. *Biochimica et Biophysica Acta (BBA) - Proteins and Proteomics* **1764**:1677-1687.

Artursson P (1990) Epithelial Transport of Drugs in Cell Culture. I: A Model for Studying the Passive Diffusion of Drugs Over Intestinal Absorbtive (Caco-2) Cells. *J Pharm Sci* **79**:476-482.

Asano N (2003) Naturally Occurring Iminosugars and Related Compounds: Structure, Distribution, and Biological Activity. *Current Topics in Medicinal Chemistry* **3**:471-484.

Asano N (2009) Sugar-Mimicking Glycosidase Inhibitors: Bioactivity and Application. *Cellular and Molecular Life Sciences* **66**:1479-1492.

Asano N, Kato A, Kizu H and Matsui K (1996a) 1β-Amino-2α,3β,5β-Trihydroxycycloheptane From *Physalis Alkekengi* Var. *Francheti. Phytochemistry* **42**:719-721.

Asano N, Kato A, Kizu H, Matsui K, Griffiths RC, Jones MG, Watson AA and Nash RJ (1997a) Enzymatic Synthesis of the Glycosides of Calystegines B_1 and B_2 and Their Glycosidase Inhibitory Activities. *Carbohydrate Research* **304**:173-178.

Asano N, Kato A, Kizu H, Matsui K, Watson AA and Nash RJ (1996b) Calystegine B4, a Novel Trehalase Inhibitor From *Scopolia Japonica. Carbohydrate Research* **293**:195-204.

Asano N, Kato A, Matsui K, Watson AA, Nash RJ, Molyneux RJ, Hackett L, Topping J and Winchester B (1997b) The Effects of Calystegines Isolated From Edible Fruits and Vegetables on Mammalian Liver Glycosidases. *Glycobiology* **7**:1085-1088.

Asano N, Kato A, Miyauchi M, Kizu H, Tomimori T, Matsui K, Nash RJ and Molyneux RJ (1997c) Specific α-Galactosidase Inhibitors, *N*-Methylcalystegines Structure/Activity Relationships of Calystegines From *Lycium Chinense. European Journal of Biochemistry* **248**:296-303.

Asano N, Kato A, Oseki K, Kizu H and Matsui K (1995a) Calystegins of *Physalis Alkekengi* Var. *Francheti* (Solanaceae). *European Journal of Biochemistry* **229**:369-376.

Asano N, Kato A, Yokoyama Y, Miyauchi M, Yamamoto M, Kizu H and Matsui K (1996c) Calystegin N_1, a Novel Nortropane Alkaloid With a Bridgehead Amino Group From *Hyoscyamus Niger*: Structure Determination and Glycosidase Inhibitory Activities. *Carbohydrate Research* **284**:169-178.

Asano N, Kizu H, Oseki K, Tomioka E, Matsui K, Okamoto M and Baba M (1995b) *N*-Alkylated Nitrogen-in-the-Ring Sugars: Conformational Basis of Inhibition of Glycosidases and HIV-1 Replication. *Journal of Medicinal Chemistry* **38**:2349-2356.

Asano N, Nash RJ, Molyneux RJ and Fleet GWJ (2000) Sugar-Mimic Glycosidase Inhibitors: Natural Occurrence, Biological Activity and Prospects for Therapeutic Application. *Tetrahedron: Asymmetry* **11**:1645-1680.

Asano N, Oseki K, Kizu H and Matsui K (1994a) Nitrogen-in-the-Ring Pyranoses and Furanoses: Structural Basis of Inhibition of Mammalian Glycosidases. *Journal of Medicinal Chemistry* **37**:3701-3706.

Asano N, Oseki K, Tomioka E, Kizu H and Matsui K (1994b) *N*-Containing Sugars From *Morus Alba* and Their Glycosidase Inhibitory Activities. *Carbohydrate Research* **259**:243-255.

Asano N, Tomioka E, Kizu H and Matsui K (1994c) Sugars With Nitrogen in the Ring Isolated From the Leaves of *Morus Bombycis*. *Carbohydrate Research* **253**:235-245.

Asano N, Yamashita T, Yasuda K, Ikeda K, Kizu H, Kameda Y, Kato A, Nash RJ, Lee HS and Ryu KS (2001a) Polyhydroxylated Alkaloids Isolated From Mulberry Trees (*Morus Alba* L.) and Silkworms (*Bombyx Mori* L.). *J Agric Food Chem* **49**:4208-4213.

Asano N, Yokoyama K, Sakurai M, Ikeda K, Kizu H, Kato A, Arisawa M, Höke D, Dräger B, Watson AA and Nash RJ (2001b) Dihydroxynortropane Alkaloids From Calystegine-Producing Plants. *Phytochemistry* **57**:721-726.

Bekkouche K, Daali Y, Cherkaoui S, Veuthey JL and Christen P (2001) Calystegine Distribution in Some Solanaceous Species. *Phytochemistry* **58**:455-462.

Bernier V, Lagacé M, Bichet DG and Bouvier M (2004) Pharmacological Chaperones: Potential Treatment for Conformational Diseases. *Trends in Endocrinology & Metabolism* **15**:222-228.

Bhandari MR, Jong-Anurakkun N, Hong G and Kawabata J (2008) α-Glucosidase and α-Amylase Inhibitory Activities of Nepalese Medicinal Herb Pakhanbhed (*Bergenia Ciliata*, Haw.). *Food Chemistry* **106**:247-252.

Biastoff S and Dräger B (2007) Chapter 2 Calystegines, in *The Alkaloids: Chemistry and Biology* (Geoffrey AC ed) pp 49-102, Academic Press.

Bischoff H (1994) Pharmacology of α-Glucosidase Inhibition. *Eur J Clin Invest* **24**:3-10.

Blais A, Bissonnette P and Berteloot A (1987) Common Characteristics for Na^+-Dependant Sugar Transport in Caco-2 Cells and Human Fetal Colon. *Journal of Membrane Biology* **99**:113-125.

Boden J and Bächmann K (1996) Investigation of Matrix Effects in Capillary Zone Electrophoresis. *Journal of Chromatography A* **734**:319-330.

Boulenc X, Marti E, Joyeux H, Roques C, Berger Y and Fabre G (1993) Importance of the Paracellular Pathway for the Transport of a New Bisphosphonate Using the Human Caco-2 Monolayers Model. *Biochemical Pharmacology* **46**:1591-1600.

Bourne Y and Henrissat B (2001) Glycoside Hydrolases and Glycosyltransferases: Families and Functional Modules. *Current Opinion in Structural Biology* **11**:593-600.

Boyer FD, Ducrot PH, Henryon V, Soulié J and Lallemand JY (1992) Studies on the Synthesis of the 1-Hydroxynortropane System; Part II.[1] Synthesis of Calystegine A_3 and Physoperuvine. *Synlett* **1992**:357-359.

Boyer FD and Lallemand JY (1992) Synthetic Studies on the 1-Hydroxy Nortropane System,- Part III:[1] Total Enantioselective Synthesis of (-)-Calystegine B_2. *Synlett* **1992**:969-971.

Boyer FD and Lallemand JY (1994) Enantioselective Syntheses of Polyhydroxylated Nortropane Derivatives: Total Synthesis of (+) and (−)-Calystegine B_2. *Tetrahedron* **50**:10443-10458.

Bradford MM (1976) A Rapid and Sensitive Method for the Quantitation of Microgram Quantities of Protein Utilizing the Principle of Protein-Dye Binding. *Analytical Biochemistry* **72**:248-254.

Brand-Miller J, McMillan-Price J, Steinbeck K and Caterson I (2009) Dietary Glycemic Index: Health Implications. *Journal of the American College of Nutrition* **28**:446-449.

Breitmeier D, Günther S and Heymann H (1997) Acarbose and 1-Deoxynojirimycin Inhibit Maltose and Maltooligosaccharide Hydrolysis of Human Small Intestinal Glucoamylase-Maltase in Two Different Substrate-Induced Modes. *ARCHIVES OF BIOCHEMISTRY AND BIOPHYSICS* **346**:7-14.

Brock A, Bieri S, Christen P and Dräger B (2005) Calystegines in Wild and Cultivated *Erythroxylum* Species. *Phytochemistry* **66**:1231-1240.

Brock A, Herzfeld T, Paschke R, Koch M and Dräger B (2006) Brassicaceae Contain Nortropane Alkaloids. *Phytochemistry* **67**:2050-2057.

Camire ME, Kubow S and Donnelly DJ (2009) Potatoes and Human Health. *Critical Reviews in Food Science and Nutrition* **49**:823-840.

Chang HH, Asano N, Ishii S, Ichikawa Y and Fan JQ (2006) Hydrophilic Iminosugar Active-Site-Specific Chaperones Increase Residual Glucocerebrosidase Activity in Fibroblasts From Gaucher Patients. *FEBS Journal* **273**:4082-4092.

Chantret I, Barbat A, Dussaulx E, Brattain MG and Zweibaum A (1988) Epithelial Polarity, Villin Expression, and Enterocytic Differentiation of Cultured Human Colon Carcinoma Cells: A Survey of Twenty Cell Lines. *Cancer Research* **48**:1936-1942.

Chen F, Nakashima N, Kimura I and Kimura M (1995) Hypoglycemic Activity and Mechanisms of Extracts From Mulberry Leaves (Folium Mori) and Cortex Mori Radicis in

Streptozotocin-Induced Diabetic Mice. *Yakugaku zasshi: Journal of the Pharmaceutical Society of Japan* **115**:476-482.

Cheng Y-C and Prusoff WH (1973) Relationship Between the Inhibition Constant (KI) and the Concentration of Inhibitor Which Causes 50 Per Cent Inhibition (I50) of an Enzymatic Reaction. *Biochemical Pharmacology* **22**:3099-3108.

Cholich LA, Gimeno EJ, Teibler PG, Jorge NL and Acosta de Pérez OC (2009) The Guinea Pig As an Animal Model for *Ipomoea Carnea* Induced α-Mannosidosis. *Toxicon* **54**:276-282.

Clark M, Cramer RD and Van Opdenbosch N (1989) Validation of the General Purpose Tripos 5.2 Force Field. *J Comput Chem* **10**:982-1012.

Cogburn JN, Donovan MG and Schasteen CS (1991) A Model of Human Small Intestinal Absorptive Cells. 1. Transport Barrier. *Pharmaceutical Research* **8**:210-216.

Cogoli A and Semenza G (1975) A Probable Oxocarbonium Ion in the Reaction Mechanism of Small Intestinal Sucrase and Isomaltase. *Journal of Biological Chemistry* **250**:7802-7809.

Conklin KA, Yamashiro KM and Gray GM (1975) Human Intestinal Sucrase-Isomaltase. Identification of Free Sucrase and Isomaltase and Cleavage of the Hybrid into Active Distinct Subunits. *Journal of Biological Chemistry* **250**:5735-5741.

Cox TM, Aerts JMFG, Andria G, Beck M, Belmatoug N, Bembi B, Chertkoff R, Vom Dahl S, Elstein D, Erikson A, Giralt M, Heitner R, Hollak C, Hrebicek M, Lewis S, Mehta A, Pastores GM, Rolfs A, Sa Miranda MC and Zimran A (2003) The Role of the Iminosugar *N*-Butyldeoxynojirimycin (Miglustat) in the Management of Type I (Non-Neuronopathic) Gaucher Disease: A Position Statement. *J Inherit Metab Dis* **26**:513-526.

Cox T, Lachmann R, Hollak C, Aerts J, van Weely S, Hrebícek M, Platt F, Butters T, Dwek R, Moyses C, Gow I, Elstein D and Zimran A (2000) Novel Oral Treatment of Gaucher's Disease With *N*-Butyldeoxynojirimycin (OGT 918) to Decrease Substrate Biosynthesis. *The Lancet* **355**:1481-1485.

Csuk R, Prell E and Reißmann S (2008) Total Synthesis of Calystegine A_7. *Tetrahedron* **64**:9417-9422.

Daali Y, Bekkouche K, Cherkaoui S, Christen P and Veuthey JL (2000) Use of Borate Complexation for the Separation of Non-UV-Absorbing Calystegines by Capillary Electrophoresis. *Journal of Chromatography A* **903**:237-244.

Dahlqvist A (1968) Assay of Intestinal Disaccharidases. *Analytical Biochemistry* **22**:99-107.

Davies GJ, Ducros VMA, Varrot A and Zechel DL (2003) Mapping the Conformational Itinerary of B-Glycosidases by X-Ray Crystallography. *Biochemical Society Transactions* **31**:523-527.

Dawson DC (1977) Na and Cl Transport Across the Isolated Turtle Colon: Parallel Pathways for Transmural Ion Movement. *Journal of Membrane Biology* **37**:213-233.

Desnick RJ (2004) Enzyme Replacement and Enhancement Therapies for Lysosomal Diseases. *J Inherit Metab Dis* **27**:385-410.

Di Carli MF, Janisse J, Grunberger G and Ager J (2003) Role of Chronic Hyperglycemia in the Pathogenesis of Coronary Microvascular Dysfunction in Diabetes. *Journal of the American College of Cardiology* **41**:1387-1393.

Dräger B (1995) Identification and Quantification of Calystegines, Polyhydroxyl Nortropane Alkaloids. *Phytochem Anal* **6**:31-37.

Dräger B (2002) Analysis of Tropane and Related Alkaloids. *Journal of Chromatography A* **978**:1-35.

Dräger B (2004) Chemistry and Biology of Calystegines. *Nat Prod Rep* **21**:211-223.

Dräger B, Funck C, Höhler A, Mrachatz G, Nahrstedt A, Portsteffen A, Schaal A and Schmidt R (1994) Calystegines As a New Group of Tropane Alkaloids in Solanaceae. *Plant Cell Tiss Organ Cult* **38**:235-240.

Dräger B, van Almsick A and Mrachatz G (1995) Distribution of Calystegines in Several Solanaceae. *Planta Med* **61**:577-579.

Duclos O, Mondange M, Duréault A and Depezay JC (1992) Polyhydroxylated Nortropanes Starting From D-Glucose: Synthesis of Homochiral (+) and (−)-Calystegines B2. *Tetrahedron Letters* **33**:8061-8064.

Ducrot PH and Lallemand JY (1990) Structure of the Calystegines: New Alkaloids of the Nortropane Family. *Tetrahedron Letters* **31**:3879-3882.

Eckel RH, Grundy SM and Zimmet PZ (2005) The Metabolic Syndrome. *The Lancet* **365**:1415-1428.

Ek KL, Brand-Miller J and Copeland L (2012) Glycemic Effect of Potatoes. *Food Chemistry* **133**:1230-1240.

Ernst HA, Lo Leggio L, Willemoës M, Leonard G, Blum P and Larsen S (2006) Structure of the *Sulfolobus Solfataricus* α-Glucosidase: Implications for Domain Conservation and Substrate Recognition in GH31. *Journal of Molecular Biology* **358**:1106-1124.

Faitg T, Soulié J, Lallemand JY and Ricard L (1999) General Access to Polyhydroxylated Nortropane Derivatives Through Hetero Diels−Alder Cycloadditions. Part 3: Synthesis of Natural (+)-Calystegine B$_2$. *Tetrahedron: Asymmetry* **10**:2165-2174.

Fan JQ, Ishii S, Asano N and Suzuki Y (1999) Accelerated Transport and Maturation of Lysosomal α-Galactosidase A in Fabry Lymphoblasts by an Enzyme Inhibitor. *Nat Med* **5**:112-115.

Ferrannini E, Simonson DC, Katz LD, Reichard Jr G, Bevilacqua S, Barrett EJ, Olsson M and DeFronzo RA (1988) The Disposal of an Oral Glucose Load in Patients With Non-Insulin-Dependent Diabetes. *Metabolism* **37**:79-85.

Ferruzza S, Rossi C, Scarino ML and Sambuy Y (2012) A Protocol for Differentiation of Human Intestinal Caco-2 Cells in Asymmetric Serum-Containing Medium. *Toxicology in Vitro* **26**:1252-1255.

Firth RG, Bell PM, Marsh HM, Hansen I and Rizza RA (1986) Postprandial Hyperglycemia in Patients With Noninsulin-Dependent Diabetes Mellitus. Role of Hepatic and Extrahepatic Tissues. *Journal of Clinical Investigation* **77**:1525.

Fischer W, Bernhagen J, Neubert RHH and Brandsch M (2010) Uptake of Codeine into Intestinal Epithelial (Caco-2) and Brain Endothelial (RBE4) Cells. *European Journal of Pharmaceutical Sciences* **41**:31-42.

Fowler MJ (2008) Microvascular and Macrovascular Complications of Diabetes. *Clinical Diabetes* **26**:77-82.

Friedman M, McDonald GM and Filadelfi-Keszi M (1997) Potato Glycoalkaloids: Chemistry, Analysis, Safety, and Plant Physiology. *Critical Reviews in Plant Sciences* **16**:55-132.

Friedman M, Roitman JN and Kozukue N (2003) Glycoalkaloid and Calystegine Contents of Eight Potato Cultivars. *J Agric Food Chem* **51**:2964-2973.

Gasteiger J and Marsili M (1978) A New Model for Calculating Atomic Charges in Molecules. *Tetrahedron Letters* **19**:3181-3184.

Gasteiger J and Marsili M (1980) Iterative Partial Equalization of Orbital Electronegativity - a Rapid Access to Atomic Charges. *Tetrahedron* **36**:3219-3228.

Gloster TM, Madsen R and Davies GJ (2006) Dissection of Conformationally Restricted Inhibitors Binding to a B-Glucosidase. *ChemBioChem* **7**:738-742.

Goldmann A, Milat ML, Ducrot PH, Lallemand JY, Maille M, Lepingle A, Charpin I and Tepfer D (1990) Tropane Derivatives From *Calystegia Sepium*. *Phytochemistry* **29**:2125-2127.

Goto Y, Yamada K, Ohyama T, Matsuo T, Odaka H and Ikeda H (1995) An α-Glucosidase Inhibitor, AO-128, Retards Carbohydrate Absorption in Rats and Humans. *Diabetes Research and Clinical Practice* **28**:81-87.

Grasset E, Pinto M, Dussaulx E, Zweibaum A and Desjeux JF (1984) Epithelial Properties of Human Colonic Carcinoma Cell Line Caco-2: Electrical Parameters. *American Journal of Physiology - Cell Physiology* **247**:C260-C267.

Griffiths DW, Shepherd T and Stewart D (2008) Comparison of the Calystegine Composition and Content of Potato Sprouts and Tubers From *Solanum Tuberosum* Group Phureja and *Solanum Tuberosum* Group Tuberosum. *J Agric Food Chem* **56**:5197-5204.

Grover JK, Yadav S and Vats V (2002) Medicinal Plants of India With Anti-Diabetic Potential. *Journal of Ethnopharmacology* **81**:81-100.

Hanozet G, Pircher HP, Vanni P, Oesch B and Semenza G (1981) An Example of Enzyme Hysteresis. The Slow and Tight Interaction of Some Fully Competitive Inhibitors With Small Intestinal Sucrase. *Journal of Biological Chemistry* **256**:3703-3711.

Hansawasdi C, Kawabata J and Kasai T (2001) Hibiscus Acid As an Inhibitor of Starch Digestion in the Caco-2 Cell Model System. *Bioscience, Biotechnology, and Biochemistry* **65**:2087-2089.

Haraguchi M, Gorniak SL, Ikeda K, Minami Y, Kato A, Watson AA, Nash RJ, Molyneux RJ and Asano N (2003) Alkaloidal Components in the Poisonous Plant, *Ipomoea Carnea* (Convolvulaceae). *J Agric Food Chem* **51**:4995-5000.

Hashimoto T, Nakajima K, Ongena G and Yamada Y (1992) Two Tropinone Reductases With Distinct Stereospecificities From Cultured Roots of *Hyoscyamus Niger*. *Plant Physiology* **100**:836-845.

Hauri HP, Sterchi EE, Bienz D, Fransen JA and Marxer A (1985) Expression and Intracellular Transport of Microvillus Membrane Hydrolases in Human Intestinal Epithelial Cells. *The Journal of Cell Biology* **101**:838-851.

Heightman TD and Vasella AT (1999) Recent Insights into Inhibition, Structure, and Mechanism of Configuration-Retaining Glycosidases. *Angewandte Chemie International Edition* **38**:750-770.

Henrissat B and Davies G (1997) Structural and Sequence-Based Classification of Glycoside Hydrolases. *Current Opinion in Structural Biology* **7**:637-644.

Heymann H and Günther S (1994) Calculation of Subsite Affinities of Human Small Intestinal Glucoamylase-Maltase. *Biological Chemistry Hoppe-Seyler* **375**:451-455.

Hidalgo IJ, Raub TJ and Borchardt RT (1989) Characterization of the Human Colon Carcinoma Cell Line (Caco-2) As a Model System for Intestinal Epithelial Permeability. *Gastroenterology* **96**:736-749.

Hikino H, Mizuno T, Oshima Y and Konno C (1985) Isolation and Hypoglycemic Activity of Moran A, a Glycoprotein of *Morus Alba* Root Barks1. *Planta Med* **51**:159-160.

Hilgers AR, Conradi RA and Burton PS (1990) Caco-2 Cell Monolayers As a Model for Drug Transport Across the Intestinal Mucosa. *Pharm Res* **7**:902-910.

Ikeda K, Kato A, Adachi I, Haraguchi M and Asano N (2003) Alkaloids From the Poisonous Plant *Ipomoea Carnea*: Effects on Intracellular Lysosomal Glycosidase Activities in Human Lymphoblast Cultures. *J Agric Food Chem* **51**:7642-7646.

Jayawardena MHS, de Alwis NMW, Hettigoda V and Fernando DJS (2005) A Double Blind Randomised Placebo Controlled Cross Over Study of a Herbal Preparation Containing *Salacia Reticulata* in the Treatment of Type 2 Diabetes. *Journal of Ethnopharmacology* **97**:215-218.

Jenkins DJ, Wolever TM, Taylor RH, Barker H, Fielden H, Baldwin JM, Bowling AC, Newman HC, Jenkins AL and Goff DV (1981) Glycemic Index of Foods: a Physiological Basis for Carbohydrate Exchange. *The American Journal of Clinical Nutrition* **34**:362-366.

Jensen JL, Tsuang SC and Uslan AH (1986) Mechanism of Acid-Catalyzed Anomerization of Methyl D-Glucopyranosides. *J Org Chem* **51**:816-819.

Johansson G, Isaksson R and Harang V (2003) Migration Time and Peak Area Artifacts Caused by Systemic Effects in Voltage Controlled Capillary Electrophoresis. *Journal of Chromatography A* **1004**:91-98.

Johnson CR and Bis SJ (1995) Enzymic Asymmetrization of 6-Amino-2-Cycloheptene-1,4-Diol Derivatives: Synthesis of Tropane Alkaloids (+)- and (-)-Calystegine A$_3$. *J Org Chem* **60**:615-623.

Jones G, Willett P and Glen RC (1995) A Genetic Algorithm for Flexible Molecular Overlay and Pharmacophore Elucidation. *Journal of Computer-Aided Molecular Design* **9**:532-549.

Jones K, Sim L, Mohan S, Kumarasamy J, Liu H, Avery S, Naim HY, Quezada-Calvillo R, Nichols BL, Mario Pinto B and Rose DR (2011) Mapping the Intestinal Alpha-Glucogenic Enzyme Specificities of Starch Digesting Maltase-Glucoamylase and Sucrase-Isomaltase. *Bioorganic & Medicinal Chemistry* **19**:3929-3934.

Kato A, Asano N, Kizu H, Matsui K, Suzuki S and Arisawa M (1997) Calystegine Alkaloids From *Duboisia Leichhardtii*. *Phytochemistry* **45**:425-429.

Kawanishi K and Farnsworth NR (2000) Current status of the chemistry and synthesis of natural antimalarial compounds and natural substances used to alleviate symptoms of diabetes (aldose reductase and α-glucosidase inhibitors), in *Studies in Natural Products Chemistry Bioactive Natural Products (Part C)* (Atta-ur Rahman ed) pp 145-193, Elsevier.

Keiner R and Dräger B (2000) Calystegine Distribution in Potato (*Solanum Tuberosum*) Tubers and Plants. *Plant Science* **150**:171-179.

Keiner R, Kaiser H, Nakajima K, Hashimoto T and Dräger B (2002) Molecular Cloning, Expression and Characterization of Tropinone Reductase II, an Enzyme of the SDR Family in *Solanum Tuberosum* (L.). *Plant Mol Biol* **48**:299-308.

Kimura M (1995) Antihyperglycemic Effects of N-Containing Sugars Derived From Mulberry Leaves in Streptozocin-Induced Diabetic Mice. *J Trad Med* **12**:214-219.

Kimura T, Nakagawa K, Kubota H, Kojima Y, Goto Y, Yamagishi K, Oita S, Oikawa S and Miyazawa T (2007) Food-Grade Mulberry Powder Enriched With 1-Deoxynojirimycin Suppresses the Elevation of Postprandial Blood Glucose in Humans. *J Agric Food Chem* **55**:5869-5874.

Krasikov VV, Karelov DV and Firsov LM (2001) α-Glucosidases. *Biochemistry (Moscow)* **66**:267-281.

Kuriyama C, Kamiyama O, Ikeda K, Sanae F, Kato A, Adachi I, Imahori T, Takahata H, Okamoto T and Asano N (2008) In Vitro Inhibition of Glycogen-Degrading Enzymes and Glycosidases by Six-Membered Sugar Mimics and Their Evaluation in Cell Cultures. *Bioorganic & Medicinal Chemistry* **16**:7330-7336.

Ludwig DS (2002) The Glycemic Index: Physiological Mechanisms Relating to Obesity, Diabetes, and Cardiovascular Disease. *Jama* **287**:2414-2423.

Martin-Latil S, Cotte-Laffitte J, Beau I, Quéro AM, Géniteau-Legendre M and Servin AL (2004) A Cyclic AMP Protein Kinase A-Dependent Mechanism by Which Rotavirus Impairs the Expression and Enzyme Activity of Brush Border-Associated Sucrase-Isomaltase in Differentiated Intestinal Caco-2 Cells. *Cellular Microbiology* **6**:719-731.

Meunier V, Bourrié M, Berger Y and Fabre G (1995) The Human Intestinal Epithelial Cell Line Caco-2; Pharmacological and Pharmacokinetic Applications. *Cell Biology and Toxicology* **11**:187-194.

Mitrakou A, Kelley D, Veneman T, Jenssen T, Pangburn T, Reilly J and Gerich J (1990) Contribution of Abnormal Muscle and Liver Glucose Metabolism to Postprandial Hyperglycemia in NIDDM. *Diabetes* **39**:1381-1390.

Miura T, Koide T, Ohichi R, Kako M, Usami M, Ishihara E, Yasuda N, Ishida H, Seino Y and Tanigawa K (1998) Effect of Acarbose (α-Glucosidase Inhibitor) on Disaccharase Activity in Small Intestine in KK-Ay and DdY Mice. *J Nutr Sci Vitaminol* **44**:371-379.

Miyahara C, Miyazawa M, Satoh S, Sakai A and Mizusaki S (2004) Inhibitory Effects of Mulberry Leaf Extract on Postprandial Hyperglycemia in Normal Rats. *J Nutr Sci Vitaminol (Tokyo)* **50**:161-164.

Molyneux RJ, Pan YT, Goldmann A, Tepfer DA and Elbein AD (1993) Calystegines, a Novel Class of Alkaloid Glycosidase Inhibitors. *ARCHIVES OF BIOCHEMISTRY AND BIOPHYSICS* **304**:81-88.

Moosophon P, Baird MC, Kanokmedhakul S and Pyne SG (2010) Total Synthesis of Calystegine B_4. *Eur J Org Chem* **2010**:3337-3344.

Motulsky HJ and Christopoulos A (2003) *Fitting Models to Biological Data Using Linear and Nonlinear Regression. A Practical Guide to Curve Fitting*. GraphPad Software Inc., San Diego.

Nash RJ, Rothschild M, Porter EA, Watson AA, Waigh RD and Waterman PG (1993) Calystegines in *Solanum* and *Datura* Species and the Death's-Head Hawk-Moth (*Acherontia Atropus*). *Phytochemistry* **34**:1281-1283.

Nerinckx W, Desmet T and Claeyssens M (2003) A Hydrophobic Platform As a Mechanistically Relevant Transition State Stabilising Factor Appears to Be Present in the Active Centre of *All* Glycoside Hydrolases. *FEBS Letters* **538**:1-7.

Nichols BL, Avery S, Sen P, Swallow DM, Hahn D and Sterchi E (2003) The Maltase-Glucoamylase Gene: Common Ancestry to Sucrase-Isomaltase With Complementary Starch Digestion Activities. *Proceedings of the National Academy of Sciences* **100**:1432-1437.

Nichols BL, Eldering J, Avery S, Hahn D, Quaroni A and Sterchi E (1998) Human Small Intestinal Maltase-Glucoamylase CDNA Cloning. *Journal of Biological Chemistry* **273**:3076-3081.

Nishioka T, Kawabata J and Aoyama Y (1998) Baicalein, an α-Glucosidase Inhibitor From *Scutellaria Baicalensis*. *J Nat Prod* **61**:1413-1415.

Nissink JW, Murray C, Hartshorn M, Verdonk ML, Cole JC and Taylor R (2002) A New Test Set for Validating Predictions of Protein-Ligand Interaction. *Proteins* **49**:457-471.

Odaka H, Miki N, Ikeda H and Matsuo T (1992) Effect of a Disaccharidase Inhibitor, AO-128, on Postprandial Hyperglycemia in Rats. *Journal of Japanese Society of Nutrition and Food Science (Japan)* **45**:27-31.

Odaka H, Shino A, Ikeda H and Matsuo T (1992) Antiobesity and Antidiabetic Actions of a New Potent Disaccharidase Inhibitor in Genetically Obese-Diabetic Mice, KKA^y. *J Nutr Sci Vitaminol (Tokyo)* **38**:27-37.

Park H, Hwang KY, Oh KH, Kim YH, Lee JY and Kim K (2008) Discovery of Novel α-Glucosidase Inhibitors Based on the Virtual Screening With the Homology-Modeled Protein Structure. *Bioorganic & Medicinal Chemistry* **16**:284-292.

Pastores GM, Weinreb NJ, Aerts H, Andria G, Cox TM, Giralt M, Grabowski GA, Mistry PK and Tylki-Szymañska A (2004) Therapeutic Goals in the Treatment of Gaucher Disease. *Seminars in Hematology* **41,** Supplement 5:4-14.

Pinto M, Robine-Leon S, Appay M-D, Kedinger M, Triadou N, Dussaulx E, Lacroix B, Simon-Assmann P, Haffen K, Fogh J and Zweibaum A (1983) Enterocyte-Like Differentiation and Polarization of the Human Colon Carcinoma Cell Line Caco-2 in Culture. *Biology of the Cell* **47**:323-330.

Platt FM, Neises GR, Dwek RA and Butters TD (1994) *N*-Butyldeoxynojirimycin Is a Novel Inhibitor of Glycolipid Biosynthesis. *Journal of Biological Chemistry* **269**:8362-8365.

Portsteffen A, Dräger B and Nahrstedt A (1992) Two Tropinone Reducing Enzymes From *Datura Stramonium* Transformed Root Cultures. *Phytochemistry* **31**:1135-1138.

Portsteffen A, Dräger B and Nahrstedt A (1994) The Reduction of Tropinone in *Datura Stramonium* Root Cultures by Two Specific Reductases. *Phytochemistry* **37**:391-400.

Puls W, Keup U, Krause HP, Thomas G and Hoffmeister F (1977) Glucosidase Inhibition. *Naturwissenschaften* **64**:536-537.

Quezada-Calvillo R, Robayo-Torres CC, Ao Z, Hamaker BR, Quaroni A, Brayer GD, Sterchi EE, Baker SS and Nichols BL (2007) Luminal Substrate "Brake" on Mucosal Maltase-Glucoamylase Activity Regulates Total Rate of Starch Digestion to Glucose. *Journal of Pediatric Gastroenterology and Nutrition* **45**:32-43.

Quezada-Calvillo R, Sim L, Ao Z, Hamaker BR, Quaroni A, Brayer GD, Sterchi EE, Robayo-Torres CC, Rose DR and Nichols BL (2008) Luminal Starch Substrate "Brake" on Maltase-Glucoamylase Activity Is Located Within the Glucoamylase Subunit. *J Nutr* **138**:685-692.

Ranilla LG, Kwon YI, Apostolidis E and Shetty K (2010) Phenolic Compounds, Antioxidant Activity and in Vitro Inhibitory Potential Against Key Enzymes Relevant for Hyperglycemia and Hypertension of Commonly Used Medicinal Plants, Herbs and Spices in Latin America. *Bioresource Technology* **101**:4676-4689.

Rasmussen TS and Jensen HH (2011) Chiral Pool Synthesis of Calystegine A$_3$ From 2-Deoxyglucose Via a Brown Allylation. *Carbohydrate Research* **346**:2855-2861.

Ratner RE (2001) Controlling Postprandial Hyperglycemia. *The American Journal of Cardiology* **88**:26-31.

Richter U, Sonnewald U and Dräger B (2007) Calystegines in Potatoes With Genetically Engineered Carbohydrate Metabolism. *Journal of Experimental Botany* **58**:1603-1615.

Römpp H, Falbe J and Regitz M (1992) *Römpp-Chemie-Lexikon*. Georg Thieme Verlag, Stuttgart-New York.

Rossi EJ, Sim L, Kuntz DA, Hahn D, Johnston BD, Ghavami A, Szczepina MG, Kumar NS, Sterchi EE, Nichols BL, Pinto BM and Rose DR (2006) Inhibition of Recombinant Human Maltase Glucoamylase by Salacinol and Derivatives. *FEBS Journal* **273**:2673-2683.

Rothe G, Garske U and Dräger B (2001) Calystegines in Root Cultures of *Atropa Belladonna* Respond to Sucrose, Not to Elicitation. *Plant Science* **160**:1043-1053.

Rousset M, Chantret I, Darmoul D, Trugnan G, Sapin C, Green F, Swallow D and Zweibaum A (1989) Reversible Forskolin-Induced Impairment of Sucrase-Isomaltase MRNA Levels, Biosynthesis, and Transport to the Brush Border Membrane in Caco-2 Cells. *J Cell Physiol* **141**:627-635.

Rüttinger HH and Dräger B (2001) Pulsed Amperometric Detection of Calystegines Separated by Capillary Electrophoresis. *Journal of Chromatography A* **925**:291-296.

Saltiel AR and Kahn CR (2001) Insulin Signalling and the Regulation of Glucose and Lipid Metabolism. *Nature* **414**:799-806.

Schimming T, Tofern B, Mann P, Richter A, Jenett-Siems K, Dräger B, Asano N, Gupta MP, Correa MD and Eich E (1998) Distribution and Taxonomic Significance of Calystegines in the Convolvulaceae. *Phytochemistry* **49**:1989-1995.

Scholl Y, Asano N and Dräger B (2001) Automated Multiple Development Thin Layer Chromatography for Calystegines and Their Biosynthetic Precursors. *Journal of Chromatography A* **928**:217-224.

Semenza G and Auricchio S (1989) in *The Metabolic Basis of Inherited Disease II* (Scriver CR, Beaudet A, Sly W, Valle D, Stanbury J, Wyngaarden J and Frederickson D eds) pp 2975-2997, McGraw-Hill Inc., New York.

Sherwood L (1997) *Human Physiology: From Cells to Systems*. Wadsworth Pub. Co., Belmont, CA.

Sim L, Quezada-Calvillo R, Sterchi EE, Nichols BL and Rose DR (2008) Human Intestinal Maltase-Glucoamylase: Crystal Structure of the N-Terminal Catalytic Subunit and Basis of Inhibition and Substrate Specificity. *Journal of Molecular Biology* **375**:782-792.

Sim L, Willemsma C, Mohan S, Naim HY, Pinto BM and Rose DR (2010) Structural Basis for Substrate Selectivity in Human Maltase-Glucoamylase and Sucrase-Isomaltase N-Terminal Domains. *Journal of Biological Chemistry* **285**:17763-17770.

Sinanoglu O and Fernández A (1985) The Denaturation Maxima of Proteins and of Drug-Biomolecule Complex Formation in a Wide Range of Methanol/Water Mixtures: Solvophobic Theory Predictions As Compared to Experiments. *Biophysical Chemistry* **21**:157-162.

Skaanderup PR and Madsen R (2001) Short Syntheses of Enantiopure Calystegine B_2, B_3, and B_4. *Chem Commun I*:1106-1107.

Skaanderup PR and Madsen R (2003) A Short Synthetic Route to the Calystegine Alkaloids. *J Org Chem* **68**:2115-2122.

Stegelmeier BL, Molyneux RJ, Asano N, Watson AA and Nash RJ (2008) The Comparative Pathology of the Glycosidase Inhibitors Swainsonine, Castanospermine, and Calystegines A3, B2, and C1 in Mice. *Toxicologic Pathology* **36**:651-659.

Stenzel O, Teuber M and Dräger B (2006) Putrescine *N*-Methyltransferase in *Solanum Tuberosum* L., a Calystegine-Forming Plant. *Planta* **223**:200-212.

Stevens RJ, Kothari V, Adler AI, Stratton IM and (2001) The UKPDS Risk Engine: a Model for the Risk of Coronary Heart Disease in Type II Diabetes (UKPDS 56). *Clin Sci* **101**:671-679.

Sweeley CC, Bentley R, Makita M and Wells WW (1963) Gas-Liquid Chromatography of Trimethylsilyl Derivatives of Sugars and Related Substances. *J Am Chem Soc* **85**:2497-2507.

Tepfer D, Goldmann A, Pamboukdjian N, Maille M, Lepingle A, Chevalier D, Dénarié J and Rosenberg C (1988) A Plasmid of *Rhizobium Meliloti* 41 Encodes Catabolism of Two Compounds From Root Exudate of *Calystegium Sepium*. *Journal of Bacteriology* **170**:1153-1161.

Toda M, Kawabata J and Kasai T (2000) α-Glucosidase Inhibitors From Clove (*Syzgium Aromaticum*). *Bioscience, Biotechnology, and Biochemistry* **64**:294-298.

Trugnan G, Rousset M and Zweibaum A (1986) Castanospermine: a Potent Inhibitor of Sucrase From the Human Enterocyte-Like Cell Line Caco-2. *FEBS Letters* **195**:28-32.

Vasella A, Davies GJ and Böhm M (2002) Glycosidase Mechanisms. *Current Opinion in Chemical Biology* **6**:619-629.

Venn BJ and Green TJ (2007) Glycemic Index and Glycemic Load: Measurement Issues and Their Effect on Diet−Disease Relationships. *European Journal of Clinical Nutrition* **61**:122-131.

Verdonk ML, Cole JC, Hartshorn MJ, Murray CW and Taylor RD (2003) Improved Protein−Ligand Docking Using GOLD. *Proteins* **52**:609-623.

Vuong TV and Wilson DB (2010) Glycoside Hydrolases: Catalytic Base/Nucleophile Diversity. *Biotechnol Bioeng* **107**:195-205.

Watson AA, Fleet GWJ, Asano N, Molyneux RJ and Nash RJ (2001) Polyhydroxylated Alkaloids − Natural Occurrence and Therapeutic Applications. *Phytochemistry* **56**:265-295.

Willett W, Manson J and Liu S (2002) Glycemic Index, Glycemic Load, and Risk of Type 2 Diabetes. *The American Journal of Clinical Nutrition* **76**:274-280.

Yagi M, Kouno T, Aoyagi Y and Murai H (1976) The Structure of Moranoline, a Piperidine Alkaloid From *Morus* Species. *Journal of the Agricultural Chemical Society of Japan* **50**:571-572.

Yoshikawa M, Murakami T, Yashiro K, Matsuda K (1998) Kotalanol, a Potent α-Glucosidase Inhibitor With Thiosugar Sulfonium Sulfate Structure, From Antidiabetic Ayurvedic Medicine *Salacia Reticulata*. *Chem Pharm Bull* **46**:1339-1340.

Yoshikawa M, Murakami T, Shimada H, Matsuda H, Yamahara J, Tanabe G and Muraoka O (1997) Salacinol, Potent Antidiabetic Principle With Unique Thiosugar Sulfonium Sulfate Structure From the Ayurvedic Traditional Medicine *Salacia Reticulata* in Sri Lanka and India. *Tetrahedron Letters* **38**:8367-8370.

Yoshikuni Y (1988) Inhibition of Intestinal α-Glucosidase Activity and Postprandial Hyperglycemia by Moranoline and Its *N*-Alkyl Derivatives. *Agricultural and Biological Chemistry* **52**:121-128.

Yun DJ, Hashimoto T and Yamada Y (1992) Metabolic Engineering of Medicinal Plants: Transgenic Atropa Belladonna With an Improved Alkaloid Composition. *Proceedings of the National Academy of Sciences* **89**:11799-11803.

Zweibaum A, Hauri HP, Sterchi E, Chantret I, Haffen K, Bamat J and Sordat B (1984) Immunohistological Evidence, Obtained With Monoclonal Antibodies, of Small Intestinal Brush Border Hydrolases in Human Colon Cancers and Foetal Colons. *Int J Cancer* **34**:591-598.

6. Appendix

6.1. GC-chromatograms of calystegine standards

Figure 24: GC chromatogram of calystegine A₃ standard
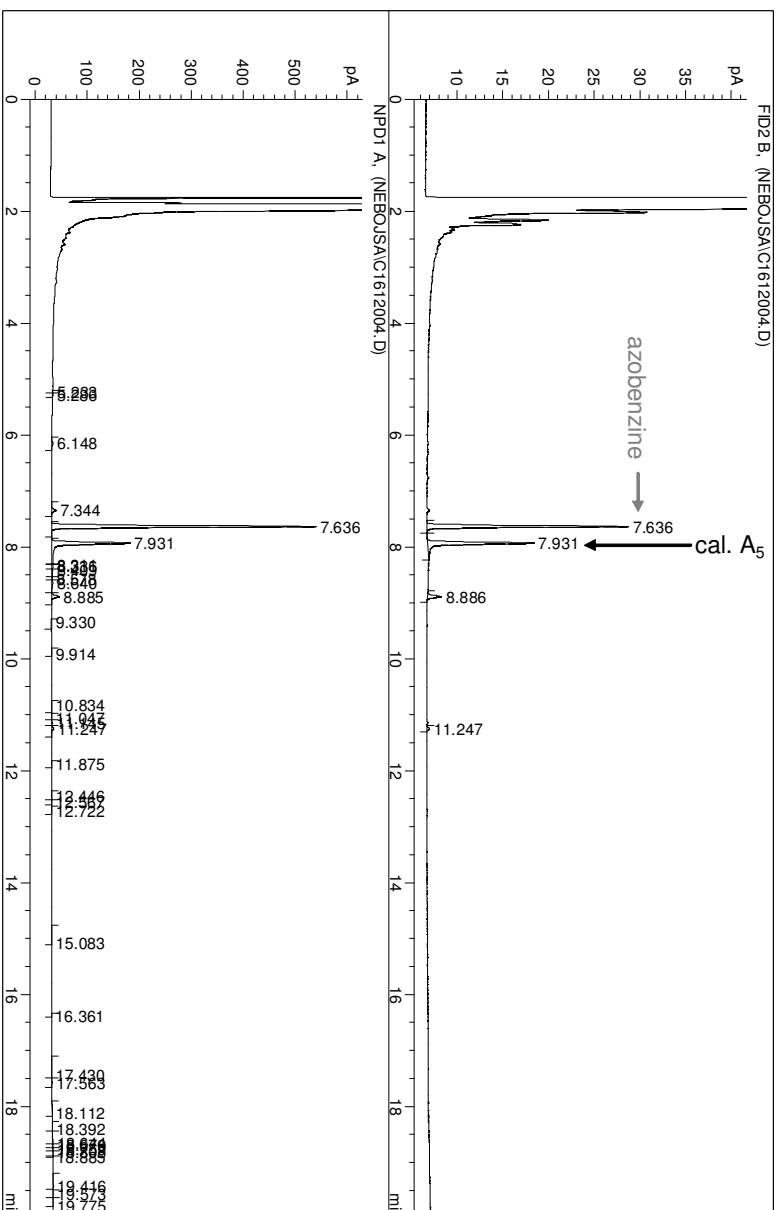
Figure 25: GC chromatogram of calystegine A₅ standard

Figure 26: GC chromatogram of calystegine B₁ standard

Figure 27: GC chromatogram of calystegine B₂ standard (mixture of calystegines)
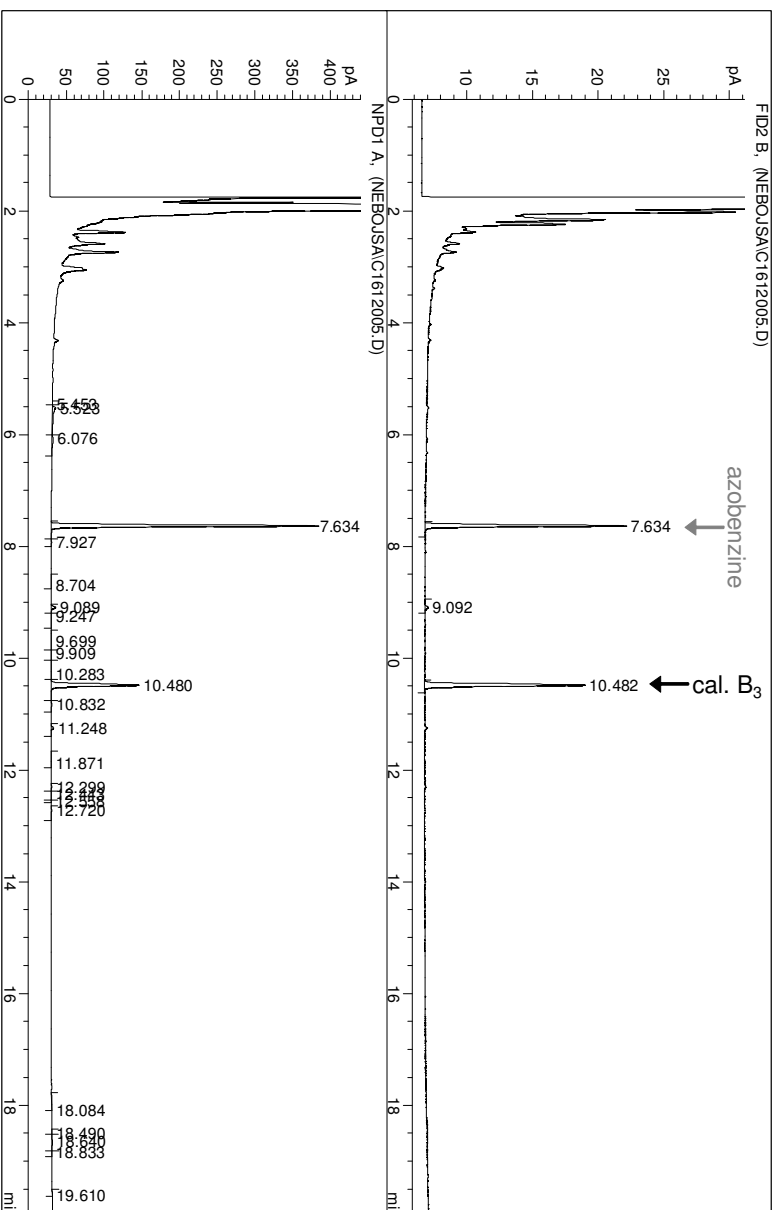
Figure 28: GC chromatogram of calystegine B₃ standard

Figure 29: GC chromatogram of calystegine B₄ standard
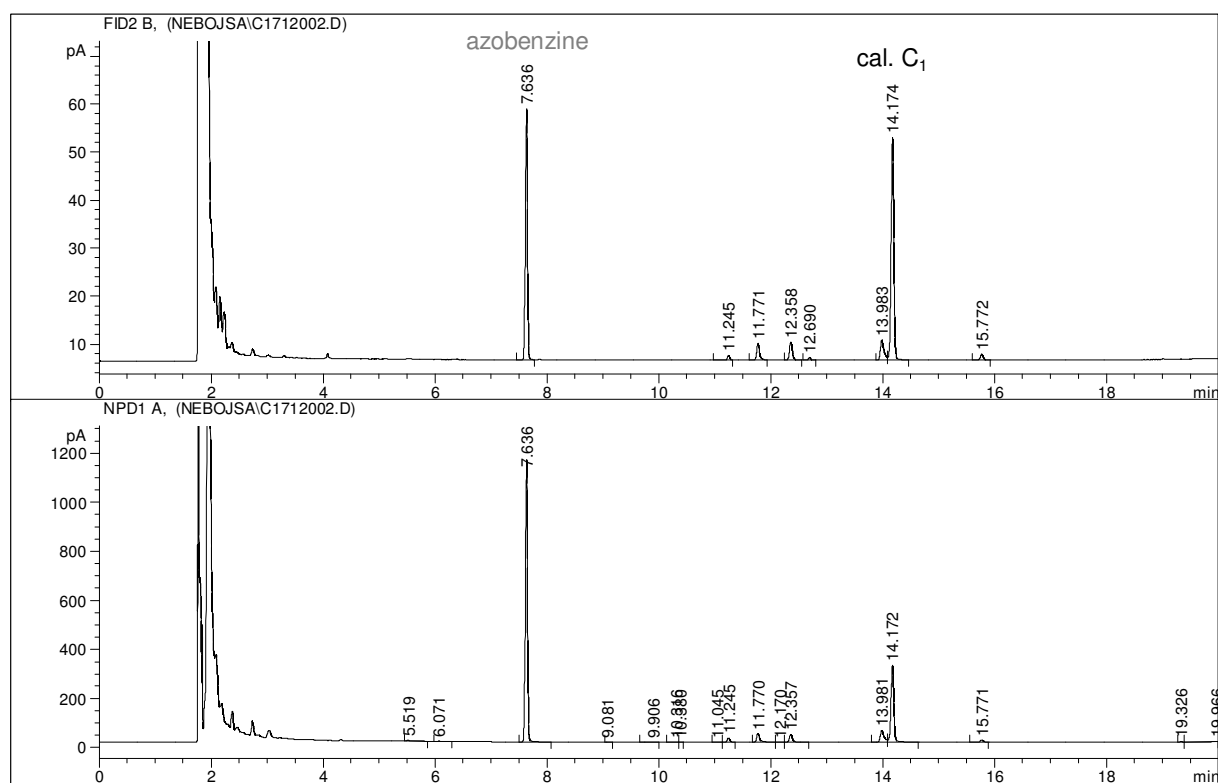
Figure 30: GC chromatogram of calystegine C₁ standard
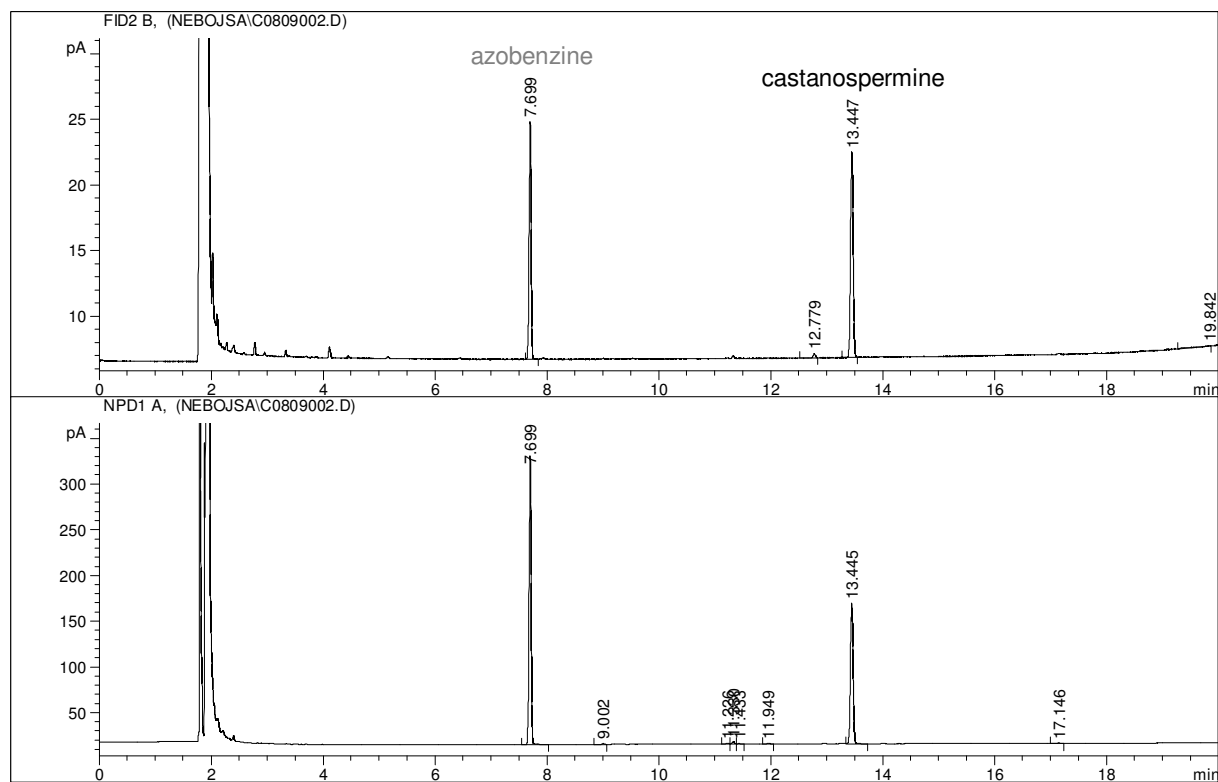
Figure 31: GC chromatogram of castanospermine standard

6.2. GC-MS-chromatograms of calystegine standards
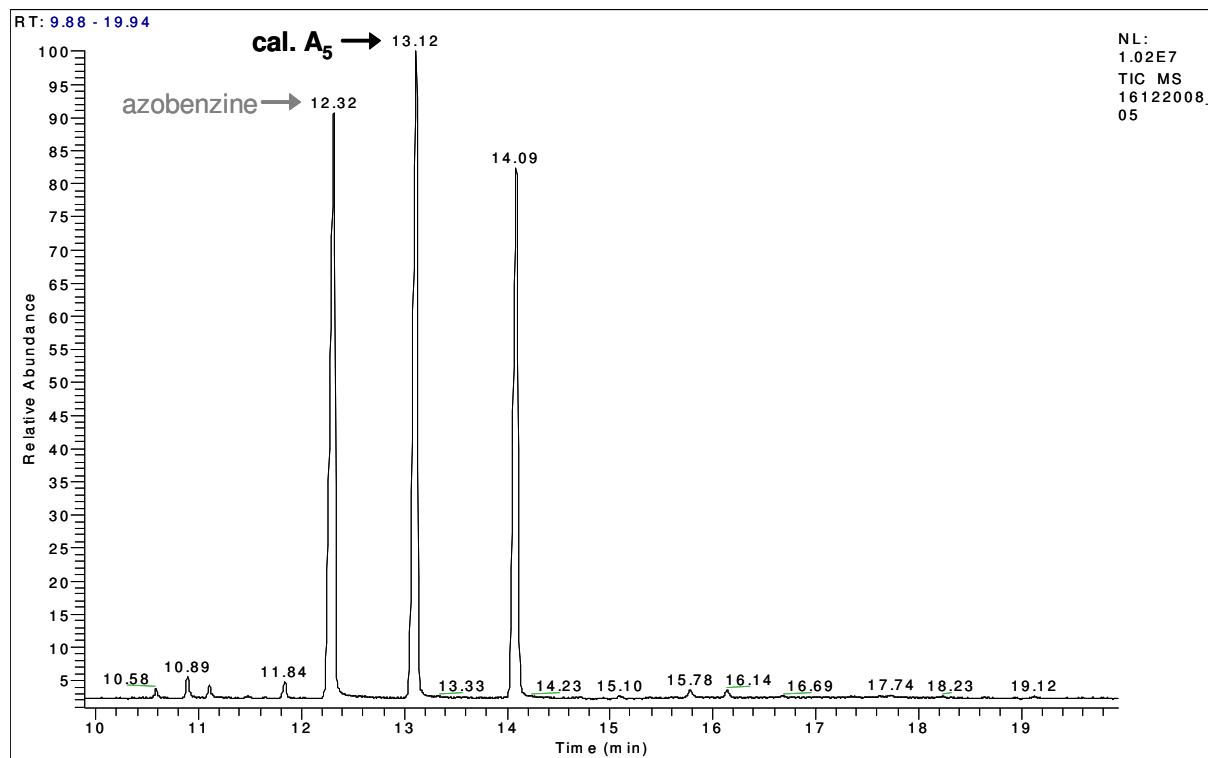
Figure 32: GC-MS chromatogram of calystegine A$_5$ standard
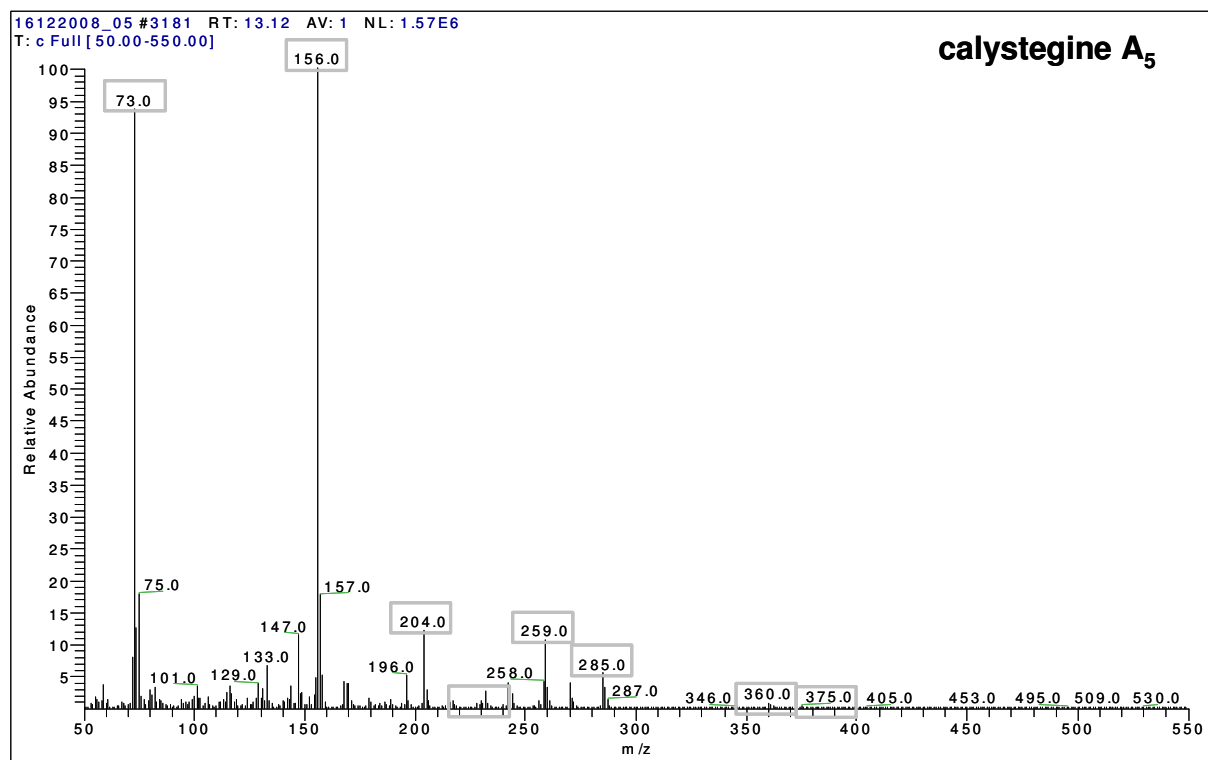
Figure 33: MS spectrum of calystegine A$_5$ standard
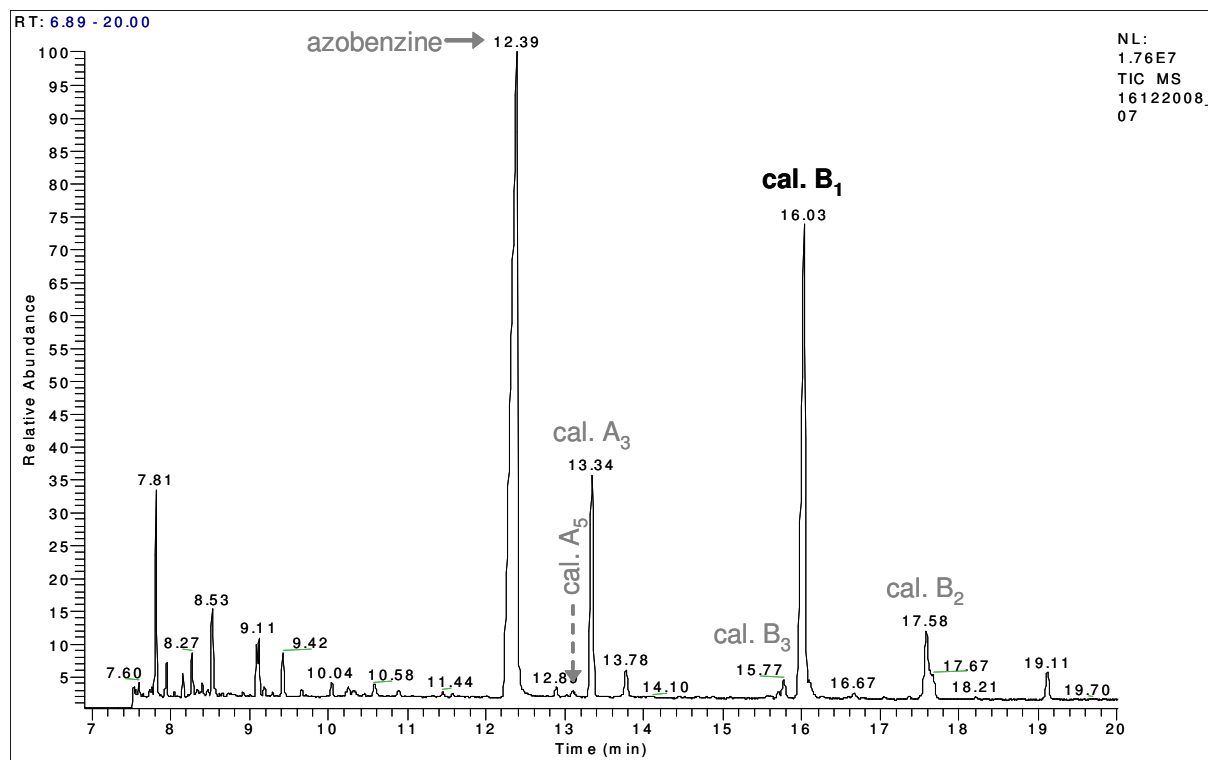
Figure 34: GC-MS chromatogram of calystegine B$_1$ standard
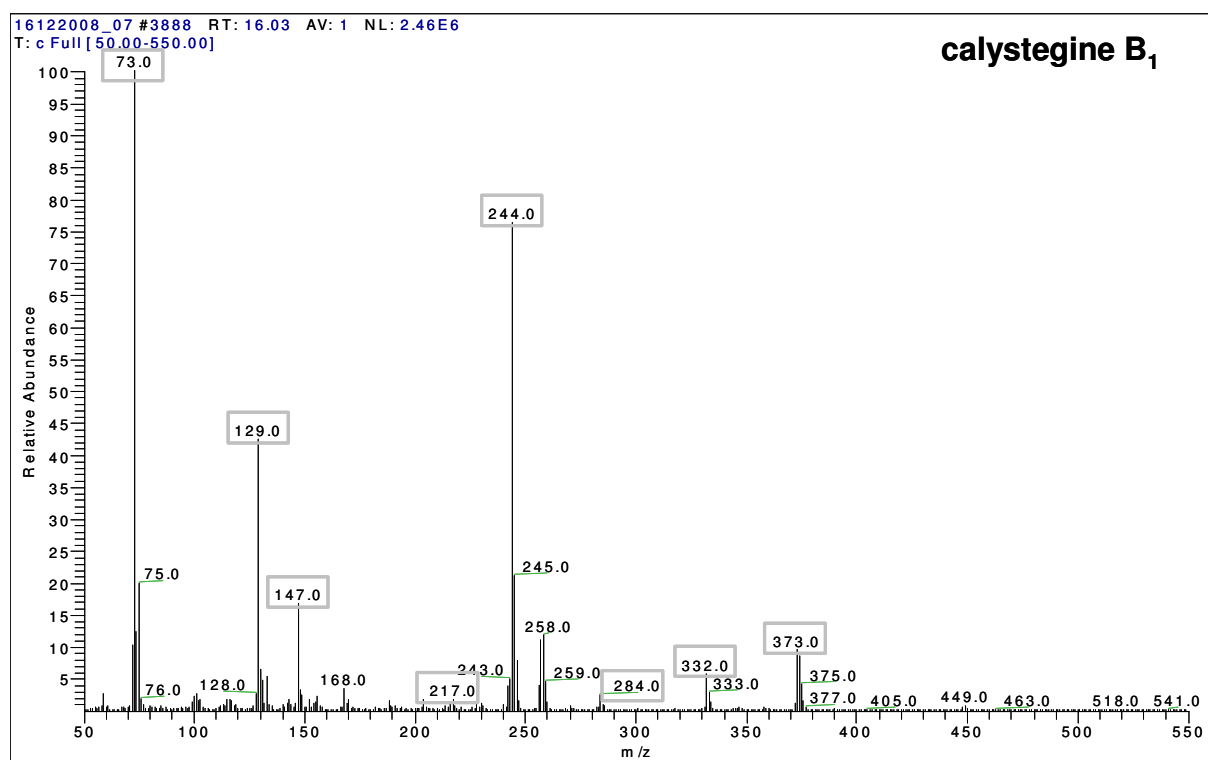
Figure 35: MS spectrum of calystegine B$_1$ standard
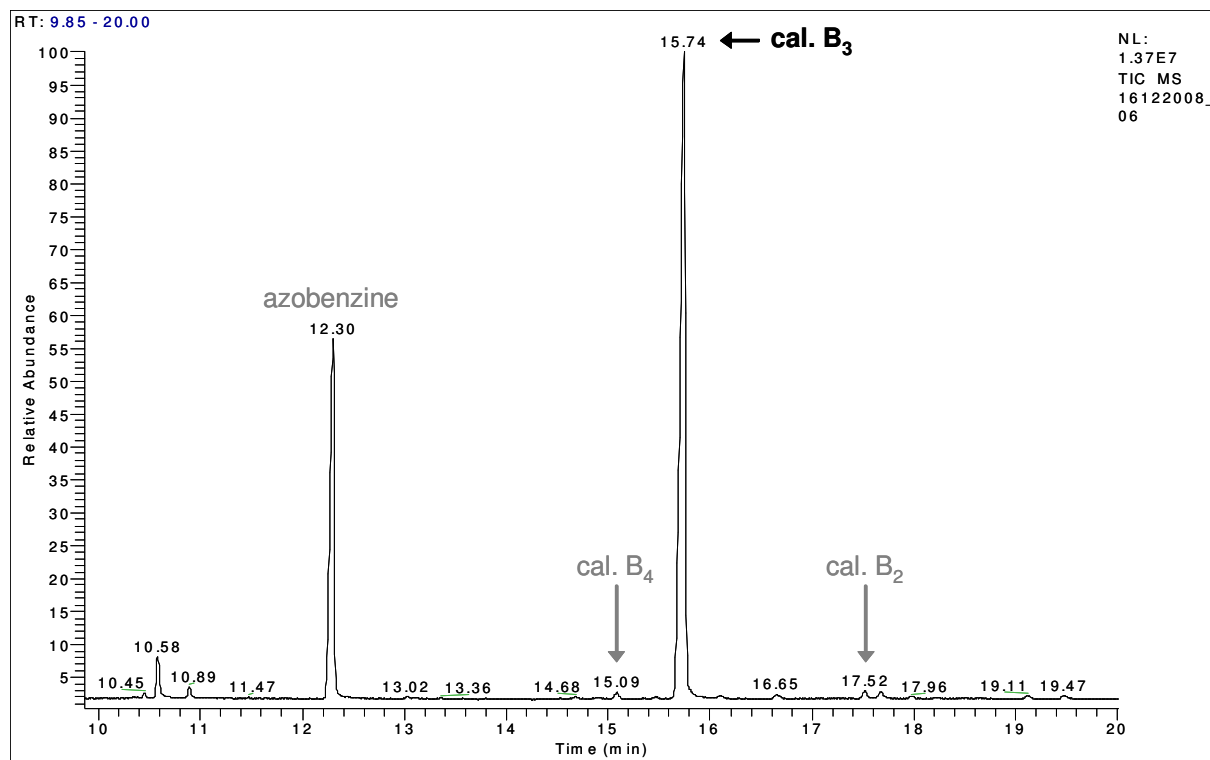
Figure 36: GC-MS chromatogram of calystegine B₃ standard
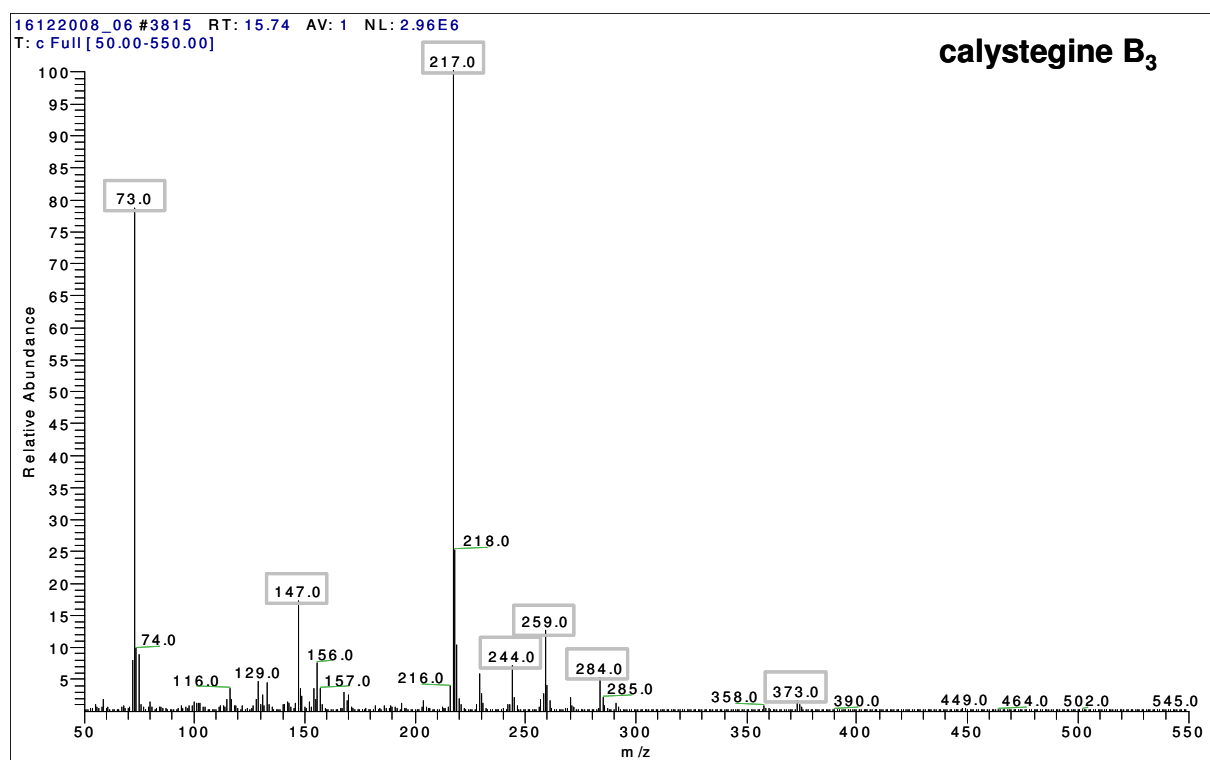
Figure 37: MS spectrum of calystegine B₃ standard
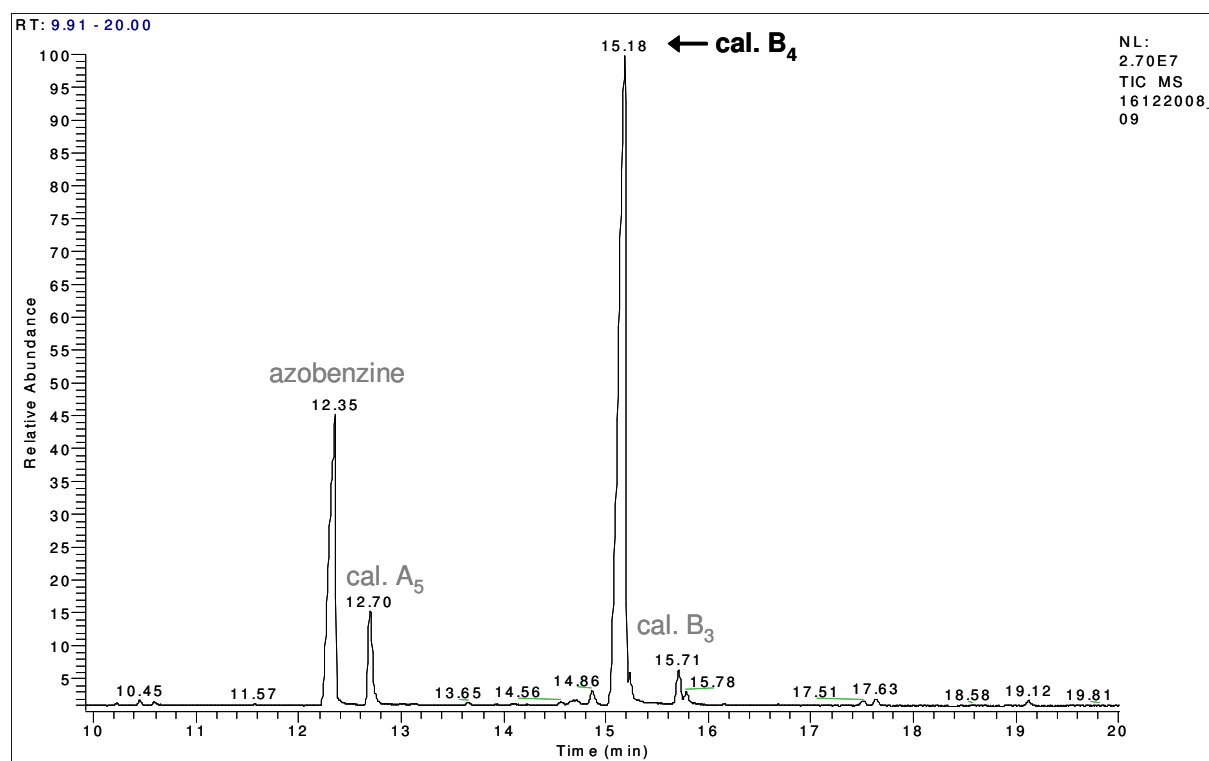
Figure 38: GC-MS chromatogram of calystegine B$_4$ standard
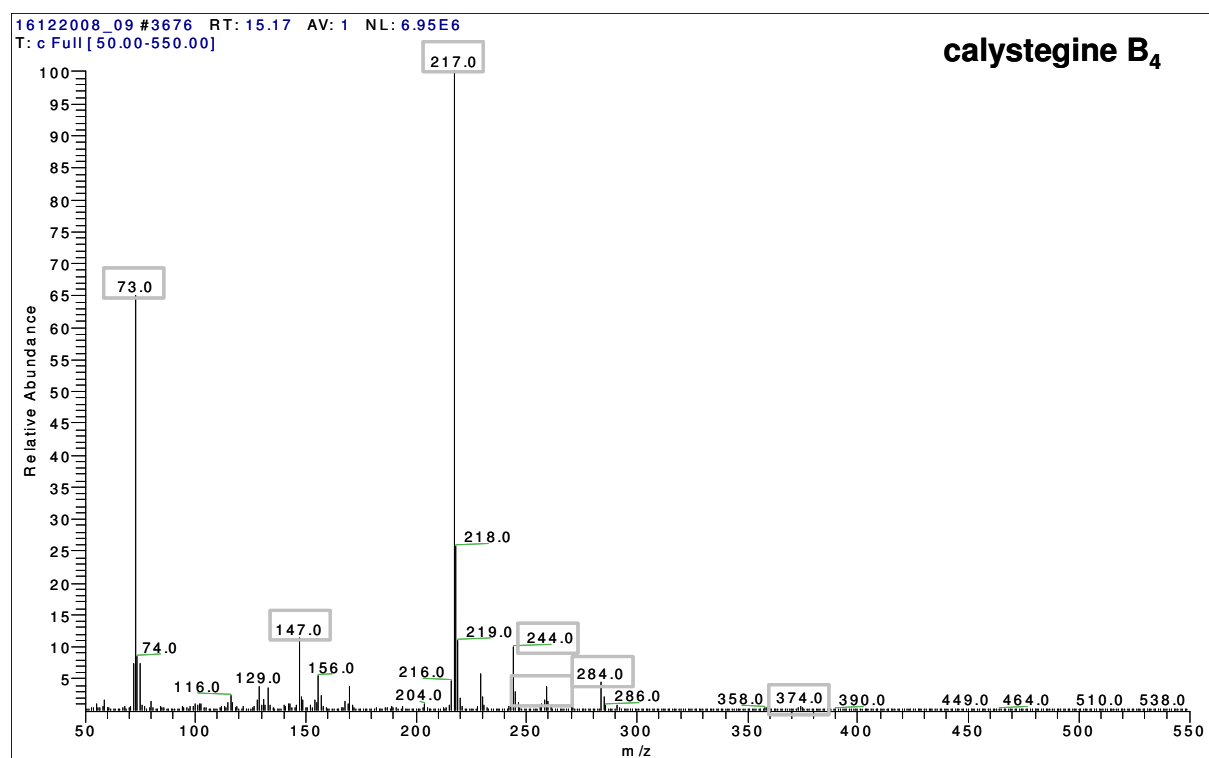
Figure 39: MS spectrum of calystegine B$_4$ standard
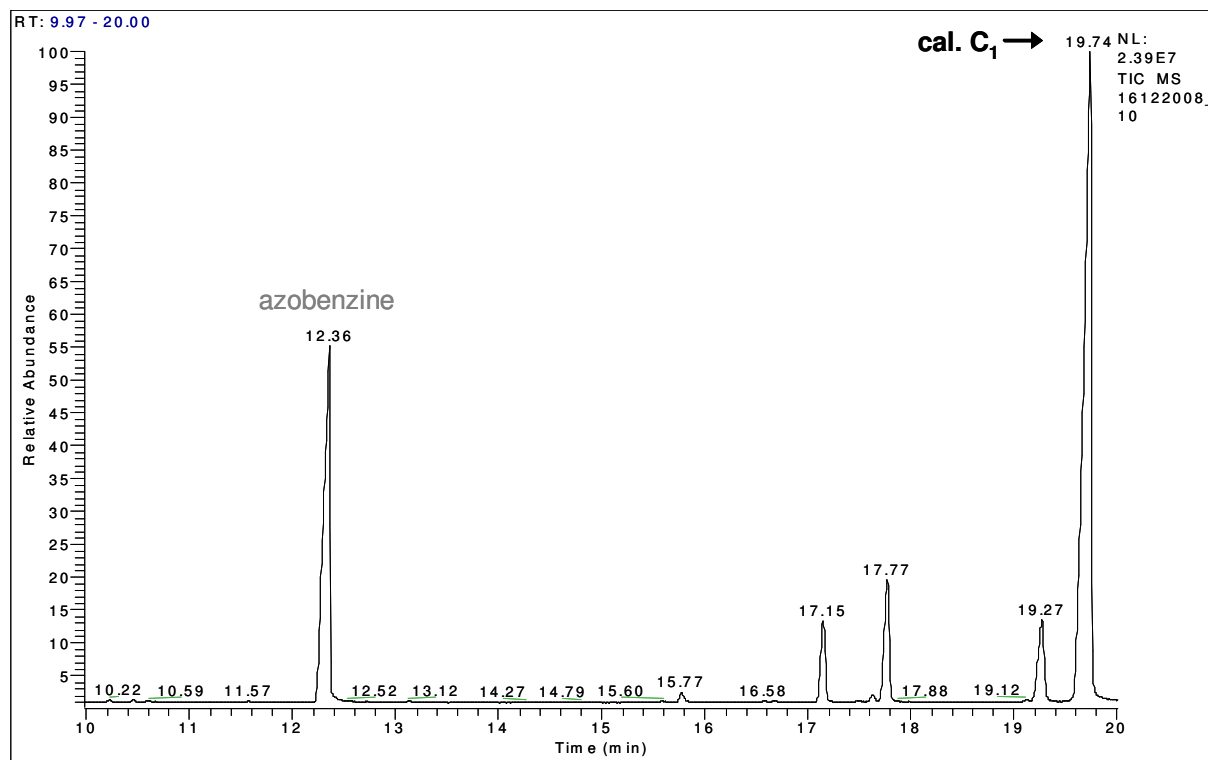
Figure 40: GC-MS chromatogram of calystegine C₁ standard
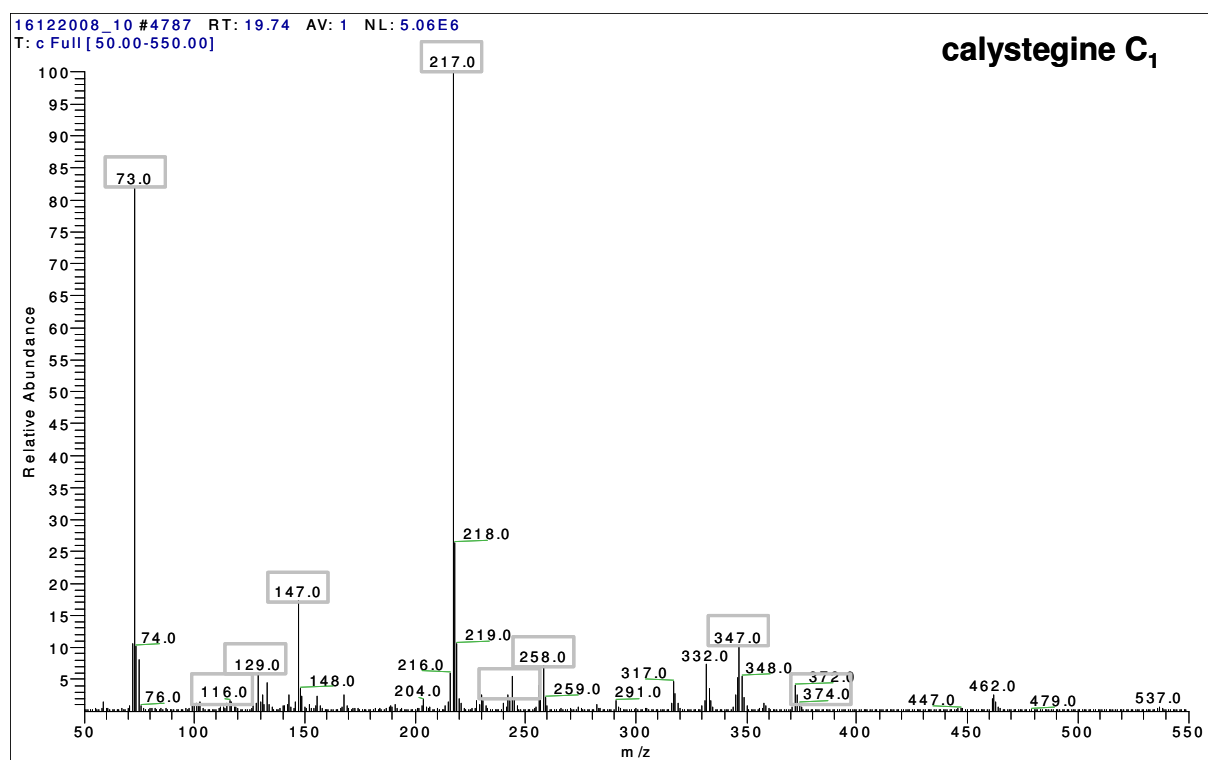
Figure 41: MS spectrum of calystegine C₁ standard

6.3. GC-chromatograms of calystegine purification

Figure 42: GC chromatogram of potato sprouts raw extract flow-through fraction 1 during purification on Merck I column

FID2 B, (NEBOJSAC1805011.D)

- compounds present in the NH₃ eluate
- compounds eliminated with flow fraction
- azobenzine
- fructose peaks
- glucose peak 1
- glucose peak 2
- sucrose

NPD1 A, (NEBOJSAC1805011.D)

Figure 43: GC chromatogram of potato sprouts raw extract flow-through fraction 2 during purification on Merck I column

FID2 B, (NEBOJSAC1405015.D)

- compounds eliminated with flow fraction
- compounds present in the NH₃ eluate
- azobenzine
- fructose peaks
- glucose peak 1; peak 2
- no sucrose

NPD1 A, (NEBOJSAC1405015.D)

Figure 44: GC chromatogram of ammonium eluate of potato sprouts raw extract purification on Merck I column (Merck I extract)
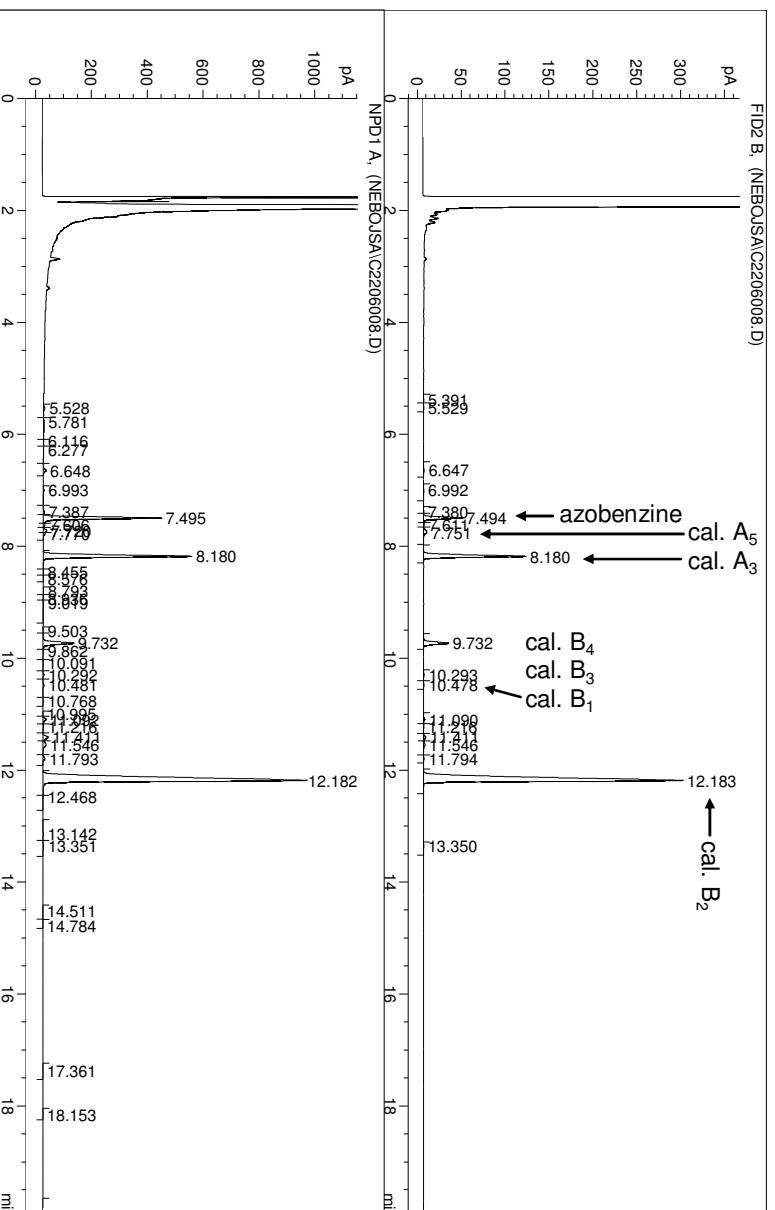
Figure 45: GC chromatogram of aqueous wash of potato sprouts extract on Merck III column (Merck III extract)
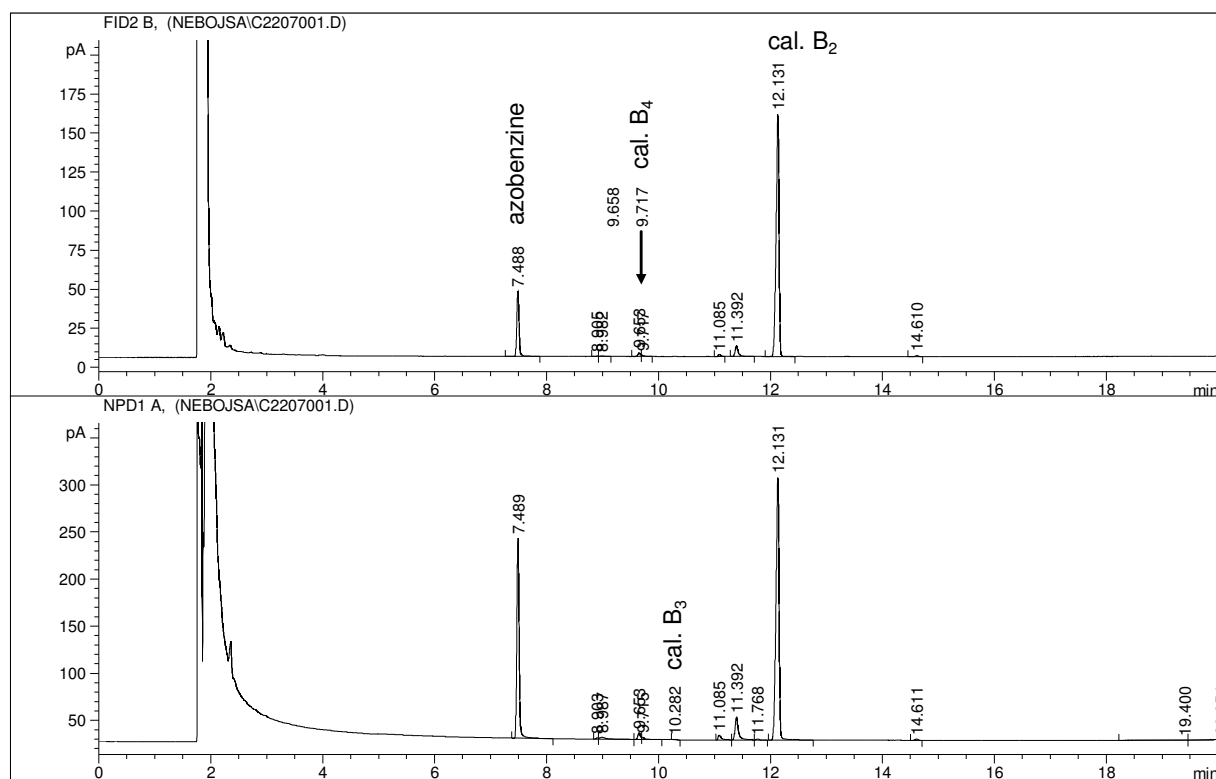
Figure 46: GC chromatogram of calystegine B$_2$ pool (fractions [15, 90])
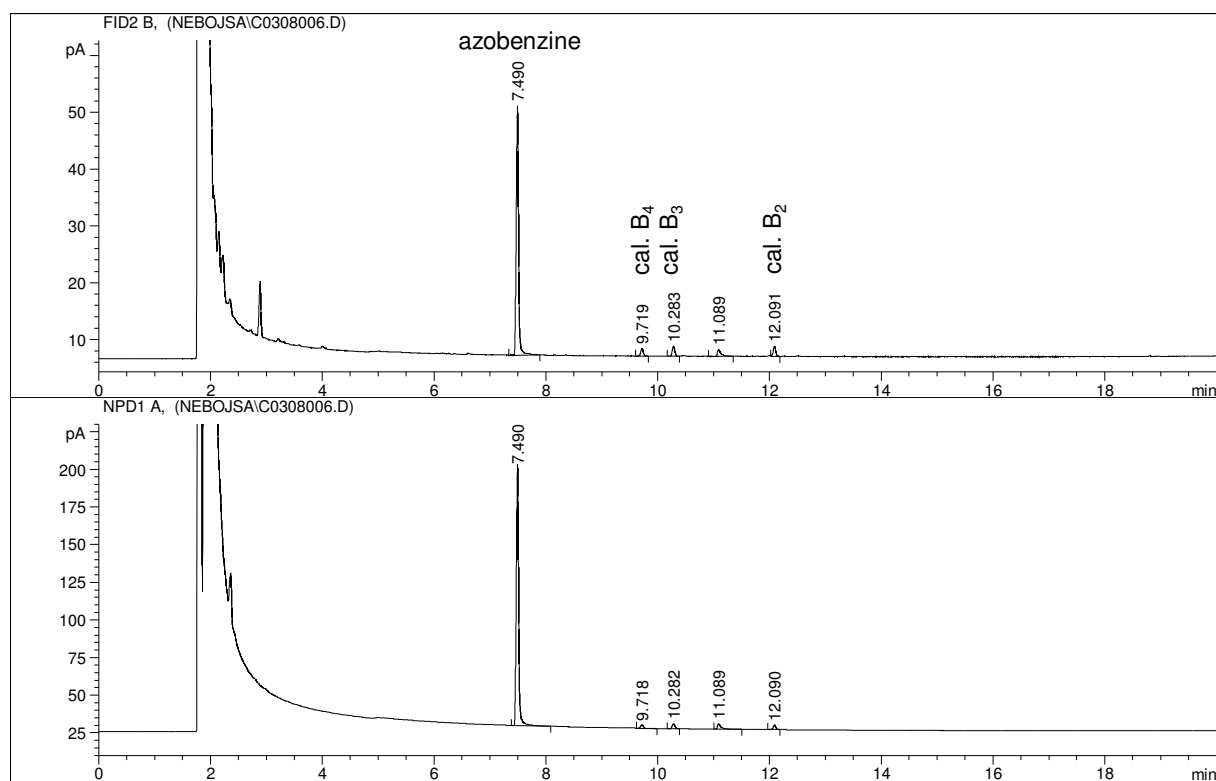
Figure 47: GC chromatogram of calystegine B$_2$, B$_3$ and B$_4$ mix pool (fractions [91, 109])
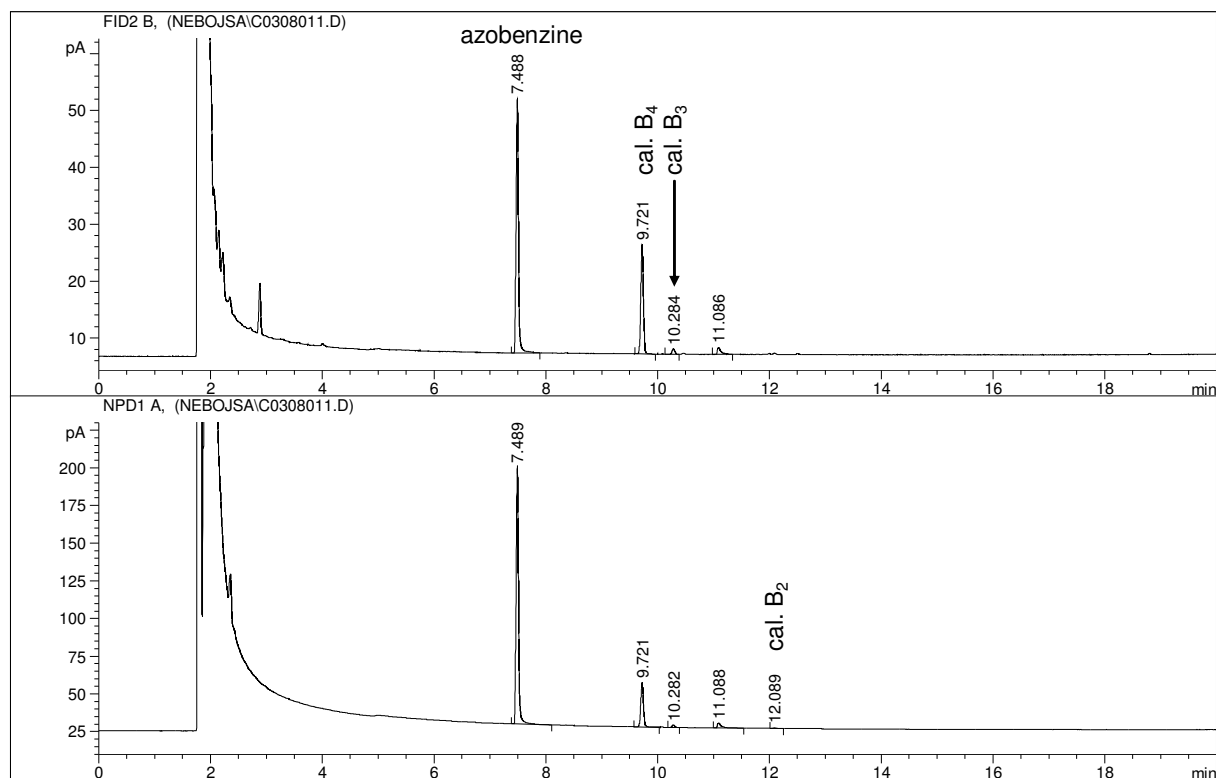
Figure 48: GC chromatogram of calystegine B_4 pool (fractions [110, 234])
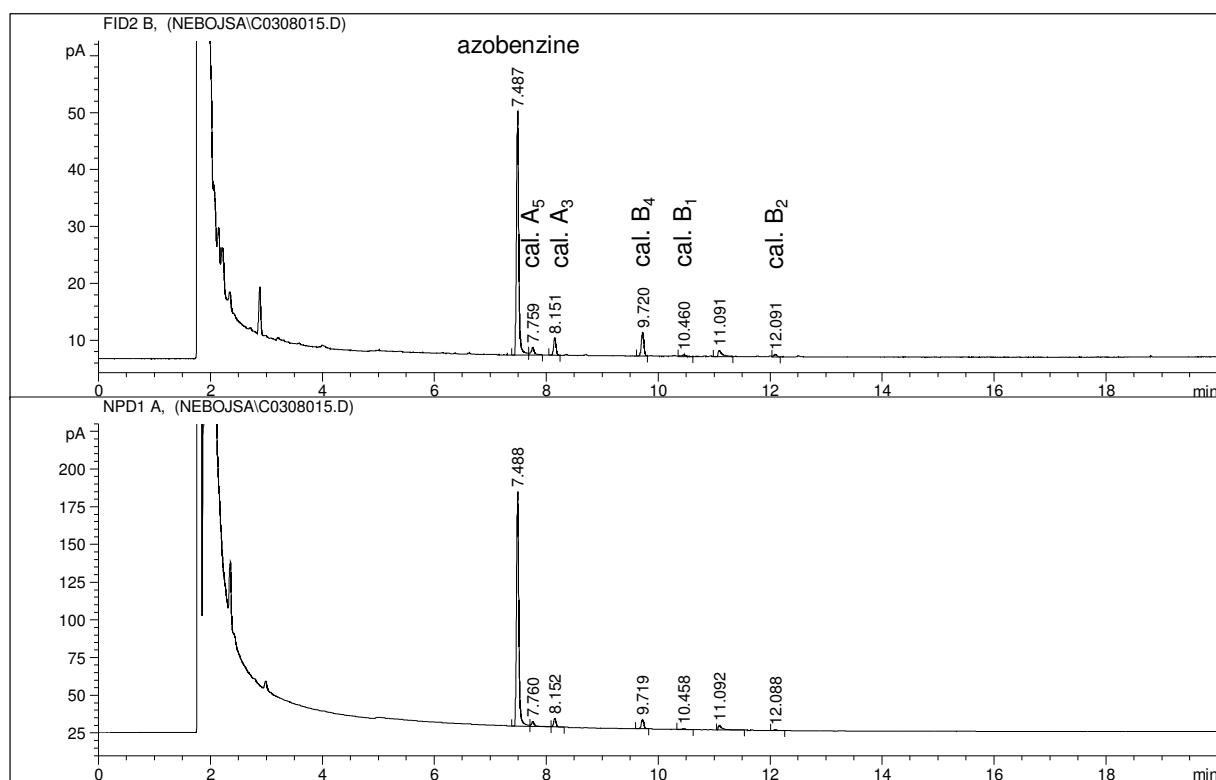
Figure 49: GC chromatogram of calystegine mix (A_3, A_5, and B_4) pool (fractions [235, 299])
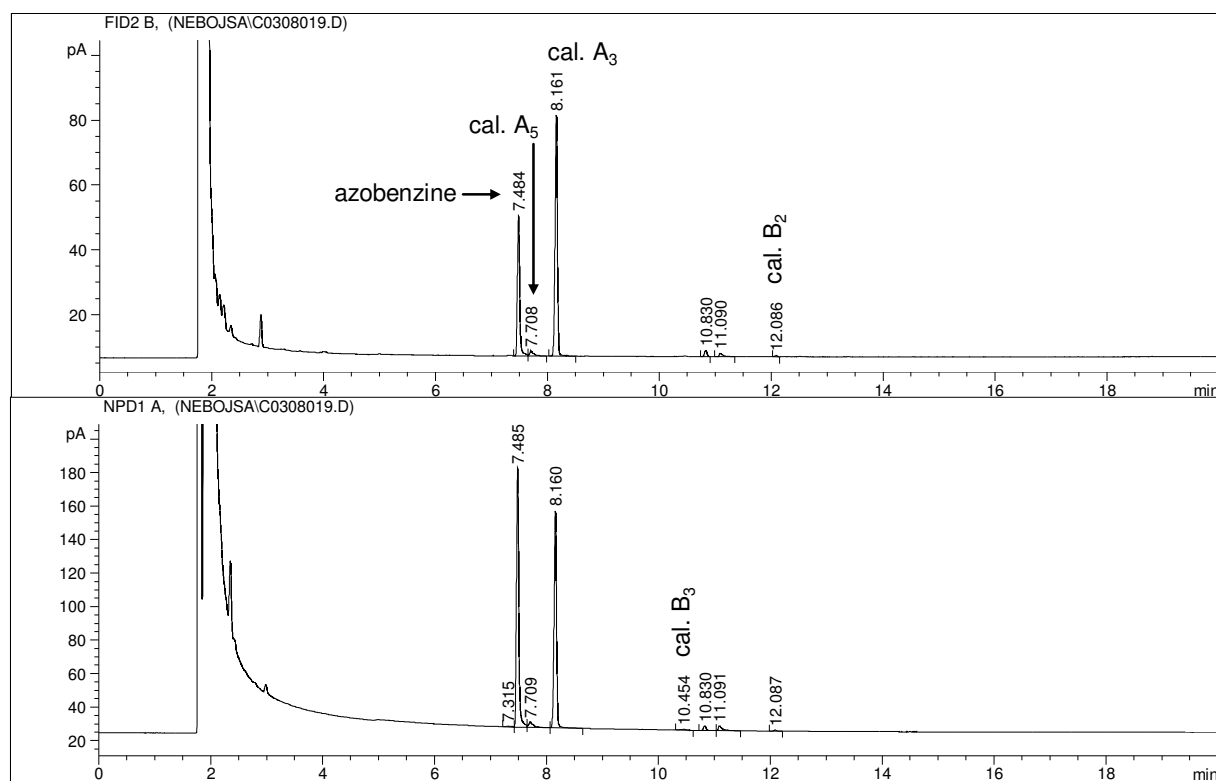
Figure 50: GC chromatogram of calystegine A_3 pool (fractions [300, 630])

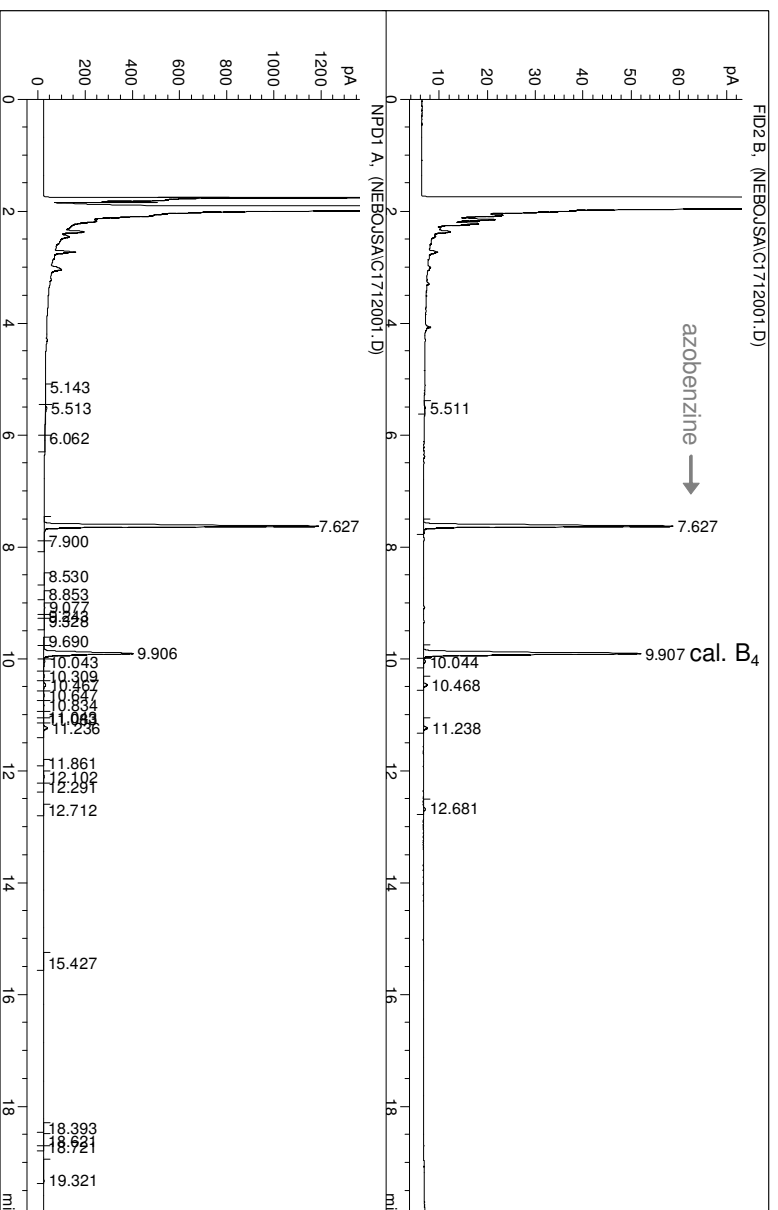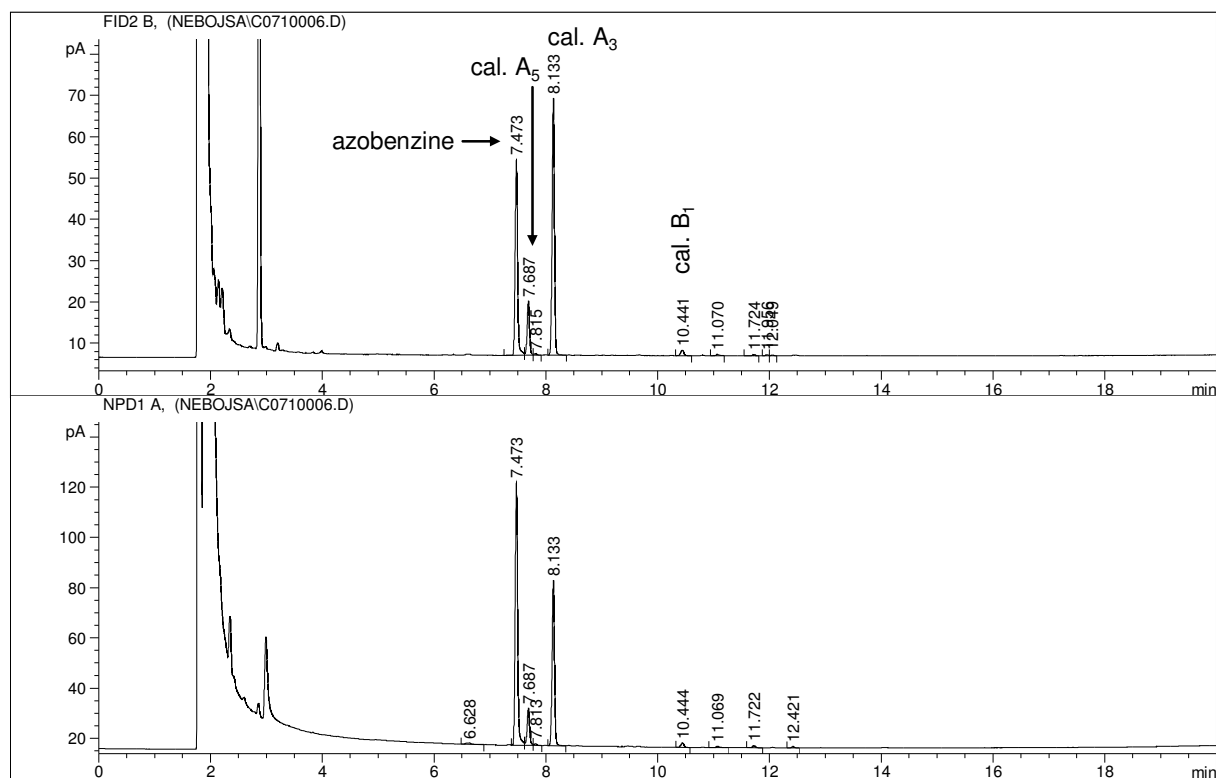**Figure 51: GC chromatogram of calystegine A_3 and A_5 mix pool (fractions [631, 797])**
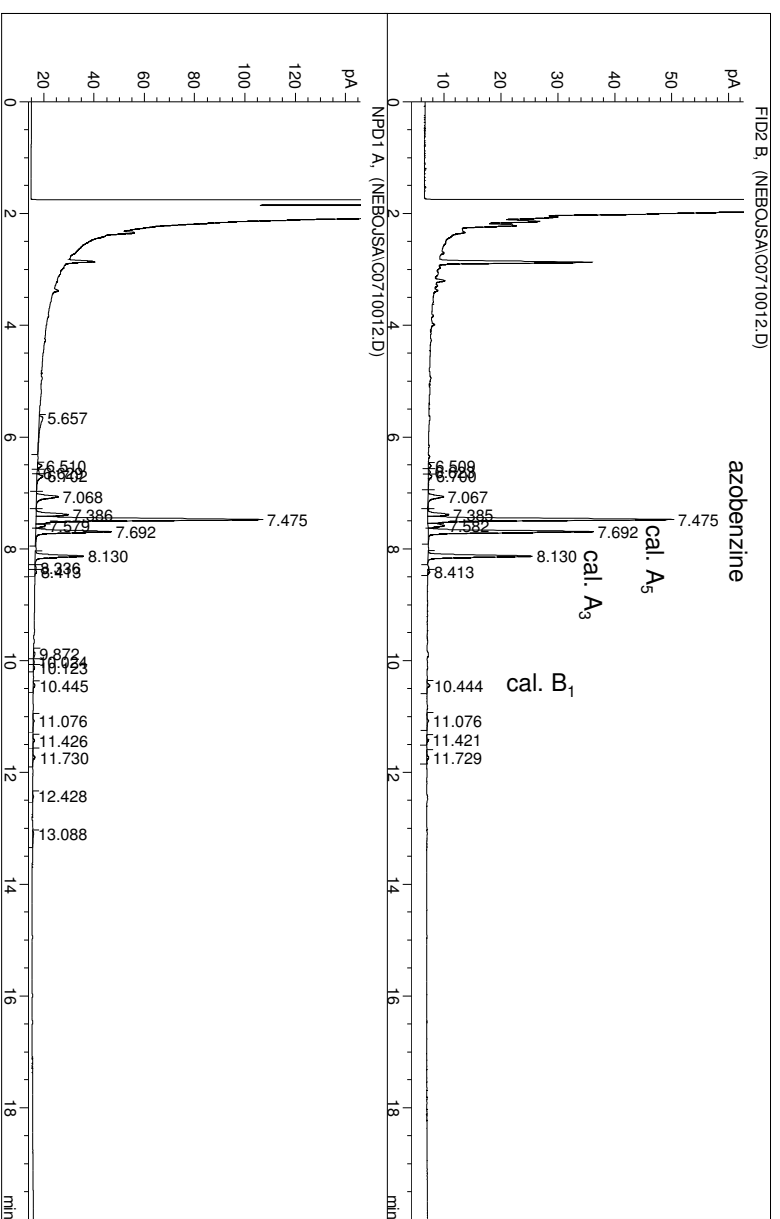
Figure 52: GC chromatogram of calystegine A$_5$ and A$_3$ mix pool (fractions [798; 800])

6.4. GC-MS chromatograms of purified calystegine pools

Pools appearance shown according to the calystegine elution order.
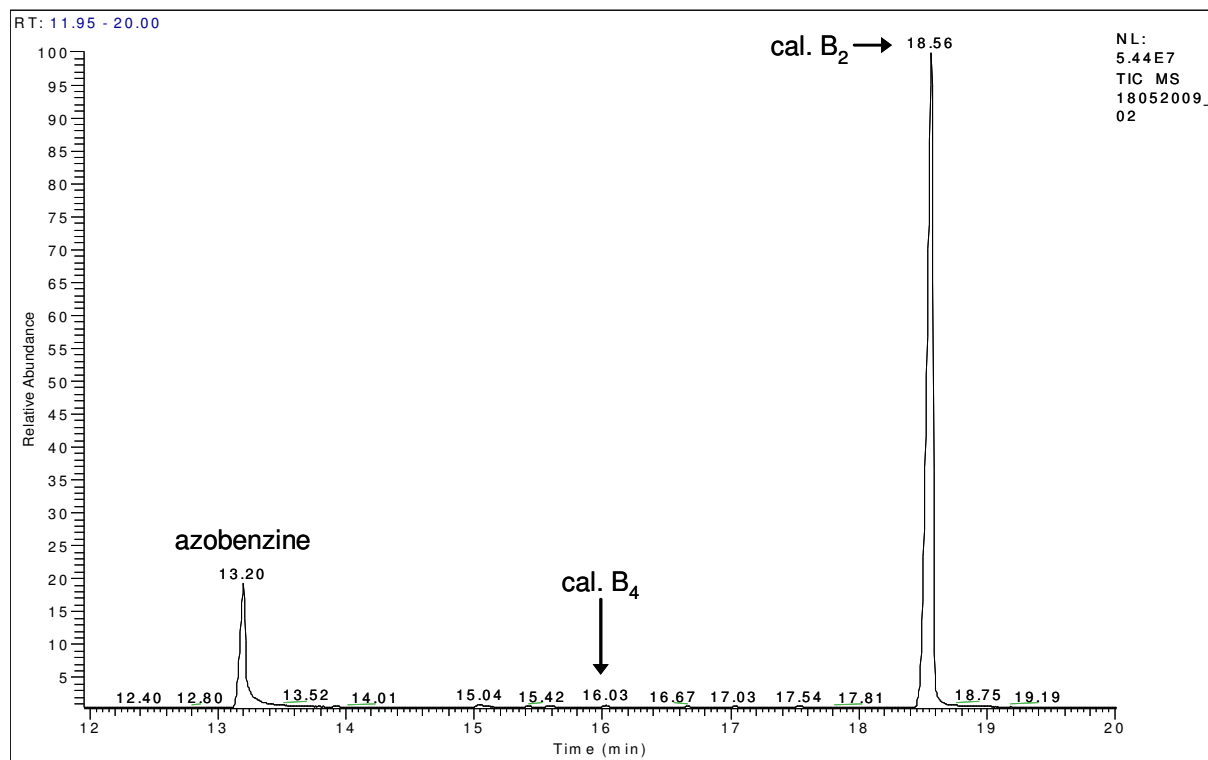
Figure 53: GC-MS chromatogram of calystegine B₂ pool
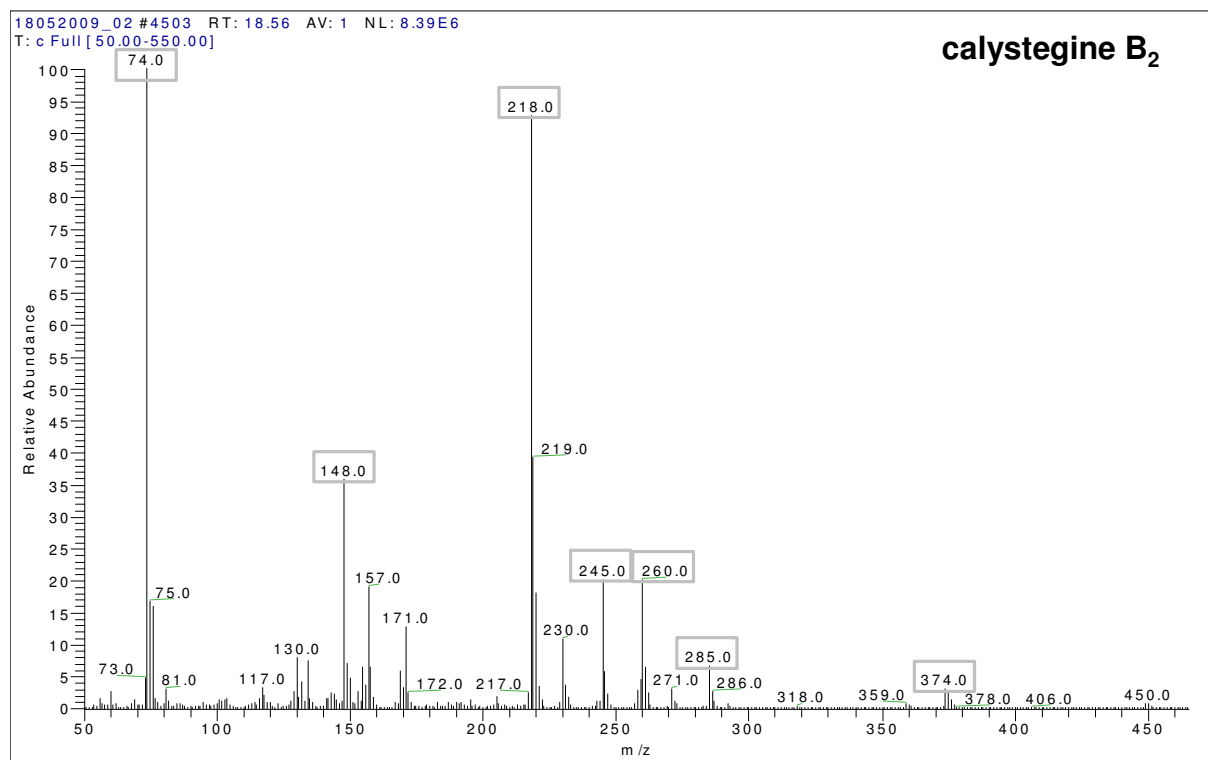
Figure 54: MS spectrum of calystegine B₂ in its pool
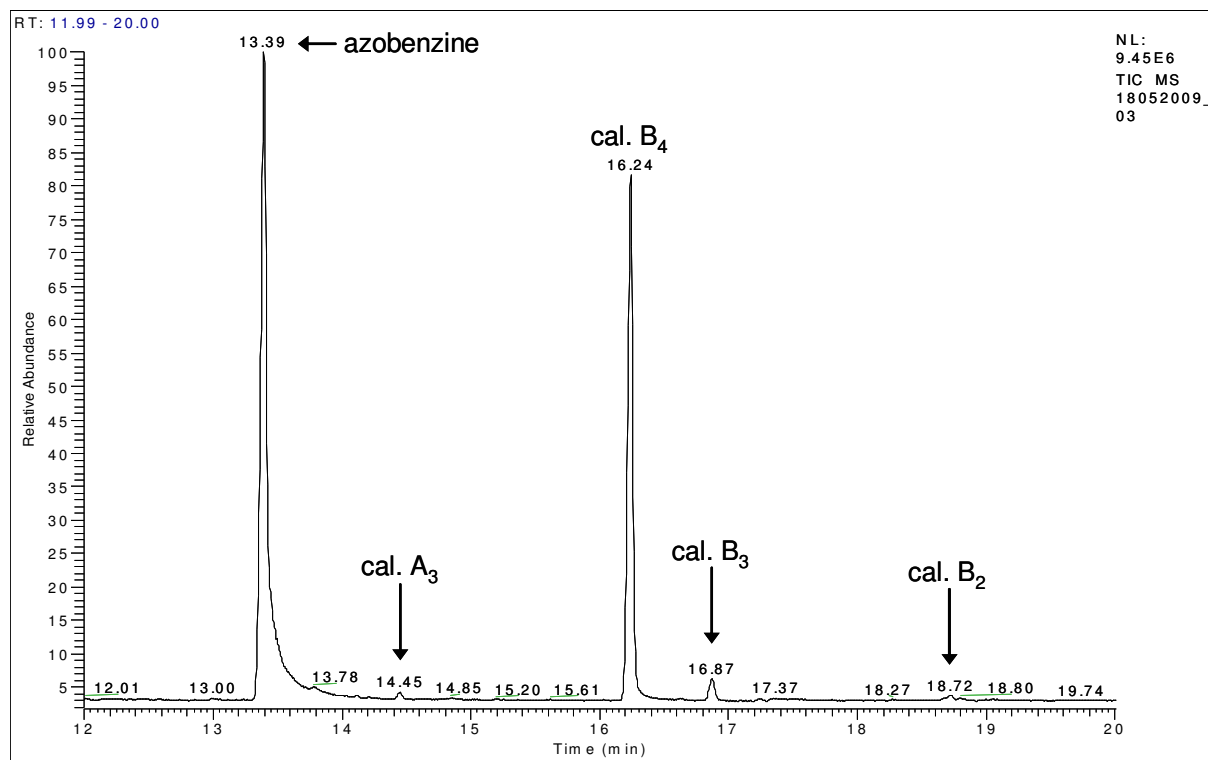
Figure 55: GC-MS chromatogram of calystegine B$_4$ pool
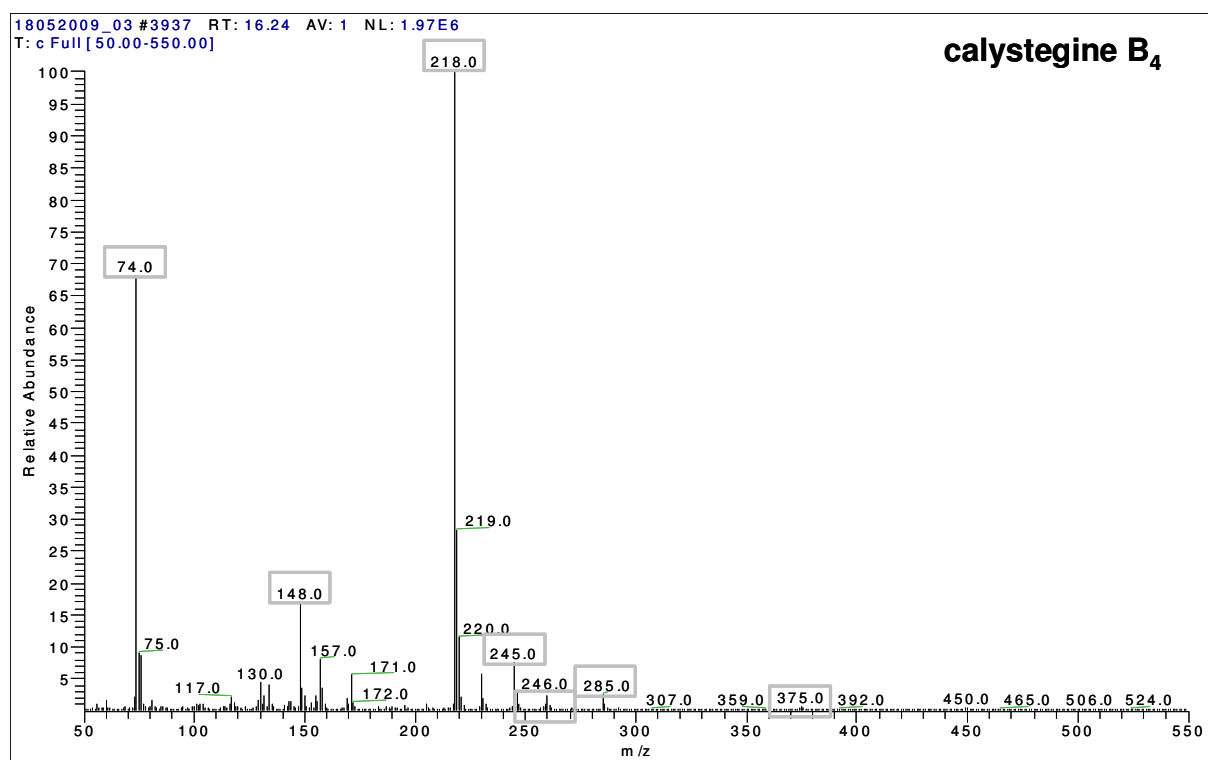
Figure 56: MS spectrum of calystegine B$_4$ in its pool
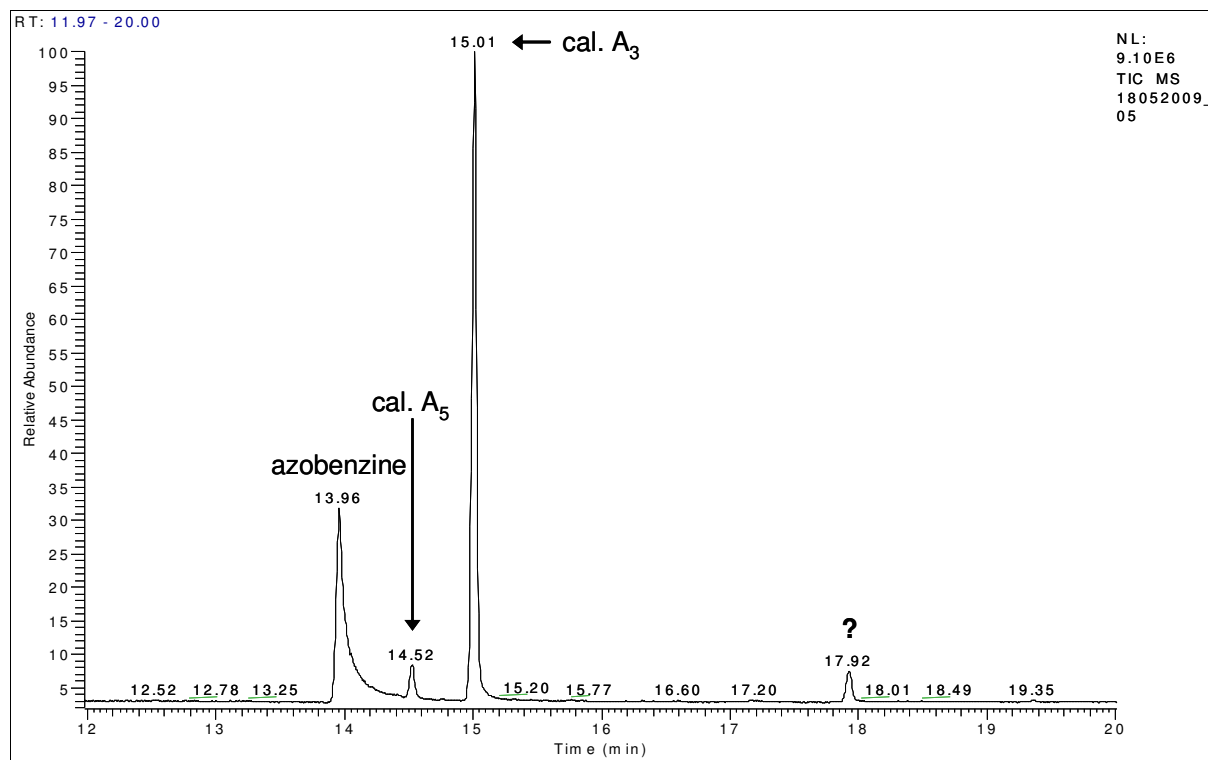
Figure 57: GC-MS chromatogram of calystegine A$_3$ pool
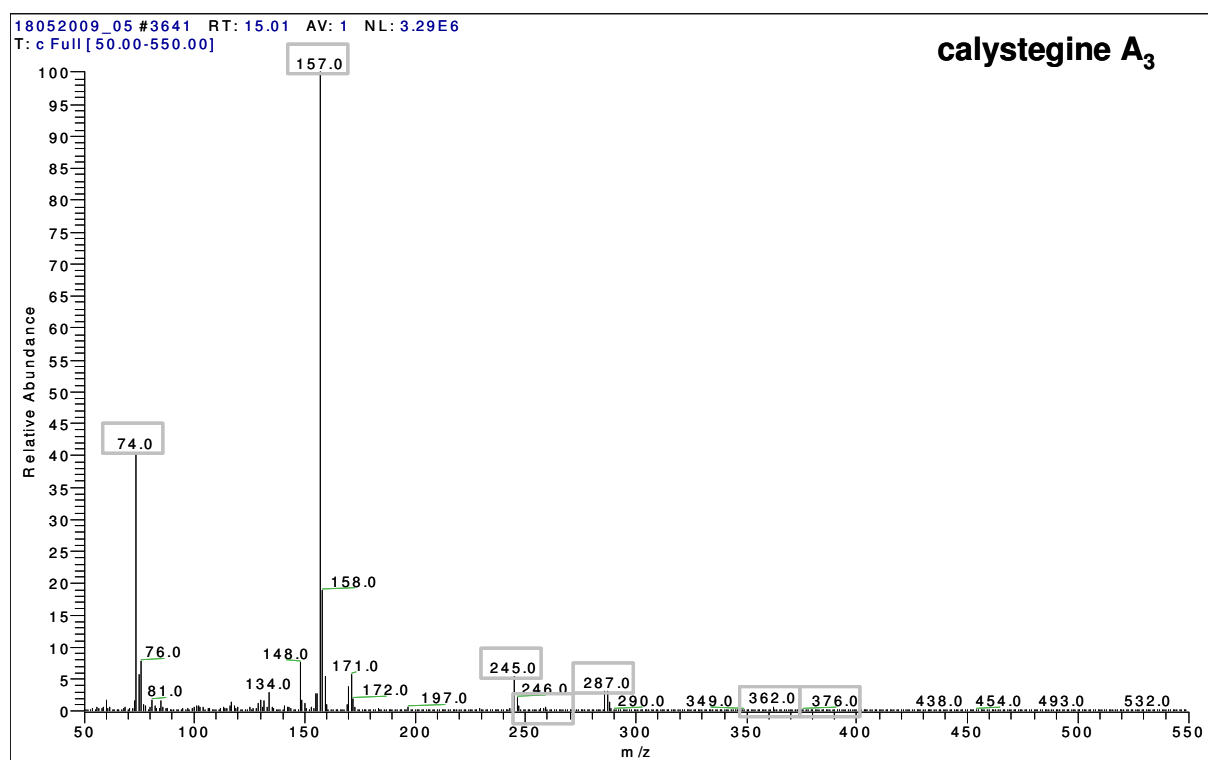
Figure 58: MS spectrum of calystegine A$_3$ in its pool

6.5. NMR spectra of purified calystegine pools
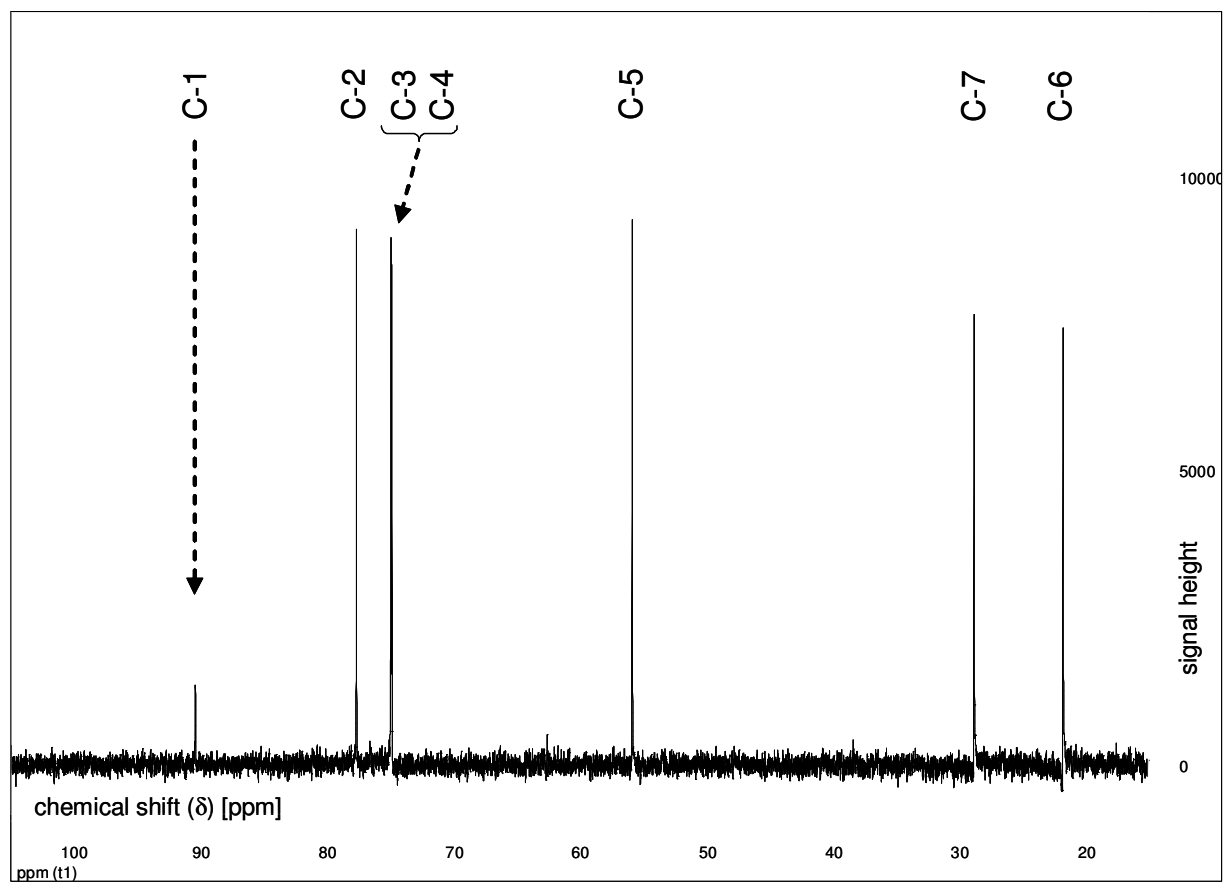
Figure 59: ^{13}**C NMR spectrum (100 MHz) of calystegine B$_2$ pool**
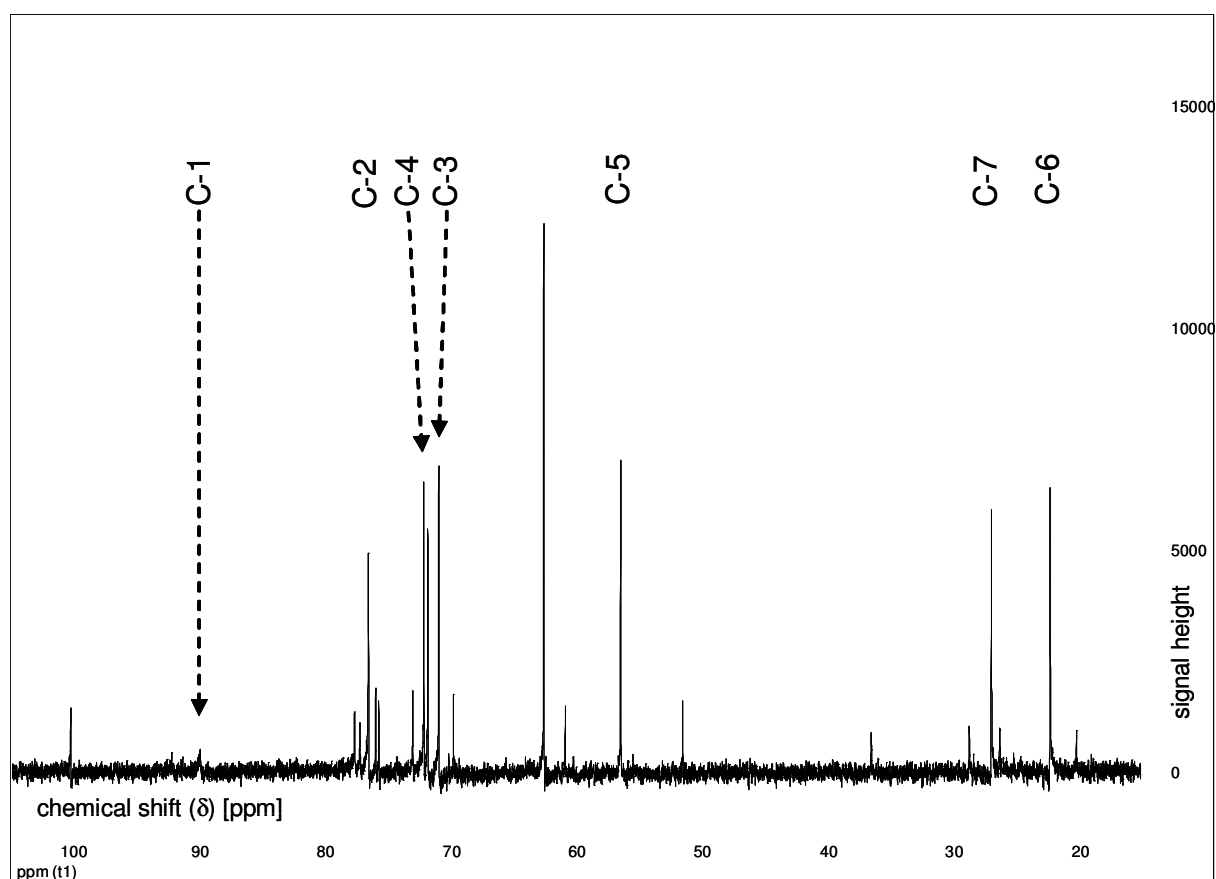
Figure 60: ^{13}C NMR spectrum (100 MHz) of calystegine B$_4$ pool
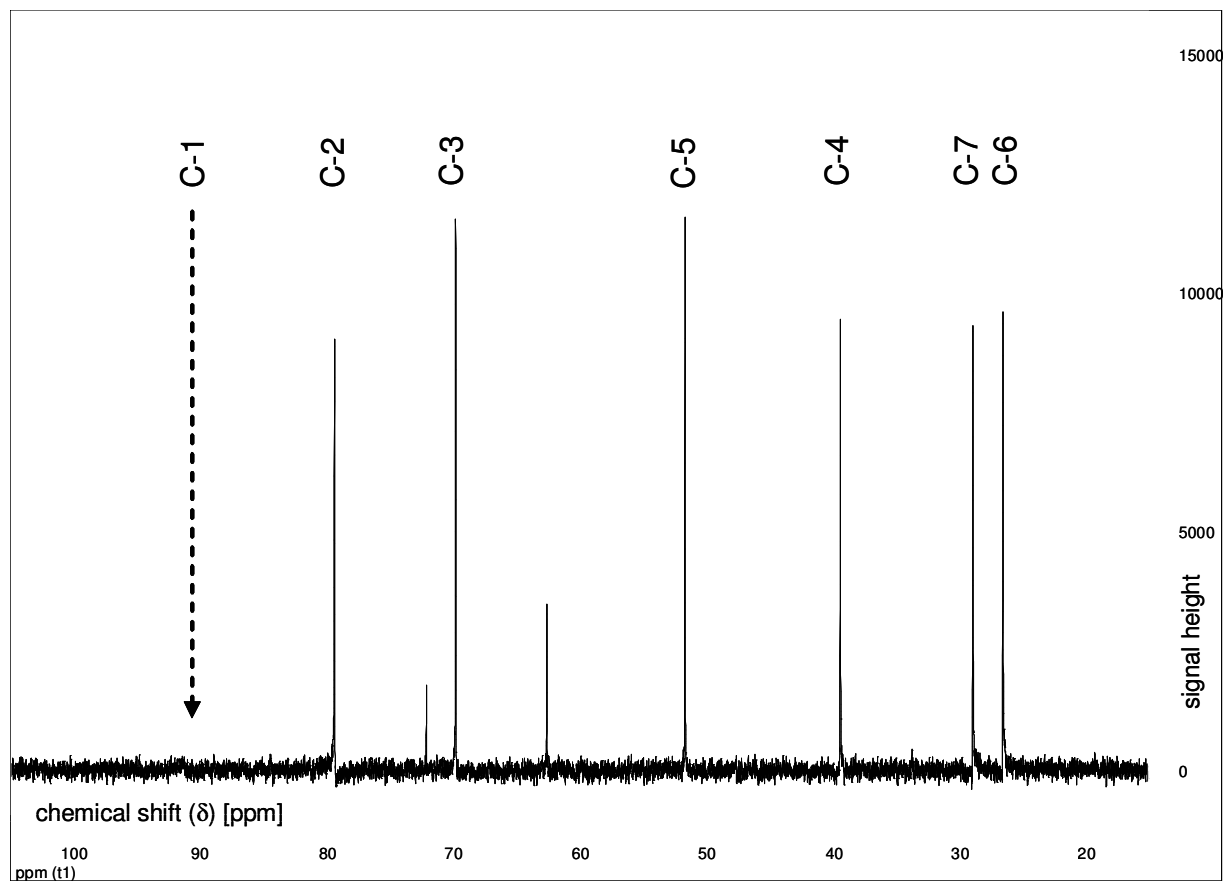
Figure 61: ^{13}**C NMR spectrum (100 MHz) of calystegine A$_3$ pool**

6.6.   Pipetting scheme and enzyme kinetics for *β*-glycosidase assay

Scheme 3: Pipetting scheme for generation of *p*-nitrophenol calibration curve

step 1: fill the column wells with 75 µL each of a *p*-nitrophenol dilution series; first column filled with PB5 ("+" = 25 µL)

	PB5 blind value	p-NP sol. 1 0.01 mM	p-NP sol. 2 0.02 mM	p-NP sol. 3 0.03 mM	p-NP sol. 4 0.05 mM	p-NP sol. 5 0.1 mM	p-NP sol. 6 0.15 mM	p-NP sol. 7 0.2 mM	p-NP sol. 8 0.25 mM	p-NP sol. 9 0.3 mM	empty –	empty –
	1	2	3	4	5	6	7	8	9	10	11	12
A	+++	+++	+++	+++	+++	+++	+++	+++	+++	+++	–	–
B	+++	+++	+++	+++	+++	+++	+++	+++	+++	+++	–	–
C	+++	+++	+++	+++	+++	+++	+++	+++	+++	+++	–	–
D	+++	+++	+++	+++	+++	+++	+++	+++	+++	+++	–	–
E	+++	+++	+++	+++	+++	+++	+++	+++	+++	+++	–	–
F	+++	+++	+++	+++	+++	+++	+++	+++	+++	+++	–	–
G	+++	+++	+++	+++	+++	+++	+++	+++	+++	+++	–	–
H	+++	+++	+++	+++	+++	+++	+++	+++	+++	+++	–	–

step 2: agitation (1 min, 960 rpm), 10 min incubation (37 °C)

step 3: add 50 µL 1M sodium carbonate (stop solution) in every well ("+" = 25 µL)

	1	2	3	4	5	6	7	8	9	10	11	12
A	++	++	++	++	++	++	++	++	++	++	++	++
B	++	++	++	++	++	++	++	++	++	++	++	++
C	++	++	++	++	++	++	++	++	++	++	++	++
D	++	++	++	++	++	++	++	++	++	++	++	++
E	++	++	++	++	++	++	++	++	++	++	++	++
F	++	++	++	++	++	++	++	++	++	++	++	++
G	++	++	++	++	++	++	++	++	++	++	++	++
H	++	++	++	++	++	++	++	++	++	++	++	++

step 4: agitation (1 min, 960 rpm); photometric absorbance measurement (wavelength 405 nm)

Scheme 4: Determination of K$_m$ value of substrate (*p*-NPG) for *β*-D-glycosidase

step 1: fill the odd columns with PB5 ("+" = 25 µL)

	1	2	3	4	5	6	7	8	9	10	11	12
A	+		+		+		+		+		+	
B	+		+		+		+		+		+	
C	+		+		+		+		+		+	
D	+		+		+		+		+		+	
E	+		+		+		+		+		+	
F	+		+		+		+		+		+	
G	+		+		+		+		+		+	
H	+		+		+		+		+		+	

step 2: in every column, add 25 µL PB5 per well; for determination of enzyme K$_m$ with flux assay samples: 25 µL FAB6 or 7.5 ("+" = 25 µL)

	1	2	3	4	5	6	7	8	9	10	11	12
A	+	+	+	+	+	+	+	+	+	+	+	+
B	+	+	+	+	+	+	+	+	+	+	+	+
C	+	+	+	+	+	+	+	+	+	+	+	+
D	+	+	+	+	+	+	+	+	+	+	+	+
E	+	+	+	+	+	+	+	+	+	+	+	+
F	+	+	+	+	+	+	+	+	+	+	+	+
G	+	+	+	+	+	+	+	+	+	+	+	+
H	+	+	+	+	+	+	+	+	+	+	+	+

step 3: add 25 µL per well of substrate solution 1−10 (one substrate concentration in two columns, four rows); "Sub" = *p*-nitrophenyl *β*-D-glycoside solution ("+" = 25 µL)

	1	2	3	4	5	6	7	8	9	10	11	12
A	Sub 3	Sub 3	Sub 1	Sub 1	Sub 2	Sub 2	Sub 3	Sub 3	Sub 4	Sub 4	Sub 5	Sub 5
B	Sub 4	Sub 4	Sub 1	Sub 1	Sub 2	Sub 2	Sub 3	Sub 3	Sub 4	Sub 4	Sub 5	Sub 5
C	Sub 5	Sub 5	Sub 1	Sub 1	Sub 2	Sub 2	Sub 3	Sub 3	Sub 4	Sub 4	Sub 5	Sub 5
D	Sub 6	Sub 6	Sub 1	Sub 1	Sub 2	Sub 2	Sub 3	Sub 3	Sub 4	Sub 4	Sub 5	Sub 5
E	Sub 7	Sub 7	Sub 6	Sub 6	Sub 7	Sub 7	Sub 8	Sub 8	Sub 9	Sub 9	Sub10	Sub10
F	Sub 8	Sub 8	Sub 6	Sub 6	Sub 7	Sub 7	Sub 8	Sub 8	Sub 9	Sub 9	Sub10	Sub10
G	Sub 9	Sub 9	Sub 6	Sub 6	Sub 7	Sub 7	Sub 8	Sub 8	Sub 9	Sub 9	Sub10	Sub10
H	Sub10	Sub10	Sub 6	Sub 6	Sub 7	Sub 7	Sub 8	Sub 8	Sub 9	Sub 9	Sub10	Sub10

step 4: 5 min incubation (37 °C)

step 5: add 25 µL per well of enzyme solution (0.01 mg/mL) in even columns, ("+" = 25 µL)

	1	2	3	4	5	6	7	8	9	10	11	12
A		+		+		+		+		+		+
B		+		+		+		+		+		+
C		+		+		+		+		+		+
D		+		+		+		+		+		+
E		+		+		+		+		+		+
F		+		+		+		+		+		+
G		+		+		+		+		+		+
H		+		+		+		+		+		+

step 6: agitation (1 min, 960 rpm); 10 min incubation (37 °C)

step 7: add 50 µL 1M sodium carbonate (stop solution) in every well ("+" = 25 µL)

	1	2	3	4	5	6	7	8	9	10	11	12
A	++	++	++	++	++	++	++	++	++	++	++	++
B	++	++	++	++	++	++	++	++	++	++	++	++
C	++	++	++	++	++	++	++	++	++	++	++	++
D	++	++	++	++	++	++	++	++	++	++	++	++
E	++	++	++	++	++	++	++	++	++	++	++	++
F	++	++	++	++	++	++	++	++	++	++	++	++
G	++	++	++	++	++	++	++	++	++	++	++	++
H	++	++	++	++	++	++	++	++	++	++	++	++

step 8: agitation (1 min, 960 rpm); photometric absorbance measurement (wavelength 405 nm)

Scheme 5: Inhibition of *β*-D-glycosidase with calystegine. Determination of K*i* value

step 1: add 25 µL PB5 per well in odd columns, first two columns 25 µL FAB6 or 7.5 per well ("+" = 25 µL)

	1	2	3	4	5	6	7	8	9	10	11	12
A	++	+	+		+		+		+		+	
B	++	+	+		+		+		+		+	
C	++	+	+		+		+		+		+	
D	++	+	+		+		+		+		+	
E	++	+	+		+		+		+		+	
F	++	+	+		+		+		+		+	
G	++	+	+		+		+		+		+	
H	++	+	+		+		+		+		+	

step 2: add calystegine solution (1−6), one single concentration per plate, i.e. assay run; calystegine solution in PB5, FAB6 or 7.5 ("+" = 25 µL)

	1	2	3	4	5	6	7	8	9	10	11	12
A			+	+	+	+	+	+	+	+	+	+
B			+	+	+	+	+	+	+	+	+	+
C			+	+	+	+	+	+	+	+	+	+
D			+	+	+	+	+	+	+	+	+	+
E			+	+	+	+	+	+	+	+	+	+
F			+	+	+	+	+	+	+	+	+	+
G			+	+	+	+	+	+	+	+	+	+
H			+	+	+	+	+	+	+	+	+	+

step 3: add 25 µLof substrate solution 1−10 per well (one substrate concentration in two columns, four rows); "Sub" = *p*-nitrophenyl *β*-D-glycoside solution ("+" = 25 µL); first two column with Sub 3−10 for observation the enzyme activity ([***])

	1	2	3	4	5	6	7	8	9	10	11	12
A	Sub 3	Sub 3	Sub 1	Sub 1	Sub 2	Sub 2	Sub 3	Sub 3	Sub 4	Sub 4	Sub 5	Sub 5
B	Sub 4	Sub 4	Sub 1	Sub 1	Sub 2	Sub 2	Sub 3	Sub 3	Sub 4	Sub 4	Sub 5	Sub 5
C	Sub 5	Sub 5	Sub 1	Sub 1	Sub 2	Sub 2	Sub 3	Sub 3	Sub 4	Sub 4	Sub 5	Sub 5
D	Sub 6	Sub 6	Sub 1	Sub 1	Sub 2	Sub 2	Sub 3	Sub 3	Sub 4	Sub 4	Sub 5	Sub 5
E	Sub 7	Sub 7	Sub 6	Sub 6	Sub 7	Sub 7	Sub 8	Sub 8	Sub 9	Sub 9	Sub10	Sub10
F	Sub 8	Sub 8	Sub 6	Sub 6	Sub 7	Sub 7	Sub 8	Sub 8	Sub 9	Sub 9	Sub10	Sub10
G	Sub 9	Sub 9	Sub 6	Sub 6	Sub 7	Sub 7	Sub 8	Sub 8	Sub 9	Sub 9	Sub10	Sub10
H	Sub10	Sub10	Sub 6	Sub 6	Sub 7	Sub 7	Sub 8	Sub 8	Sub 9	Sub 9	Sub10	Sub10

step 4: 5 min incubation (37 °C)

step 5: add 25 µL of enzyme solution per well (0.01 mg/mL) in even columns ("+" = 25 µL)

	1	2	3	4	5	6	7	8	9	10	11	12
A		+		+		+		+		+		+
B		+		+		+		+		+		+
C		+		+		+		+		+		+
D		+		+		+		+		+		+
E		+		+		+		+		+		+
F		+		+		+		+		+		+
G		+		+		+		+		+		+
H		+		+		+		+		+		+

step 6: agitation (1 min, 960 rpm); 10 min incubation (37 °C)

step 7: add 50 µL 1M sodium carbonate (stop solution) in every well ("+" = 25 µL)

	1	2	3	4	5	6	7	8	9	10	11	12
A	++	++	++	++	++	++	++	++	++	++	++	++
B	++	++	++	++	++	++	++	++	++	++	++	++
C	++	++	++	++	++	++	++	++	++	++	++	++
D	++	++	++	++	++	++	++	++	++	++	++	++
E	++	++	++	++	++	++	++	++	++	++	++	++
F	++	++	++	++	++	++	++	++	++	++	++	++
G	++	++	++	++	++	++	++	++	++	++	++	++
H	++	++	++	++	++	++	++	++	++	++	++	++

step 8: agitation (1 min, 960 rpm); photometric absorbance measurement (wavelength 405 nm)
([***]) columns 1 and 2 used for approximate estimation of enzyme specific activity to judge if the kinetic parameters are approximately in the range of desirable values

Scheme 6: Inhibition of *β*-ᴅ-glycosidase with calystegine. Generation of the equation for calystegine quantification in flux assay samples

step 1: add 25 µL PB5 per well in odd columns ("+" = 25 µL)

	1	2	3	4	5	6	7	8	9	10	11	12
A	+		+		+		+		+		+	
B	+		+		+		+		+		+	
C	+		+		+		+		+		+	
D	+		+		+		+		+		+	
E	+		+		+		+		+		+	
F	+		+		+		+		+		+	
G	+		+		+		+		+		+	
H	+		+		+		+		+		+	

step 2: add calystegine sol. (1−6) in FAB6, each concentration pipetted pairwise in rows A−D, 25 µL per well

	1	2	3	4	5	6	7	8	9	10	11	12
A	cal. 1	cal. 1	cal. 2	cal. 2	cal. 3	cal. 3	cal. 4	cal. 4	cal. 5	cal. 5	cal. 6	cal. 6
B	cal. 1	cal. 1	cal. 2	cal. 2	cal. 3	cal. 3	cal. 4	cal. 4	cal. 5	cal. 5	cal. 6	cal. 6
C	cal. 1	cal. 1	cal. 2	cal. 2	cal. 3	cal. 3	cal. 4	cal. 4	cal. 5	cal. 5	cal. 6	cal. 6
D	cal. 1	cal. 1	cal. 2	cal. 2	cal. 3	cal. 3	cal. 4	cal. 4	cal. 5	cal. 5	cal. 6	cal. 6
E												
F												
G												
H												

step 3: add calystegine sol. (1−6) in FAB7.5, each concentration pipetted pairwise in rows E−H, 25 µL per well

	1	2	3	4	5	6	7	8	9	10	11	12
A												
B												
C												
D												
E	cal. 1	cal. 1	cal. 2	cal. 2	cal. 3	cal. 3	cal. 4	cal. 4	cal. 5	cal. 5	cal. 6	cal. 6
F	cal. 1	cal. 1	cal. 2	cal. 2	cal. 3	cal. 3	cal. 4	cal. 4	cal. 5	cal. 5	cal. 6	cal. 6
G	cal. 1	cal. 1	cal. 2	cal. 2	cal. 3	cal. 3	cal. 4	cal. 4	cal. 5	cal. 5	cal. 6	cal. 6
H	cal. 1	cal. 1	cal. 2	cal. 2	cal. 3	cal. 3	cal. 4	cal. 4	cal. 5	cal. 5	cal. 6	cal. 6

step 4: add 25 µL of substrate solution 5 per well (9 mM *p*-nitrophenyl *β*-ᴅ-glycoside solution in 150 mM PB5)   ("+" = 25 µL) → c(*p*-NPG) = 3 mM in assay mixture

	1	2	3	4	5	6	7	8	9	10	11	12
A	+	+	+	+	+	+	+	+	+	+	+	+
B	+	+	+	+	+	+	+	+	+	+	+	+
C	+	+	+	+	+	+	+	+	+	+	+	+
D	+	+	+	+	+	+	+	+	+	+	+	+
E	+	+	+	+	+	+	+	+	+	+	+	+
F	+	+	+	+	+	+	+	+	+	+	+	+
G	+	+	+	+	+	+	+	+	+	+	+	+
H	+	+	+	+	+	+	+	+	+	+	+	+

step 5: 5 min incubation (37 °C)

step 6: add 25 µL of enzyme solution per well (0.01 mg/mL) in even columns ("+" = 25 µL)

	1	2	3	4	5	6	7	8	9	10	11	12
A		+		+		+		+		+		+
B		+		+		+		+		+		+
C		+		+		+		+		+		+
D		+		+		+		+		+		+
E		+		+		+		+		+		+
F		+		+		+		+		+		+
G		+		+		+		+		+		+
H		+		+		+		+		+		+

step 7: agitation (1 min, 960 rpm); 10 min incubation (37 °C)

step 8: add 50 µL 1M sodium carbonate (stop solution) in every well ("+" = 25 µL)

	1	2	3	4	5	6	7	8	9	10	11	12
A	++	++	++	++	++	++	++	++	++	++	++	++
B	++	++	++	++	++	++	++	++	++	++	++	++
C	++	++	++	++	++	++	++	++	++	++	++	++
D	++	++	++	++	++	++	++	++	++	++	++	++
E	++	++	++	++	++	++	++	++	++	++	++	++
F	++	++	++	++	++	++	++	++	++	++	++	++
G	++	++	++	++	++	++	++	++	++	++	++	++
H	++	++	++	++	++	++	++	++	++	++	++	++

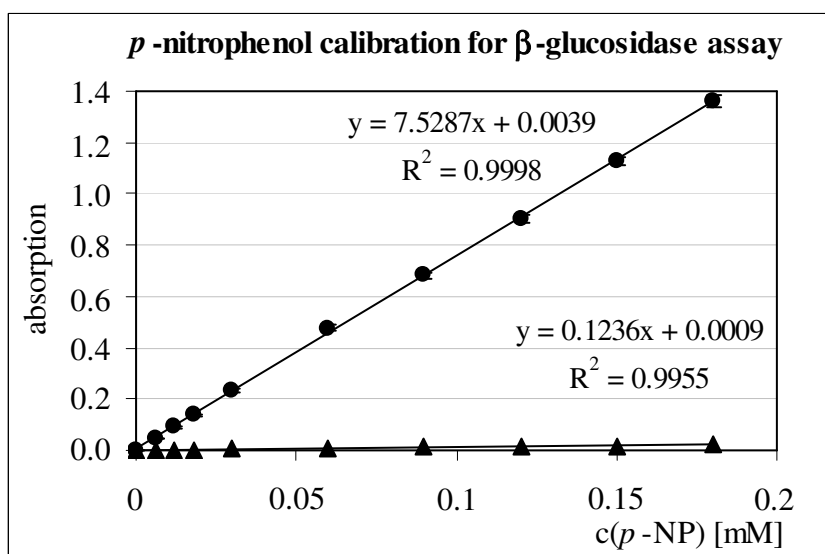**step 9:** agitation (1 min, 960 rpm); photometric absorbance measurement (wavelength 405 nm)

Figure 62: *p*-nitrophenol calibration curve for *β*-glycosidase assay.

Full black dotted points represent *p*-NP absorption values in the stop assay mixture; black triangles represent *p*-NP absorption values in the assay mixture, before stopping the assay.

Table 47: Replications of the *β*-glycosidase assay for determination of the enzyme kinetic parameters and confirmation of the assay reliability

β-glycosidase assay replicate No.	V_{max} ± Std. Error [nkat/mg]	K_m ± Std. Error [mM]	R^2
1	133 ± 2	2.9 ± 0.1	0.9962
2	153 ± 2	3.0 ± 0.1	0.9948
3	136 ± 3	2.7 ± 0.2	0.9877
4	131 ± 3	2.7 ± 0.2	0.9857
5	129 ± 1	2.8 ± 0.1	0.9975
6	121 ± 2	3.0 ± 0.2	0.9896
7	120 ± 3	2.6 ± 0.2	0.9841
8	146 ± 3	2.7 ± 0.2	0.9875
8 replicates (*β*-glycosidase assay)			
m.v.	134	2.8	0.9904
s.d.	11	0.2	0.0051
% s.d.(m.v.)	9	5.6	0.5

For single assay results, values are shown with standard errors (number of samples n = 4);

Final result are represented as mean values of the appropriate kinetic parameters for eight single assay runs with standard deviations.
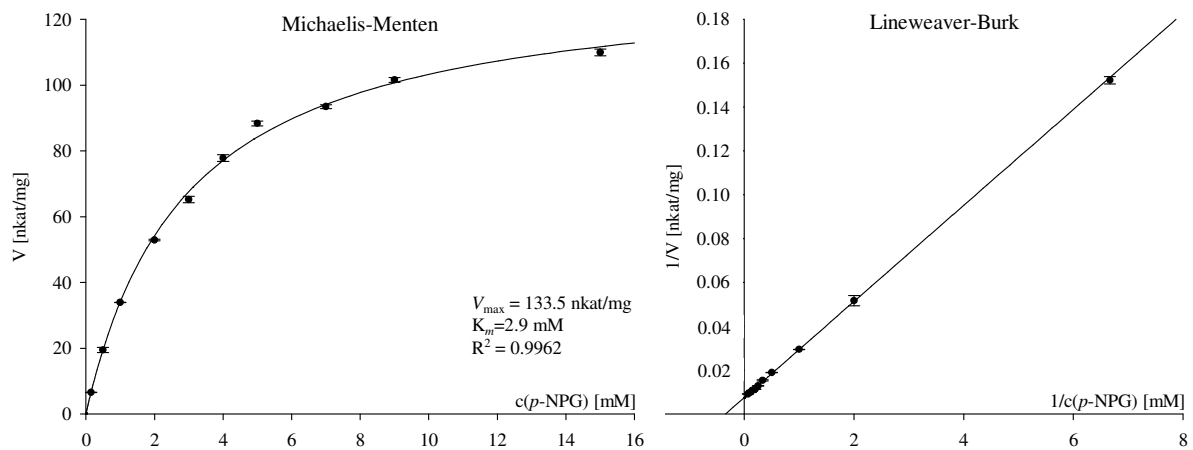
Figure 63: Michaelis-Menten and Lineweaver-Burk diagrams showing β-glycosidase specific activity curve
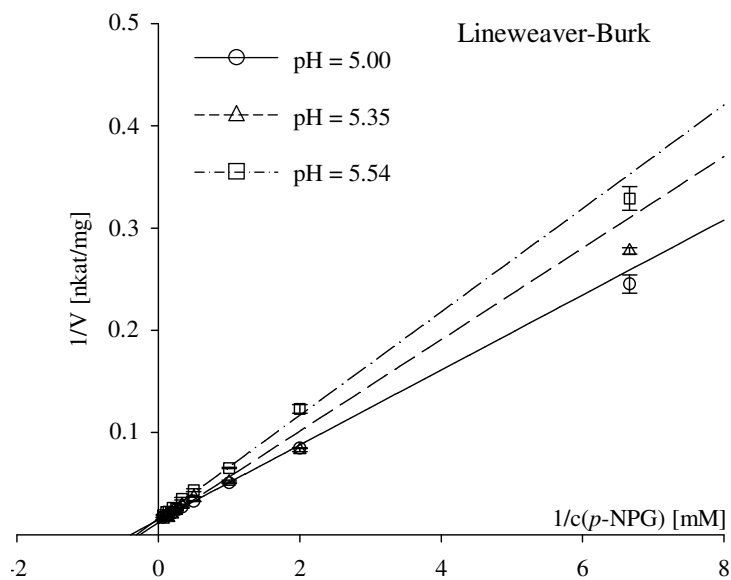

Figure 64: Comparison of the specific activity lines of β-glycosidase according to Lineweaver-Burk in three different pH-environments (enzyme assay PB5 alone, compared with the combinations with Transwell® compartment samples from the flux test)

Table 48: Kinetic parameters of *β*-glycosidase in determination of K*i* with enzyme inhibition by 0.5-50 µM calystegine B₂ in FAB6

c(cal. B₂)/assay [µM]	V_{max} ± Std. Error [nkat/mg]	K_m ± Std. Error [mM]	R^2 -
0	108 ± 2	3.2 ± 0.2	0.9871
0.17	90 ± 3	2.5 ± 0.2	0.9738
0.83	89 ± 3	3.7 ± 0.3	0.9748
1.67	94 ± 3	4.8 ± 0.3	0.9863
8.33	79 ± 4	8.1 ± 0.7	0.9830
16.67	62 ± 4	9.8 ± 1.0	0.9788

Table 49: Kinetic parameters of *β*-glycosidase in determination of K*i* with enzyme inhibition by 0.5-50 µM calystegine B₂ in FAB7.5

c(cal. B₂)/assay [µM]	V_{max} ± Std. Error [nkat/mg]	K_m ± Std. Error [mM]	R^2
0	96 ± 3	3.3 ± 0.3	0.9746
0.17	87 ± 4	3.7 ± 0.5	0.9501
0.83	83 ± 2	4.3 ± 0.2	0.9898
1.67	110 ± 3	5.9 ± 0.4	0.9898
8.33	71 ± 5	7.7 ± 1.0	0.9633
16.67	74 ± 6	14.7 ± 1.9	0.9769
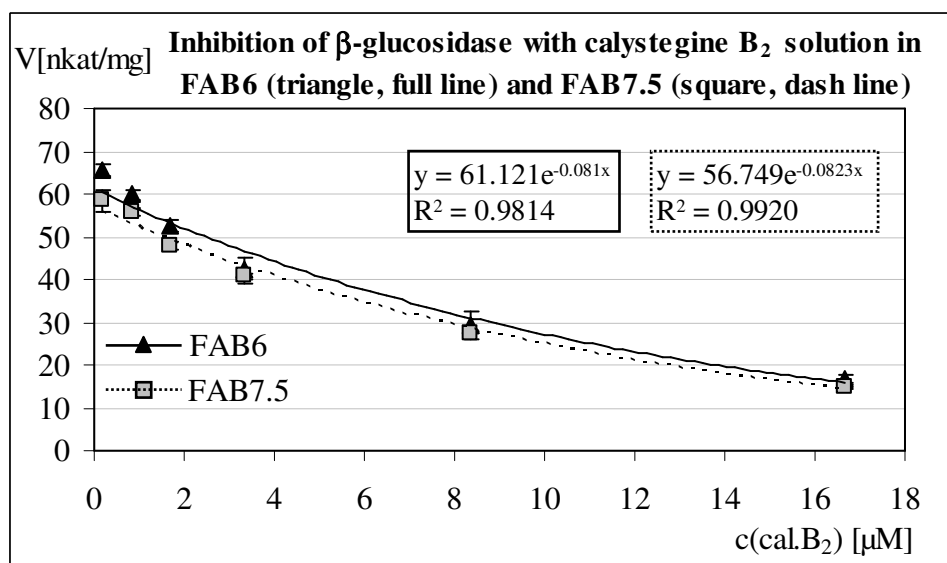
Figure 65: Regression lines of *β*-glycosidase activity in FAB6 and 7.5 inhibited with calystegine B$_2$

Specific activity of sweet almond *β*-glycosidase at 3 mM *p*-NPG (nkat/mg), inhibited by calystegine B$_2$ in concentrations ranging from 0.16 to 16.67 µM in the assay. Black full triangles and full line: calystegine solution in FAB6; full grey squares and dash line: calystegine solution in FAB7.5. Regression line equations were used for generation of calystegine B$_2$ calibration curves in the *β*-glycosidase assay for the calystegine quantification after the transepithelial flux test. Black bars on value marks represent standard deviations of the samples measurements (n = 4).

6.7.   Enzyme kinetics of *α*-glycosidases inhibition with calystegines

maltase / no inhibitor

V_{max}= 827.4 pkat/mg
K_m= 7.3 mM
c(maltose) [mM]

maltase / 5 µM acarbose

V_{max}= 725.2 pkat/mg
K_m= 15.6 mM
c(maltose) [mM]

maltase / 119 µM calystegine A$_3$

V_{max}= 955.5 pkat/mg
K_m= 9.1 mM
c(maltose) [mM]

maltase / 476 µM calystegine A$_3$

V_{max}= 939.1 pkat/mg
K_m= 11.1 mM
c(maltose) [mM]

maltase / 119 µM calystegine B$_2$

V_{max}= 741.6 pkat/mg
K_m= 8.6 mM
c(maltose) [mM]

maltase / 476 µM calystegine B$_2$

V_{max}= 1016.2 pkat/mg
K_m= 25.4 mM
c(maltose) [mM]

Figure 66: Michaelis-Menten enzyme activity curves of maltase for various conditions tested: 0, 119 and 476 µM calystegine (A$_3$ and B$_2$), 5 µM acarbose as inhibition positive control
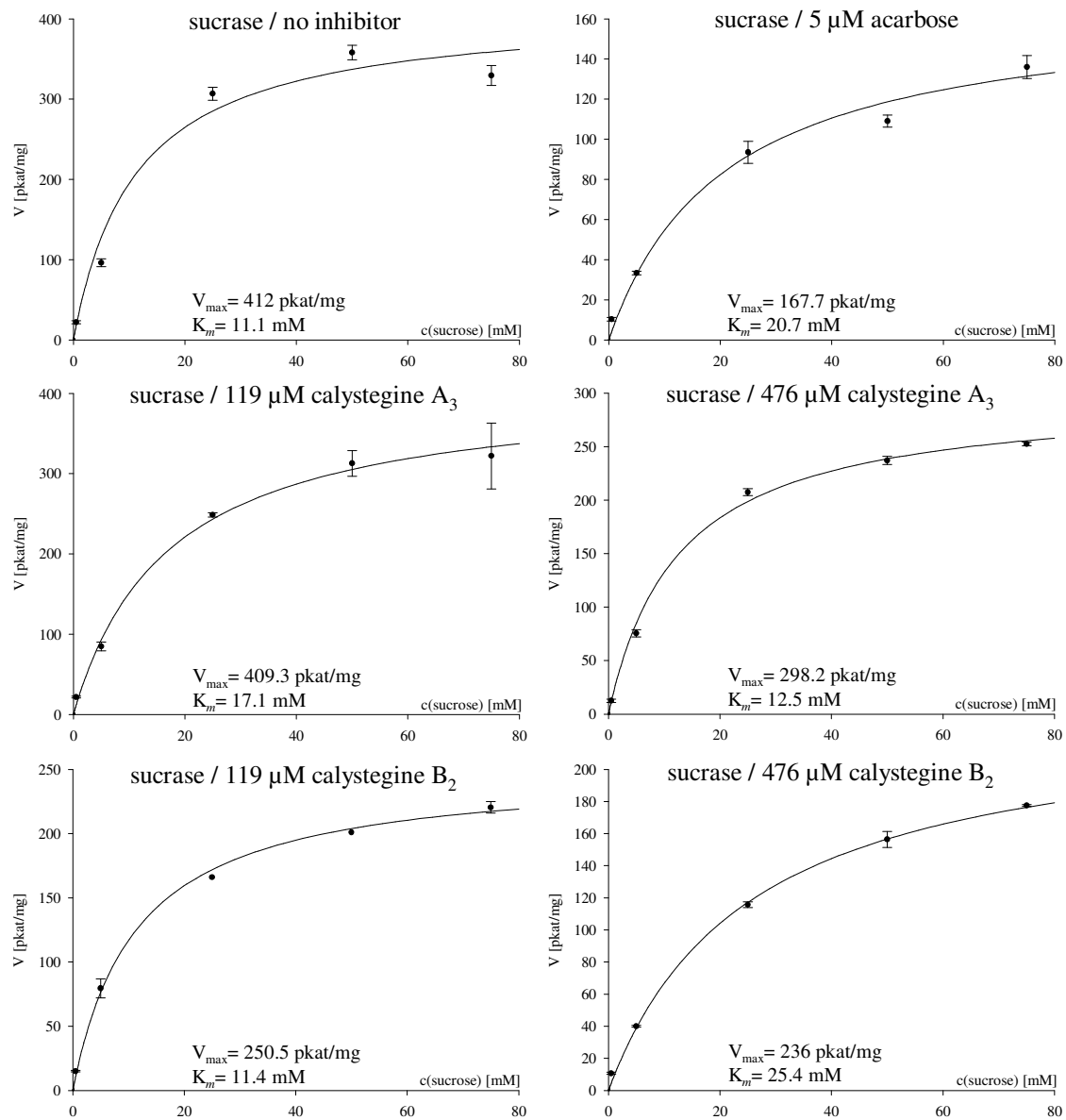
Figure 67: Michaelis-Menten enzyme activity curves of sucrase for various conditions tested: 0, 119 and 476 μM calystegine (A₃ and B₂), 5 μM acarbose as inhibition positive control

7. Acknowledgements

Nebojša Jocković thanks to:

- the KAAD (Catholic academic exchange organisation) for a PhD fellowship, and the association "Die Vereinigung der Freunde und Förderer der Martin-Luther-Universität Halle-Wittenberg e.V. (VFF)" for additional financial support during the writing of the thesis. Work in the laboratory in Halle was financially supported by the DFG (German Research Foundation).
- Prof. Dr. Birgit Dräger for providing the subject and working conditions for the thesis
- Prof. Ing. František Kvasnička for cooperation and publication on CZE and cITP
- Prof. Dr. Hans-Hermann Rüttinger and his working group for investigation on CZE
- PD Dr. Matthias Brandsch and his working group for providing the working space, support and advices in the area of membrane transport investigation.
- PD Dr. Wolfgang Brandt and his working group for performing and evaluating the docking of calystegines
- Prof. Dr. Goran Kaluđerović for consulting support and heartening tips
- Dr. Jorrit Jan Krijger for the generous technical support by the script corrections

Special thanks go to the previous and contemporary members of AG Dräger and the technical staff for generous help, helpful advices, encouraging discussions and making the hard times inside and outside the laboratory easier or easier to get over.

8. Declaration

I, Nebojša Jocković, declare that this thesis, submitted in fulfilment of the requirement for the award of Doctor of Philosophy, at the Institute of Pharmacy, Faculty of Natural Science I, Martin-Luther-University Halle-Wittenberg, is wholly my own work unless due reference is provided. This document has not been submitted for qualifications at any other academic institution.

Nebojša Jocković

Halle (Saale), October, 2014

9. Curriculum vitae

Personal information:

Name: Nebojša Jocković

Date and place of birth: 06.11.1979, Novi Sad, Serbia

Education:

1986 – 1988   Primary school "11. Novembar", Senta

1988 – 1994   Primary school "Kralj Petar II", Belgrade

1994 – 1998   Third Belgrade Grammar School, Belgrade

Academic education and training:

1998 – 2004   Faculty of Pharmacy, University of Belgrade

Jul. 2003   IPSF Students Exchange Programme:
               Institute of Pharmacognosy , Faculty of Pharmacy,
               University of Porto, Portugal
               Topic: Extraction and determination of phenolic compounds from natural
               matrices using HPLC/DAD and LC/MS

Dec. 2004   Diploma thesis: Institute of Pharmacognosy, Faculty of Pharmacy,
               University of Belgrade
               Topic: Chemical investigation of some bryophyte species: *Brachythecium*,
               Eurhynchium, *Polytrichum*, *Lunularia* and *Pellia*

2005 – 2006   Practical training for pharmacist: "Božur" community pharmacy, Belgrade

Aug. 2006   State exam for pharmacists, Belgrade

May 2014   Approbation for apothecary, Halle (Saale)

Ph. D. studies:

2006 – 2014   Institute of Pharmacy, Department of Pharmacognosy and Pharmacology,
               Martin-Luther-University Halle-Wittenberg, Group Biogenic Drugs
               (Prof. Dr. Birgit Dräger)

Work experience:

Apr. – Aug.
   2006   Pharmacist, "Javor" community pharmacy, Belgrade

Oct. 2013 –
Apr. 2014   Pharmacist, Humanitas-Apotheke, Halle (Saale)

Sep. 2014 →   Pharmacist, Apotheke im Neustadt-Centrum, Halle (Saale)